National Library
of Canada

Acquisitions and
Bibliographic Services Branch

395 Wellington Street
Ottawa, Ontario
K1A 0N4

Bibliothèque nationale
du Canada

Direction des acquisitions et
des services bibliographiques

395, rue Wellington
Ottawa (Ontario)
K1A 0N4

Your file Votre référence

Our file Notre référence

NOTICE

The quality of this microform is heavily dependent upon the quality of the original thesis submitted for microfilming. Every effort has been made to ensure the highest quality of reproduction possible.

If pages are missing, contact the university which granted the degree.

Some pages may have indistinct print especially if the original pages were typed with a poor typewriter ribbon or if the university sent us an inferior photocopy.

Reproduction in full or in part of this microform is governed by the Canadian Copyright Act, R.S.C. 1970, c. C-30, and subsequent amendments.

AVIS

La qualité de cette microforme dépend grandement de la qualité de la thèse soumise au microfilmage. Nous avons tout fait pour assurer une qualité supérieure de reproduction.

S'il manque des pages, veuillez communiquer avec l'université qui a conféré le grade.

La qualité d'impression de certaines pages peut laisser à désirer, surtout si les pages originales ont été dactylographiées à l'aide d'un ruban usé ou si l'université nous a fait parvenir une photocopie de qualité inférieure.

La reproduction, même partielle, de cette microforme est soumise à la Loi canadienne sur le droit d'auteur, SRC 1970, c. C-30, et ses amendements subséquents.

Canada

UNIVERSITY OF ALBERTA

ELEMENTAL ELECTROSPRAY MASS SPECTROMETRY

BY

© George R. Agnes

A thesis submitted to the Faculty of Graduate Studies and Research in partial fulfillment of the requirements for the degree of **Doctor of Philosophy**.

DEPARTMENT OF CHEMISTRY

Edmonton, Alberta
SPRING, 1994

National Library
of Canada

Acquisitions and
Bibliographic Services Branch

395 Wellington Street
Ottawa, Ontario
K1A 0N4

Bibliothèque nationale
du Canada

Direction des acquisitions et
des services bibliographiques

395, rue Wellington
Ottawa (Ontario)
K1A 0N4

Your file Votre référence

Our file Notre référence

The author has granted an irrevocable non-exclusive licence allowing the National Library of Canada to reproduce, loan, distribute or sell copies of his/her thesis by any means and in any form or format, making this thesis available to interested persons.

L'auteur a accordé une licence irrévocable et non exclusive permettant à la Bibliothèque nationale du Canada de reproduire, prêter, distribuer ou vendre des copies de sa thèse de quelque manière et sous quelque forme que ce soit pour mettre des exemplaires de cette thèse à la disposition des personnes intéressées.

The author retains ownership of the copyright in his/her thesis. Neither the thesis nor substantial extracts from it may be printed or otherwise reproduced without his/her permission.

L'auteur conserve la propriété du droit d'auteur qui protège sa thèse. Ni la thèse ni des extraits substantiels de celle-ci ne doivent être imprimés ou autrement reproduits sans son autorisation.

ISBN 0-612-11143-1

Canada

UNIVERSITY OF ALBERTA

RELEASE FORM

NAME OF AUTHOR:	**George R. Agnes**
TITLE OF THESIS:	**Elemental Electrospray Mass Spectrometry**
DEGREE:	**Doctor of Philosophy**
YEAR THIS DEGREE GRANTED:	**1994**

Permission is hereby granted to the University of Alberta Library to reproduce single copies of this thesis and to lend or sell such copies for private, scholarly or scientific research purposes only.

The author reserves all other publication rights and other rights in association with the copyright in the thesis, and except as hereinbefore provided neither the thesis nor any substantial portion thereof may be printed or otherwise reproduced in any material form whatever without the author's prior written permission.

Department of Chemistry
Simon Fraser University
Burnaby, British Columbia
Canada, V5A 1S6

Date: April 21/1994

"It does not take a genius, just a different way of thinking"

UNIVERSITY OF ALBERTA

FACULTY OF GRADUATE STUDIES AND RESEARCH

The undersigned certify that they have read, and recommend to the Faculty of Graduate Studies and Research for acceptance, a thesis entitled **Elemental Electrospray Mass Spectrometry** submitted by **George R. Agnes** in partial fulfillment of the requirements for the degree of **Doctor of Philosophy**.

Professor G. Horlick

Professor D. J. Harrison

Professor P. Kebarle

Professor L. Li

Professor J. Gray

Professor J. A. Caruso

DATE: April 21/1994

To my wife Jackie,

to our families and friends,

and in memory of my father H. V. Agnes,

memories are forever.

Abstract

The use of Electrospray Mass Spectrometry as a technique for elemental analysis is presented. The electrospray source provides a method of transferring preformed ions in solution to the gas phase at atmospheric pressure. The potential to directly differentiate the chemical forms of an element in solution with an electrospray source provided the impetus with which the research presented in this thesis was initiated.

The characterization of the electrospray ion source through the use of well defined solutions of simple inorganic analytes provided the framework from which the results presented in this thesis were developed. The speciation capabilities of electrospray mass spectrometry were investigated. Kinetically inert species were shown to be quite easily determined with this technique and the potential exists for accurate determinations of kinetically labile species with this technique. Quantitation methodology was developed that exhibits four orders of magnitude linear dynamic range.

The use of well defined solutions of inorganic salts in solution permitted an investigative study of the electrospray source with the directive of understanding the fundamental nature of the technique. The mechanism by which ions are transferred to the gas phase was clarified as being Rayleigh fission in the limit, better known in the literature as the Single Ion Droplet Theory. Results obtained were not supportive of the Ion Evaporation Theory, an alternative theory that has been proposed as the mechanism by which ions within charged droplets are transferred to the gas phase. Furthermore, a model to predict the composition of the charged droplets produced by the electrospray source was developed. The key assumption of the model is that all electrostatically atomized droplets have the same surface electric field strength. Calculations based on this model are used to explain the experimental results obtained.

Acknowledgments

I would like to thank all the people who supported me through either their encouragement and or contribution to the research that was done during the course of completing this thesis. Henry Stolk went well above and beyond the call of duty to not only provide excellent technical assistance, but also his friendship. Dieter Stark assisted me in the numerous times of dire need (like the time(s) I required an 'o' ring five minutes after quitting time). Pat Cambell did a wonderful recruiting job. A gracious thank you to Ian Stewart for listening to my endless electrospray bable over at Java Jive. To all the people who assisted me at the University of Alberta, thank you.

I am also indebted to the people that assisted me in getting to the University of Alberta in the first place.

Professor Gary Horlick performed wonderfully in his ability to see the big picture regardless of how hard I inadvertently tried to confuse him. Gary you are indeed a wonderful teacher and thank you for sharing some of your vision, philosophy, 'magic', and most especially, your version of the perturbation theory with me. Honorable mention goes to Professor Paul Kebarle who was able to set me straight in a but a few short moments during our (unfortunately) few hall conversations. Thanks also to Professor Liang Li for the continuous support.

My savior through all of this was my wife Jackie. Thanks for your wonderful support and endless patience. Also, thanks for accompanying me on those frequent, but required excursions to the Canadian Rocky Mountain National Parks and beyond. P.S. The best is yet to come.

The financial support that was provided by the Department of Chemistry at the University of Alberta, SCIEX, and the Natural Science and Engineering Research Council (NSERC) is gratefully acknowledged.

Table of Contents

Chapter		Page
1	**Introduction**	1
	1.1 Why This Project Was Undertaken	2
	1.2 Development of Electrospray Mass Spectrometry as a Technique for Elemental Analysis	4
	1.3 Recent Developments of the Technique	6
	1.4 References	13
2	**Electrospray Mass Spectrometry as a Technique for Elemental Analysis: Preliminary Results**	17
	2.1 Introduction	18
	2.2 Experimental	19
	2.3 Results and Discussion	21
	2.4 Conclusions	24
	2.5 References	32
3	**Electrospray Mass Spectrometry as a Technique for Elemental Analysis: Quantitative Aspects**	35
	3.1 Introduction	36
	3.2 Experimental	37
	3.3 Results and Discussion	38
	3.4 Conclusions	41
	3.5 References	51
4	**Background Spectral Characteristics of Quantitative Elemental ES-MS**	53
	4.1 Introduction	54
	4.2 Experimental	54
	4.3 Results and Discussion	55
	4.4 Conclusions	58
	4.5 References	64

Chapter Page

5 Determination of Solution Ions by Electrospray Mass Spectrometry 65
5.1 Introduction 66
5.2 Experimental 67
5.3 Results 68
5.3.1 Ion-Cluster Mode 69
5.3.2 Metal-Ion Mode 70
5.3.3 Intermediate Mode 71
5.3.4 Negative Ion Mode 73
5.4 Conclusions 74
5.5 References 86

6 Effect of Operating Parameters on Analyte Signals in Elemental Electrospray Mass Spectrometry 88
6.1 Introduction 89
6.2 Experimental 90
6.3 Results and Discussion 91
6.3.1 The Alkali Metals 91
6.3.2 The Alkaline Earths 95
6.3.3 A Transition Metal: Cobalt II 98
6.4 Conclusions 101
6.5 References 116

7 Elemental Speciation Measurements with Electrospray Mass Spectrometry: An Assessment 119
7.1 Introduction 120
7.2 Speciation Strategies 120
7.3 Experimental 121
7.4 Results and Discussion 123
7.4.1 Differentiation of Kinetically Inert Species with Different Oxidation States and Different Inner Coordination Sphere Composition 123

Chapter Page

7.4.2 Differentiation of Kinetically Inert Species with Different Oxidation States 126
7.4.3 Inorganic complexes 127
7.4.4 Organometallics 130
7.5 Summary 131
7.6 Conclusions 133
7.7 References 144

8 Mechanistic Investigations of Electrospray Mass Spectrometry: Part I, On the Transfer of Ions from within a Charged Droplet to the Gas Phase 152
8.1 Introduction 153
8.2 A Review of the Literature 153
8.3 Experimental 157
8.4 Results and Discussion 158
8.4.1 Suppression of Ion Signal Intensity Levels from Solutions with High Total Electrolyte Concentration 158
8.4.2 Is there a Preferential Desorption Mechanism? 161
8.4.3 Suppression Effects Due to Similarly Charged Ions 163
8.4.4 Suppression Effects Due to Dissimilarly Charged Ions 165
8.4.5 Indirect Evidence of a Single Ion Droplet Mechanism 168
8.5 Conclusions 171
8.6 References 185

9 Mechanistic Investigations of Electrospray Mass Spectrometry: Part II, Prediction of the Physical Parameters of the Charged Droplets 188
9.1 Introduction 189
9.2 Experimental 192
9.3 Results 192
9.4 Discussion: Charged Droplet Composition Prediction with a Constant Surface Electric Field Model 194

Chapter **Page**

9.5 Conclusions 203
9.6 References 213

10 Conclusions 217
10.1 Summary 218
10.2 Future Directions 219
10.2.1 Potential Applications for Elemental ES-MS 219
10.2.1 Instrumental Modifications 220

List of Tables

Table		Page
2.1	Salts used to prepare solutions	25
5.1	Operational Parameters of the Elemental ES Source	75
7.1	Electrospray source and interface parameter set points	134
8.1	Measured electrospray capillary current as a function of the total electrolyte concentration in HPLC grade methanol	172
8.2	Experimentally observed suppressions in the analyte ion signal intensity as predicted by Eqn. 8.3 from a similarly charged ion in solution, equimolar with the analyte ion	173
8.3	Experimentally observed suppressions in the analyte ion signal intensity as predicted by Eqn. 8.3 from a dissimilarly charged ion in solution equimolar with the analyte ion	174
8.4	Experimentally observed suppressions in the analyte ion signal intensity as predicted by Eqn. 8.3 from a dissimilary charged ion in solution, equimolar with the analyte ion. Data was acquired ten minutes after application of the high voltage to the electrospray capillary	175
9.1	Measured electrospray capillary current as a function of electrolyte concentration in HPLC grade methanol	205
9.2	Predicted charged droplet composition for electrospraying simple inorganic electrolytes dissolved in methanol	206
9.3	Corrected third generation charged droplet composition for electrospraying simple inorganic electrolytes dissolved in methanol	207

List of Figures

Figure **Page**

1.1 Cartoon representing the steps involved in generating gas phase ions from ions in a liquid solution sample by classic atomic spectrometry techniques 8
1.2 A cartoon representing a simple electrospray source 9
1.3 A schematic diagram of the electrospray source and interface 10
1.4 A cartoon representing the electrospray process and the ion sampling interface 11
1.5 A schematic diagram of the electrospray source interfaced to the Perkin Elmer/SCIEX ELAN Model 250 quadrupole based mass spectrometer 12

2.1 ES-MS interface and voltage biasing arrangement 26
2.2 ES mass spectrum for a $1x10^{-4}$ molar solution (methanol) of Li, Na, K, Rb, and Cs 27
2.3 Single element mass spectra for (a) Cr, (b) Fe, (c) Mn, (d) Ni, (e) Cu, (f) Zn, (g) Ag, and (h) Cd 28
2.4 The ES mass Spectra of Co ($1x10^{-3}$ molar) in (a) water and (b) methanol 29
2.5 A multielement ES mass spectrum of Cr, Mn, Fe, Co, Cu, and Ni ($1x10^{-4}$ molar) and V and Zn ($1x10^{-3}$ molar) in methanol 30
2.6 ES mass spectra of vanadyl sulfate (a and c) and uranyl nitrate (b and d). 31

3.1 Attempted calibration curves for (a) cesium and (b) cobalt 43
3.2 Mass spectra for a solution of KNO_3 in methanol: (a) $1x10^{-6}$ molar and (b) $1x10^{-3}$ molar 44
3.3 Signal intensities of cesium and potassium as a function of cesium concentration 45
3.4 (a) Calibration curve for cesium with potassium as the electrospray stabilizer and internal standard. (a) Calibration curve for cobalt with zinc as the electrospray stabilizer and internal standard. 46
3.5 (a) Calibration curve for cobalt with potassium as the electrospray stabilizer and internal standard. (b) Calibration curve for potassium with cobalt as the electrospray stabilizer and internal standard 47
3.6 Calibration curves for cesium with protonated solvent species as the ..... electrospray stabilizer and internal standard 48

Figure **Page**

3.7 Multi-element solution (Li, Na, K, Rb, and Cs) calibration curves with protonated methanol as the electrospray stabilizer and internal standard 49
3.8 Multi-element solution (Co, Ni, Cu, and Zn) calibration curves with nickel as the electrospray stabilizer and internal standard 50

4.1 Mass Spectrum of RbCl ($1x10^{-4}$ molar) in methanol. Nitrogen curtain gas 59
4.2 Mass spectrum of RbCl ($1x10^{-4}$ molar) in methanol. Oxygen curtain gas 60
4.3 Mass spectrum of RbCl ($1x10^{-4}$ molar) in methanol. Argon curtain gas 61
4.4 Mass spectrum of RbCl ($1x10^{-4}$ molar) in acetonitrile. Argon curtain gas 62
4.5 Mass spectrum of RbCl ($1x10^{-4}$ molar) in methanol/water (1:1). Argon curtain gas 63

5.1 A schematic diagram of the electrospray source and interface 76
5.2 Mass spectrum of a cobalt chloride solution ($CoCl_2$, $1x10^{-3}$ molar) in the ion cluster mode 77
5.3 Mass spectrum of a manganese chloride solution ($MnCl_2$, $1x10^{-4}$ molar) in the ion cluster mode 78
5.4 Mass spectrum of a cobalt bromide solution ($CoBr_2$), $1x10^{-4}$ molar) in the metal ion mode 79
5.5 Mass spectra for (a) copper, (b) zinc, (c) cadmium, and (d) lead solutions ($1x10^{-4}$ molar) in the metal ion mode 80
5.6 Mass spectra of (a) cobalt chloride, (b) cobalt nitrate, (c) cobalt bromide, and (d) cobalt sulfate solutions ($1x10^{-3}$ molar) with intermediate conditions 81
5.7 Mass spectra of a manganese chloride solution ($1x10^{-4}$ molar) acquired with (a) the ion cluster mode, (b) intermediate conditions, and (c) the metal ion mode 82
5.8 Negative ion mode mass spectra for (a) a solution containing F^-, Cl^-, Br^-, and I^- (each halide is $1x10^{-4}$ molar), (b) a solution of sodium thiocyanate ($1x10^{-4}$ molar), and (c) a $1x10^{-4}$ molar solution of nitric acid 83
5.9 Negative ion mass spectra for solutions ($1x10^{-4}$ molar) of (a) potassium dichromate and (b) potassium permanganate 84

Figure **Page**

5.10 (a) Positive ion mode mass spectrum of vanadyl sulfate ($VO(SO_4)$) and (b) negative ion mode mass spectrum of sodium vanadate ($NaVO_3$) 85

6.1 Schematic diagram of the electrospray ion source 102
6.2 Mass spectrum of lithium chloride in 97:3 methanol:water 103
6.3 Effect of electrospray capillary voltage bias on $^{85}Rb^+$ and $H(MeOH)_1^+$ signal intensities 104
6.4 Effect of curtain gas flow rate on the total lithium signal 105
6.5 $^{85}Rb^+$ and $H(MeOH)_1^+$ signal intensities for (a) front plate voltage, (b) sampling plate voltage, (c) skimmer voltage, and (d) barrel ion extractor voltage 106
6.6 Mass spectra of potassium chloride 107
6.7 Mass spectra of strontium chloride 108
6.8 Effect of curtain gas flow rate on the total strontium signal 109
6.9 Effect of curtain gas flow rate on (a) doubly charged bare alkaline earths and (b) bare singly charged alkaline earths 110
6.10 Mass spectra of cobalt chloride. Curtain gas flow rate was (a) 0 lpm, (b) 0.21 lpm, (c) 0.39 lpm, and (d) 1.93 lpm 111
6.11 Mass spectra of cobalt chloride. Sampling plate voltage was (a) 35 V, (b) 44 V, (c) 70 V, and (d) 120 V 112
6.12 Major ion intensities from Fig. 6.10 as a function of (a) curtain gas flow rate and from Fig. 6.11 as a function of (b) sampling plate voltage 113
6.13 Mass spectra of cobalt nitrate acquired while varying the sampling plate voltage and the curtain gas flow rate 114
6.14 (a) $^{59}Co^+$ and (b) the sum of charge reduced cobalt molecular ion (Σ(cr-$^{59}Co^+$))signal intensities as a function of sampling plate voltage bias at the curtain gas flow rate of 0.70 lpm 115

7.1 A schematic diagram of the Electrospray source and interface 135
7.2 Mass spectra of (a) chloride, (b) chlorite, (c) perchlorate, and (d) an equimolar mixture of chloride, chlorate, and perchlorate acquired with negative mode ES-MS 136

Figure **Page**

7.3 Mass spectra of (a) iodide and (b) iodate acquired with negative mode ES-MS 137
7.4 Negative mode ES-MS spectra of (a) thiocyanate, (b) sulfite, (c) sulfate, (d) thiosulfate, and (e) peroxodisulfate.... 138
7.5 Negative mode mass spectrum of an equimolar mixture ($3x10^{-5}$ molar) of thiocyanate, sulfite, sulfate, thiosulfate, and peroxodisulfate 139
7.6 Positive mode mass spectra of (a) Fe(II), (b) Fe(III), and an equimolar mixture of Fe(II) and Fe(III) for both (c) and (d).... 140
7.7 Negative mode mass spectra obtained while electrospraying (a) no Ag^+ added and (b) $1x10^{-4}$ molar Ag^+ in the presence of a fixed level of CN^- ($3x10^{-4}$ molar) 141
7.8 Positive mode mass spectra obtained while electrospraying a solution of (a) no added F^-, (b) $1x10^{-4}$ molar F^-, (c) $3x10^{-4}$ molar F^-, and (d) $9x10^{-4}$ molar F^-. A fixed level of Fe(III) ($1x10^{-4}$ molar) was present in each of the solutions electrosprayed 142
7.9 Electrospray mass spectrum of trimethyltin chloride ($1x10^{-4}$ molar).... 143

8.1 A schematic diagram of the electrospray source and interface to the mass spectrometer.... 176
8.2 A schematic diagram of the SCIEX/Perkin-Elmer ELAN Model 250 mass spectrometer interfaced with the electrospray source.... 177
8.3 Attempted calibration curve for cesium nitrate in HPLC grade methanol 178
8.4 Dependency of ES-MS analyte signal intensities (Cl^- and CH_3COO^- at $1x10^{-4}$ molar) as a function of sodium hydroxide concentration 179
8.5 Total rubidium ion signal as a function of the curtain gas flow rate 180
8.6 Normalized total ion signal intensities for an equimolar ($1x10^{-4}$ molar) two component mixture of rubidium and cesium as a function of curtain gas flow rate.... 181
8.7 Normalized total ion signal intensities for a two component mixture of (a) potassium and strontium where both analyte ions were $1x10^{-4}$ molar and (b) sodium ($2x10^{-4}$ molar) and cobalt ($1x10^{-4}$ molar) as a function of curtain gas flow rate 182

Figure **Page**

8.8 Lithium ion cluster distributions being shifted to lower ligand coordination numbers 183
8.9 Histogram of the number of ion counts per integration period for two different electrospray interface operating conditions 184

9.1 Cartoon depicting electrostatic atomization of a liquid 208
9.2 Cartoon that depicts the electrostatic atomization steps occurring at the electrospray capillary tip 209
9.3 Attempted calibration curve for cesium nitrate in HPLC grade methanol 210
9.4 A schematic diagram of the electrospray source and interface 211
9.5 Total lithium ion signal as a function of the curtain gas flow rate as the composition of the water/methanol solvent was changed 212

Chapter 1

1.0 Introduction

1.1 Why this project was undertaken.

The phenomenon of electrical dispersement of liquids into fine aerosols, a process which has long been termed electrospray, is used in a wide variety of applications [1,2]. Mass spectrometric measurement of charged particles produced by electrospray was first performed by M. Dole and co-workers in 1968 [3,4]. The significance of the efforts of Dole and co-workers was that not just charged particles, but inorganic polymers added to the solution electrosprayed were observed in the gas phase as charged ions. The significance of this result was ignored until 1989 when J. Fenn and co-workers published an article in Science in which they demonstrated that large bio-organic polymers were readily detected by electrospray mass spectrometry [5]. Since that time, the use of electrospray mass spectrometry has been witness to very prolific growth, primarily in the bio-molecular field where peptides and proteins up to molecular weight of ~100,000 Daltons are now routinely determined by mass spectrometry when just five years ago such determinations were simply not possible by any method [6-21].

An earlier investigation of electrospray mass spectrometry from the research group directed by J. B. Fenn utilized solutions of simple inorganic electrolytes (i.e. A^+B^-) and small organic bases to characterize the electrospray ion source [22,23]. In particular, no doubly charged inorganic ions (M^{2+}) from solution were detected. This observation reiterated what Iribarne and Thomson had previously concluded in their investigations of gas phase ions generated by pneumatic nebulization of liquid solutions [24,25]. Consequently these reports generated very little interest within the atomic spectroscopy community.

This all changed when Kebarle and co-workers reported the observation of multiple charged inorganic solution ions (M^{2+} and M^{3+}) by electrospray mass spectrometry [26-29], thereby opening up the technique to elemental analysis in a broad context. It was the appearance of these publications that provided the impetus to investigate and develop electrospray mass spectrometry for the purpose of analytical determinations of inorganic ions in solution.

At this point it is useful to review the nature of classical atomic spectroscopic techniques in order to provide the reader with the conceptual framework that directed the research presented in this thesis. Conventional solution sample introduction and free atom formation processes are summarized pictorially in Fig. 1.1. Solution samples are mechanically dispersed (nebulized) to form a droplet plume which is then transported to a

high temperature environment such as a flame, furnace, or plasma. The high temperature environment, commonly referred to as the atom (or ion) source desolvates and vaporizes the salt particle residues of the droplets to free atoms and ions. Spectroscopic techniques such as absorption, emission, fluorescence, or mass spectrometry can be used to detect and measure the elemental composition of the vaporized solution sample.

While atomic spectroscopic techniques are quite simple in concept, the implementation of the concepts in Fig. 1.1 has proven non-trivial and development of improved atomic spectroscopic techniques has inevitably lead to expensive instrumentation. This is not to say that atomic spectroscopic techniques are not successful, rather atomic absorption and in particular the inductively coupled plasma represent nearly ideal atomic spectroscopic atom (and atomic ion) sources. Still there remains much development work to not just improve but develop new technologies to supplement or replace each of the sample processing steps denoted by an arrow in Fig. 1.1.

Enter electrospray. Very simply ions present in solution can be transferred to the gas phase at atmospheric pressure with an electrospray source. Implicit in this statement was a radically different approach to performing atomic spectroscopic measurements of ions in solution: a high temperature environment was not required!

An electrospray source consists of a capillary biased to a high potential ($\geq$ 3 kV) relative to a counterelectrode through which a solution is pumped. Fig. 1.2 is a cartoon of the simplest electrospray source. The solution is electrically dispersed into charged droplets at the electrospray capillary tip and ultimately solution ions are transferred to the gas phase where they can then be sampled into an atmospheric pressure sampling mass spectrometer for mass to charge separation and quantitation. Fig. 1.3 is a schematic of the electrospray source used in this work. Details of this electrsopray source are described in Chapter 2. The mechanism by which charged droplets are formed and also the transfer of ions within the charged droplets to the gas phase is referred to as the electrospray process. Discussion of the details of the electrospray process is reserved until section 1.3 of this introduction. For the present it is sufficient to mention that ions are thought to be stabilized by a solvation sphere during the transfer to the gas phase [26]. Hence a gas phase ion produced by an electrospray source is best described as an ion cluster at atmospheric pressure. Much of the work described in this thesis was concerned with the extent to which the ion clusters are broken apart during the ion sampling transfer step from atmospheric pressure into the mass spectrometer. Ion molecule collisions between the electrospray source generated ion

clusters and neutral curtain gas molecules (or atoms) in the jet expansion were responsible for the preservation, or decomposition of the ion clusters. Low electric field gradients between the sampling plate and the skimmer were employed for minimal ion molecule collisional energies. Conversely, high electric field gradients between the sampling plate and the skimmer were employed for maximum ion molecule collisional energies causing removal of the solvation sphere molecules from the analyte ion. See Fig. 1.4 for a cartoon of the electrospray process where the solution form of the ion is stabilized in the gas phase and depending on the ion sampling conditions, the ion clusters could be either preserved or decomposed.

On this premise, an electrospray source should provide a direct method for solution ion species determinations. The conceptual removal of an ion, intact with its solvation sphere from solution, and placing it in the gas phase represented a radically different approach to elemental speciation methodology. The possibilities for and potential of electrospray mass spectrometry for elemental analysis represented an exciting and information rich alternative to classical atomic spectroscopic techniques.

1.2 Development of Electrospray Mass Spectrometry as a Technique for Elemental Analysis.

In the beginning, simple mass spectra showing inorganic solution ions generated by an electrospray source were proposed as a very satisfying objective to fulfill, particularly in light of the hot temperature environment bias of this atomic spectroscopic investigator. The electrospray source employed throughout was fabricated in-house and retrofitted onto a SCIEX/Perkin Elmer ELAN Model 250 mass spectrometer. A schematic of this quadrupole based mass spectrometer is shown in Fig. 1.5 interfaced to the electrospray source. Of note is that the ion optical arrangement used to transfer ions but not photons to the quadrupole mass filter was not changed from that used with the standard ion source for this mass spectrometer, an inductively coupled plasma [30].

An initial concern was the ability to remove the solvation sphere from an ion to leave a single bare metal ion to be detected. The presence of solvation sphere ligands coordinated with the analyte ion was considered a potentially serious spectral interference problem with respect to direct multielement analysis by electrospray mass spectrometry (ES-MS). Subjecting the ion clusters to energetic collisions in the jet expansion between the sampling

plate orifice and the skimmer orifice (See Fig. 1.4) was the only feasible way to break up the ion-solvent clusters. Preliminary ES-MS results obtained in this regard constitute Chapter 2 of this thesis.

Delineation of the quantitative aspects of this ion source is the subject of Chapter 3. First attempts in establishing a calibration curve proved very successful in exposing an inherent non-linearity of the electrospray source. Workable calibration curves (slope of the log-log plot = 1) were obtained through the addition of an external electrolyte that was called an electrospray stabilizer.

An inspection of the chemical background associated with the operation of the electrospray source such that the solvation sphere is removed from the ion is the focus of Chapter 4. Attempts to obtain respresentative background spectra from various solvents while using an inorganic acid or salt as an electrospray stabilizer proved much more involved than originally intended. The results that are presented should not be construed as definitive ES-MS background spectra. Upon completion of the body of this thesis, reflection on how chemical information was obtained through manipulation of the electrospray source, it is recommended that every electrospray mass spectrum comprise a mass scan from m/z =1 to the upper limit of the mass spectrometer. More so than any other atomic spectroscopy technique, an electrospray mass spectrum is very dependent on the properties of the individual solution being electrosprayed.

From the outset, the speciation potential afforded by the electrospray process focused the nature of way the electrospray source was operated. Chapter 5 is a summary of a few specific electrospray source operating conditions that can provide characteristic information regarding ions in the solution sample (i.e. total metal content for quantitation purposes and oxidation state and associated ligands for qualitative information purposes).

A detailed study of how the inorganic mass spectrum is affected by the electrospray source parameters is the purpose of Chapter 6. The variables that were investigated in that chapter were the curtain gas flow rate and the voltage bias of the electrospray capillary, front plate, sampling plate, skimmer, and barrel ion extraction lens. The two single most important electrospray source parameters in determining the nature of the resultant mass spectra were found to be the curtain gas flow rate and the sampling plate voltage bias (refer to Fig. 1.3). More correctly, these two variables should be termed interface parameters as they are not directly involved with charged droplet production at the electrospray capillary. The flow

rate of curtain, or drying gas was shown to be very useful in the desolvation of ions in the interface zone. (The curtain gas used was dry with respect to the solvent being electrosprayed (i.e. low electrospray-solvent vapour pressure). The reader should be well aware that the physically important variable is the vapour pressure of the solvent. However, no attempt was made to measure the solvent vapour pressure in these experiments, comsequently, all parameter plots are plotted as a function of the curtain gas flow rate. Moreover, the experiments discussed herein were dynamic in that the experimental system was dynamic, droplets passing through a countercurrent stream of curtain gas.) The sampling plate voltage bias was used to control the extent of collisional declustering experienced by ions sampled from atmospheric pressure in the jet expansion (refer to Fig. 1.4).

The assessment of the potential for speciation measurements by ES-MS in Chapter 7 exploited the knowledge gained in Chapter 6 regarding the electrospray source parameter study and in particular, how the source can be manipulated to extract the sought for chemical species in the solution. Examples are provided to support the statement that ES-MS will prove to be an extremely useful technique with which speciation determinations can be performed. However it can not be overstated that ES-MS does not meet all requirements of the ideal speciation technique. The single most serious flaw with respect to speciation measurements is that solvent evaporation from the charged droplets is a required step in the electrospray process. Therefore kinetically labile species equilibria will be altered before the ions in the droplets are transferred by the electrospray process to the gas phase. Estimation of the degree to which kinetically labile species distributions are altered lead to an investigation of the electrospray process, the results of which are presented in Chapters 8 and 9.

1.3 Recent Developments of the Technique.

Several instrumentation developments were reported in the past few years such as interfacing the electrospray source with a variety of mass spectrometers [9,10,31-33] and new and improved electrospray source designs [18,34-38]. However, the significance of these developments pales in comparison to the mechanistic interpretation of the transfer process of ions in the charged droplet to the gas phase at atmospheric pressure that was provided by L. Tang and P. Kebarle [39-41].

Without going into detail here, basically two mechanisms are thought to be possible in the transfer of solution ions to the gas phase. Both mechanisms assume some degree of ion solvation during the transfer from the solution phase to the gas phase, but a different degree of solvation is assumed for each mechanism. One of the mechansims, the single ion droplet theory (SIDT) assumes that solvation is equivalent to a micro-droplet [3,4,42] whereas the other mechanism known as the ion evaporation theory (IET) assumes the ion is stabilized only by its solvation sphere [24,25]. Until recently a number of experimental results were best rationalized with the IET [6]. The recent contributions from Tang and Kebarle however, which have shown that the SIDT is equally capable of explaining experimental results [39-41]. In spite of this development, Tang and Kebarle were still not able to provide clear evidence as to which mechanism is ultimately responsible for the transfer of solution ions to the gas phase.

Investigations performed in this study using simple well defined systems of simple inorganic electrolytes proved very illuminating with respect to clarifying the underlying mechanism by which ions in the charged droplets are transferred to the gas phase. Results of this investigation are presented in Chapter 8 where it is argued that because no data to support the IET were found, the SIDT can be considered a much more plausible mechanism by which the experimental results obtained may be explained.

An interpretation of charged droplet formation steps is presented in Chapter 9. Calculations based on this model predict well the experimental ES-MS observations. In particular, this model can be used to explain the inherent non-linearity of an electrospray source that was recently reported [43].

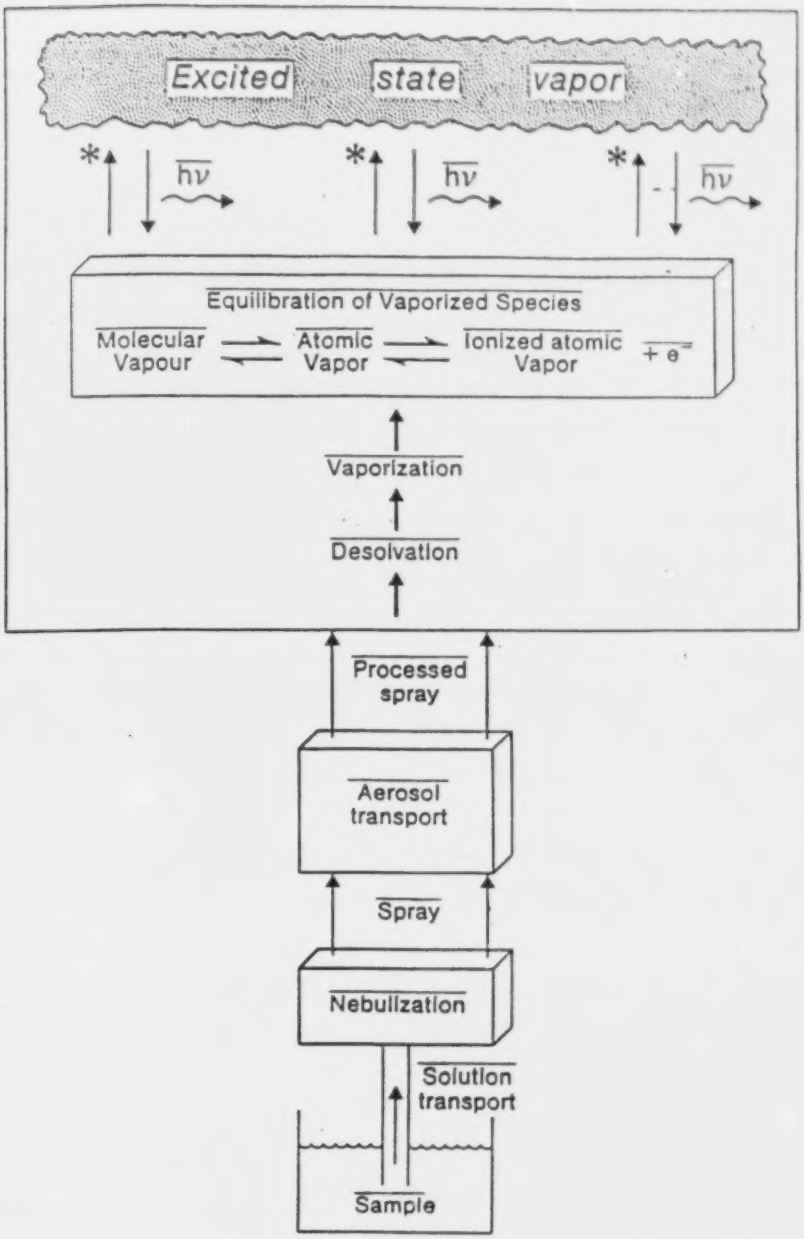

Figure 1.1 Cartoon representing the steps involved in generating gas phase atoms from ions in a liquid solution sample by classic atomic spectroscopy techniques.

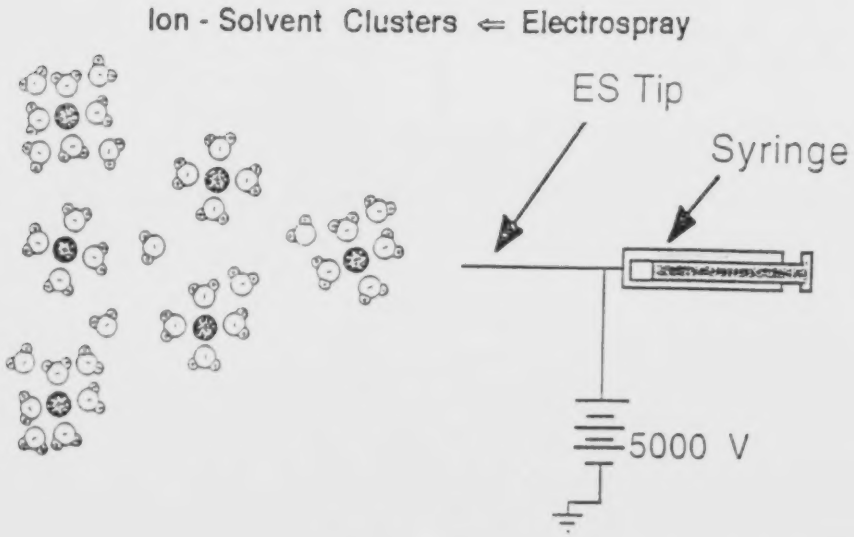

Figure 1.2 A cartoon representing a simple electrospray source.

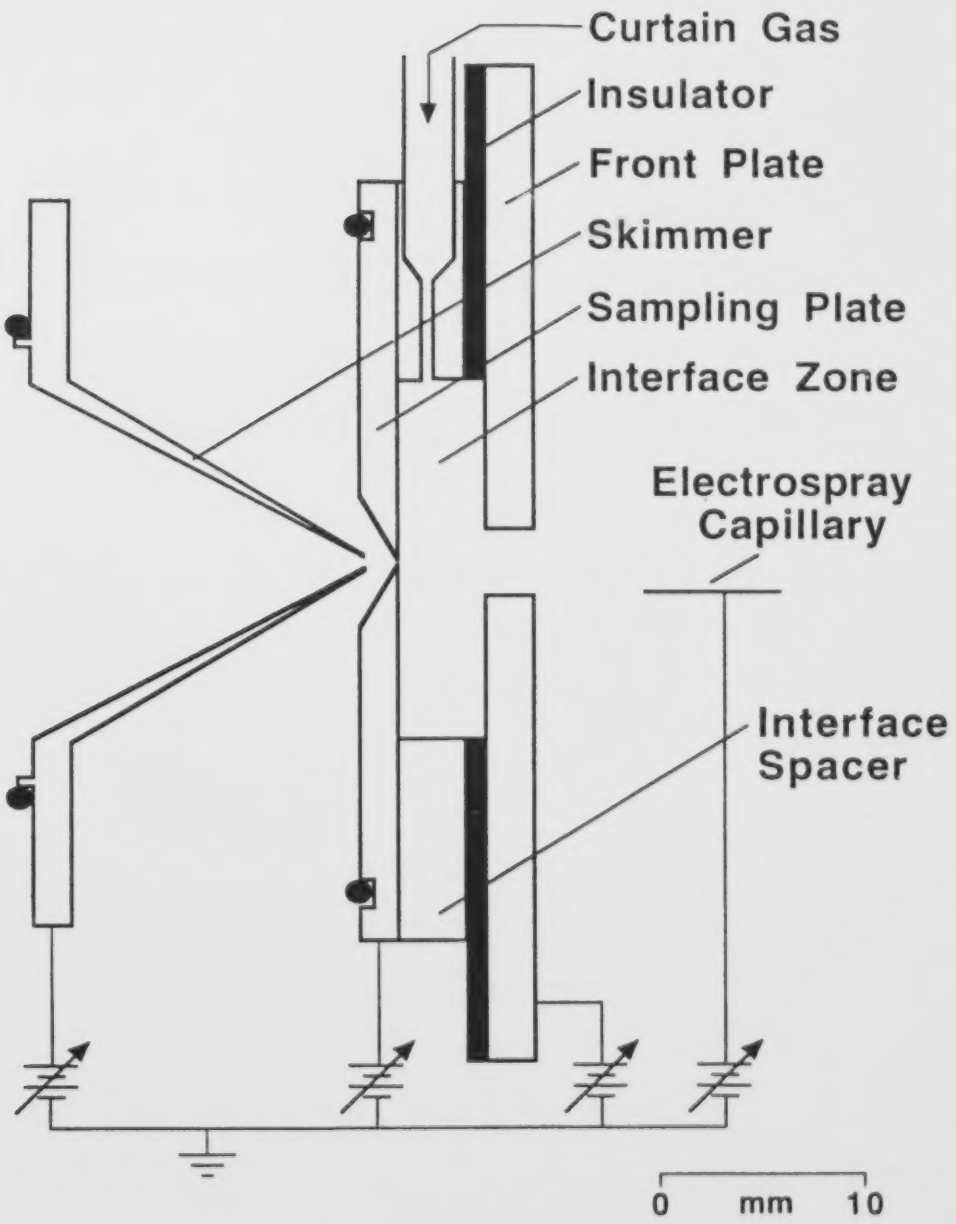

Figure 1.3 A schematic diagram of the electrospray source and interface.

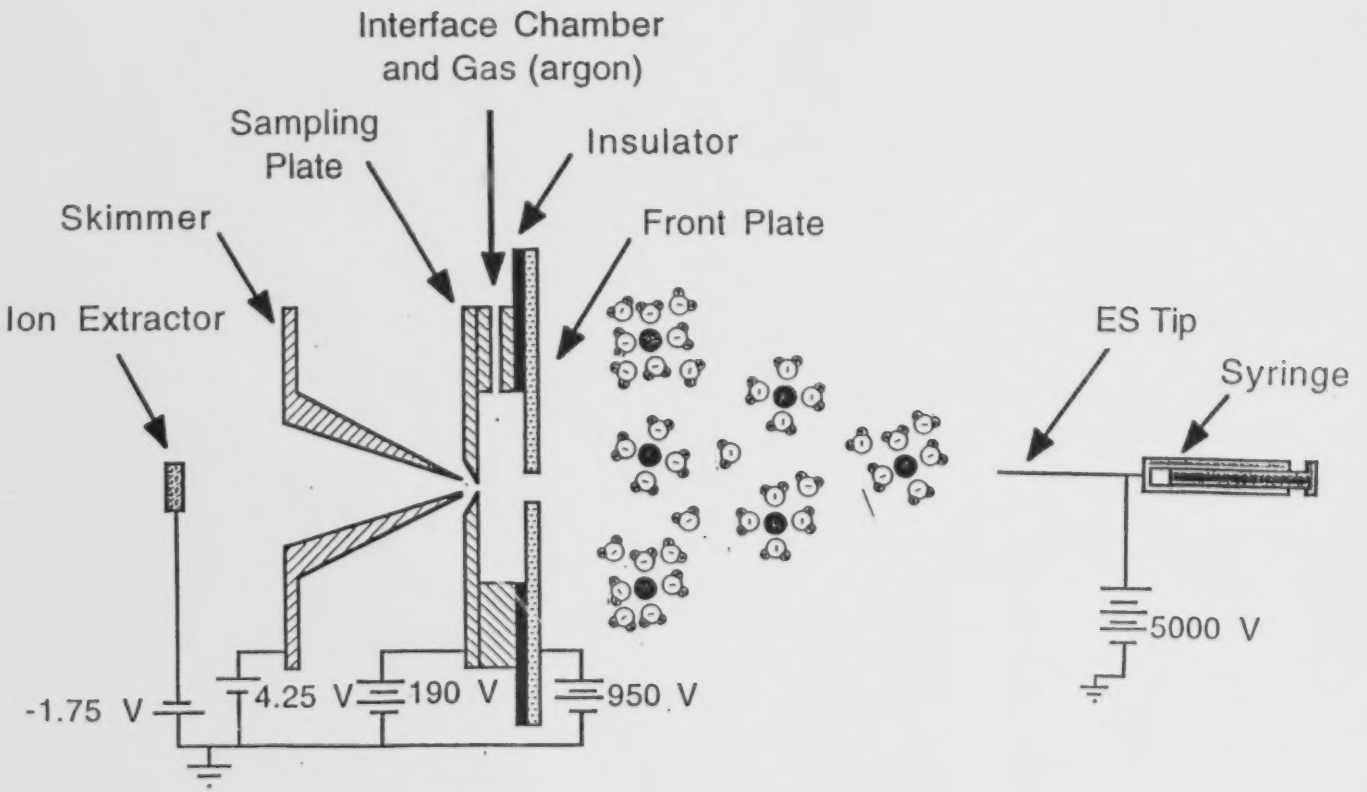

Figure 1.4 A cartoon representing the electrospray process. A plume of charged droplets can be created by electrostatic atomization of a liquid flowing through a charged capillary. Charges (solvated ions) within the droplets are then released to the gas phase by as yet an unknown mechanism. Ion clusters can then be sampled into the mass spectrometer by the interface.

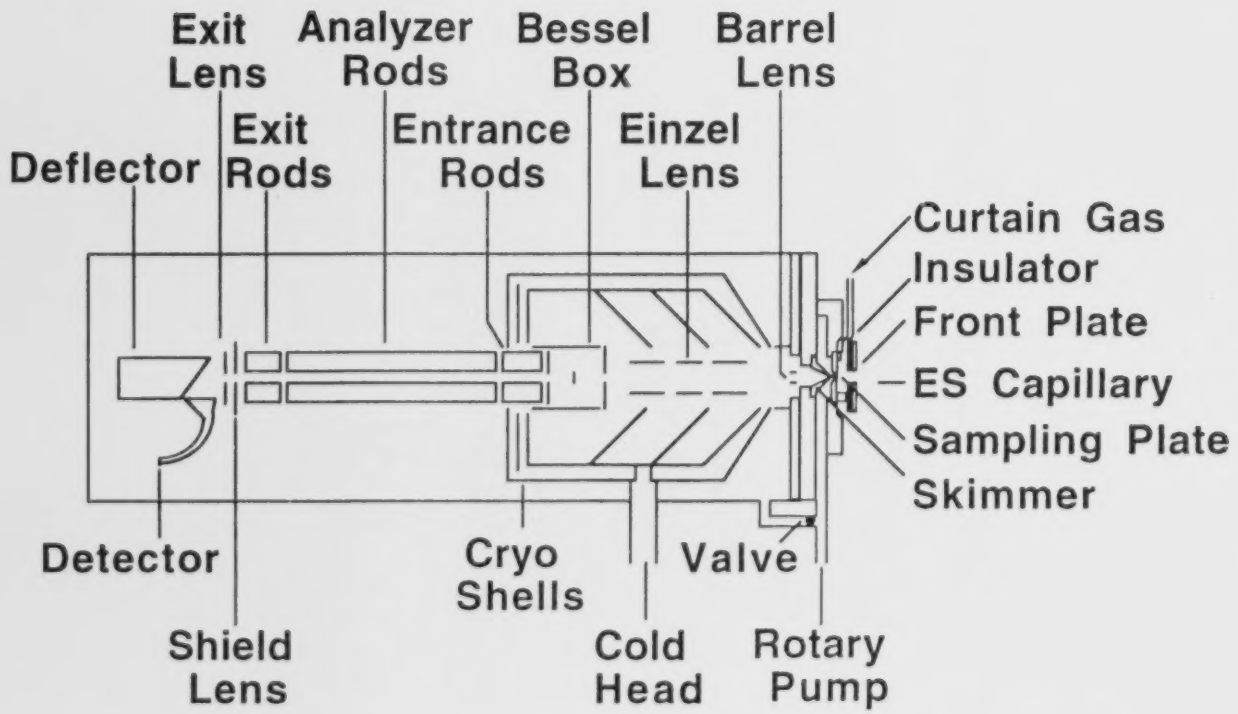

Figure 1.5 A schematic diagram of the electrospray source interfaced to the Perkin Elmer/SCIEX ELAN Model 250 quadrupole based mass spectrometer.

1.4 References

1. A. G. Bailey, *Electrostatic Spraying of Liquids*, Research Studies Press, Ltd., (1988).

2. M. Cloupeay and B. Prunet-Foch, J. Electrostatics, **25**, 165 (1990).

3. M. Dole, L. L. Mack, R. L. Hines, R. C. Mobley, L. P. Ferguson, and M. B. Alice, J. Chem. Phys., **49**, 2240 (1968).

4. L. L. Mack, P. Kralik, A. Rheuda, and M. Dole, J. Chem. Phys., **52**, 4977 (1970).

5. J. B. Fenn, M. Mann, C. K. Meng, S. F. Wong, and C. M. Whitehouse, Science, **246**, 64 (1989).

6. J. B. Fenn, J. Am. Soc. Mass Spectrom., 4, 524 (1993).

7. B. E. Winger, K. L. Light-Wahl, R. R. Ogorzalek Loo, H. R. Udseth, and R. D. Smith, J. Am. Soc. Mass Spectrom., **4**, 536 (1993).

8. R. B. Cole and A. K. Harrata, J. Am. Soc. Mass Spectrom., **4**, 546 (1993).

9. S. C. Beu, M. W. Senko, J. P. Quinn, F. M. Wampler, and F. W. McLafferty, J. Am. Soc. Mass Spectrom., **4**, 557 (1993).

10. B. E. Winger, S. A. Hofsadler, J. E. Bruce, H. R. Udseth, and R. D. Smith, J. Am. Soc. Mass Spectrom., **4**, 566 (1993).

11. T. R. Covey and D. Douglas, J. Am. Soc. Mass Spectrom., **4**, 616 (1993).

12. E. C. Huang, B. N. Pramanik, A. Tsarbopoulos, P. Reichert, A. K. Ganguly, P. P. Trotta, T. L. Nagabhushan, and T. R. Covey, J. Am. Soc. Mass Spectrom., **4**, 624 (1993).

13. Y.-T. Li, Y.-L. Hsieh, J. D. Henion, and B. Ganem, J. Am. Soc. Mass Spectrom., **4**, 631 (1993).

14. R. Feng and Y. Konishi, J. Am. Soc. Mass Spectrom., **4**, 638 (1993).

15. C. L. Stevenson, R. J. Anderegg, and R. T. Borchardt, J. Am. Soc. Mass Spectrom., **4**, 646 (1993).

16. D. Fabris, M. Kelly, C. Murphy, Z. Wu, and C. Fenseleu, J. Am. Soc. Mass Spectrom., **4**, 652 (1993).

17. J. R. Perkins, B. Smith, R. T. Gallagher, D. S. Jones, S. C. Davis, A. D. Hoffman, and K. B. Tomer, J. Am. Soc. Mass Spectrom., **4**, 670 (1993)

18. R. D. Smith, J. H. Wahl, D. R. Goodlett, and S. A. Hofstadler, Anal. Chem., **65**, 574A (1993).

19. M. Mann, Org. Mass Spectrom., **25**, 575 (1990).

20. R. D. Smith, J. A. Loo, R. R. Ogorzalek Loo, M. Busman, and H. R. Udseth, Mass Spectrom. Rev., **10**, 359 (1991).

21. J. B. Fenn, M. Mann, C. K. Meng, S. K. Wong, and C. M. Whitehouse, Mass Spectrom. Rev., **9**, 37 (1990).

22. M. Yamashita and J. B. Fenn, J. Phys. Chem., **88**, 4451 (1984).

23. M. Yamashita and J. B. Fenn, J. Phys. Chem., **88**, 4671 (1984).

24. J. V. Iribarne and B. A. Thomson, J. Chem. Phys., **64**, 2287 (1976).

25. B. A. Thomson and J. V. Iribarne, J. Chem. Phys., **71**, 4451 (1979).

26. P. Jayweera, A. T. Blades, M. G. Ikonomou, and P. Kebarle, J. Am. Chem. Soc., **112**, 2452 (1990).

27. A. T. Blades, P. Jayaweera, M. G. Ikonomou, and P. Kebarle, J. Chem. Phys., **92**, 5900 (1990).

28. A. T. Blades, P. Jayaweera, M. G. Ikonomou, and P. Kebarle, Int. J. Mass Spectrom. Ion Processes, **102**, 251 (1990).

29. A. T. Blades, P. Jayaweera, M. G. Ikonomou, and P. Kebarle, Int. J. Mass Spectrom. Ion Processes, **101**, 325 (1990).

30. G. Horlick and Y. Shao, "Inductively Coupled Plasma-Mass Spectrometry for Elemental Analysis," in Inductively Coupled Plasmas in Analytical Atomic Spectrometry, A. Montaser and D. W. Golightly, Ed., 2nd ed., VCH Publishers, Inc., 1992.

31. G. J. Van Berkel, G. L. Glish, and S. A. McLuckey, Anal. Chem., **62**, 1284 (1990).

32. J. G. Boyle and C. M. Whitehouse, Anal. Chem., **64**, 2084 (1992).

33. B. M. Chien, S. M. Michael, and D. M. Lubman, **65**, 1916 (1993).

34. J. W. Finch, B. D. Musselman, J. F. Banks, and C. M. Whitehouse, "Electrospray Ionization at LC Compatible Flow Rates on a Magnetic Sector Mass Spectrometer," in Proceedings of the 41st ASMS Conference on Mass Spectrometry and Allied Topics, San Francisco, CA, May 30-June 4, 1993, p287a.

35. N. Sproch and T. Kruger, J. Am. Soc. Mass Spectrom., **4**, 964 (1993).

36. D. R. Knapp, K. L. Schey, and D. I. Papic, Anal. Chem., **63**, 1658 (1991).

37. S. K. Chowdhury and B. T. Chait, Anal. Chem., **63**, 1660 (1991).

38. M. G. Ikonomou, A. T. Blades, and P. Kebarle, Anal. Chem., **63**, 1989 (1991).

39. L. Tang and P. Kebarle, Anal. Chem, **65**, 3654 (1993).

40. P. Kebarle and L. Tang, Anal. Chem., **65**, 972A (1993).

41. L. Tang, Ph. D. Dissertation, University of Alberta, 1993.

42. G. Schmelzeisen-Redeker, G. Butfering, and F. W. Rollgen, Int. J. Mass Spectrom. Ion Processes, **90**, 139 (1989).

43. G. R. Agnes and G. Horlick, "Electrospray Mass Spectrometry as a Technique for Elemental Analysis: Quantitative Aspects", Appl. Spectrosc., (accepted for publication).

Chapter 2

Electrospray Mass Spectrometry as a Technique for Elemental Analysis: Preliminary Results

2.1 Introduction[1]

Recently there has been considerable interest in the utilization of the phenomenon of Electrospray (ES) as an atmospheric-pressure ionization source for Mass Spectrometry (MS) [1-4]. In this technique, first demonstrated by Yamashita and Fenn[5,6] a solution is pumped (1-10 μL/min) through a charged capillary (~ 3-5 kV) and a spray emerges from the capillary that contains gas-phase ionic species generated from components in the solution. These gas-phase ions, often clustered with solvent and/or polar atmospheric gases [7,8], are then sampled directly into a mass spectrometer capable of sampling at atmospheric pressure [9].

The electrospray technique has proven to be particularly powerful for the determination of the molecular weight of proteins by the utilization of the mass spectral pattern of multiply charged ions [10], and it has also been used as an ionization technique in the coupling of liquid chromatography [11-14] and capillary electrophoresis [15] to mass spectrometers. Recently Siu et al. [16] have presented data illustrating the coupling of ion-exchange and ion-pairing chromatography to mass spectrometry using ES for the analysis of organo-arsenic compounds. In addition, Siu et al. [17] have used ion-spray MS/MS for the determination of tributyltin.

Although the focus of most researchers has been on the utilization of ES as an ionization technique for organic species, Kebarle and co-workers have focused much of their efforts on the generation and study of ion-molecule clusters generated by ES which involve metal ions [18,19]. They have been able to generate ion-molecule clusters for a wide range of metal ions, and it is clear from their work that ES has the potential to evolve into a generic ion source for elemental mass spectrometry. Indeed, Douglas [20], Cheng et al. [21], and Van Berkel et al. [22] have already presented some preliminary results indicating the potential of ES-MS as a technique for inorganic analysis.

In this report, preliminary results are presented that further indicate the potential of ES-MS as a technique for elemental analysis. These results have been obtained by interfacing a

---

[1] A version of this chapter has been published. George R. Agnes and Gary Horlick, Appl. Spectrosc., **46**(3), 403 (1992).

laboratory-constructed electrospray source to a mass spectrometer normally used for inductively coupled plasma-mass spectrometry (ICP-MS). In fact, the results indicate that ES-MS could very well become competitive with ICP-MS as a technique for elemental analysis.

2.2 Experimental

A diagram of the electrospray source and the interface used to transfer ions into the mass spectrometer (SCIEX/Perkin-Elmer ELAN Model 250) is shown in Fig. 2.1. The ES source consists of a syringe pump (Sage Instruments, Model 341A), a glass sample syringe (1 mL), and an ES capillary. The ES capillary is a stainless steel capillary (0.2 mm outside dia., 0.1 mm inside dia.) with a length of 1.5 cm. This capillary is welded onto a short length (~ 20 cm) of larger bore (1.6 mm outside dia., 1.1 mm inside dia.) stainless steel tubing that is coiled and is attached to the glass sample syringe with the use of standard fittings. The syringe pump was set to deliver sample solution at 10 μL/min.

The ES capillary tip was positioned 8-12 mm from the front plate and about 4 mm off axis with respect to the central axis of the mass spectrometer entrance apertures. The ES capillary tip was biased at +3.9 kV for aqueous solutions and at +5.0 kV for methanol solutions. The bias range over which signals could be observed was only +3.8 to +4.1 kV for aqueous solutions, but was considerably broader (+3 to +6 kV) for methanol solutions. The bias voltage was supplied by an EH-series (0-10 kV) Glassman high-voltage supply.

The interface consists of two circular plates, a sampling plate, and a front plate. The sampling plate takes the place of the normal sampling cone used in ICP-MS measurements. The orifice dia. in the flat sampling plate is 0.1 mm, which contrasts with the orifice dia. in sampling cones used in ICP-MS, which can range from 0.75 to 1 mm. A front plate with a 3-mm-dia. hole is mounted 4 mm in front of the sampling plate. This creates a chamber in front of the sampling plate. A "curtain" gas (Argon or Nitrogen) is introduced into this chamber at a flow rate of 0.2 L/min. The function of this curtain gas zone is to decluster the ions that enter into the mass spectrometer and is similar in concept and design to that used for several years on API systems manufactured by SCIEX [9,23].

Both the sampling plate and the front plate could be independently biased. For the results presented in this study, the sampling plate was typically biased at +200 V and the front plate was biased at +900 V. These bias voltages were supplied with a Glassman EH-series high-voltage supply and a BHK Model 2000-0.1 M high-voltage supply, both of which have a range of 0 to 2 kV.

The skimmer was identical to that normally used in ICP-MS. The orifice diameter was 1 mm and the skimmer was grounded, although it is planned to bias the skimmer in future studies.

The ion extractor shown in Fig. 2.1 is, in fact, the so-called shadow stop of the ICP-MS [24]. In contrast to normal ICP-MS operation where this stop is grounded, it is now biased at -12 V. This is similar to the biasing arrangement that was required when glow discharge ion sources were interfaced to this mass spectrometer [25].

The rest of the mass spectrometer was unchanged, and it was operated much as it would be in ICP-MS applications. The pressure in the differentially pumped region between the skimmer and the sampling plate was 0.2 Torr, and in the main chamber of the mass spectrometer the pressure was 5×10^{-6} Torr.

While the ion optics of the mass spectrometer were unchanged, this aspect of the mass spectrometer should, in all likelihood, be re-designed from the point of view of coupling to an ES source rather than to an ICP. In particular, the ion optics of the ELAN contain two photon stops and a Bessel box [24], which are probably not required for an ES source. One approach would be to completely replace the current input ion optics with an input rf-only quadrupole. This so-called Q0 input quadrupole approach has recently been evaluated by Douglas and French [26].

Sample solutions were prepared by dissolving the metal salt (see Table 2.1) in ACS-grade methanol or distilled deionized water. The mass scan rate was 0.3 s/point, and the mass spectral data were transferred to a Mac IIci computer, where the spectra were processed with SpectroPlot [27] and Igor (WaveMetrics, Lake Oswego, OR, USA).

2.3 Results and Discussion

The ES mass spectrum of an equimolar mixture of Li, Na, K, Rb, and Cs is shown in Fig. 2.2. The concentration of the alkali metals is $1x10^{-4}$ molar and the solvent is methanol. While some residual clustering is evident by the presence of the metal-methanol clusters [M(MeOH)+], the spectrum shown in Fig. 2.2 clearly indicates that the singly ionized metal ions are the dominant species.

One characteristic of the ES spectra of elemental species observed in most previous studies has been a much higher degree of clustering. Typically a metal ion was clustered with a range of solvent molecules [i.e., $Na(H_2O)_3^+$, $Na(H_2O)_4^+$, and $Na(H_2O)_5^+$ for a methanol-water solvent], and the free-metal ion was not normally observed [18,21,22]. A number of the previous results have been obtained with SCIEX TAGA-type mass spectrometers [23] in which there is no skimmer and hence no input differentially pumped zone. While the curtain gas zone in front of the sampling plate is known to aid declustering, it is likely, in the interface design used in this study, that considerable declustering is also occurring in the differentially pumped zone. In particular, Douglas has shown that the degree of declustering for inorganic species is directly dependent on the voltage between the sampling plate and the skimmer [20]. In addition, relatively high voltages between the front plate and the sampling plate (700 V) and the sampling plate and the skimmer (200 V) also facilitate declustering.

The ES mass spectra for eight transition metals (Cr, Fe, Mn, Ni, Cu, Zn, Ag, and Cd) are shown in Fig. 2.3. All solutions were $1x10^{-3}$ molar. Mn, Cd, and Ag were in aqueous solutions as Mn^{2+}, Cd^{2+}, and Ag^+, and Cr, Fe, Ni, Cu, and Zn were in methanol solutions as Cr^{3+}, Fe^{2+}, Ni^{2+}, Cu^{2+}, and Zn^{2+} (see Table 2.1). Although these spectra are somewhat more complex than the spectrum shown in Fig. 2.2, the singly ionized metal ion is still the dominant species. Again this is in contrast to some previously reported ES spectra of metal ion species [18,19,21,22], where a range of solvent-clustered ions [$M(H_2O)_n^{y+}$] were observed with n ranging from 5 to 14 and where multiply charged solvent-clustered ions (i.e., y = 2 or 3) were also observed. As mentioned above, the interface design and conditions used in this study seem to promote declustering. As well, declustering of multiply charged ions can also promote charge reduction, as discussed and explained by Blades et al. [18]. Some of the products of charge reduction reactions [MOH^+ and $MOH(H_2O)_1^+$] lead to the complexity of the spectra shown in Fig. 2.3. Those species (Ag^+ and the alkali metals) for which charge reduction does not occur yield simpler spectra.

From one analytical point of view, that of straightforward elemental analysis, an ionization source that yields only bare singly charged metal ions would be advantageous and it will have to be seen whether ES ionization conditions can be adjusted to cleanly achieve this goal. However, from another analytical point of view, that of elemental speciation, it would be desirable if ES ionization conditions could also be adjusted to retain solution speciation. Such a goal may not be quite as elusive as it seems and could become a unique strength of ES-MS (more on this point later in this paper).

Some differences exist when water or methanol is used as the ES solvent. As noted in the Experimental section, the voltage biasing conditions for methanol are less restrictive, and water is generally regarded as a more difficult solvent to electrospray [28]. The ES mass spectra for $1x10^{-3}$ molar solutions of cobalt in water and methanol are shown in Fig. 2.4. The sensitivity for Co is about a factor of three greater in methanol (Fig. 2.4b) than it is in water (Fig. 2.4a). The change in sensitivity of ES with different solvents has been discussed by Ikonomou et al. [29]. Another effect is that the $CoO^+/CoOH^+$ signal ratio is different in the two solvents. The CoO^+ signal intensity is greater than the $CoOH^+$ signal intensity in methanol solvent, while the opposite is true for water solvent. This can also be seen in the spectra shown in Fig. 2.3 for Cr, Ni, and Zn (methanol) and for Mn and Cd (water).

Interestingly, this trend is not followed by the spectrum shown for Fe in a methanol solvent (Fig. 2.3b). A quick glance at this spectrum would lead to the conclusion that the signal for $^{56}FeOH^+$ is more intense than that for $^{56}FeO^+$ as observed in aqueous solutions. However, it is actually felt that the peak at mass 73 is really $^{56}Fe(NH_3)_1^+$ and not $^{56}FeOH^+$. First and foremost, the solution was prepared with the use of ferrous ammonium sulfate. Since iron is complexed with ammonia in solution, it would follow that gaseous iron-amine, because ES is a soft ionization technique, should exist. In fact, Cheng et al. [21] observed both $Ag(NH_3)_1^+$ and $Ag(NH_3)_2^+$ in their study of ES-MS of aqueous solutions involving metal salts.

Second, given the trend observed for the MO^+/MOH^+ ratio between solvents, $FeOH^+$ should be smaller than FeO^+, and the natural abundance of ^{57}Fe is not enough to tip the scales via $^{57}FeO^+$ contributing to the signal at mass 73. Finally, the presence of NH_3 can alter the charge reduction reactions and is likely responsible for the absence of the species $FeOH(H_2O)_1^+$. This has been discussed by Blades et al. [18].

In a different vein, perhaps the most important aspect of the spectrum shown in Fig. 2.3b is that ES spectra may, in part, be used to directly measure total solution components, including elemental ions and ligands.

ES can be used for multielement determinations. This is indicated by the mass spectrum shown in Fig. 2.5. This spectrum is for a solution containing Cr, Mn, Fe, Co, Cu, and Ni ($1x10^{-4}$ molar) and V and Zn ($1x10^{-3}$ molar) in methanol. Of particular note in this spectrum is the fact that the dominant vanadium species is VO^+ and not V^+. Note, from Table 2.1 that vanadium solutions were prepared starting with vanadyl sulfate [$VO(SO_4)•2H_2O$]. The VO^+ is the result of the charge reduction of VO^{2+} in the gas phase. This is clear and exciting evidence that ES-MS should be useful for the direct speciation of solution components.

The potential for this capability is further illustrated in Fig. 2.6. The single-element ES spectra for vanadyl sulfate and uranyl nitrate are shown in this figure. The solution species of vanadium ($^{51}VO^{2+}$) and uranium ($^{138}UO_2^{2+}$) were detected as $^{51}VO^+$ (Fig. 2.6a) and $^{138}UO_2^+$ (Fig. 2.6b). Thus, while ES did preserve the molecular form of the metal, the oxidation state of the species was not preserved as charge reduction occurred, resulting in the plus-one species. As well, if the interface (curtain) gas flow rate is increased by 50% (Figs. 2.6c and 2.6d), the relative populations of the detected metal species are shifted towards the bare metal ion.

Thus the attainment of this highly desirable goal, that of being able to directly determine the speciation of solution components, is tantalizingly close, as depicted by the data shown in Figs. 6a and 6b. However, considerable characterization, study, and development of ES conditions will be required in order to ensure reliable and accurate results.

While the focus of this report has been on the qualitative analysis aspects of ES-MS, the technique should also be applicable to quantitative analysis. Certainly others have illustrated that ES-MS can be used for quantitative analysis [11,17]. For the system reported on here, the detection limit for potassium was determined to be 1 ng/mL (1 ppb). This is a 3σ detection limit based on a 10 second integration time with the background count standard deviation determined at mass 35. This is probably a rather conservative estimate of what is possible.

Our sensitivity for $^{39}K^+$ is about a factor of 50 lower than that reported by Ikonomou et al. [30]. They used a TAGA system designed for API work. As mentioned earlier, the input ion optics of our mass spectrometer are those designed for ICP-MS, and ion optics optimized for ES-MS should considerably improve ion throughput. In addition, our ICP-MS is a very early Model 250 ELAN, and even for ICP-MS it does not provide state-of-the-art detection limits by about two orders of magnitude. Thus it is felt that detection limits in the 1 pg/mL range are within reach for elemental ES-MS, which would make it competitive with ICP-MS.

Finally, in quantitative analysis, one cannot ignore matrix effects. They are essentially completely uninvestigated, will likely prove to be problematic (as always), and will certainly require extensive investigation.

2.4 Conclusions

Owing to the success and rapid development of ICP-MS, mass spectrometry is now firmly established as a major technique for elemental analysis. This in turn has paved the way for the development and assessment of additional ion sources that would either complement or improve on the ICP. This preliminary assessment of ES as a source for elemental mass spectrometry represents one development in this direction. Clearly, more work is required.

ES is a complex process. The nature of the resulting ions depends on the solvent, solution composition, gas-phase reactions, and interface design. Overall, it is felt that the preliminary results reported here and by others [18,19,21,22] for elemental ES-MS are very encouraging. That ever-elusive analytical technique that would be able to provide direct solution speciation information may well prove to be ES-MS. Although only positive-mode ES-MS was demonstrated here, speciation of anions (i.e., sulfate, nitrate, chloride) using negative-mode ES-MS should also be possible. The prospect of an ES-MS instrument that could directly provide a complete picture of the cationic and anionic composition of a solution is not out of the question. Certainly it appears that ES-MS has an important role to play in the future of elemental analysis.

Table 2.1 Salts used to prepare solutions.

LiCl	$Fe(NH_4)_2(SO_4)_2 \cdot 6H_2O$
NaCl	$Co(NO_3)_2 \cdot 6H_2O$
KNO_3	$NiCl_2 \cdot 6H_2O$
RbCl	$Cu(NO_3)_2 \cdot 3H_2O$
CsCl	$Zn(NO_3)_2 \cdot 6H_2O$
$VO(SO_4) \cdot 2H_2O$	$Cd(NO_3)_2 \cdot 4H_2O$
$Cr(NO_3)_3 \cdot 9H_2O$	$AgNO_3$
$MnCl_2 \cdot 4H_2O$	$UO_2(NO_3)_2 \cdot 6H_2O$

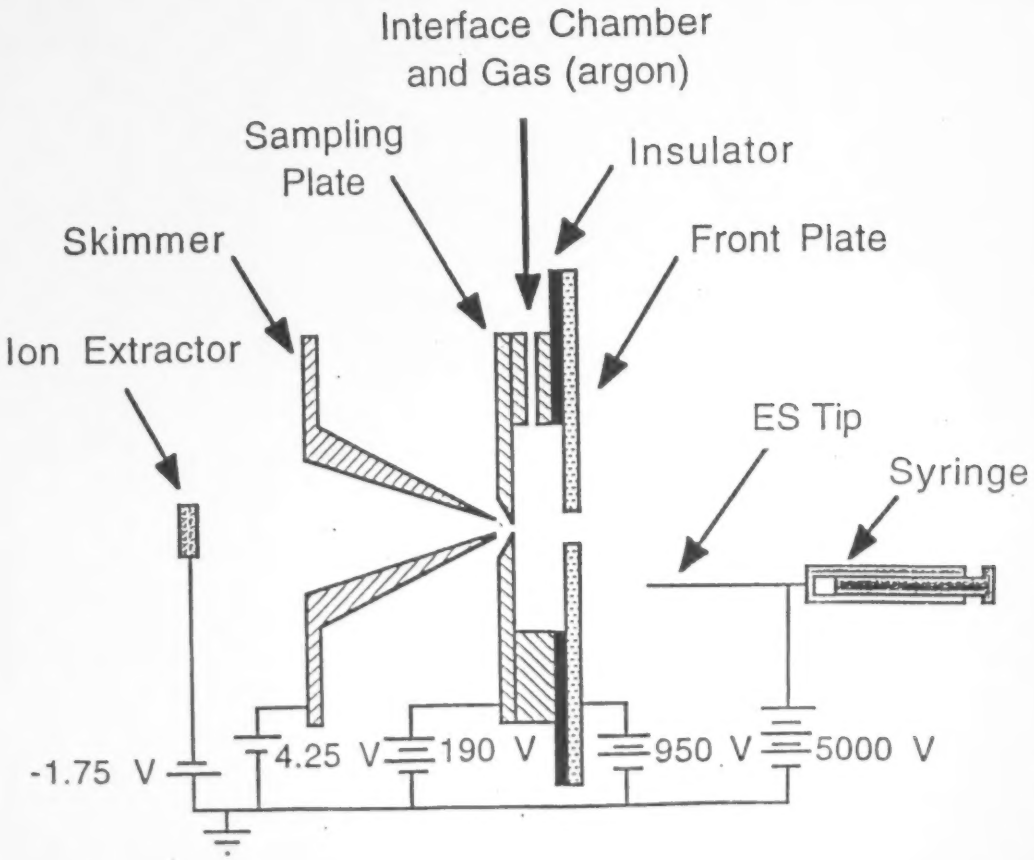

Figure 2.1 ES-MS interface and voltage biasing arrangement. The syringe is not drawn to scale and is larger than depicted.

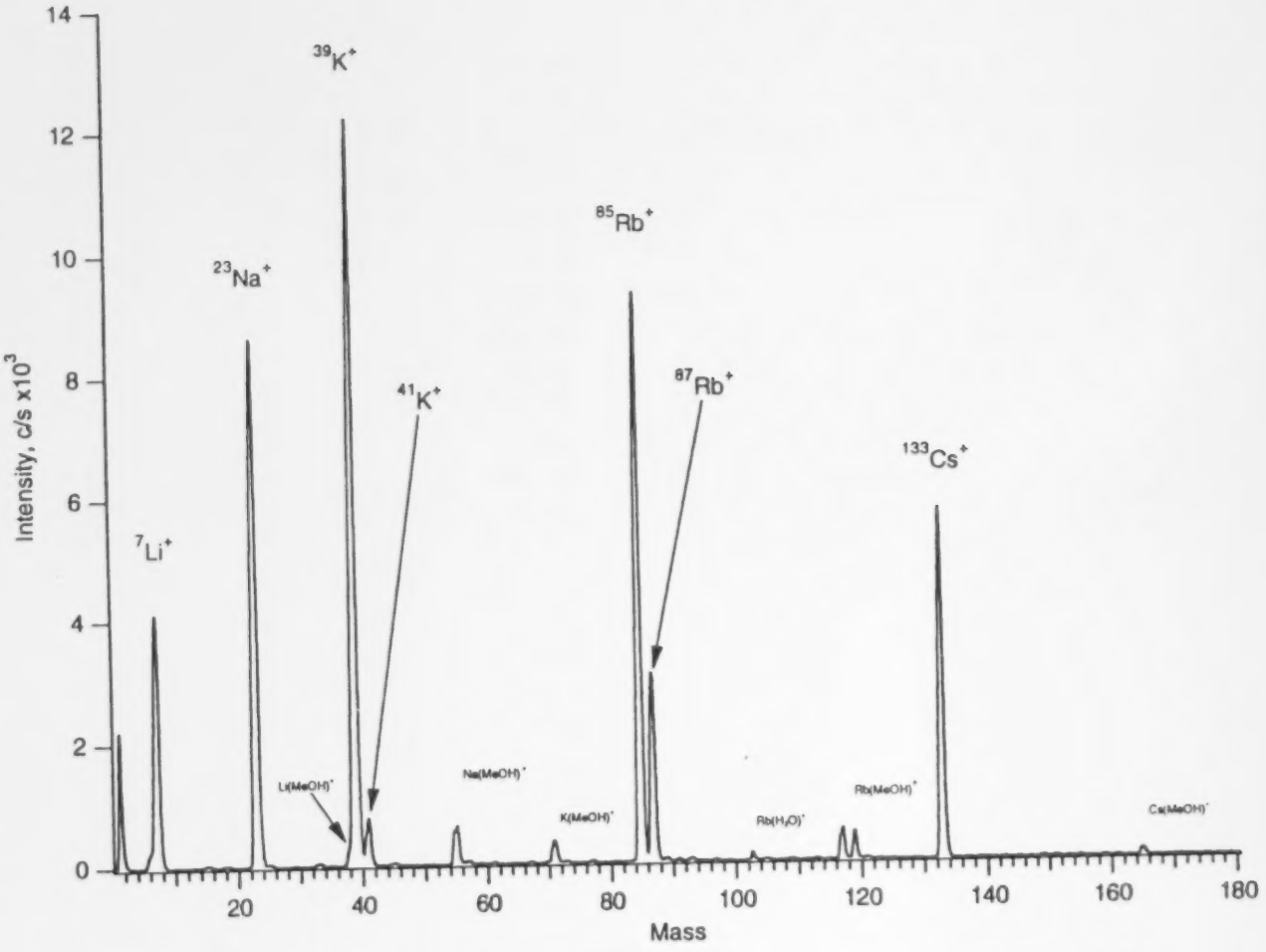

Figure 2.2 ES mass spectrum for a $1x10^{-4}$ molar solution (methanol) of Li, Na, K, Rb, and Cs.

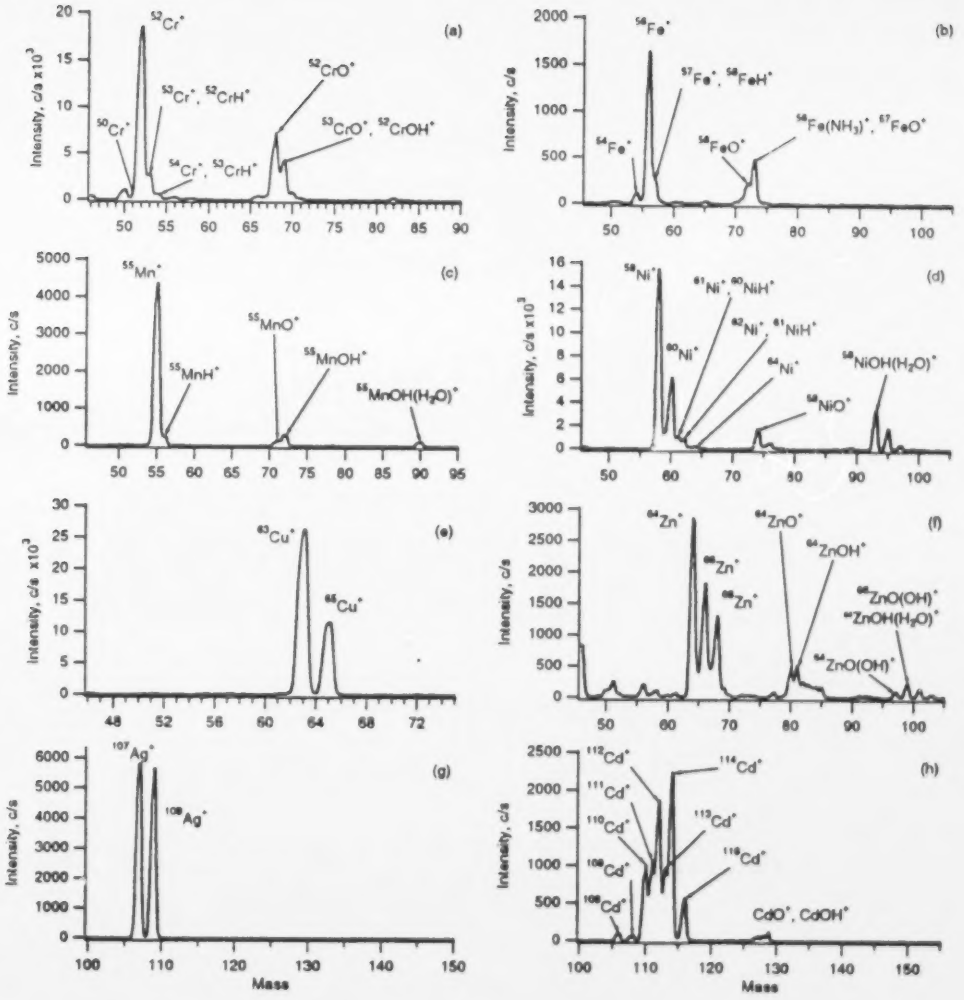

Figure 2.3 Single-element ES mass spectra for (a) Cr, (b) Fe, (c) Mn, (d) Ni, (e) Cu, (f) Zn, (g) Ag, and (h) Cd. All solutions were $1x10^{-3}$ molar. Mn, Cd, and Ag were in water, and Cr, Fe, Ni, Cu, and Zn were in methanol.

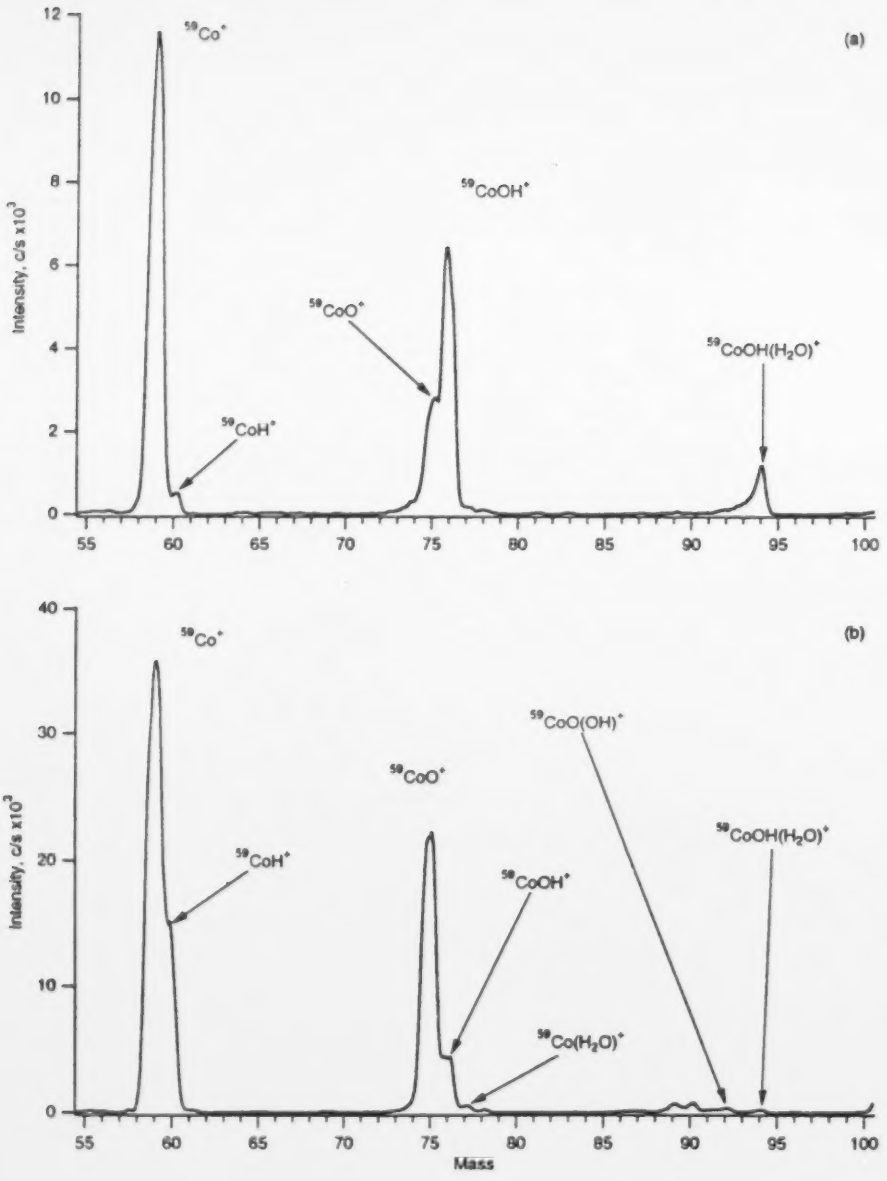

Figure 2.4 The ES mass spectra of Co ($1x10^{-3}$ molar) in (a) water and (b) methanol.

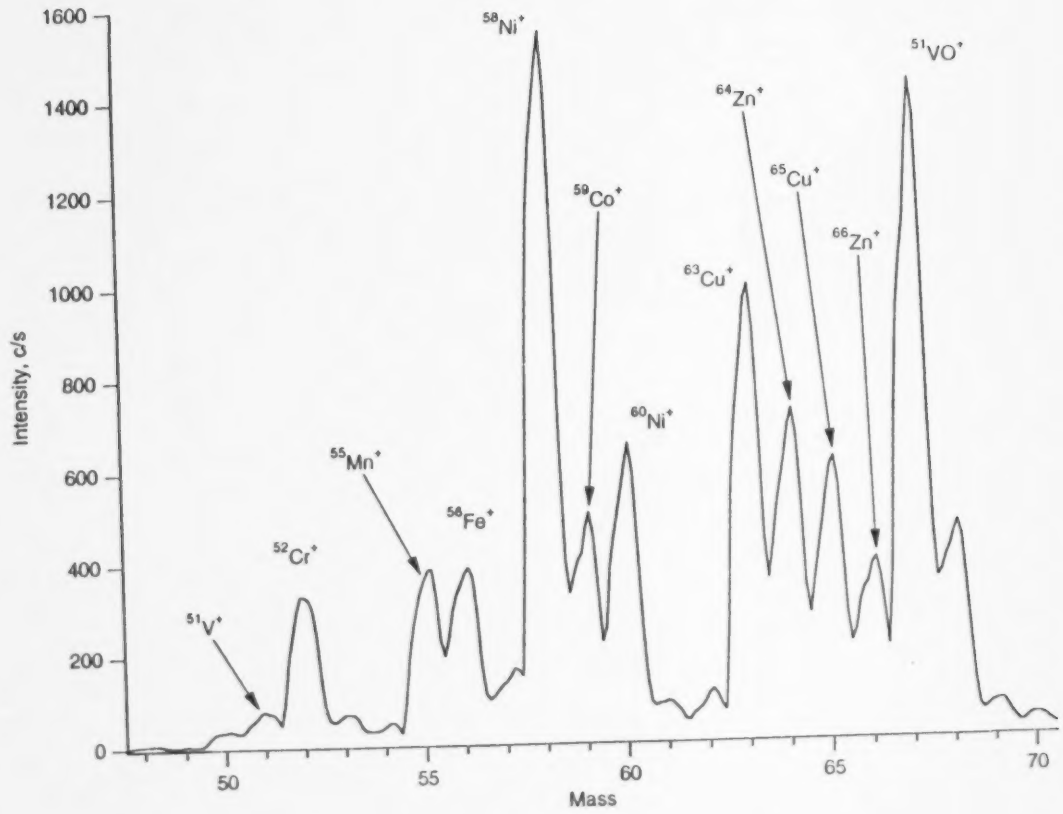

Figure 2.5 A multielement ES mass spectrum of Cr, Mn, Fe, Co, Cu, and Ni ($1x10^{-4}$ molar) and V and Zn ($1x10^{-3}$ molar) in methanol.

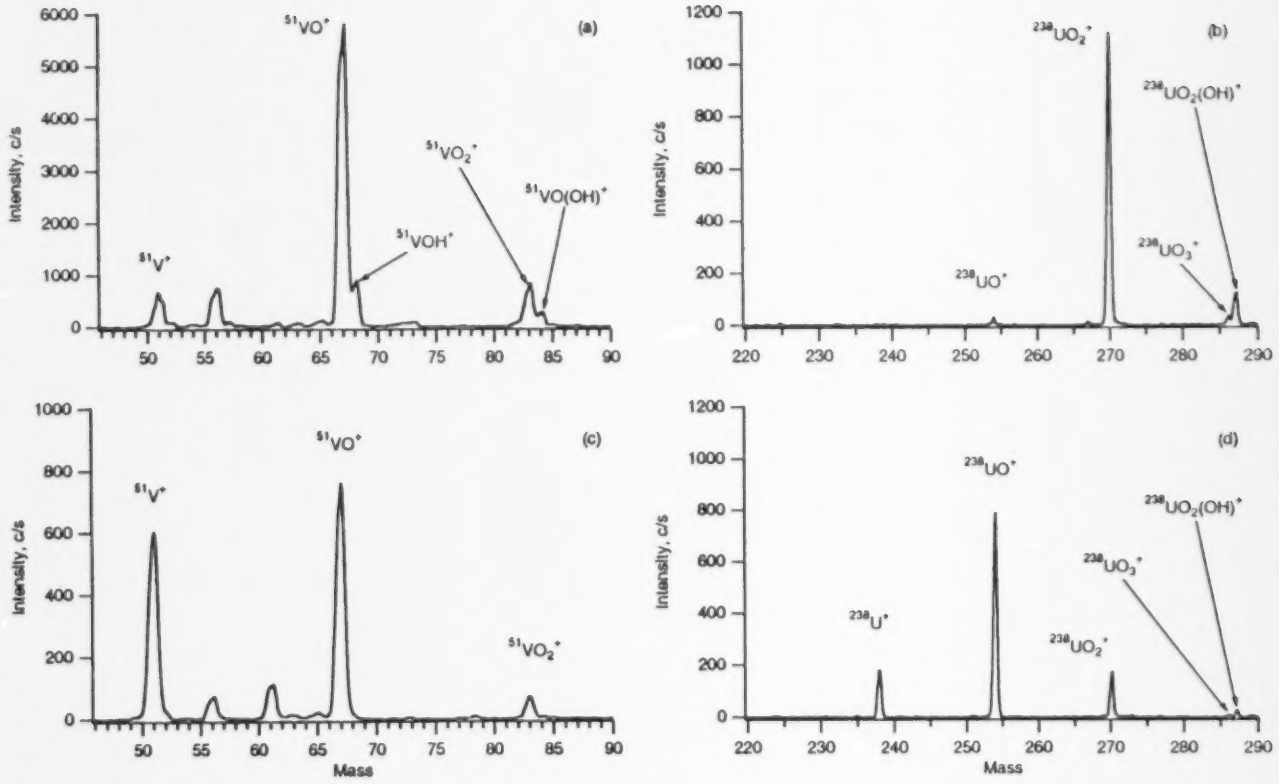

Figure 2.6 ES mass spectra of vanadyl sulfate (a and c) and uranyl nitrate (b and d). See text for discussion.

2.5 References

1. J. B. Fenn, M. Mann, C. K. Meng, S. F. Wong, and C. M. Whitehouse, Mass Spectrom. Rev. **9**, 37 (1990).

2. R. D. Smith, J. A. Loo, C. G. Edmonds, C. J. Barinaga, and H. R. Udseth, Anal. Chem. **62**, 882 (1990).

3. E. C. Huang, T. Wachs, J. J. Conboy, and J. D. Henion, Anal. Chem. **62**, 713A (1990).

4. M. Hamdan and O. Curcuruto, Int. J. Mass Spectrom. Ion Processes **108**, 93 (1991).

5. M. Yamashita and J. B. Fenn, J. Phys. Chem. **88**, 4451 (1984).

6. M. Yamashita and J. B. Fenn, J. Phys. Chem. **88**, 4671 (1984).

7. J. V. Iribarne and B. A. Thomson, J. Chem. Phys. **64**, 2287 (1976).

8. B. A. Thomson and J. V. Iribarne, J. Chem. Phys. **71**, 4451 (1979).

9. A. P. Bruins, Mass Spectrom. Rev. **10**, 53 (1991).

10. J. B. Fenn, M. Mann, C. K. Meng, S. K. Wong, and C. M. Whitehouse, Science **246**, 64 (1989).

11. C. M. Whitehouse, R. N. Dreyer, M. Yamashita, and J. B. Fenn, Anal. Chem. **57**, 675 (1985).

12. R. P. Schneider, M. J. Lynch, J. F. Ericson, and H. G. Fouda, Anal. Chem. **63**, 1789 (1991).

13. T. Wachs, J. C. Conboy, F. Garcia, and J. D. Henion, J. Chromatogr. Sci. **29**, 357 (1991).

14. A. P. Bruins, T. R. Covey, and J. D. Henion, Anal. Chem. **59**, 2642 (1987).

15. R. D. Smith, C. J. Barinaga, and H. R. Udseth, Anal. Chem. **60**, 1948 (1988).

16. K. W. M. Siu, R. Guevremont, J. C. Y. Le Blanc, G. J. Gardner, and S. S. Berman, J. Chromatogr. **554**, 27 (1991).

17. K. W. M. Siu, G. J. Gardner, and S. S. Berman, Anal. Chem. **61**, 2320 (1989).

18. A. T. Blades, P. Jayaweera, M. G. Ikonomou, and P. Kebarle, Int. J. Mass Spectrom. Ion Processes **102**, 251 (1990).

19. A. T. Blades, P. Jayaweera, M. G. Ikonomou, and P. Kebarle, Int. J. Mass Spectrom. Ion Processes **101**, 325 (1990).

20. D. J. Douglas, "Fundamental Aspects of Inductively Coupled Plasma Mass Spectrometry," in *Inductively Coupled Plasmas in Analytical Atomic Spectroscopy*, A. Montaser and D. W. Golightly, Eds. (VCH Publishers, New York, 1992), 2nd ed.

21. Z. L. Cheng, K. W. M. Siu, R. Guevremont, and S. S. Berman, "Electrospray Mass Spectrometry: A Study on Some Aqueous Solutions of Metal Salts," in *Proceedings of the 39th ASMS Conference on Mass Spectrometry and Allied Topics* (ASMS, East Lansing, Michigan, 1991), p. 1255.

22. G. J. Van Berkel, S. A. McLuckey, and G. L. Glish, "Analysis of Metals in Solution Using Electrospray Ionization Mass Spectrometry," in *Proceedings of the 39th ASMS Conference on Mass Spectrometry and Allied Topics* (ASMS, East Lansing, Michigan, 1991), p. 292.

23. *The API III Book* (SCIEX, Thornhill, Ontario, Canada).

24. M. A. Vaughan and G. Horlick, Spectrochim. Acta **45B**, 1301 (1990).

25. Y. Shao and G. Horlick, Spectrochim. Acta **46B**, 165 (1991).

26. D. J. Douglas and J. B. French, J. Am. Soc. Mass Spectrom., **3**, 398 (1992).

27. G. B. King and G. Horlick, Spectrochim. Acta Electronica **47B**, E353 (1992).

28. S. K. Chowdhury and B. T. Chait, Anal. Chem. **63**, 1660 (1991).

29. M. G. Ikonomou, A. T. Blades, and P. Kebarle, Anal. Chem. **63**, 1989 (1991).

30. M. G. Ikonomou, A. T. Blades, and P. Kebarle, Anal. Chem. **62**, 957 (1990).

Chapter 3

Electrospray Mass Spectrometry as a Technique for Elemental Analysis: Quantitative Aspects

3.1 Introduction[2]

In a preliminary report, it has been shown that the phenomenon of electrospray can be used as an ion source for elemental mass spectrometry [1]. In that report the qualitative aspects of the technique were emphasized and several mass spectra of solution samples were presented indicating that trace levels of both elemental and molecular inorganic ions could be observed. This preliminary study actually followed on the work by Kebarle and co-workers who showed that inorganic ions, other than the alkali metals, could be determined by electrospray mass spectrometry [2-4]. Their results were significant in that earlier attempts to observe divalent and trivalent inorganic solution ions had been unsuccessful [5,6], although it is clear in a recent report that Douglas [7] had made some successful, but previously unreported, measurements of divalent inorganic ions by electrospray mass spectrometry.

In this current study the quantitative aspects of elemental electrospray mass spectrometry are investigated. In particular, it is important to establish factors that affect dynamic range and linearity, and to determine the existence and extent of matrix effects. To date, there have only been limited studies of the quantitative characteristics of electrospray mass spectrometry (ES-MS). Raffaelli and Bruins [8] discussed the effect of variables such as solvent and the size and shape of the counter-ion on the measured ES current. They concluded that the ES current was very dependent on the analyte ion-solvent interaction, but independent of the counter-ion type. The linear dynamic range for two different quaternary ammonium salts (tetrabutylammonium bromide and oxyphenonium bromide) extended over only one order of magnitude. Mann was able to obtain linear log-log calibration plots extending over four orders of magnitude for two bio-polymers [9], however, the slopes for the log-log plots presented were 0.78 and 0.73 indicating that the response actually was non-linear.

Kebarle and coworkers have published a series of papers where they have systematically investigated ES ionization and in doing so have contributed considerable information to the understanding of the charged droplet and ion production processes [2-4,10-13]. With

---

[2] A version of this chapter has been accepted for publication. George R. Agnes and Gary Horlick, Appl. Spectrosc.

respect to quantitation, a calibration curve extending almost three orders of magnitude was obtained for cocaine hydrochloride in methanol however, the slope of the log-log plot was 0.85 [10]. In addition, calibration curves (again as log-log plots) presented for Cs and K in the same report had non-unity slopes and exhibited significant curvature over just two orders of magnitude variation in concentration ($3x10^{-6}$ to $3x10^{-4}$ molar).

In a recent report, Fenn [14] presented linear calibration curves extending 3 orders of magnitude for tetramethyl, tetrabutyl, and tetraheptyl ammonium halides. Fenn also noted that signal levels were greatest for the most solvophobic species (*i.e.* the tetraheptyl ammonium halide). Tang and Kebarle [15] have also observed a similar correlation when relating signal levels to solvation energies of tetraalkyl ammonium ions and alkaloids.

The variety of results for linear dynamic range and sensitivity indicates that it is not yet clear which variables in electrospray are important in establishing quantitative performance. In this work we have chosen to study simple inorganic metal ions as the analyte. Such species have no solvophobic moieties and should provide simple probes of quantitative performance and the ion evaporation process. It will be seen that the overall solution composition can have a profound effect on the signal for a metallic analyte ion. In particular, the presence of a second ion at a moderately high concentration is beneficial in establishing stable and quantitative electrospray conditions for a trace component.

3.2 Experimental

The electrospray source and mass spectrometer used for this study have been described [1]. In this study the ES capillary was biased at 5000 V, the front plate at 950 V, the sampling plate at 190 V, the skimmer at 4.25 V, and the ion extractor at -1.75 V. Significant changes from the previous study include the fact that the skimmer is now biased and the ion extractor has been changed to a cylinder from a solid disk. These changes improved the signal intensity by about a factor of 20. The curtain gas flow rate was 0.1 L/min for singly charged solution ions (*i.e.* Cs^+) and was 0.4 L/min for doubly charged solution ions (*i.e.* Co^{2+}). With these source and interface conditions, all ions, regardless of their charge state in solution, were detected as singly charged atomic ions (M^+). It should be noted that the source and interface conditions can exert a strong influence on the nature of the resulting mass spectrum. These effects have been delineated in a separate study [16].

The bias voltage applied to the electrospray capillary was provided by an EH-series (0-10 kV) Glassman high-voltage supply. Test points are provided in the back of this supply that allow monitoring of the current flow to the capillary. The value of this current was monitored in order to note any onset of a corona discharge at the ES capillary tip. Such a discharge is disruptive to the electrospray process and conditions should be avoided that lead to the formation of such a discharge (*i.e.* voltage too high or lack of any electrolyte in the solvent).

All solutions were made by dissolving the ACS grade salt in a minimum of distilled deionized water, then diluting to volume with HPLC-grade methanol. This results in most solutions being essentially methanol-based with a trace of water present (< 1 %).

3.3 Results and Discussion

A first attempt at establishing a calibration curve is shown in Fig. 3.1a. The calibration curve is for cesium and pure solutions containing only $CsNO_3$ ($1x10^{-7}$ to $3x10^{-3}$ molar) were run. The response is clearly non-linear. There is a minimum concentration (~ $1x10^{-5}$ molar) at which the signal abruptly increases in intensity and then quickly levels off. A similar response was found for solutions of KNO_3 and two "calibration curves" are shown (superimposed) for cobalt ($Co(NO_3)_2$) in Fig. 3.1b, again illustrating a similar response. These results indicate that there is a minimum concentration at which there is onset of a stable electrospray process and that the overall phenomenon is inherently non-linear. It is interesting to observe the mass spectra of the solutions before and after the onset of the electrospray signal for the analyte. These are shown in Fig. 3.2. The mass spectrum for a solution containing $1x10^{-6}$ molar KNO_3 is shown in Fig. 3.2a. The species observed appear to be entirely based on the solvent and, in addition, the electrospray current was not particularly stable, tending to fluctuate rapidly between 300-1000 nanoamperes. The mass spectrum represents the species resulting from a corona discharge. However, for a solution containing $1x10^{-3}$ molar KNO_3 the electrospray current was steady at about 600 nanoamperes and the mass spectrum shown in Fig. 3.2b was obtained clearly indicating the presence of potassium and a stable electrospray phenomenon. This requirement for the presence of a minimum level of ionized electrolyte in the solvent to be electrosprayed (*i.e.* a minimum conductivity) has been noted in the literature [11,13] and the results shown in

Fig. 3.1 indicate the consequences to analytical performance if such a minimum level is not present.

These observations lead to the idea that it might be possible to stabilize the electrospray process for quantitation of a trace analyte component by adding a constant amount of a second ion at a moderate concentration level (*i.e.* $1x10^{-4}$ to $1x10^{-3}$ molar). Following this rationale, $1x10^{-4}$ molar KNO_3 was added to all the $CsNO_3$ solutions used to establish the calibration curve. A plot of both the cesium and the potassium signals as a function of cesium concentration is shown in Fig. 3.3. Although not perfect, the presence of the constant amount of potassium has indeed allowed the observation of signals for the lower concentration values of cesium in an approximately linear manner. Note that the potassium signal at first slowly decreases as the cesium concentration increases, and then as the cesium concentration exceeds about $1x10^{-4}$ molar (*i.e.* the level of potassium in these solutions) the potassium signal falls dramatically as the cesium signal reaches a plateau. Thus at high concentrations, cesium is suppressing the potassium signal. Interestingly, the suppression is approximately linearly related to the increase in cesium concentration above the cross-over point. This means that the entire cesium calibration curve may be linearized by dividing the cesium signals by the corresponding potassium signals. This is shown by the plot presented in Fig. 3.4a. Now a linear calibration curve is obtained (slope = 1.08) over a dynamic range of four orders of magnitude. Potassium can be thought of as carrying out a multi-function control role by both stabilizing and monitoring the electrospray process and also by acting as an internal standard.

While not the focus of this study, the data presented in Fig. 3.3 for the potassium ion signal as a function of Cs concentration could also be viewed as a matrix effect study, with the conclusion that the presence of Cs suppresses the K signal. In a recent study modeling the dependence of ion intensity in ES-MS on the concentration of analytes in solution Tang and Kebarle [15] have also noted this suppression effect. This indicates that the nature and control of the matrix will be important to clarify quantitative ES-MS measurements.

The electrospray process and the process of generating singly charged metal ions as the solvated electrosprayed ion clusters are extracted into the mass spectrometer are not the same for singly and doubly charged solution ions. In particular, for doubly charged ion-solvent clusters, the metal ion is reduced to the singly charged state as solvent molecules are stripped off (see references 3 and 16 for more details and discussion). Thus, it is reasonable to assume that a doubly charged analyte solution ion would be best monitored

by another doubly charged ion. The calibration curve for cobalt (Fig. 3.1b) can be linearized (slope of the log-log calibration plot = 1.00) by use of zinc ($1x10^{-4}$ molar) as an electrospray stabilizer and internal standard (see Fig. 3.4b). In contrast, if potassium ($1x10^{-4}$ molar) is used as an electrospray stabilizer and internal standard for cobalt the plot shown in Fig. 3.5a is the result. There are now two distinct regions within the calibration curve. Likewise, cobalt fails to provide effective electrospray stabilization and internal standardization for potassium as an analyte (see Fig. 3.5b) over the full concentration range. It appears that at low concentration of analyte (< $1x10^{-4}$ molar) the internal standard element, in someway, controls the electrospray process and at concentrations greater than $1x10^{-4}$ molar, control switches over to the analyte ion. Other than the fact that doubly charged ions undergo a charge reduction step in the gas phase, the exact nature of the step that transfers ions from solution to ions in the gas phase is not known [17]. The data presented in Fig. 3.5 imply that this step is different for mono and divalent inorganic ions.

An interesting variation of the electrospray stabilizer theme is to create ions to control the electrospray process through acidification of the solvent, thereby using a built-in solution ion. The properties required of an electrospray stabilizer appear to be met when protonated solvent ions are used as both the electrospray stabilizer and the internal standard for singly charged metal ions. Addition of a small amount of nitric acid ($1x10^{-4}$ molar) to the methanol-based solutions provides stable signals for $H(MeOH)_1^+$ (m/z = 33) and $H(H_2O)_1^+$ (m/z = 19), both of which can be used to linearize a cesium calibration curve (see Fig. 3.6). The slope of the calibration curve obtained from the ratio of the analyte ion signal intensity to the $H(H_2O)^+$ signal intensity ratio and to the $H(MeOH)^+$ signal intensity is 1.03 and 1.09 respectively.

Linear calibration curves were also obtained for a multielement solution (Li, Na, K, Rb, and Cs), again through the use of a species from the acidified solvent (see Fig. 3.7). In this case, however, the acid level (HNO_3) had to be raised to $1x10^{-3}$ molar in order to maintain linearity at the high concentration end of the calibration curves. If only $1x10^{-4}$ molar HNO_3 was present, the curves tended to roll-off at the upper end. The slopes for the log-log plots shown in Fig. 3.7 are Li (1.04), Na (0.98), K (1.04), Rb (1.02), and Cs (1.07).

A slightly different approach to electrospray stabilization and calibration curve linearization was tested for a set of multielement solutions of doubly charged solution ions (Co, Mn, Cu, and Zn). For these solutions, $1x10^{-4}$ molar Ni^{2+} was added to all solutions and they

were also acidified with HNO_3 at the level of $1x10^{-3}$ molar. The resulting calibration curves that were obtained by ratioing the analyte ion signal intensity to the $^{58}Ni^+$ signal intensity are shown in Fig. 3.8. The slopes for these calibration curves are Co (1.03), Mn (0.99), Cu (1.06), and Zn (0.86).

Finally, using the data presented in Fig. 3.4, the detection limit (3σ) for Cs was $2x10^{-8}$ molar (2.7 ng/mL) and that for Co was $8x10^{-8}$ molar (4.7 ng/mL). Detection limits were not a focus of this study and a parametric optimization of signal levels has yet to be carried out. However, ppb to sub-ppb level detection limits appear to be easily in sight as Corr and Douglas [18] have already reported sub-ppb detection limits for elemental ion spray-mass spectrometry.

3.4 Conclusions

It is interesting to review the results presented here and to see how the data fit the two theoretical models proposed to describe the nature of the electrospray process leading to the formation of gas-phase ions. The two models are the so-called single ion in droplet theory (SIDT) first proposed by Dole [19,20] and the ion evaporation theory (IET) proposed by Iribarne and Thomson [5,21]. Both theories have recently been reviewed in some detail by Kebarle and Tang [17].

The electrospray process requires charged droplets to be created by a flow of solution through a capillary held at a high potential. The resultant droplets, charged with an excess of cations relative to anions (capillary positive) experience solvent evaporation as they drift through the ambient, atmospheric pressure environment. With sufficient solvent evaporation the droplets become unstable and undergo Rayleigh fission. Rayleigh fission occurs when the field strength of the charge contained within the droplet exceeds the retentive forces acting within the droplet, namely the surface tension of the solvent. After sufficient Rayleigh fissions, gas phase ions are produced from the remains of the charged droplets either by a SIDT or an IET process. The SIDT is based upon simple Rayleigh fission for smaller and smaller droplets until ultimately, a very small droplet containing a single ion is produced. The IET states that ions are desorbed from small charged droplets (radius ~ 7-9 nm, number of excess charges ~ 40-100). The IET states that the rate of ion desorption is dependent on the solvation energy of each ion. The matter of which, or a combination of these two models is responsible for the generation of gas phase ions has

been the subject of numerous reviews and is still a matter of considerable debate [14,17,22].

The "calibration curves" shown in Fig. 3.1 imply that a minimum electrolyte concentration must be present in order to observe the electrospray phenomenon. This observation is not implicit in the models of the electrospray process and needs to be incorporated into any model of the process. The calibration plots of Figs. 3.7 and 3.8 for multi-element solutions of inorganic ions all have unity slopes for the log-log plots independent of the nature of the inorganic ion. Thus ion signals from the multi-element solutions depend simply on concentration. Redundant as the following statement is, it cannot be over emphasized that the inorganic ions employed in this study were detected proportional only to concentration. This result would not be expected if there was an additional dependency on the ion solvation energy. Certainly there is a change in solvation energy in going from Li to Cs, that is, for the alkali metals depicted in Fig. 3.7. If there was a solvation energy dependency for ion generation, one analyte, preferentially formed, might suppress other ion signals as the concentration level is increased as that ion would preferentially carry off the excess charge.

Thus, these results tend to favor the SIDT over the IET as the IET has a solution energy dependency for ion desorption. In all of our data only the plot for Zn in Fig. 3.8 has a significant non-unity slope (0.86). However, there was a large background associated with m/z = 64 (the isotope used to quantitate the zinc signal in this study) which may account for the non-unity slope of the log-log plot. Certainly this evidence is very circumstantial but in a way, the simple inorganic ions studied here provide simple and direct probes of the electrospray process compared to the large organic molecules and bio-molecules often used to model the electrospray process. It is felt that further work using inorganic ions will help to clarify the electrospray process. In the end, however, from a practical point of view, two desirable quantitative characteristics of an analytical technique are that the calibration curves are linear and that it is possible to determine an analyte over a wide dynamic range of concentration. In this study it has been shown that conditions can be established and methodology utilized that achieve both of these goals for elemental electrospray mass spectrometry.

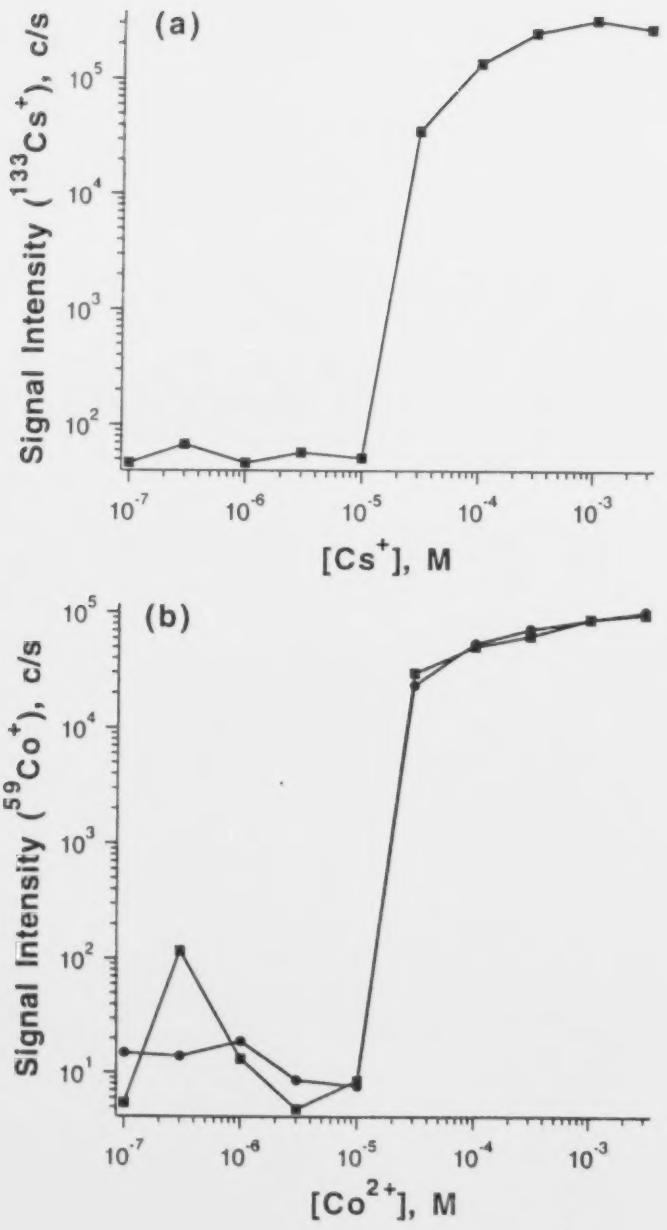

Figure 3.1 Attempted calibration curves for (a) cesium and (b) cobalt.

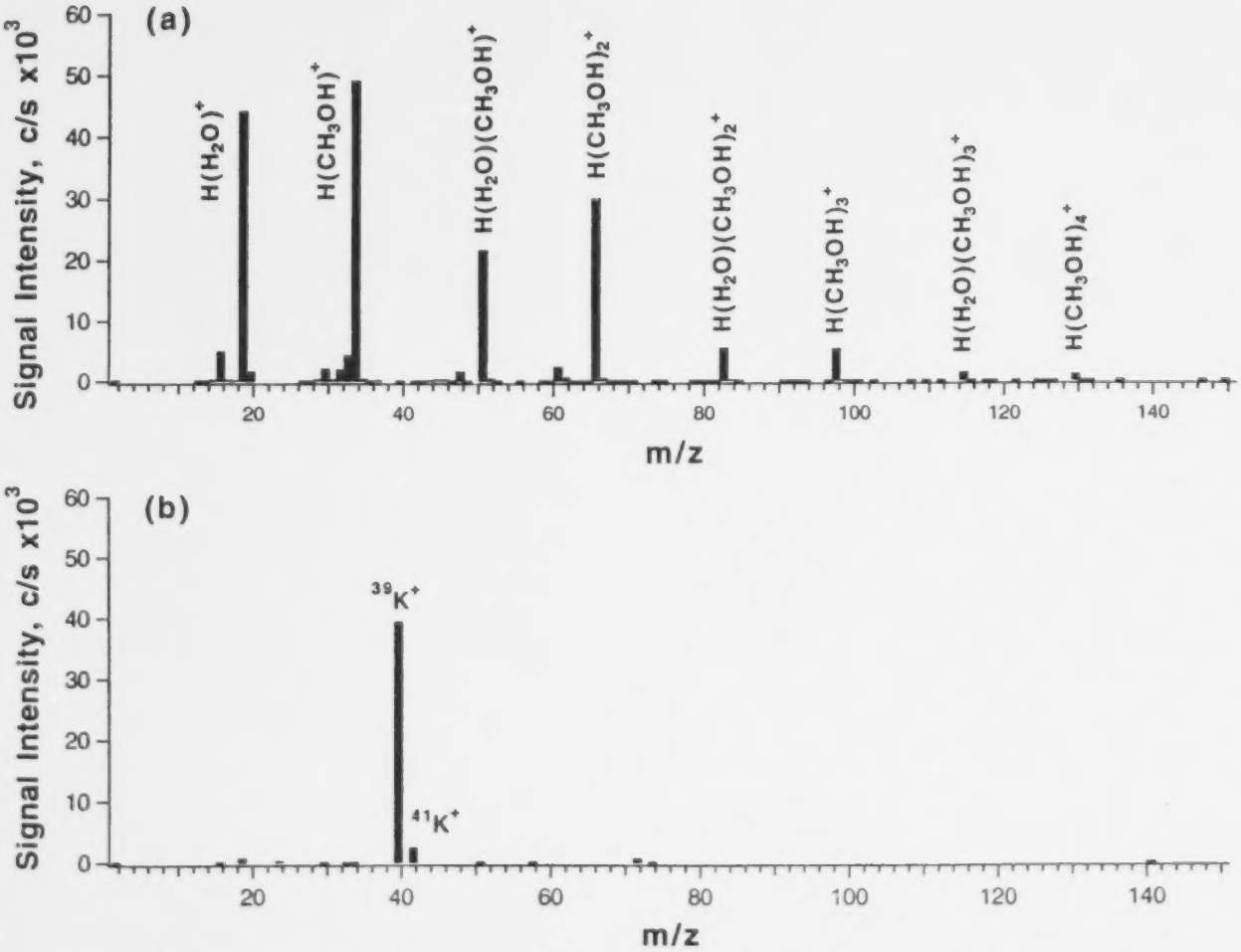

Figure 3.2 Mass spectra for a solution of KNO_3 in methanol: (a) $1x10^{-6}$ molar and (b) $1x10^{-3}$ molar.

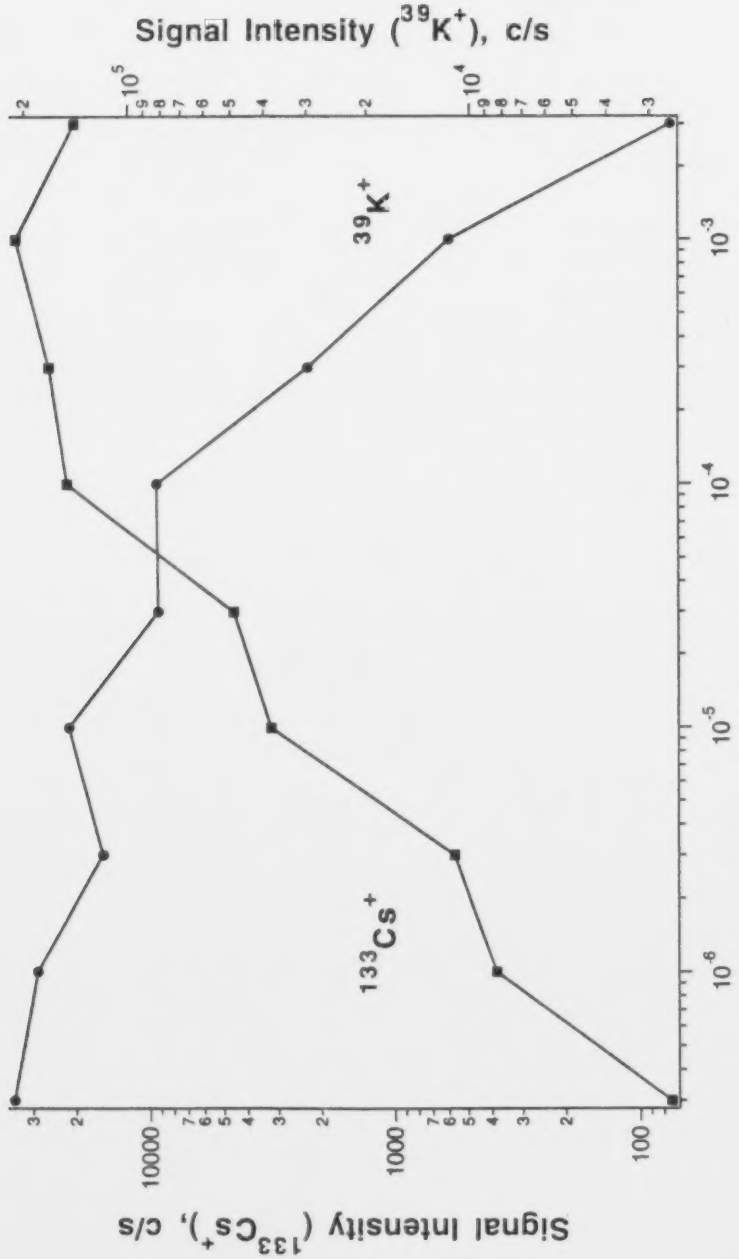

Figure 3.3 Signal intensities of cesium and potassium as a function of cesium concentration. The potassium ion concentration was constant at 1×10^{-4} molar.

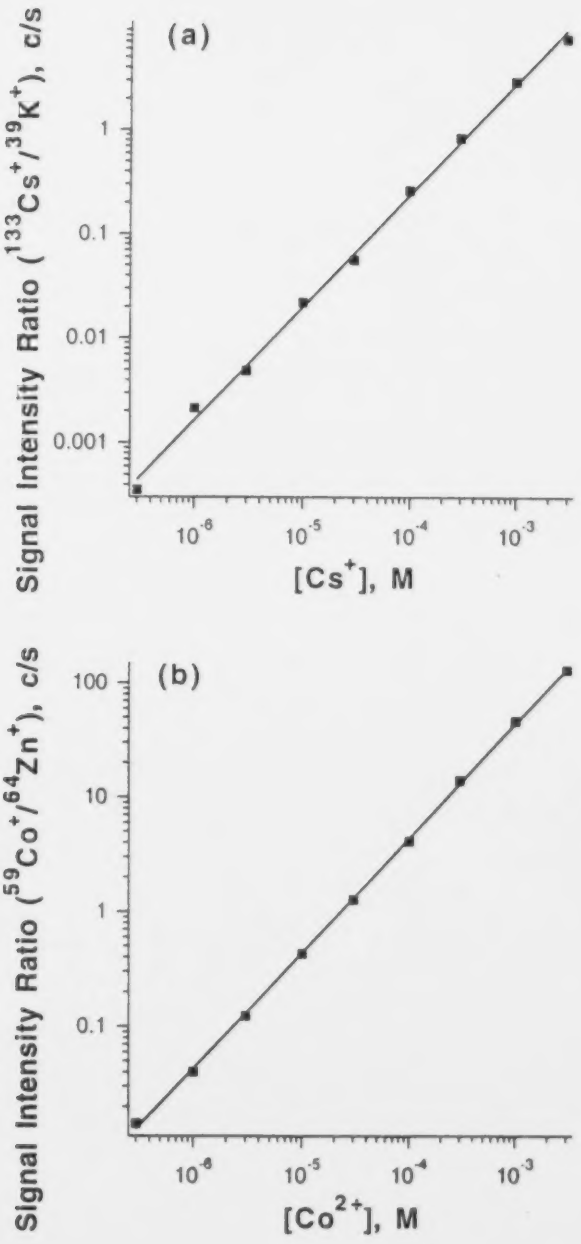

Figure 3.4 (a) Calibration curve for cesium with potassium as the electrospray stabilizer and internal standard. (b) Calibration curve for cobalt with zinc as the electrospray stabilizer and internal standard.

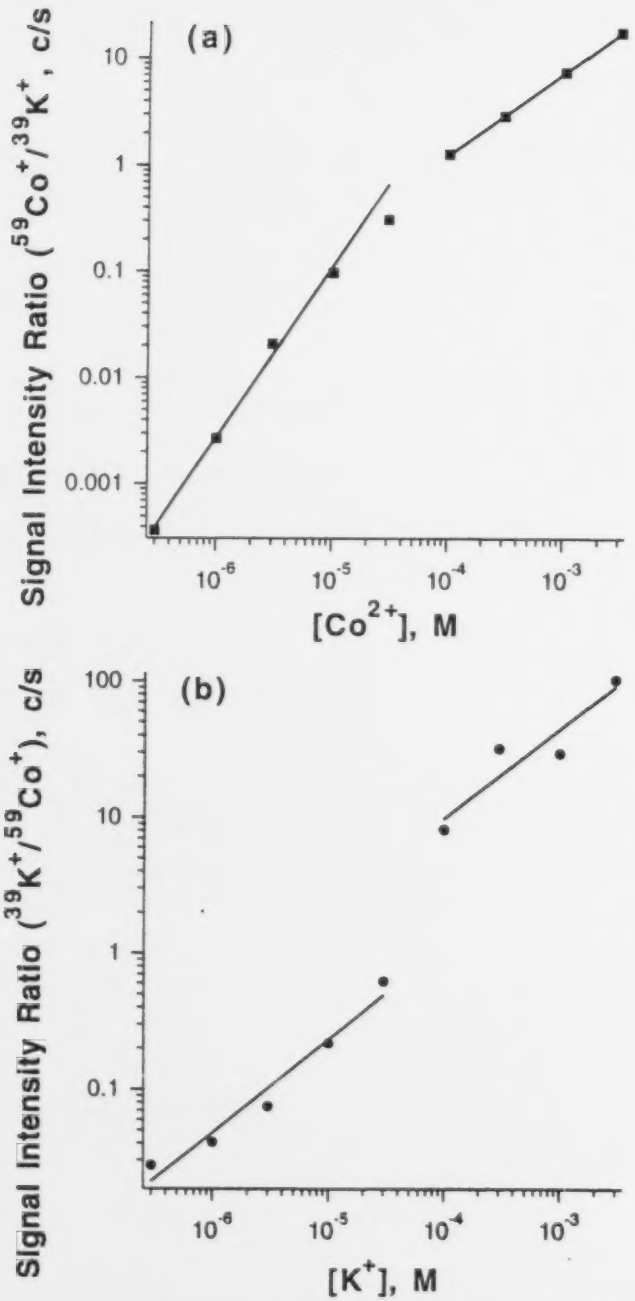

Figure 3.5 (a) Calibration curve for cobalt with potassium as the electrospray stabilizer and internal standard. (b) Calibration curve for potassium with cobalt as the electrospray stabilizer and internal standard.

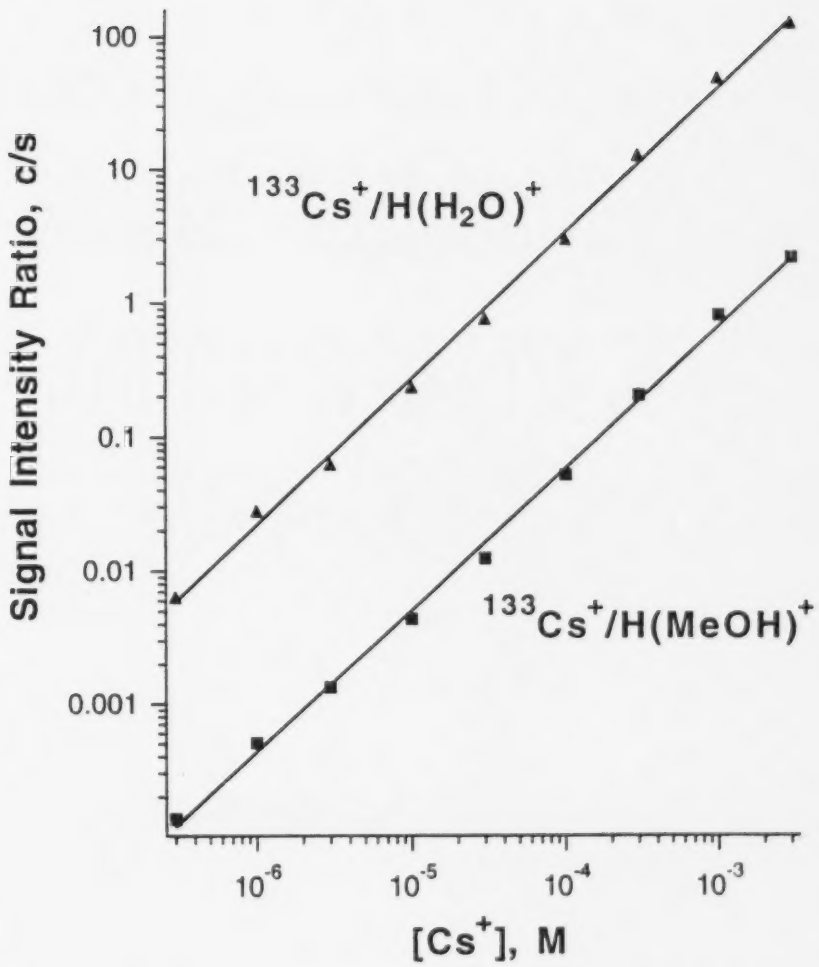

Figure 3.6 Calibration curves for cesium with protonated solvent species as the electrospray stabilizer and internal standard.

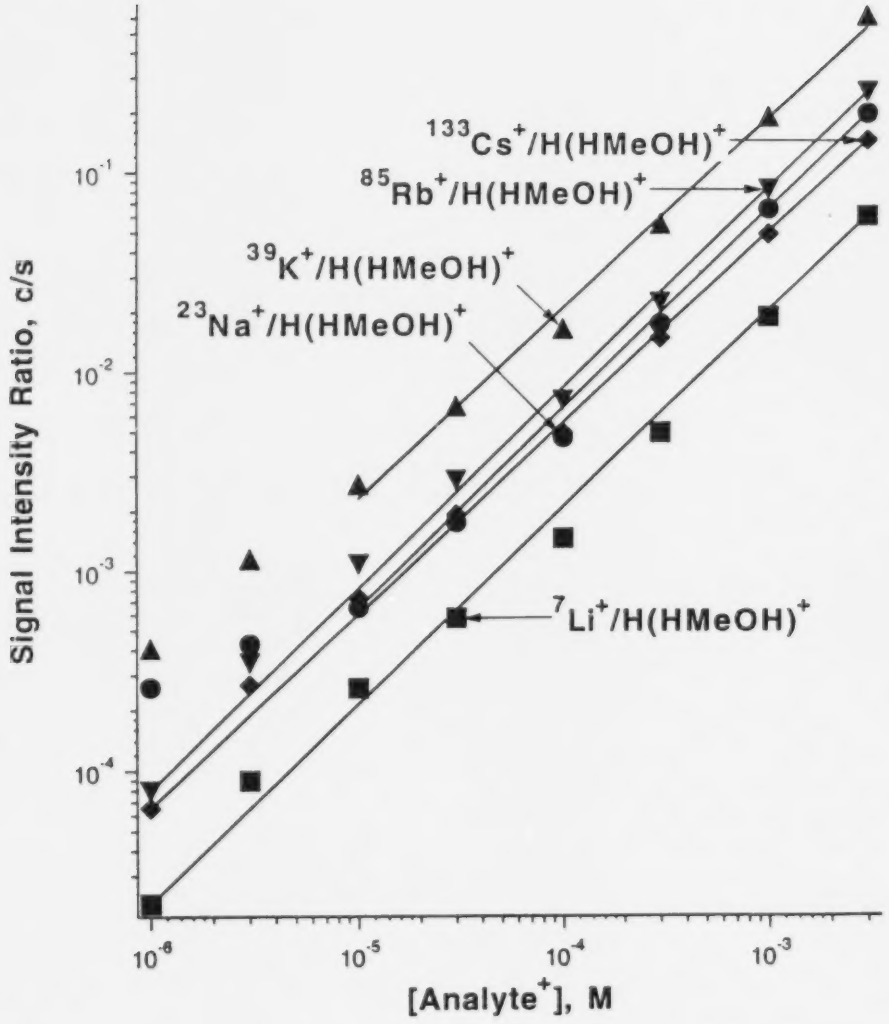

Figure 3.7 Multielement solution (Li, Na, K, Rb, and Cs) calibration curves with protonated methanol as the electrospray stabilizer and internal standard.

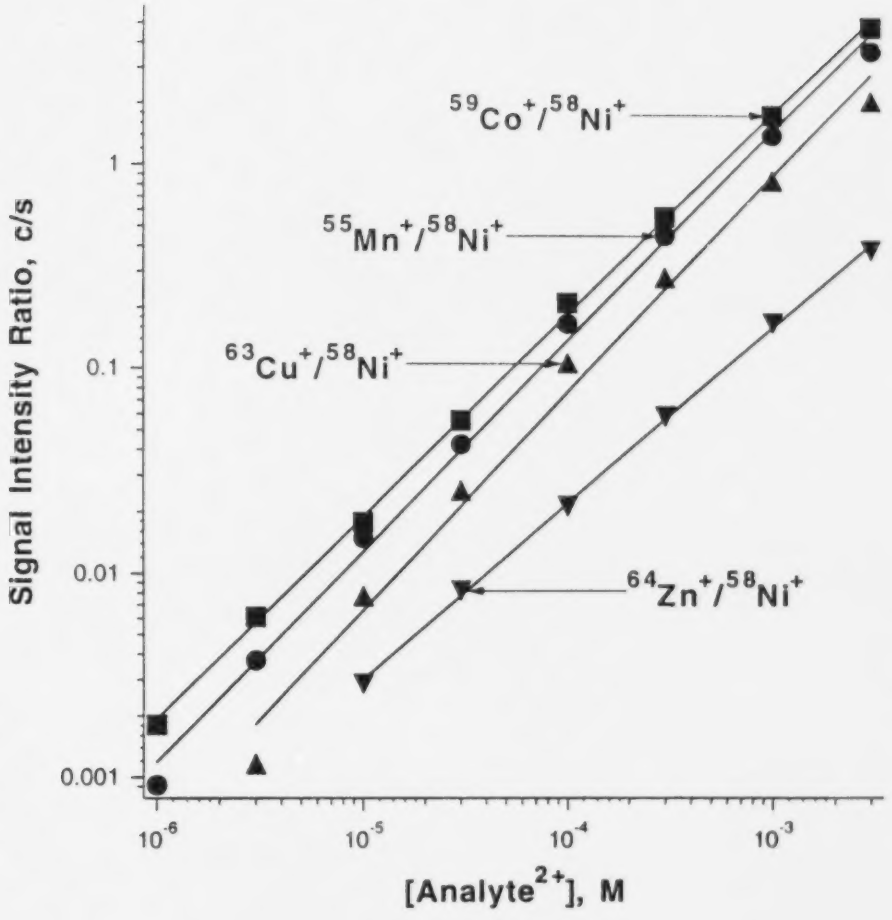

Figure 3.8 Multi-element solution (Co, Ni, Cu, and Zn) calibration curves with nickel as the electrospray stabilizer and internal standard. Note: The solutions were also acidified with HNO_3 at the level of $1x10^{-3}$ molar .

3.5 References

1. G. R. Agnes and G. Horlick, Appl. Spectrosc. **46**, 401 (1992).

2. A. T. Blades, P. Jayaweera, M. G. Ikonomou, and P. Kebarle, Int. J. Mass Spectrom. and Ion Processes **102**, 251 (1990).

3. A. T. Blades, P. Jayaweera, M. G. Ikonomou, and P. Kebarle, Int. J. Mass Spectrom. and Ion Processes **101**, 325 (1990).

4. A. T. Blades, P. Jayaweera, M. G. Ikonomou, and P. Kebarle, J. Chem. Phys. **92**(10), 5900 (1990).

5. B. A. Thomson and J. V. Iribarne, J. Chem. Phys. **71**, 4451 (1979).

6. M. Yamashita and J. B. Fen, J. Phys. Chem. **88**, 4451 (1984).

7. D. J. Douglas, "Fundamental Aspects of Inductively Coupled Plasma Mass Spectrometry", in *Inductively Coupled Plasmas in Analytical Atomic Spectroscopy*, A. Montaser and D. W. Golightly, Eds. (VCH Publishers, New York, 1992), 2nd ed., p. 642.

8. A Raffaelli and A. P. Bruins, Rapid Commun. Mass Spectrom. **5**, 269 (1991).

9. M. Mann, Organic Mass Spectrometry **25**, 575 (1990).

10. M. G. Ikonomou, A. T. Blades, and P. Kebarle, Anal. Chem. **62**, 957 (1990).

11. M. G. Ikonomou, A. T. Blades, and P. Kebarle, Anal. Chem. **63**, 1989 (1991).

12. A. T. Blades, M. G. Ikonomou, and P. Kebarle, Anal. Chem. **63**, 109 (1991).

13. L. Tang and P. Kebarle, Anal. Chem. **63**, 2709 (1991).

14. J. B. Fenn, J. Am. Soc. Mass Spectrom. **4**, 524 (1993).

15. L. Tang and P. Kebarle, Anal. Chem. **65**, 3654 (1993).

16. G. R. Agnes and G. Horlick, "Determination of Solution Ions by Electrospray Mass Spectrometry", Appl. Spectrosc. (accepted for publication).

17. P. Kebarle and L. Tang, Anal. Chem. **65**, 972A (1993).

18. J. J. Corr and D. J. Douglas, "Elemental Ion Spray-Mass Spectrometry: Analysis of Solutions of Metal Salts", in *Proceedings of the 41st ASMS Conference on Mass Spectrometry and Applied Topics*, San Francisco (1993), p. 732a.

19. M. Dole, L. L. Mach, R. L. Hines, R. C. Mobley, L. P. Ferguson, and M. B. Alice, J. Chem. Phys. **49**, 2240 (1968).

20. L. L. Mach, P. Kralik, A. Rheude, and M. Dole, J. Chem. Phys. **52**, 4977 (1970).

21. J. V. Iribarne and B. A. Thomson, J. Chem. Phys. **64**, 2287 (1976).

22. B. E. Winger, K. J. Light-Wahl, R. R. Ogurzalek Loo, H. R. Udseth, and R. D. Smith, J. Am. Soc. Mass Spectrom. **4**(7), 536 (1993).

Chapter 4

Background Spectral Characteristics of Quantitative Elemental ES-MS.

4.1 Introduction

Quantitative analysis of solution components by ES-MS is most easily achieved when the electrospray ion source is operated in a manner such that all ions, regardless of their solution form are detected as singly charged gas phase ions. Ion clusters formed via the electrospray process are collisionally declustered in the jet expansion in the zone between the sampling plate and skimmer. Few molecular-analyte ion clusters remain and a "simple" elemental mass spectrum is generated. (See references 1 and 2 for further details regarding the quantitative and qualitative aspects of operating the electrospray source in this manner.)

Aside from matrix effects, spectral interferences arising from background components pose one of the most serious sources of error for quantitative analysis. A previous report focused on the quantitative aspects of elemental ES-MS [2]. This report presents the basic background spectral features characteristic to elemental electrospray mass spectrometry (ES-MS).

4.2 Experimental

The effect of solvent (methanol, methanol/water (1:1), and acetonitrile) and the curtain gas type (Nitrogen, Oxygen, and Argon) on the basic background spectral features were investigated. A stock solution of $1x10^{-2}$ molar RbCl was prepared by dissolving the ACS grade salt into distilled deionized water, then diluting with the appropriate solvent so that the RbCl concentration in the solution electrosprayed was $1x10^{-4}$ molar. The methanol and acetonitrile solvents were HPLC grade.

The electrospray ion source was operated with the similar conditions as used previously [2]. The electrospray capillary was biased at 4500 V (except for acetonitrile solutions where the electrospray capillary bias was reduced to 4000 V), the front plate at 950 V, the sampling plate at 190 V, the skimmer at 6 V and the barrel ion extractor at -4.0 V. The curtain gas flow rate was kept constant at 0.70 lpm. Signal intensities of analyte molecular species were found to be more completely removed from the 'ICP-like' mass spectrum at the higher curtain gas flow rate than at the 0.4 lpm flow rate used in reference 2.

4.3 Results and Discussion

Electrospraying a pure solvent at the conditions we employ for elemental analysis would create an electric discharge between the electrospray capillary tip and the front plate [3]. Addition of an electrolyte (rubidium chloride) increases the voltage bias that can be applied to the electrospray capillary tip before an electric discharge is struck [2]. The added electrolyte permits stable charged droplet generation and in turn quantitation of trace elements in the solution. Also the rubidium chloride provides a measure of the relative analyte sensitivity as the solvent and curtain gas types are changed.

The spectra displayed in Figs. 4.1, 4.2, and 4.3 were acquired while electrospraying the same rubidium chloride solution ($1x10^{-4}$ molar in methanol), but a nitrogen, oxygen, and argon curtain gas was used respectively. Within each figure the vertical axis is a) full scale, b) expanded by a factor of ten, and c) expanded by a factor of one hundred (note that different vertical scales were however used in Figs. 4.1, 4.2, and 4.3). The signal intensity of the $^{85}Rb^+$ peak decreases in changing the curtain gas from nitrogen to oxygen to argon. The mean background signal level (i.e. at m/z = 98) also decreases in the same order. This trend is likely due to a decreasing level of electric discharging. $^{12}C^+$ provides a relative measure of the electric discharge, and the $^{12}C^+$ signal intensity decreases in changing the curtain gas from nitrogen to oxygen to argon (methanol is ionized by the electric discharge, collision induced dissociation of $MeOH^+$ in the jet expansion produces $^{12}CH_n^+$, n = 0, 1, 2, 3). Matching the $^{12}C^+$ signal intensity in Fig. 4.1 (nitrogen curtain gas) to the $^{12}C^+$ signal intensity in Fig. 4.3 (argon curtain gas) by lowering the electrospray capillary voltage would reduce the $^{85}Rb^+$ signal intensity and background signal intensities from that shown in Fig. 4.1. Hence the signal to background ratio is largely unaffected by the type of curtain gas employed. Also, the presence of an electric discharge is suppressed in the presence of the higher dielectric strength nitrogen and oxygen gases than in the presence of argon gas. (This contradicts what was stated above, but less harsh conditions were used for Argon curtain gas, as a consequence an electric discharge was purposely suppressed in Fig. 4.3.)

Long term drift, which was not investigated, may account for any other minor differences in the $^{85}Rb^+$ ion signal intensities in Figs. 4.1, 4.2, and 4.3. Analyte sensitivity drifts by as much as a factor of (negative) 5 were observed, depending on the age of the electrospray capillary, composition of sample being electrosprayed, and time elapsed since high voltage was applied to the electrospray capillary. Upon application of high voltage to the

electrospray capillary, analyte ion signal intensity levels decay over 5 to 15 minutes before stabilizing at ~ 1/3 the initial sensitivity. Switching from positive to negative electrospray, then back, did not appear to affect analyte ion sensitivity. These observations were made over two and a half years of investigation of ES-MS. Most troubling was that none of these observations could be purposely reproduced. Clearly there are interesting phenomenon occurring inside the electrospray capillary.

Background ions in ES-MS originate from an electric discharge, oxidation of the electrospray capillary material, and trace impurities in the solvent and added electrolyte [5]. Although not immediately apparent in scanning Fig. 4.1a, background spectral features of elemental ES-MS are quite extensive, particularly in the m/z = 1 to 80 range in Figs. 4.1b, 4.2b, and 4.3b. Almost all of these peaks are due to an electric discharge and all attempts should be made to suppress the electric discharge.

Indicative of an atmospheric pressure electric discharge are N_2^+, and HN_2^+, and ionized curtain gas when nitrogen was not used. An argon curtain gas would pose potential problems in the analysis of $^{39}K^+$ and $^{40}Ca^+$. See Fig. 4.3c. Similar background spectral features are observed for all three curtain gases. Solvent molecules are also ionized in the electric discharge, but as stated earlier these ions can be decomposed in the jet expansion to create C^+, CH_1^+, CH_2^+, and CH_3^+. The origin of the ion peaks at m/z = 37, 43, and 45 are not known, but ion molecule reactions in the later stages of the jet expansion may give rise to these ion signals. The source of the chromium, iron, and nickel is the stainless steel electrospray capillary. Oxidation of the electrospray capillary was noted previously by Blades et. al. They have explained the nature of the electrospray source as an electrochemical cell of a special kind in that the medium through which charge carriers migrate is gaseous [5]. Quantitation of trace levels of solution components that are also found in the electrospray capillary material may prove difficult. It can not be overemphasized that the spectra shown in Figs. 4.1-4.5 represent a worst case scenario in that the presence of an electric discharge was purposely not suppressed, and also that the electrospray capillary had been exposed to solutions having nitric acid at 1x10-3 molar. Also present in the mass spectra shown in Figs. 4.1-4.3 are sodium impurities from the solvent [6].

Further scale expansion (Figs. 4.1c, 4.2c, and 4.3c) draws attention to the m/z = 80 to 260 region of the spectrum. Above m/z = 80, the signal level of the background is in general at least one order of magnitude less than background ion signal levels in the m/z = 1 to 80

region. The structure of the background above m/z = 80 in Fig. 4.1c implies that there may be an ion signal at each mass to charge unit. Ion clusters are not a logical explanation for these background ions since very little clustering around an ion was observed with the conditions employed for this study. Compare for example the $^{85}Rb(H_2O)_1^+$ and $^{85}Rb(MeOH)_1^+$ signal levels at m/z = 117 and 103 versus the $^{85}Rb^+$ signal intensity. The extent of declustering in Figs. 4.1, 4.2, and 4.3 as determined by the $^{85}Rb^+$ to $^{85}Rb(H_2O)_1^+$ signal intensity ratio of ~ 0.0015 was unaffected by the level of electric discharge present. For the same reason, ion clusters created by an electric discharge at atmospheric pressure would not contribute to the structured background in the region m/z = 80 to 260. It may be argued that the background structure is no more than a continuum of high energy ions. This is certainly plausible since our mass spectrometer resolution was 1.5 Daltons at ten percent of the peak height, and the baseline peak width for $^{85}Rb^+$ was ~ 4 Daltons. In a separate study, cesium ions were determined to have a mean ion energy of approximately 9 V, with an energy spread from 3 to 18 V. Ion energies were determined by raising the DC bias of the quadrupole [7-9]. Ion energy spread is determined by the spatial position, relative to the skimmer orifice, where the ion becomes collisionally free [10]. There is no doubt an ion continuum extending from m/z = 1 to 260 is present, but superimposed on top of this continuum is a structured background.

This discussion has so far ignored the ion signal at m/z = 205, 207, 209, and 211 (see Fig. 4.1c). During data acquisition, attention was focused on the mass region below m/z = 80 and these peaks were initially attributed to lead. This assignment seemed reasonable since lead solder was used in the construction of the electrospray capillary and elements comprising the electrospray capillary were being oxidized and observed in the mass spectra. However, upon closer inspection during data work-up, the mass to charge ratio and the signal intensity pattern clearly indicates that these ion peaks can not be attributed to lead isotope ions. Not until the complexity of the background signal structure was realized did the interpretation arise that these ion peaks could be ion clusters that either survived the harsh collisional conditions during transfer through the jet or from the result of ion-molecule reactions in the later portion of the jet expansion. The peaks at m/z = 205, 207, 209, and 211 have been assigned to the cluster $H((MeOH)_2(Cl_2)_2)^+$. While this sounds extremely improbable and contradictory to what was just said in the paragraph above, expansion of the chlorine isotope ratio to the fourth power does match well with the observed ion pattern. The source of the chlorine could be due to oxidation of chloride ions in the electrospray capillary or at the electrospray capillary tip [5]. Moreover, the ion signals starting at m/z = 159, 173, and 189 could be assigned to $H((H_2O)_1(Cl_2)_2)^+$,

$H((MeOH)_1(Cl_2)_2)^+$, and $H((MeOH)_1(H_2O)_1(Cl_2)_2)^+$ respectively. Such clusters would not survive the energetic collisions in the jet expansion, but such clusters could be the remnants of a charged droplet that has been sampled into the mass spectrometer. After passing through the zone between the sampling plate and the skimmer, the remnants of these droplets could give rise to the structured background. A conservative estimate of ~ $1x10^3$ charged droplet residues per second are being drawn into the mass spectrometer.

When the solvent was changed to acetonitrile, the basic spectral characteristics of the background were similar to the methanol based solutions for all three curtain gases. For this reason, only the background spectrum obtained while electrospraying an acetonitrile based solution with an argon curtain gas is shown (Fig. 4.4). The $^{85}Rb^+$ sensitivity is ~ $1.5x10^4$ counts/second/$1x10^{-4}$ molar for both methanol and acetonitrile based solutions. The one single major difference in the background of an acetonitrile based solution was the appearance of copper in the mass spectrum. See Fig. 4.4b. The source of the copper impurity was determined to be from the brass fitting on the syringe. Copper (I) is known to be very stable in acetonitrile solutions [11].

The mass spectrum acquired while electrospraying a 1:1 methanol/water based solution in the presence of an argon curtain gas is shown in Fig. 4.5. The $^{85}Rb^+$ sensitivity was ~ $1.5x10^3$ counts/second/$1x10^{-4}$ molar for each of the three curtain gases tested (N_2, O_2 and Ar). Hence, it is the nature of the solvent being electrosprayed that determines the sensitivity of analyte ions and a method or device capable of electrospraying solutions of high water content generating higher analyte ion sensitivities is required for ES-MS.

4.4 Conclusions

The nature of the solvent being electrosprayed significantly affects analyte sensitivities. Changing the curtain gas does not affect electrosprayed ion sensitivities so much as the presence of an electric discharge affects ion signal levels. The voltage bias applied to the electrospray capillary should be set while maximizing analyte ion signals and minimizing ions signals that are characteristic of electric discharges. This preliminary investigation has illuminated some of the characteristics of background ion signals in elemental ES-MS. Further studies specifically directed into uncovering the nature of the background spectral characteristics could yield a multitude of information about the mechanism of the electrospray process.

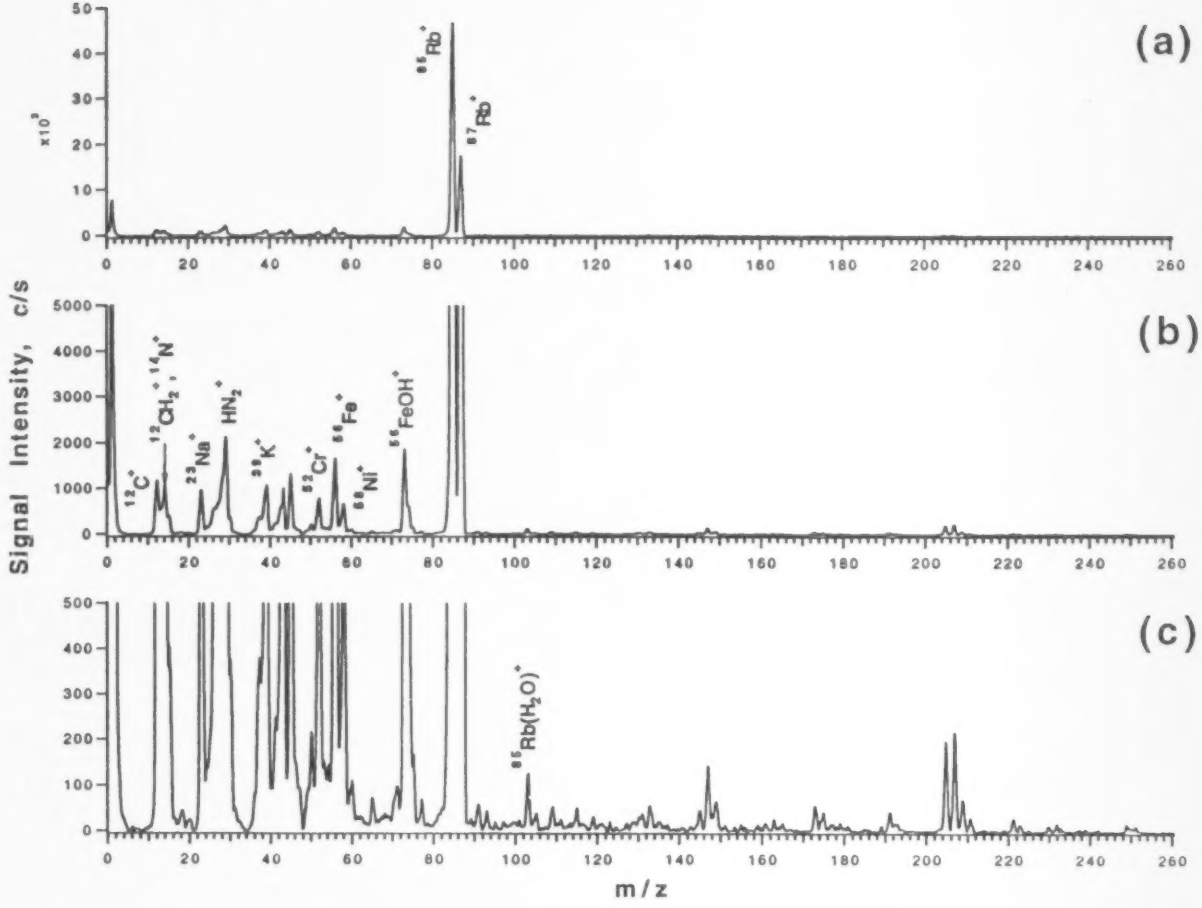

Figure 4.1 Mass spectrum of RbCl ($1x10^{-4}$ molar) in methanol. Nitrogen curtain gas. (a) full scale, (b) scale expanded by a factor of 10, and (c) scale expanded by a factor of 100.

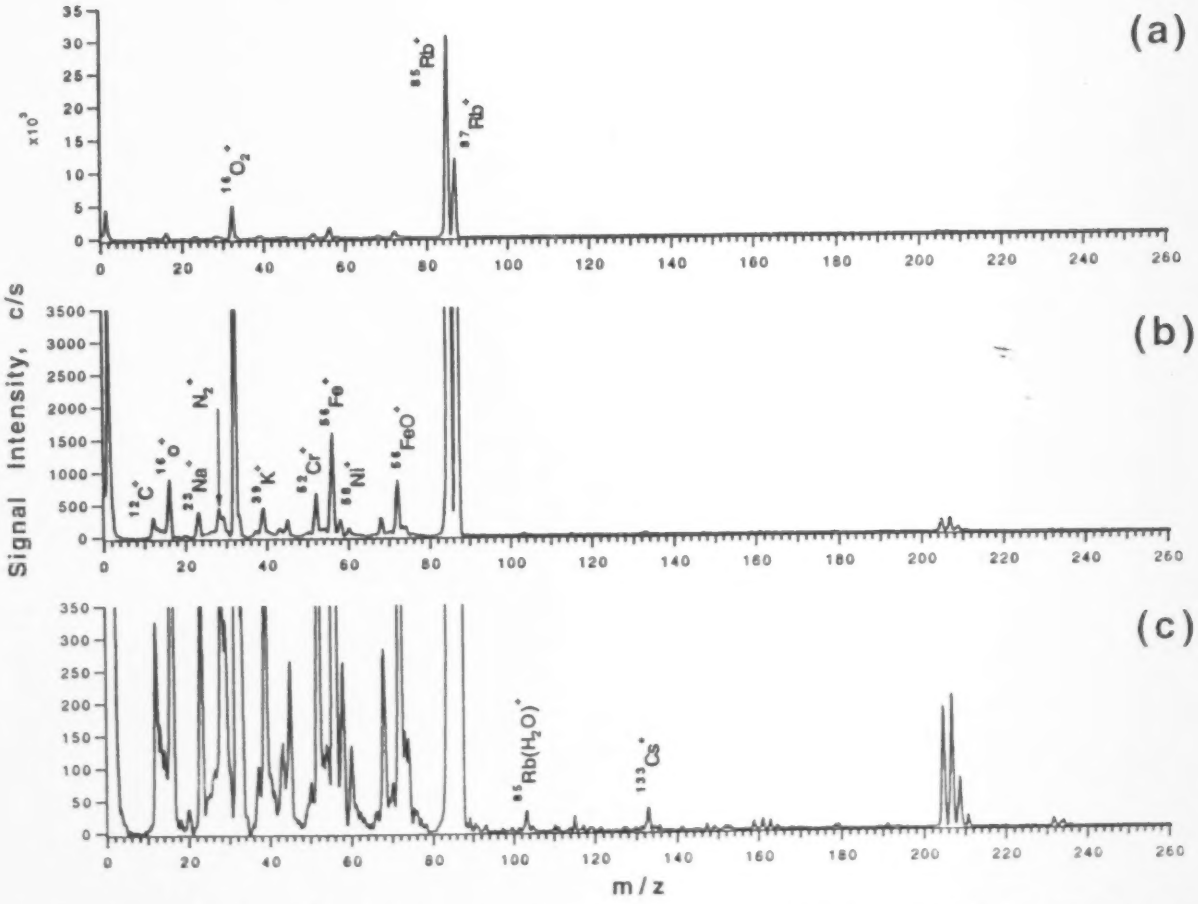

Figure 4.2 Mass spectrum of RbCl ($1x10^{-4}$ molar) in methanol. Oxygen curtain gas. (a) full scale, (b) scale expanded by a factor of 10, and (c) scale expanded by a factor of 100.

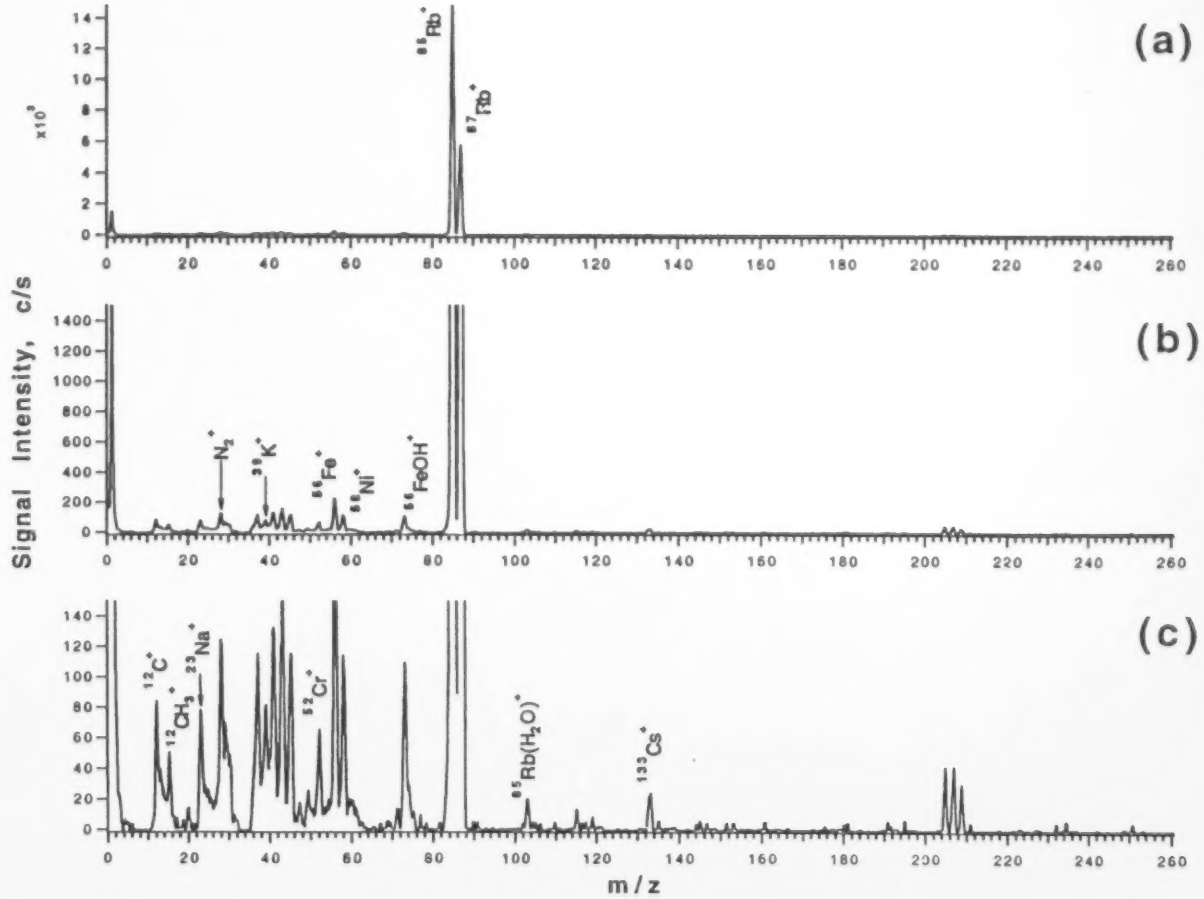

Figure 4.3 Mass spectrum of RbCl ($1x10^{-4}$ molar) in methanol. Argon curtain gas. (a) full scale, (b) scale expanded by a factor of 10, and (c) scale expanded by a factor of 100.

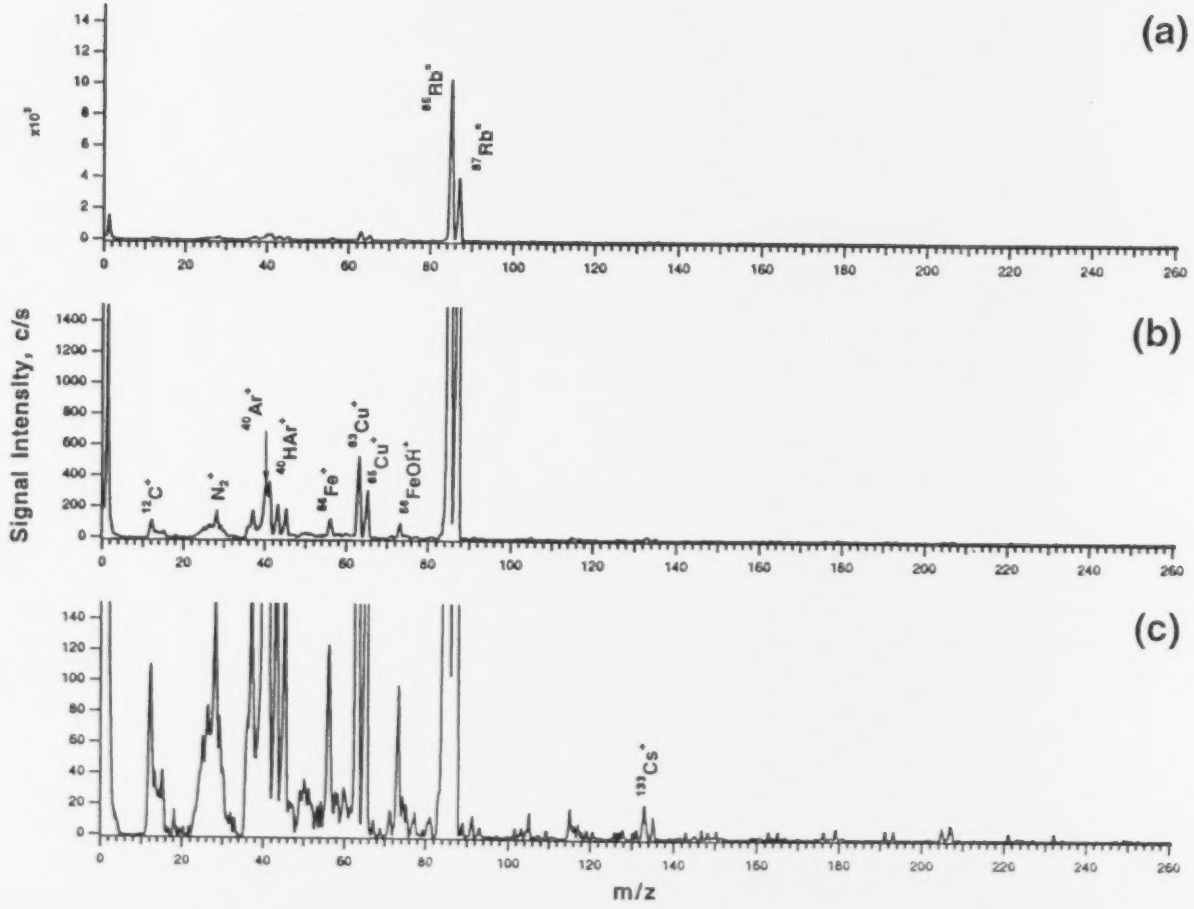

Figure 4.4 Mass spectrum of RbCl ($1x10^{-4}$ molar) in acetonitrile. Argon curtain gas. (a) full scale, (b) scale expanded by a factor of 10, and (c) scale expanded by a factor of 100.

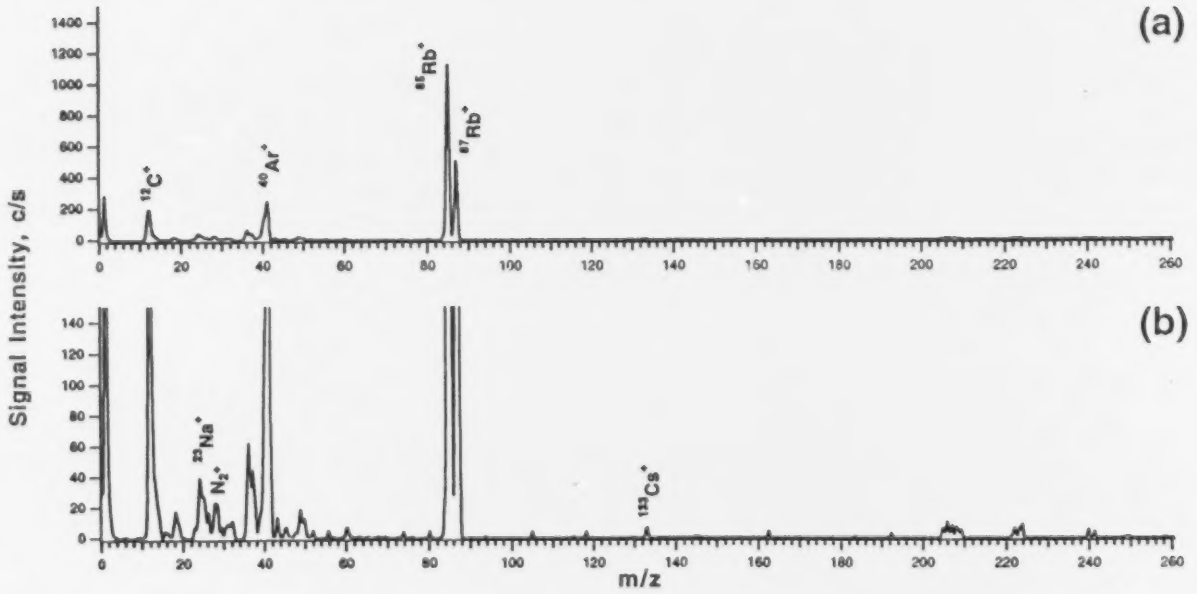

Figure 4.5 Mass spectrum of RbCl ($1x10^{-4}$ molar) in methanol/water (1:1). Argon curtain gas. (a) full scale, and (b) scale expanded by a factor of 10.

4.5 References

1. G. R. Agnes and G. Horlick, "Determination of Solution Ions by Electrospray Mass Spectrometry", Appl. Spectrosc. (accepted for publication).

2. G. R. Agnes and G. Horlick, "Electrospray Mass Spectrometry as a Technique for Elemental Analysis: Quantitative Aspects", Appl. Spectrosc. (accepted for publication).

3. G. R. Agnes and G. Horlick, Appl. Spectrosc., submitted.

4. L. Tang and P. Kebarle, Anal. Chem., **63**, 2709 (1991).

5. A. T. Blades, M. G. Ikonomou, and P. Kebarle, Anal. Chem., **63**, 2109 (1991).

6. M. G. Ikonomou, A. T. Blades, and P. Kebarle, Anal. Chem., **62**, 957 (1990).

7. J. A. Olivares and R. S. Houk, Appl. Spectrosc., **39**, 1070 (1985).

8. A. L. Gray and J. G. Williams, **2**, 599 (1987).

9. J. E. Fulford and D. J. Douglas, Appl. Spectrosc. **40**, 971 (1986).

10. E. E. Gulcicek, C. M . Whitehouse, and J. G. Boyle, "Fundamental Energy Studies of Electrospray Ions Entrained in a Free Jet Expansion" in *Proceedings of the 41st ASMS Conference on Mass Spectrometry and Allied Topics*, San Francisco, CA, May 30 - June 4, 1993 (ASMS, East Lansing, Michigan), page 746a-b.

11. F. A. Cotton and G. Wilkinson, Advanced Inorganic Chemistry, 5th edition, J. Wiley and Sons, 1988, pages 757-758.

Chapter 5

Determination of Solution Ions by Electrospray Mass Spectrometry

5.1 Introduction[3]

An ideal elemental analysis technique for solution samples would provide both qualitative and quantitative information for all solution components. Solution components include both anions and cations and they may be found in elemental, molecular, and complexed forms. The elemental analysis of solution samples is normally implemented using atomic-based elemental analysis techniques such as atomic absorption spectrometry (AAS), inductively coupled plasma-atomic emission spectrometry (ICP-AES), and inductively coupled plasma-mass spectrometry (ICP-MS). In particular, ICP-MS with its very low detection limits and wide linear dynamic range is close to the ideal technique for trace element analysis.

Unfortunately, these atomic-based techniques are just that: atomic. They provide information about the identity and quantity of the elements present in a sample. This focuses the information primarily on the metallic cations in the solution and, in general, data concerning valence state, anions, molecular form, and complexation are not directly available. To overcome this limitation, atomic methods are often coupled to separation techniques and there is a considerable body of research in this area [1-6].

Recently, electrospray mass spectrometry (ES-MS) has been applied to the generation and study of metal ion molecule clusters [7-9], to the direct determination of solution components [10,11], and as a technique for elemental analysis [12-15]. To date it has been shown that ES-MS can be used to quantitatively determine trace levels of both elemental and molecular inorganic cations and anions with ppb to sub-ppb detection limits: It can, in some cases, provide valence state information, and can be used to establish the presence of ligands and study complexation. Based on these results, electrospray mass spectrometry is a technique that could directly provide a complete picture of the cationic and anionic composition of a solution.

In this study the operation of an electrospray source in a variety of spectral acquisition modes is reported. These modes can provide a plethora of information about a solution

---

[3] A version of this chapter has been accepted for publication. George R. Agnes and Gary Horlick, Appl. Spectrosc.

sample. Three positive ion modes are described: ion cluster mode, metal ion mode, and an intermediate mode. In a positive ion mode the electrospray capillary is run at a positive potential, thus the information obtained is primarily about cationic species. Each positive ion mode has been named for the type of information available from the mass spectrum. In the ion cluster mode the electrospray source is run under so-called "mild" conditions. In general this means that relatively low voltage settings are used on the source and interface components. In this mode the mass spectra may be quite complex as the ion-solvent cluster distribution generated during the electrospray process is preserved relatively intact. With this mode it may be possible to determine the solution valence state of the cation and the data obtained in this mode are generally more representative of solution speciation. In contrast, the metal-ion mode is one in which conditions are adjusted (higher interface voltages) to decluster the cation to the bare metal ion. During this process multiply-charged cations are also reduced to the plus-one state and the resulting mass spectra are very much like those obtained in ICP-MS. This is the mode used for elemental analysis. The third mode is an intermediate mode in which partial declustering has occurred, some of the ion clusters contain counter ions (*i.e.* anions), and various charged reduced species may be observed. Thus, the mass spectra obtained in this mode provide some information about the overall solution composition.

Finally, the electrospray source can be run in a negative ion mode. In this case the electrospray capillary is run at a negative potential and the information obtained is primarily about anionic species. This mode can be used to directly observe anionic species such as the halides and metallic oxo-anions.

5.2 Experimental

The mass spectrometer used in this work was originally a SCIEX/Perkin Elmer ELAN Model 250 ICP-MS. An electrospray source was constructed in-house and attached to the front end of the mass spectrometer. Details of the interface are shown in Fig. 5.1 and the source is also described in more detail in reference 12. Sample solution is pumped through the electrospray stainless steel capillary (0.2 mm OD, 0.1 mm ID) at a rate of 10 μL/min with a syringe pump. In the positive ion mode the curtain gas was nitrogen or argon and in the negative ion mode the curtain gas was oxygen. The choice of argon or nitrogen as the curtain gas in the positive ion mode depended primarily on spectral interference considerations, while in negative ion mode, oxygen was the only curtain gas that

successfully suppressed corona formation. The diameter of the orifice in the sampling plate was 0.1 mm and the operating pressure in the first stage was 0.25 Torr. The operating pressure in the main vacuum chamber was $5x10^{-6}$ Torr.

The operating parameters for the positive and negative ion modes of the electrospray source are listed in Table 5.1. The mass spectrometer itself is switched between positive and negative ion operation by throwing two switches that are located on the ion multiplier and deflector power supply boards. This changes the polarity of the ion multiplier, the ion deflector, and appropriate ion optic elements. All solutions were made by dissolving an ACS grade salt in HPLC grade methanol. Methanol insoluble salts were first dissolved with water, then diluted with HPLC grade methanol such that the final solution electrosprayed was less than one percent water.

5.3 Results

The electrospray process is initiated with the application of a high potential to a capillary through which a solution is pumped to produce a mist of charged droplets at atmospheric pressure. An electrophoretic charging mechanism is thought to be responsible for the charging of the droplets, leaving a cation to anion imbalance, as droplets separate from the liquid jet at the end of the electrospray capillary [16]. A positively biased electrospray capillary will produce positively charged droplets. The charged droplets drift under the influence of the applied field towards the front plate. A counter flow of drying gas (curtain gas) causes the droplet charge to volume ratio to increase due to solvent evaporation. Continued solvent evaporation causes the charged droplets to become unstable and undergo Rayleigh fission, a process where nanodroplets carrying the destabilizing excess charge are expelled from the droplet such that the droplet charge to volume ratio returns to a stable state. After a few cycles of solvent evaporation-Rayleigh fission, ion-clusters are produced. Details of the mechanism as to how these gas phase ions are exactly produced are unclear and the subject of much debate. The current status of the various theories has recently been discussed and reviewed by Kebarle and Tang [17], who have also studied the electrospray process in some detail [18].

The ion clusters produced are ion-solvent clusters (*i.e.* $Co(MeOH)_n^{2+}$) and typically there is a distribution of ion-solvent clusters with n ranging from 3 or 4 to more than 12. In effect, the metal cation is surrounded by a "sphere of solvation" and it is this solvation

sphere that maintains the metal ion originally present in the solution as a stable ion in the gas phase at room temperature and at atmospheric pressure; a task that, from the point of view of an atomic spectroscopist, normally requires a high temperature source, *i.e.* an ICP. It is these gas phase ion-solvent clusters that are sampled by the atmospheric pressure sampling mass spectrometer. By varying the operating parameters of the electrospray source and the mass spectrometer inlet system the gas phase ion-solvent clusters can either be preserved or declustered giving rise to the various modes outlined in the introduction.

5.3.1 Ion-Cluster Mode

In this mode, so-called mild source and interface settings are used (see Table 5.1). The electrospray capillary voltage, the front plate voltage, and in particular, the sampling plate voltage are all relatively low compared to the other two positive ion modes.

The mass spectrum of a solution of $CoCl_2$ run under the ion-cluster mode condition is shown in Fig. 5.2. The range of solvent molecules, as detected with the mass spectrometer, is from 4 to 12 with a maximum intensity for the $Co(MeOH)_7^{2+}$ cluster. Similar results are seen for a solution of $MnCl_2$ as shown in Fig. 5.3. The spectra shown in Figs. 5.2 and 5.3 are relatively complex and would be even more so for multielement solutions. However, the information contained in the spectra correctly indicates the valence state of the metal ion in the original solution.

The exact nature of the ion-solvent cluster distribution that is observed (*i.e.* the spectra in Figs. 5.2 and 5.3) is highly dependent on the nature of the cation (*i.e.* M^+, M^{2+} or M^{3+}) and on the electrospray interface parameters, particularly the curtain gas flow rate and the sampling plate voltage. Detailed parametric studies of these solution and interface variables have been carried out and will be reported on in separate publications [19,20]. In short, as indicated by the spectra in Figs. 5.2 and 5.3, with mild interface settings for the curtain gas flow rate and sampling plate voltage, it is possible to observe solvated cations and the mass to charge ratio is directly indicative of the valence state in the original solution. It will be seen later that with appropriate source conditions, ion solvent clusters can be observed that contain anions from the solution as well as cations and solvent. Thus ES-MS has the potential to directly tell us a great deal about the composition of a solution.

All this, of course, is in marked contrast to most of the methods of introducing liquid samples into an ICP, which is now a common ion source for the elemental analysis of solution samples by mass spectrometry. With pneumatic nebulization in combination with the steps of desolvation, vaporization, and ionization/excitation in the plasma, solution sample history is erased. Moreover, electrospray is a highly efficient way to generate gas phase ions from solution. In a short but interesting discussion, Douglas [14] contrasts electrospray and ICPs as ion sources for mass spectrometry. In particular, the energy inefficiency of producing ions with an ICP is highlighted.

5.3.2 Metal-Ion Mode

For the metal-ion mode, the electrospray source and interface conditions are adjusted so that the ion-solvent clusters are declustered (increased curtain gas flow rate and sampling plate voltage). The net result is typically a bare singly charged metal ion and the resulting mass spectra, although not identical, are much like those observed in ICP-MS. The operational parameters for this mode are presented in Table 5.1 and a mass spectrum obtained for a $CoBr_2$ solution run under these conditions is shown in Fig. 5.4. Cobalt is mono-isotopic and the dominant peak in the mass spectrum is that for $^{59}Co^+$. Contrast this spectrum with that shown in Fig. 5.2. Further examples of declustered mass spectra are shown in Fig. 5.5 for Cu, Zn, Cd, and Pb. It is in this mode that the technique is most applicable to trace multielement analysis [12-15].

In contrast to the spectra shown in a preliminary report (Figs. 3 and 4 of reference 12), the oxide, hydroxide, and residual cluster levels in these spectra (Figs. 4 and 5) are quite low. The difference is simply having more experience in adjusting source and interface conditions to achieve cleaner single ion spectra. In the previous spectra the relative levels of these other species were as high as 50%. Now oxide levels for these elements are no more than 4% and for some elements they are less than 1%.

Several steps are involved in converting the original ion-solvent clusters generated by the electrospray operation into singly charged declustered metal ions. Note the parameters that have been changed to switch between these modes (Table 5.1): the electrospray capillary voltage has been increased from 3.5 kV to 5.0 kV, the front plate voltage has been increased from 700 V to 950 V, the sampling plate voltage has been increased from 35 V to 190 V, and the curtain gas flow rate has been increased from 0.4 to 0.7 l/min.

For monovalent solution ions such as the alkali metals, declustering is a relatively simple process. Some solvent molecules are removed by evaporation as the ion-solvent cluster passes through the curtain gas and then, *via* collision primarily in the zone between the sampling plate and the skimmer, they are further declustered to the free metal ion. A declustered mass spectrum of the alkali metals (Li^+, Na^+, K^+, Rb^+ and Cs^+) was shown in Fig. 2 of reference 12.

The situation is more complex for divalent solution ions such as Co^{2+}. As shown in Fig. 5.2, these ions initially retain their doubly charged state. However, as discussed in detail by Blades *et al.* [7], when these clusters lose solvent molecules by evaporation there comes a point at which there is insufficient solvation energy to maintain the metal ion in the plus-two state and charge reduction occurs with oxidation of a ligand molecule. This step is depicted by Eqn. 1.1.

$$Co(MeOH)_n^{2+} \longrightarrow Co(MeO)(MeOH)_{n-2}^{+} + H(MeOH)^{+} \qquad (5.1)$$

Note, for example, that the species $Co(MeO)(MeOH)_2^+$ is observed in the spectrum shown in Fig. 5.2. Collisions in the zone between the sampling plate and the skimmer complete the declustering of such species down to Co^+. Under the conditions for this mode there is a potential difference of 185 V between the sampling plate and the skimmer (electric field gradient about 900 V/cm). The collision processes are presented in more detail in ref. 19.

5.3.3 Intermediate Mode

Interface conditions can be adjusted to achieve an interesting mode intermediate between the ion-cluster and the bare metal ion modes. In this mode a wide range of partially declustered species are observed, most with a charge reduced metal ion and many incorporating an anion both with and without solvent. There really is a continuum of "modes" as one moves from ion-cluster conditions to the bare metal ion mode and this transition is illustrated in detail in reference 19. Spectra are presented here for one stop along the way in order to illustrate the basic nature of the species observed with intermediate conditions. Spectral features seen in this mode for solutions of $CoCl_2$, $Co(NO_3)_2$, $CoBr_2$, and $CoSO_4$ are shown in Fig. 5.6. These data were measured simply by reducing the curtain gas flow rate from 0.4 L/min to 0.1 L/min while retaining the other settings appropriate for the metal ion mode (see Table 5.1).

Ion-counter ion clusters are observed for the Cl^-, NO_3^- and Br^- salts (but not for the SO_4^{2-} salt) along with a range of partially declustered cobalt species. The absence of sulfate clusters can be rationalized on the basis that, if they exist, they would be neutral and/or negative.

Overall, these spectra are quite complex, and it is difficult to explain the geneses of all the observed species. Certainly it appears that $Co(MeO)(MeOH)_1^+$ is undergoing collision induced dissociation to yield $CoH(MeOH)_1^+$ and CH_2O. Further declustering would yield $Co(H)^+$ which is a major species in each spectrum shown in Fig. 5.6. Also, the CoO^+ peak is much stronger in the mass spectrum for $Co(NO_3)_2$ (Fig. 5.6b) than it is in the other spectra, and as well there is a peak for $CoO(MeOH)_1^+$ at m/z 107 that is not present in the other spectra in Fig. 5.6. It is speculated that these species arise from the collisional breakdown of the $Co(NO_3)(MeOH)_1^+$ cluster:

$$Co(NO_3)(MeOH)_1^+ \longrightarrow CoO(MeOH)_1^+ + NO_2 \qquad (5.2)$$

$$CoO(MeOH)_1^+ \longrightarrow CoO^+ + MeOH \quad (5.3)$$

The spectra shown in Fig. 5.6 indicate that this ion-counter ion mode is a complex mode with several species present that are the result of a mixture of ion pairing, charge reduction, and incomplete declustering reactions. However it does give a picture of some of the stages that an ion-solvent cluster proceeds through as it is declustered and these data may provide some information related to the anionic composition of the original solution. A more complete parameter study following the changes that occur in the spectra in moving from the ion cluster mode to the metal ion mode is presented in reference 19.

Finally mass spectra for the three positive ion spectral acquisition modes for ES-MS are illustrated in Fig. 5.7 for a $1x10^{-4}$ molar solution of $MnCl_2$. For a set of measurements extending over about three minutes, the solution charge state of the analyte, associated anions and quantitation of the analyte can be attained while consuming as little as 30 μL of sample solution. If the solution assay is targeted for a single data point, such as the concentration of the analyte in solution, as little as 1 μL of solution need be consumed. The three spectral acquisition modes described could, as well, be complimented with a flow injection front end to the electrospray source.

5.3.4 Negative Ion Mode

While the ion-counter ion positive ion mode can provide some indication of the anionic composition of the solution, the measurement of anions can be directly accomplished with negative ion mode electrospray mass spectrometry. The electrospray source and interface operational parameters for negative mode electrospray are listed in Table 5.1 and as well the mass spectrometer detector and deflector power supply boards must be switched to negative ion mode. Initial experiments indicated that the wide range of operational conditions possible with positive ion mode electrospray is not realized for negative ion mode electrospray. There was a very narrow electrospray capillary voltage window (-3.0 to -3.2 kV) within which a stable ion signal was possible. Increasing the electrospray capillary voltage beyond -3.2 kV initiated a discharge. The fact that the range of operational parameters with respect to the biasing of the electrospray capillary for negative ion mode electrospray is not as large as positive mode electrospray, means that the range and number of modes observed in positive electrospray may not be realized for negative ion mode ES-MS. As well, stable negative ion mode electrospray was only possible when an electronegative gas, such as oxygen, was used as the curtain gas. The electrospray source was not stable when either nitrogen or argon was used as the curtain gas when operated in the negative ion mode.

Three negative ion mode spectra are shown in Fig. 5.8. The mass spectrum for an equimolar mixture of the halides (F^-, Cl^-, Br^-, and I^-) is shown in Fig. 5.8a. The concentration of each component was $1x10^{-4}$ molar. The 3s detection limits for these species are 0.1 ng/L for $^{19}F^-$, 0.03 ng/L for $^{35}Cl^-$, 0.06 ng/L for $^{79}Br^-$, and 0.09 ng/L for $^{127}I^-$. These detection limits are at least one order of magnitude lower than those reported for negative ion ICP-MS [21,22].

The mass spectrum of a $1x10^{-4}$ molar solution of NaSCN is shown in Fig. 5.8b and the thiocyanate anion is clearly observed. Finally, the mass spectrum of $1x10^{-4}$ molar HNO_3 is shown in Fig. 5.8c. The data indicate that NO_3^- is being converted to NO_2^-. The NO_2^- species may be the result of collisions in the jet expansion and/or electrochemical reduction of the nitrate may also be occurring.

Many elements form oxo-anions and these can be measured using negative ion mode ES-MS. Two examples are presented in Fig. 5.9. The negative ion mass spectrum resulting from electrospraying a $1x10^{-4}$ molar solution of $K_2Cr_2O_7$ is shown in Fig. 5.9a.

The main species observed is chromate, $^{52}CrO_3^-$. It is not known if the dichromate ion was collisionally broken down or reduced as a result of the electrospray process. The negative ion mass spectrum of a $1x10^{-4}$ molar solution of $KMnO_4$ is shown in Fig. 5.9b and the dominant peak is for permanganate. It was noticed that permanganate ions held in the syringe reservoir were reduced to manganese dioxide over a period of approximately ten minutes when the electrospray capillary was biased to -3 kV. Therefore it is also possible that the dichromate ion was reduced to chromate ions as a result of an electrochemical reaction at the electrospray capillary and not as a consequence of the ion evaporation step or collisions.

Some elements form both oxo-cations and oxo-anions. One such element is vanadium. In our preliminary report [12] we showed a positive ion mode mass spectrum of a solution of vanadyl sulfate. That spectrum is shown in Fig. 5.10a. A charge reduced form of the vanadyl cation is observed. The negative ion mode mass spectrum of a solution of sodium vanadate ($NaVO_3$) is shown in Fig. 5.10b. In this case the vanadate anion is directly observed.

5.4 Conclusions

For an increasing number of analytical situations it is important to know the chemical form (*i.e.* cation, oxo-cation, anion, and oxo-anion) and the valence state of an element, that is to distinguish Cr(III) from Cr(VI), Mn(II) from Mn(VII) or V(IV) from V(V). By controlling the operating conditions of an electrospray source and by combining the results obtained for the negative ion mode and for the various positive ion modes, it is clear that this type of information can be determined about the ionic composition of solution samples by ES-MS. The mass spectral results presented in this report emphasize the qualitative measurement capability of "elemental" ES-MS. Results concerning the quantitative elemental analysis capabilities of ES-MS were reported in a separate study [13]. The quantitative results presented in that study and those presented by Corr and Douglas [15] indicate that the quantitative analytical capability of ES-MS is comparable to ICP-AES and may even approach that of ICP-MS. Thus, ES-MS should become an effective technique for the qualitative and quantitative analysis of solution samples.

Table 5.1. Operational Parameters of the Elemental ES Source

	Positive Ion Modes			Negative Ion Mode
Parameter	Ion Cluster Mode	Metal Ion Mode	Ion-Counter Ion Mode	
ES Capillary (kV)	3.5-4.0	5.0	5.0	-3.0
Front Plate (V)	700	950	950	-950
Sampling Plate (V)	35-40	190	190	-80
Skimmer (V)	8	5	5	-5
Curtain Gas Flow Rate (L/min)	0.4	0.7	0.1	0.4
Cylinder Lens (V)	0	-3.0	-3.0	0

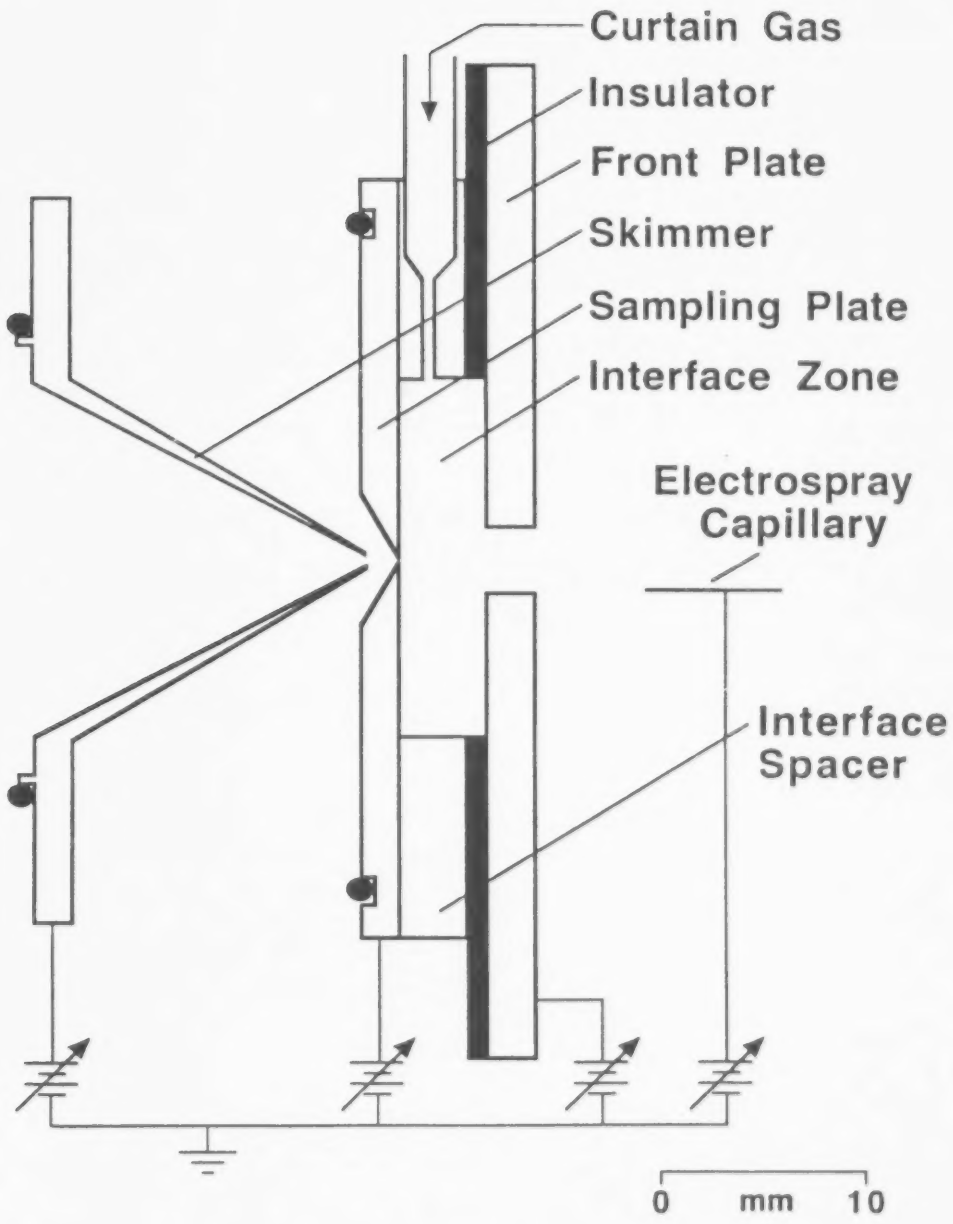

Figure 5.1 Schematic diagram of the electrospray source and interface.

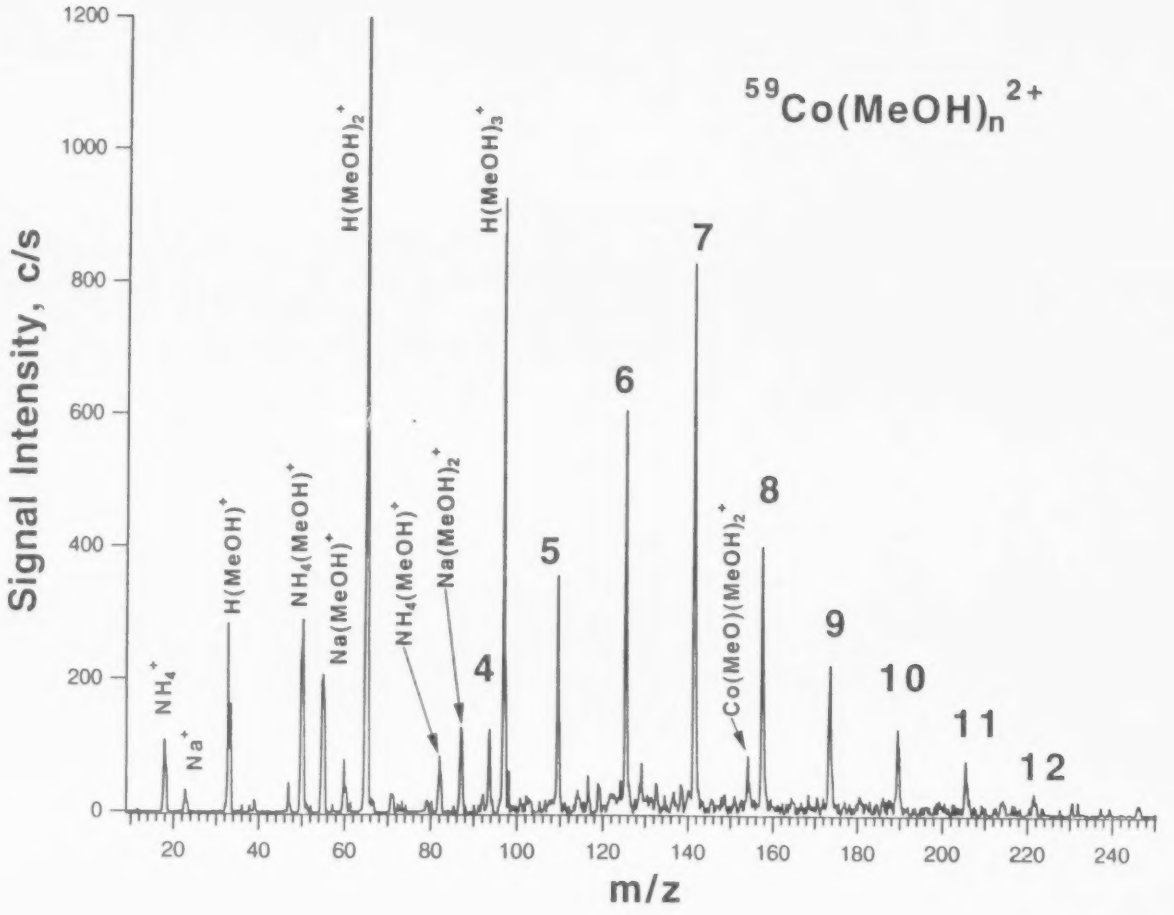

Figure 5.2 Mass spectrum of a cobalt chloride solution ($CoCl_2$, $1x10^{-3}$ molar) in the ion cluster mode.

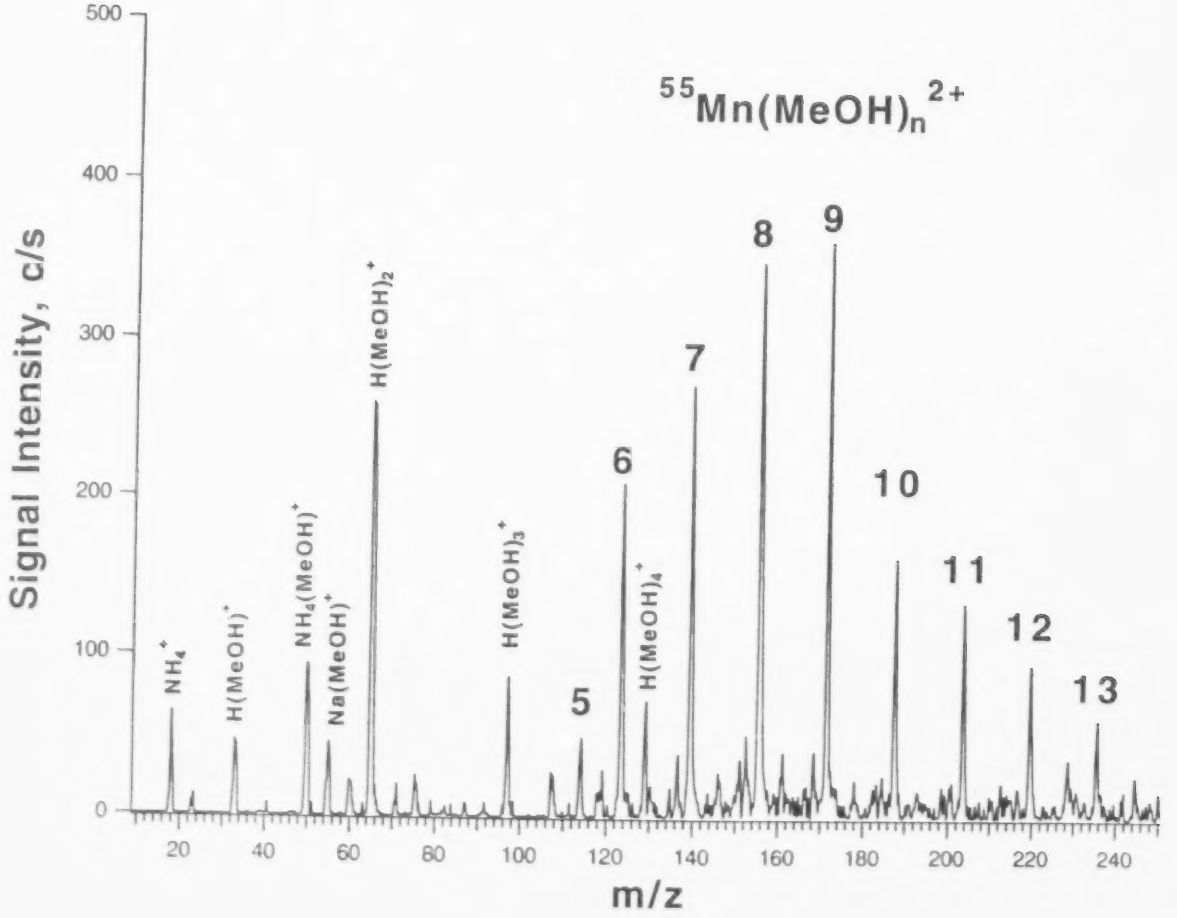

Figure 5.3 Mass spectrum of a manganese chloride solution ($MnCl_2$, $1x10^{-4}$ molar) in the ion cluster mode.

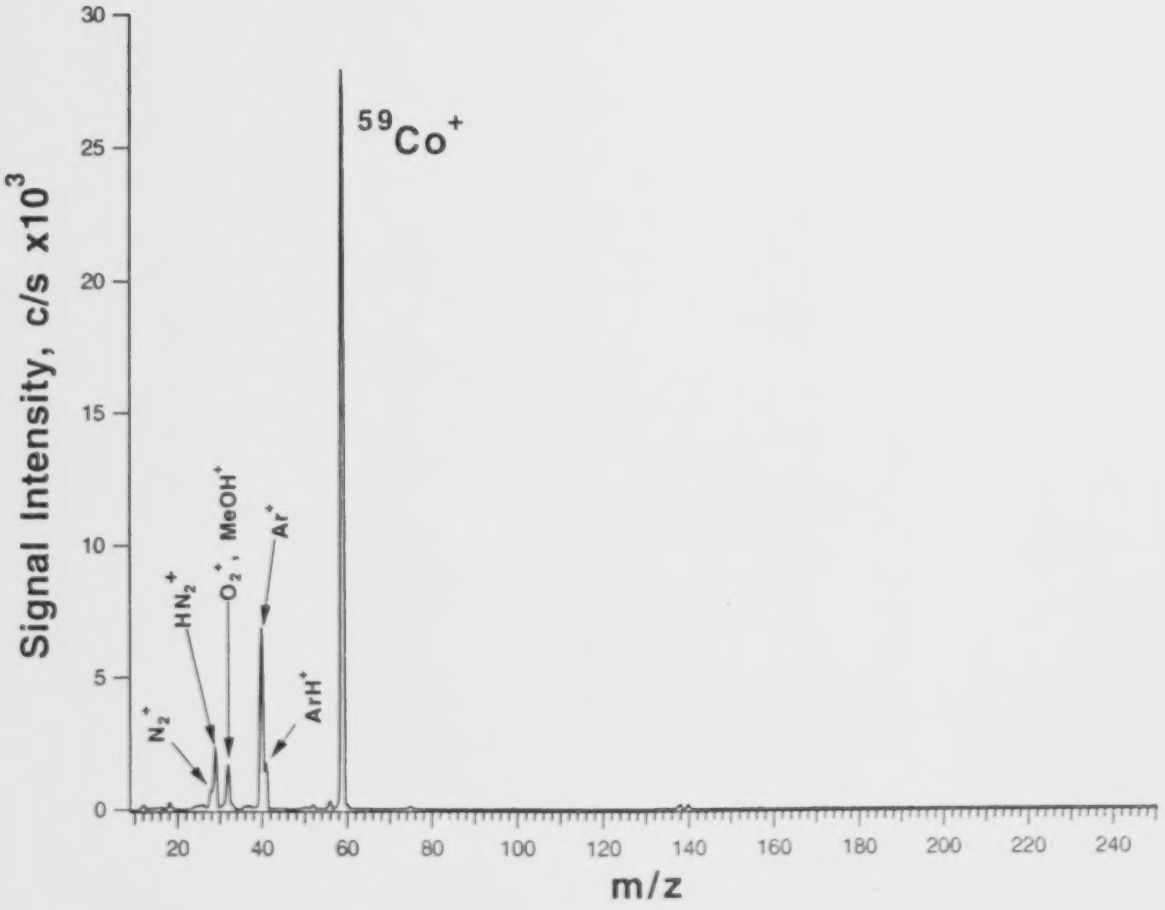

Figure 5.4 Mass spectrum of a cobalt bromide solution ($CoBr_2$, $1x10^{-4}$ molar) in the metal ion mode.

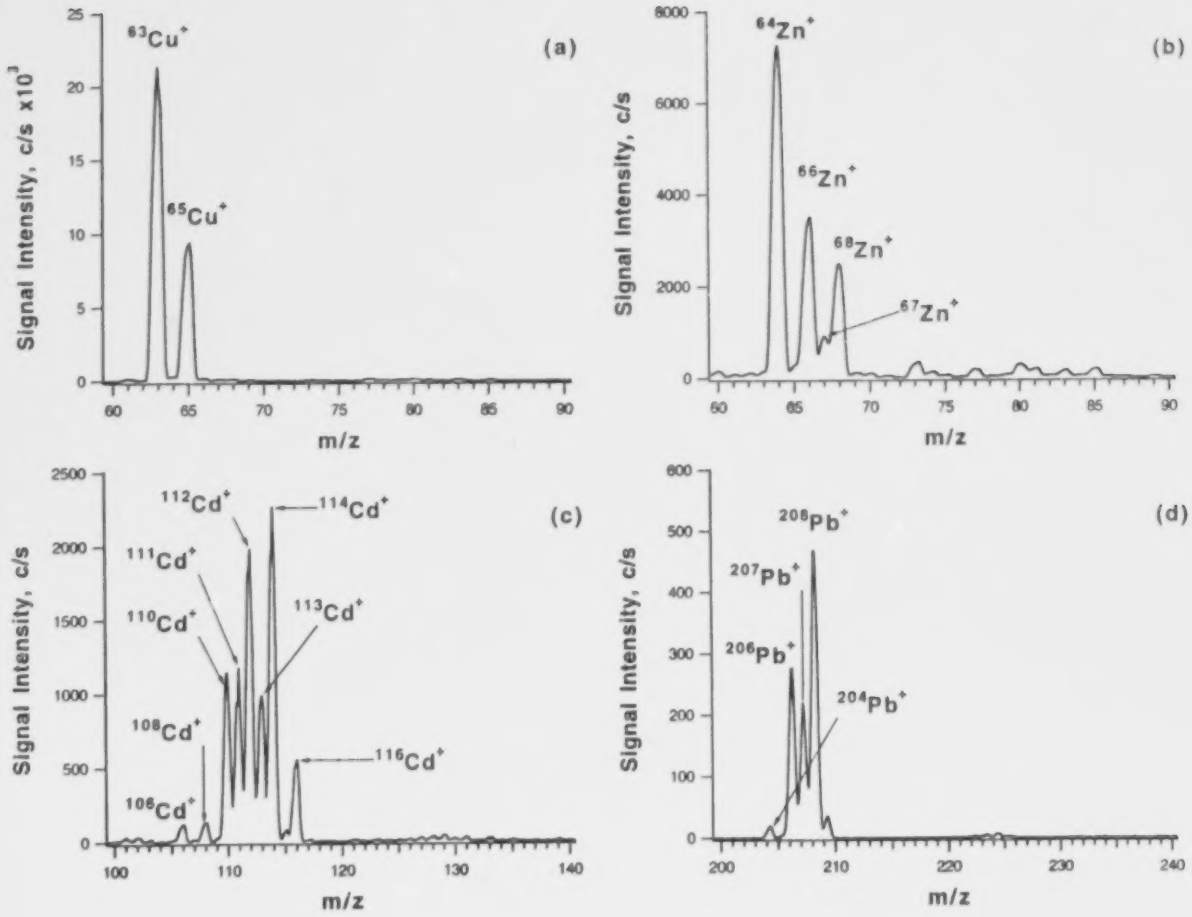

Figure 5.5 Mass spectra for (a) copper, (b) zinc, (c) cadmium, and (d) lead solutions ($1x10^{-4}$ molar) in the metal ion mode.

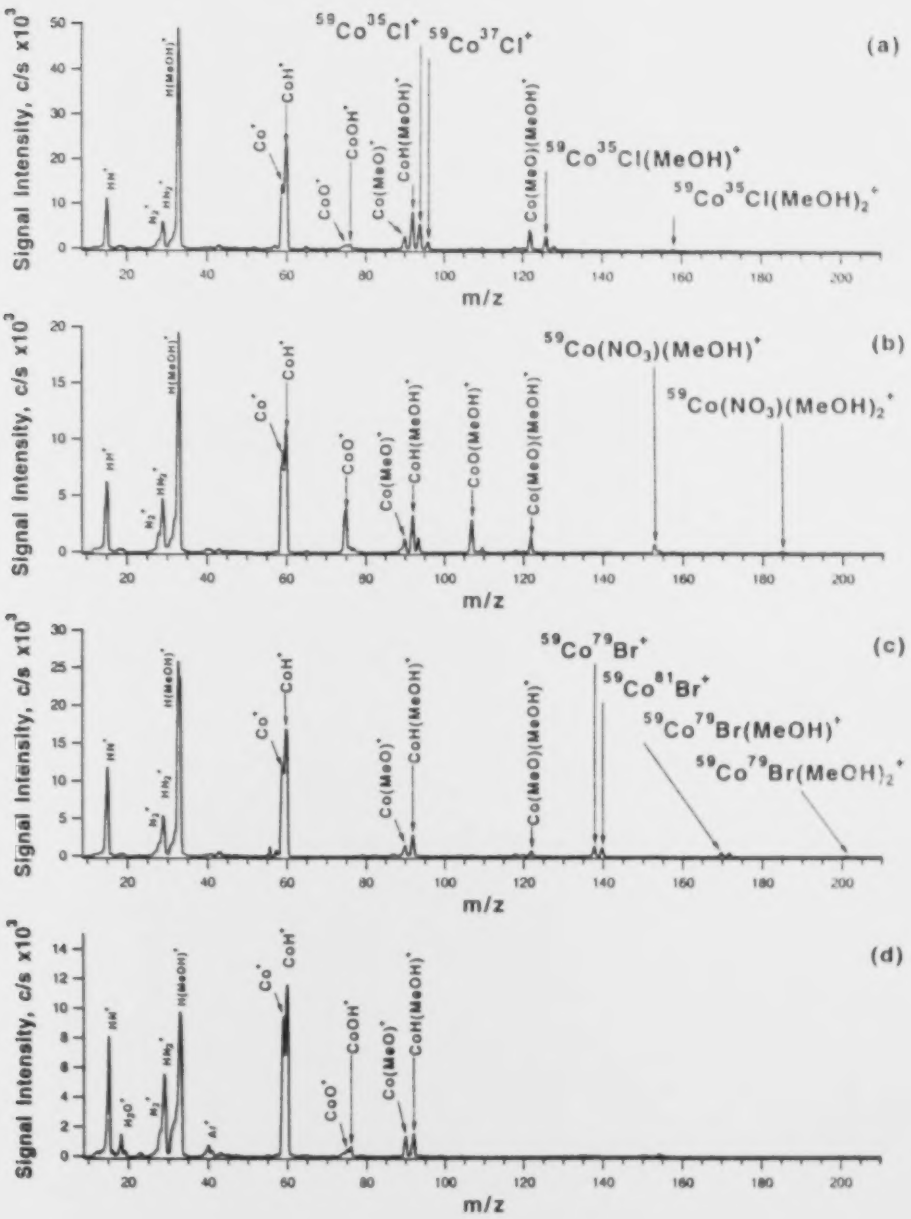

Figure 5.6 Mass spectra of (a) cobalt chloride, (b) cobalt nitrate, (c) cobalt bromide, and (d) cobalt sulfate solutions (1×10^{-3} molar) with intermediate conditions.

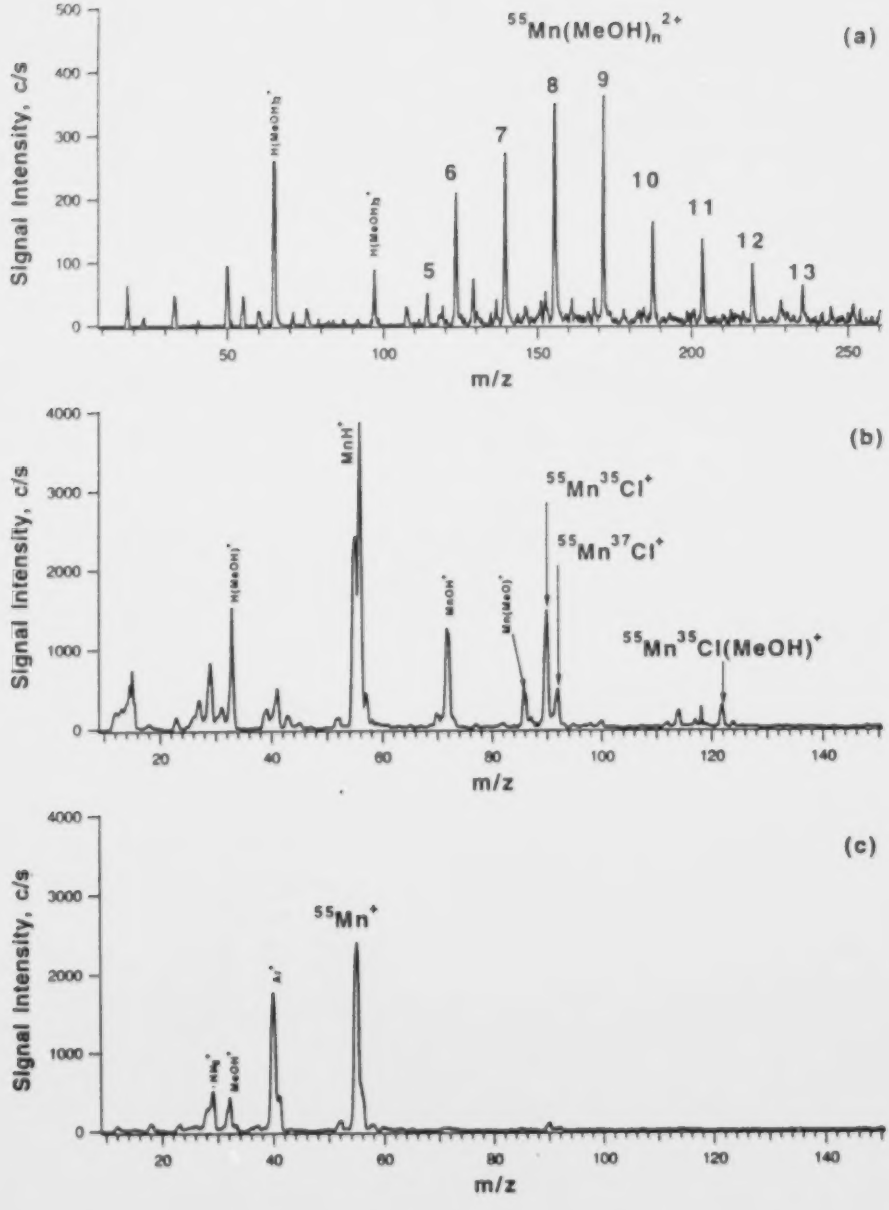

Figure 5.7 Mass spectra of a manganese chloride solution ($1x10^{-4}$ molar) acquired with (a) the ion cluster mode, (b) intermediate conditions, and (c) the metal ion mode.

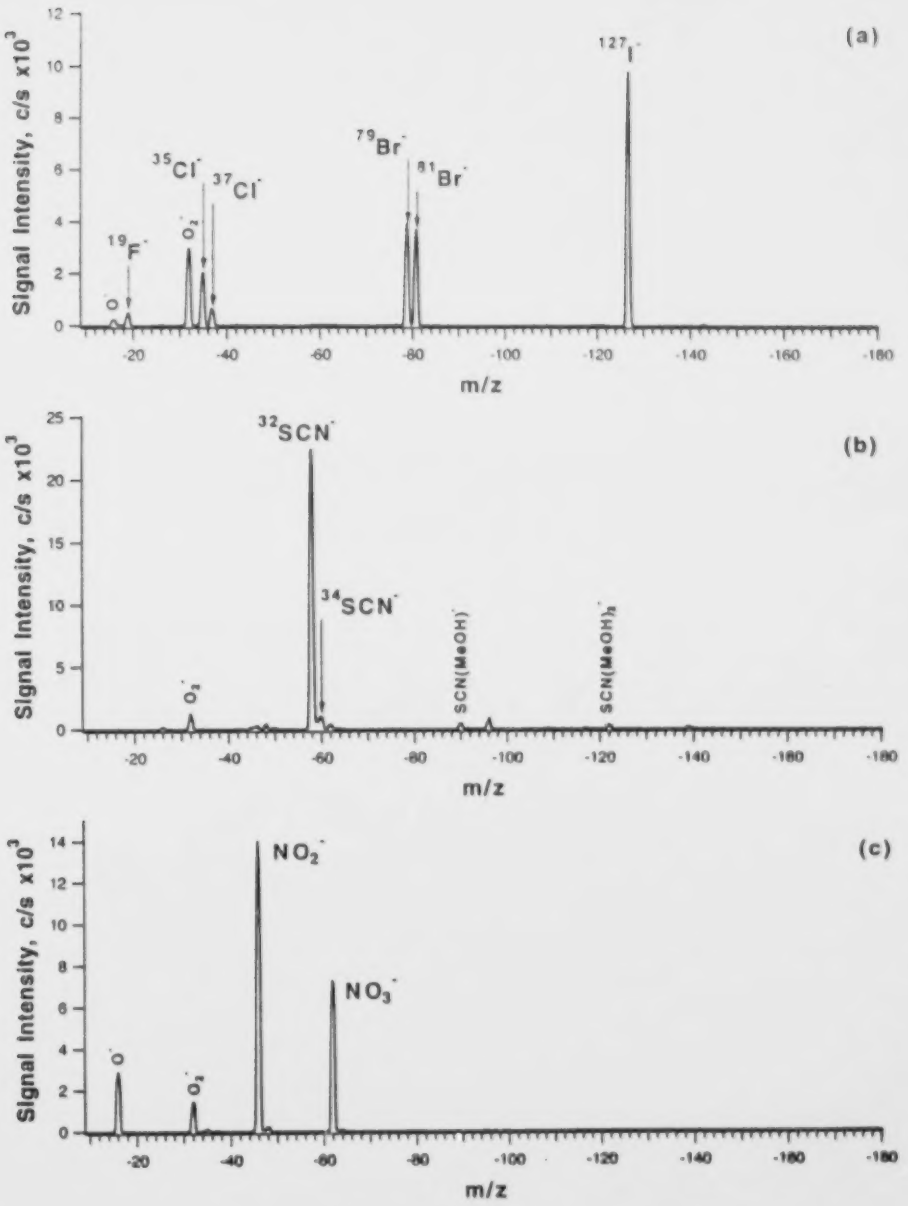

Figure 5.8 Negative ion mode mass spectra for (a) a solution containing F^-, Cl^-, Br^-, and I^- (each halide is $1x10^{-4}$ molar), (b) a solution of sodium thiocyanate ($1x10^{-4}$ molar), and (c) a $1x10^{-4}$ molar solution of nitric acid.

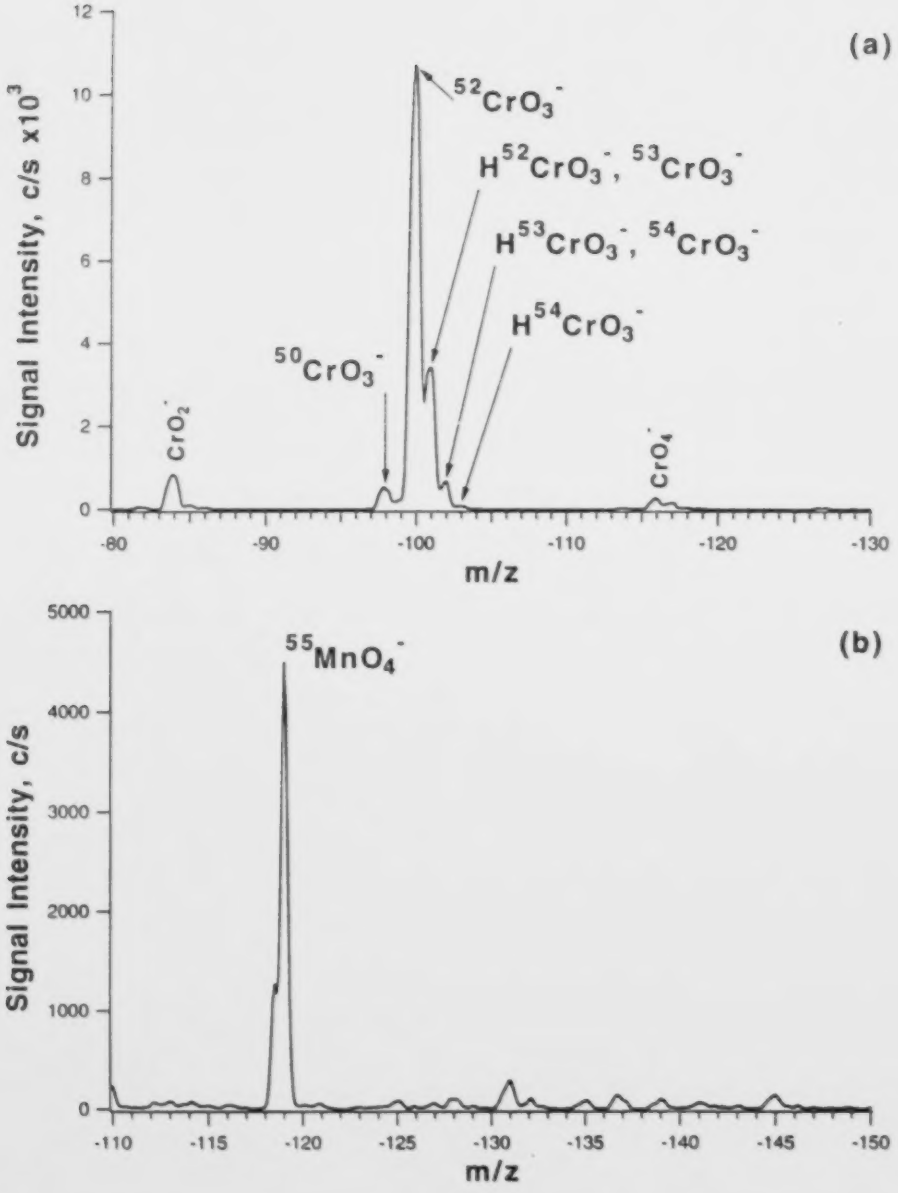

Figure 5.9 Negative ion mode mass spectra for solutions ($1x10^{-4}$ molar) of (a) potassium dichromate and (b) potassium permanganate.

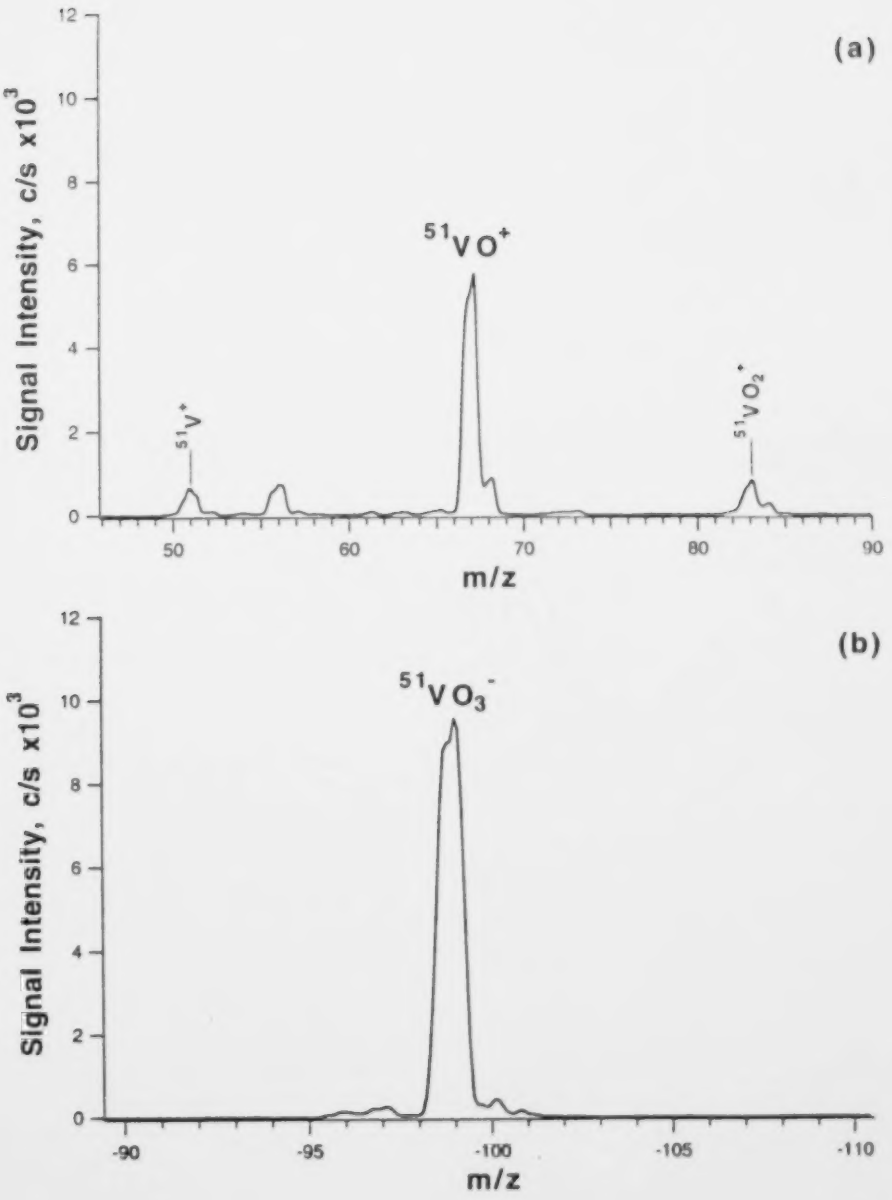

Figure 5.10 (a) Positive ion mode mass spectrum of vanadyl sulfate ($VO(SO_4)$) and (b) negative ion mode mass spectrum of sodium vanadate ($NaVO_3$). Both compounds are at $1x10^{-4}$ molar.

5.5 References

1. N. P. Vela, L. K. Olson, and J. A. Caruso, Anal. Chem. **65**, 585A (1993).

2. V. V. Salov, J. Yoshinaga, Y. Shibata, and M. Morita, Anal. Chem.**64**, 2425 (1992).

3. A. Al-Rashdam, N. P. Vela, J. A. Caruso, and D. T. Heitkember, J. Anal. At. Spectrom. **7**, 551 (1992).

4. C. P. Hanna, J. F. Tyson, and S. McIntosh, Anal. Chem. **65**, 653 (1993).

5. A. Siriraks, H. M. Kingston, and J. M. Riviello, Anal. Chem. **62**, 1185 (1990).

6. W. L. Shen, N. P. Vela, B. S. Sheppard, and J. A. Caruso, Anal. Chem. **63**, 1491 (1991).

7. A. T. Blades, P. Jayaweera, M. G. Ikonomou, and P. Kebarle, Int. J. Mass Spectrom. and Ion Processes **102**, 251 (1990).

8. A. T. Blades, P. Jayaweera, M. G. Ikonomou, and P. Kebarle, Int. J. Mass Spectrom. and Ion Processes **101**, 325 (1990).

9. A. T. Blades, P. Jayaweera, M. G. Ikonomou, and P. Kebarle, J. Chem. Phys. **92**, 5900 (1990).

10. Z. L. Cheng, K. W. M. Siu, R. Guevremont, and S. S. Berman, J. Am. Soc. Mass Spectrom. **3**, 281 (1992).

11. Z. L. Cheng, K. W. M. Siu, R. Guevremont, and S. S. Berman, Organic Mass Spectrom. **27**, 1370 (1992).

12. G. R. Agnes and G. Horlick, Appl. Spectrosc. **46**, 401 (1992).

13. G. R. Agnes and G. Horlick, "Electrospray Mass Spectrometry as a Technique for Elemental Analysis: Quantitative Aspects", Appl. Spectrosc. (accepted for publication).

14. D.J. Douglas, "Fundamental Aspects of Inductively Coupled Plasma Mass Spectrometry", in *Inductively Coupled Plasmas in Analytical Atomic Spectroscopy*, A. Montaser and D.W. Golightly, Eds. (VCH Publishers, New York, 1992), 2nd ed., p. 642.

15. J. J. Corr and D. J. Douglas, "Elemental Ion Spray-Mass Spectrometry: Analysis of Solutions of Metal Salts", in *Proceedings of the 41st ASMS Conference on Mass Spectrometry and Applied Topics*, San Francisco (1993), p. 732a.

16. M. G. Ikonomou, A. T. Blades, and P. Kebarle, Anal. Chem. **63**, 189 (1991).

17. P. Kebarle and L. Tang, Anal. Chem. **65**, 972A (1993).

18. L. Tang and P. Kebarle, Anal. Chem. **65**, 3654 (1993).

19. G. R. Agnes and G. Horlick, Appl. Spectrosc. (submitted for publication).

20. I. Stewart and G. Horlick, J. Anal. At. Spectrosc. (submitted for publication).

21. G. H. Vickers, D. A. Wilson, and G. M. Hieftje, Anal. Chem. **60**, 1808 (1988).

22. J. E. Fulford and E. S. K. Quan, Appl. Spectrosc. **42**, 425 (1988).

Chapter 6

Effect of Operating Parameters on Analyte Signals in Elemental Electrospray Mass Spectrometry

6.1 Introduction[4]

Electrospray is now widely used as an ion source for mass spectrometry and the present understanding of the mechanism by which gas phase ions are produced by an electrospray source has been reviewed by Kebarle and Tang [1]. A diagram of an electrospray ion source and interface is shown in Fig. 6.1. A solution containing an electrolyte that is pumped through a capillary held at a high voltage relative to another conductor will produce charged droplets. The charged droplets contain an excess of cations if the capillary is biased positively. The charged droplets drift toward the front plate and some of the charged droplets pass into the interface zone, the region between the sampling plate and the front plate (see Fig. 6.1). This zone is kept dry with respect to solvent vapor by adjustment of the flow rate of curtain gas. In this region the droplets undergo Rayleigh fission (sometimes termed electrohydrodynamic disintegration) producing even smaller droplets. Rayleigh fission has been measured by Taflin *et. al.* where a charged droplet expels 15% of its excess charge and 2% of its mass in the process [2]. The final stage in which gas phase ions are produced from the charged droplets remains a mechanistic mystery [3-5] although two theories are described in the literature. The single ion droplet theory (SIDT) [6-8] is a continuation of the Rayleigh fissional process to the limit where droplets containing a single ion are produced. The other mechanism is the ion evaporation theory (IET) [9,10] which describes ion desorption from the surface of a charged droplet (number of excess charges ~ 80 and a radius of ~ 8 nm). The ion is assumed to be solvated by a coordination sphere during the desorption step. Therefore the difference between the SIDT and IET is that either micro droplets or individual ion clusters are respectively created at atmospheric pressure by an electrospray source.

The work on inorganic electrospray mass spectrometry (ES-MS) by Kebarle and co-workers showed that inorganic ions, other than the alkali metals, were amenable to this technique [11-14]. Their results were significant in that earlier attempts to observe divalent and trivalent inorganic solution ions were unsuccessful [10,15].

---

[4] A version of this chapter has been submitted for publication. George R. Agnes and Gary Horlick, Appl. Spectrosc.

Following on the results of Kebarle *et al.*, we initiated a study of ES-MS with the purpose of investigating its applicability to elemental analysis. Our investigations of ES-MS have shown that this technique provides a rich window through which solution composition can be probed. The electrospray source can be adjusted to not only provide an elemental analysis of a solution sample but also to provide unique information concerning the environment of analyte ions in solution (solution state valency, molecular form, and composition of the solvation sphere (*i.e.*. ligands, counter-ions)) [16,17]. This current study was undertaken to delineate the effect of the various electrospray source parameters on the nature of the ions detected.

6.2 Experimental

All experiments were performed on a Perkin-Elmer/SCIEX ELAN Model 250 ICP mass spectrometer. This mass spectrometer is limited to the study of ions with a mass to charge ratio < 300. The ICP ion source normally coupled to this spectrometer was replaced with an in-house constructed electrospray source. A schematic of the electrospray source employed in this study is depicted in Fig. 6.1. This ion source has been described in detail elsewhere [16,17]. All results presented in this report pertain to positive ion ES-MS and the voltage bias applied to each conductor in the electrospray source was referenced to ground potential.

A variety of inorganic ions were employed as analytes in an effort to minimize errors of generalization. All solutions were prepared by dissolving an ACS grade salt in distilled/deionized water, then diluting with HPLC grade methanol such that the final solution electrosprayed was one percent water and the analyte ion concentration was $1x10^{-4}$ molar. All solutions electrosprayed contained a single salt unless otherwise stated. The curtain gas was either nitrogen or argon. An integration time of 0.1 sec/point was employed and ten points/amu were measured unless otherwise stated.

6.3 Results and Discussion

6.3.1 The Alkali Metals

To set the stage for the nature of the data to be discussed throughout this paper, a mass spectrum of lithium chloride is shown in Fig. 6.2. A range of lithium ion species are present in the mass spectrum. Depending on the conditions of the electrospray source, the population of lithium clusters ($^{7}Li(MeOH)_m(H_2O)_n^+$) can be increased and as well the population distribution can be shifted to higher values of m and n than what is shown in Fig. 6.2. With another set of operating conditions, the relative abundance of these clusters in the mass spectrum can be strongly attenuated such that the ratio of the signal intensity sum of all lithium clusters to the signal intensity of the lithium ion ($^{7}Li^+$) approaches zero. Major background ions are also labeled in Fig. 6.2. $H(MeOH)^+$, NH_4^+, and $^{23}Na^+$ are almost always present in ES mass spectra. The presence of an electric discharge (corona) at atmospheric pressure causes $H(MeOH)_m^+$ to become the major ion in the mass spectrum.

The parametric study was initiated by varying the electrospray capillary voltage and the flow rate of curtain (drying) gas. The effect of varying the electrospray capillary voltage was evaluated (Fig. 6.3) while spraying an equimolar solution of the alkali metals and holding all other electrospray source parameters constant. The alkali metals all responded similarly, and only the rubidium signal is plotted in Fig. 6.3. The electrospray source was operated such that very few analyte clusters were present. In fact, the alkali metals were chosen as analytes for this study based on the relative ease with which these ions can be declustered (e.g. > 99 % of the total rubidium signal was due to $^{85}Rb^+$). The relative signal intensities of the alkali metals were 3 : 2 : 1 for $^{85}Rb^+ \sim {}^{39}K^+ > {}^{23}Na^+ \sim {}^{133}Cs^+ > {}^{7}Li^+$. The signal for the background ion $H(MeOH)_1^+$ is also plotted in Fig. 6.3. Each data point shown in Fig. 6.3 corresponds to the mean of ten measurements. As the electrospray capillary voltage is increased from 3.0 to 4.6 kV, the analyte and background signal levels remain constant, and low. An increase of 200 volts to bring the electrospray capillary voltage bias to 4.8 kV leads to the maximum analyte signal. A further increase in the electrospray capillary voltage bias promotes the formation of a corona discharge causing suppression of the analyte signal. Yamashita *et. al.* showed similar effects of the electrospray capillary applied potential on the electrospray mass spectrum for positive and negative ES-MS [15,18]. Ikonomou *et. al.* investigated electrospray capillary tip design, composition, positioning, and voltage bias in detail [19-21]. In particular, they found that

an electrospray capillary tip with a large outer diameter (1.5 mm) allowed the maximization of the analytical signal before the onset of a corona discharge [20].

The next variable that was investigated was the effect of the curtain gas flow rate. The lithium signal is negligible at flow rates less than 0.1 lpm (see Fig. 6.4). A sharp threshold in the lithium ion signal level occurs at a flow rate of about 0.2 lpm, above which the total lithium ion signal (sum of all lithium species in the mass spectrum) levels off. Also included in Fig. 6.4 are data for the major individual lithium species in the mass spectrum. The signal intensity of $^{7}Li(MeOH)_1^+$ is shown to abruptly increase at 0.15 lpm to a maximum at 0.2 lpm and thereafter further increases in the curtain gas flow rate cause the $^{7}Li(MeOH)_1^+$ signal to fall off. The $^{7}Li^+$ signal intensity continuously increases over the same curtain gas flow rate range. The increase of the signal intensity of the $^{7}Li(H_2O)_1^+$ is due to trace amounts of water ligand in the curtain gas which preferentially displaces methanol in the cluster at atmospheric pressure [12]. At low curtain gas flow rates between 0.085 lpm and 0.15 lpm (Fig. 6.4), the sum of lithium signals is comprised primarily of large lithium solvent clusters ($^{7}Li(MeOH)_n^+$, n=3-6).

The data plotted in Fig. 6.4 were acquired with the sampling plate biased at 40 V. An electric field strength ~ 125 V/cm in the region between the sampling plate orifice and the skimmer cone orifice generates mild declustering in this zone. The pressure in this zone is nominally 0.3 Torr. The electric field strength of 125 V/cm used to acquire the data in Fig. 6.4 is small compared to the relatively large ~ 900 V/cm field strength (sampling plate biased to 190 V) used when complete removal of the solvation sphere from the ion is required.

An equimolar solution ($1x10^{-4}$ molar) containing the alkali metals (Li, Na, K, Rb, and Cs) was used as the test solution for all data shown in Fig. 6.5. Note that relatively high bias conditions were used for the sampling plate (190 V). Again, the basic behavior of the alkali metals was similar and data are presented only for rubidium. $^{85}Rb^+$ and $H(MeOH)_1^+$ signals are shown in Fig. 6.5a as a function of the front plate voltage bias. Increasing the front plate voltage bias from 200 V to 800 V causes a steady increase in the $^{85}Rb^+$ signal. Between 800 V and 1200 V applied bias the $^{85}Rb^+$ signal remains constant, but at 1300 V applied bias, the $^{85}Rb^+$ signal drops precipitously. The other alkali metals present in the test solution behaved in an identical fashion. Over the same front plate voltage range, the $H(MeOH)_1^+$ signal response curve is at a high level initially, but decreases with increasing front plate voltage bias. The trend in the signal response is that analyte signal intensities

increase while the background signal intensities decrease as the front plate voltage bias is increased. A rationale for this behavior is that increasing the front plate voltage bias decreases the electric field gradient between the electrospray capillary tip and the front plate, which amounts to reduced relative bias on the electrospray capillary. Increasing the front plate voltage bias to 1300 V created conditions where the electrospray process was sustained, but without the presence of a discharge (*i.e.* similar to Fig. 6.3 at electrospray capillary voltage biases less than 4.4 kV).

Analyte and background signal responses to changes of the sampling plate voltage are shown in Fig. 6.5b. Analyte signal rises to a maximum level at a sampling plate voltage bias of 150 V. From 150 V to 350 V, the analyte signal decreases slowly. Over the same sampling plate voltage bias range, the background signal decays much more rapidly. At sampling plate voltage biases greater than 350 V, an electric discharge is formed between the sampling plate and skimmer, causing atmospheric gases (the curtain gas) entrained in the jet expansion to become ionized. Analyte ions are not detected under these conditions.

The skimmer and barrel ion extractor serve as simple ion optic elements facilitating the transfer of atmospheric pressure ions into the mass spectrometer. Signal dependence on the voltage bias of these elements is shown in Figs. 6.5c and 6.5d. The skimmer voltage bias was optimal at 4.5 V and the barrel ion extractor at -3.5 V. However, it should be noted that when low bias conditions were used for the sampling plate (40 V) so as to preserve analyte ion clusters, the optimal skimmer voltage was 9.0 V and the barrel ion extractor voltage was 0 V.

Investigation of the effect of the electrospray source parameters on the nature of the mass spectrum indicated a correlation between the flow rate of curtain gas and the sampling plate voltage. The spectra in Fig. 6.6 will be used to illustrate the correlation between these two variables. The spectrum shown in Fig. 6.6a was acquired with the flow rate of curtain gas set to 0 lpm and with the sampling plate bias at 40 V (electric field gradient in the jet expansion ~ 150 V/cm). The total potassium signal intensity is ~ 750 counts/sec (note that the vertical axes in Fig. 6.6 are not scaled the same). Increasing the curtain gas flow rate to 0.58 lpm, with no change in the sampling plate voltage bias (Fig. 6.6c) increases the total potassium signal intensity to ~ 1.1×10^5 counts/second, representing an increase of approximately 2.5 orders of magnitude. Conversely, a similar increase in the potassium signal can also be accomplished by increasing the sampling plate voltage to 190 V (electric

field gradient in the jet expansion ~ 900 V/cm), while leaving the flow rate of curtain gas at 0 lpm. Compare Fig. 6.6a to Fig. 6.6b and Fig. 6.6b to Fig. 6.6c.

Absence of potassium clusters from the mass spectrum is not realized until both the flow rate of curtain gas and sampling plate voltage bias are set to high values (see Fig. 6.6d). The curtain gas employed for the data shown in Fig. 6.6d was argon. The lack of baseline resolution in Fig. 6.6d between the isotopes of potassium is attributed to the generation of $^{40}Ar^+$. The Ar^+ is likely formed in the jet expansion by electron impact ionization. The source of the electrons is likely sputtered from positive ions impacting on the surface of the skimmer. The $^{40}Ar^+$ ion signal was dependent on the skimmer voltage bias. Also note that an optimized flow rate of curtain gas and sampling plate voltage bias that discriminates analyte ion clusters relative to the bare metal ion signal does so at some expense to the metal ion signal.

The mass spectra shown in Figs. 6.6a and 6.6c were acquired at different times than the mass spectra shown in Figs. 6.6b and 6.6d. The reader is cautioned against making detailed direct analyte signal intensity comparisons between these spectra as ES-MS sensitivities were not reproducible from day to day. Relative sensitivities within a mass spectrum were, however, very reproducible.

Reflection upon the data contained in Fig. 6.6 as to the nature of the potassium at atmospheric pressure is informative in that the two distinct interface parameters may be used independently to define the path that is followed by the potassium clusters as they enter the mass spectrometer. Either a high flow rate of curtain gas (Fig. 6.6c) or energetic collisions in the jet expansion (Fig. 6.6b) may be used to generate a similar result.

When the curtain gas flow rate is sufficient (Fig. 6.6c), the small charged droplets are caused to release gas phase ions at atmospheric pressure. The two theories of ion release from a charged droplet are the single ion droplet theory (SIDT) or the ion evaporation theory (IET) which can be used to predict either a micro droplet containing a single charge (potassium) or ejection of a potassium ion solvated by its solvation sphere respectively. A micro droplet containing a single potassium ion may be represented as $K(MeOH)_m^+$ where $m > 7$ and the range of m is large. A potassium ion solvated by its solvation sphere may be represented as $K(MeOH)_6^+$.

If the IET mechanism was responsible for the gas phase ion production from the charged droplets, $K(MeOH)_6^+$ would have been readily detected under the conditions of Fig. 6.6a and increasing the sampling plate voltage would have simply declustered $K(MeOH)_6^+$ to K^+ and $K(MeOH)_1^+$ as shown in Fig. 6.6b. However, no potassium ions existed as $K(MeOH)_6^+$ as there were no potassium clusters detected above m/z = 140 with the interface conditions of Fig. 6.6a. Alternatively, had clusters such as $K(MeOH)_6^+$ been desorbed from charged droplets at atmospheric pressure by ion evaporation, there is the possibility that there would be growth of the cluster to $K(MeOH)_m^+$ since a low curtain gas flow rate would not efficiently sweep solvent vapor out of the interface chamber. However, this alternative is not credible in that if conditions were such that the charged droplets evaporated to such an extent that $K(MeOH)_6^+$ was desorbed, then methanol vapor attachment to $K(MeOH)_6^+$ would not be expected. In the event that the source of the potassium signal in Fig. 6.6b was collisional release of ions from a third generation Rayleigh fission charged droplet which have been described by Kebarle and Tang as containing ~ 280 excess charges in a droplet of radius ~ 0.03 μm [1], consideration of the time and energy required to first collisionally knock-out a potassium ion from a droplet of radius ~ 0.03 μm, then collisionally remove the methanol ligands from the potassium ion all within the time that the charged droplet resides in the zone between the sampling plate and skimmer orifices makes the process unlikely.

From this argument, minute droplets created at atmospheric pressure by a mechanism described by the SIDT where each droplet contains a single potassium ion $K(MeOH)_m^+$ appears to more satisfactorily account for the experimental observations than the IET.

6.3.2 The Alkaline Earths

The connection between flow rate of curtain gas and the sampling plate voltage bias observed for the alkali metal potassium is also observed for the alkaline earths. However a subtle difference between the functional dependence of these two variables on the nature of the ions detected emerges for the divalent alkaline earth solution ions. In Fig. 6.7a, the mass spectrum of strontium chloride is shown with the flow rate of curtain gas at 0.085 lpm and the sampling plate bias at 40 V. The strontium is detected as $Sr(MeOH)_n^{2+}$ where the methanol ligands stabilize the two plus valence state of strontium. Increasing the flow rate of curtain gas to 0.70 lpm (Fig. 6.7c) while keeping the sampling plate biased to 40 V causes a large increase in the strontium ion cluster signal level. The strontium signal is

largely comprised of doubly charged ion clusters at (relatively) low sampling plate voltage bias and high curtain gas flow rates. A single charge reduced strontium cluster ($^{88}Sr(MeO)^+$) is present at m/z = 119. Charge reduction is expressed in Eqn. 6.1 for a strontium cluster where collisions in the jet expansion with curtain gas molecules propel the reaction.

$$Sr(MeOH)_2^{2+} \longrightarrow Sr(MeO)^+ + H(MeOH)_1^+ \qquad (6.1)$$

The mass spectrum in Fig. 6.7b was acquired after increasing the sampling plate bias to 190 V (while the flow rate of curtain gas remained low (0.085 lpm)). Strontium ion signals in Fig. 6.7b do not contain any methanol ligands as they have been stripped away during passage through the jet expansion. In Fig. 6.7d, when the flow rate of curtain gas and sampling plate voltage bias are both optimized, it is seen that strontium methanol clusters are stripped of their solvation ligands to generate a spectrum very similar in appearance to that shown in Fig. 6.7b. In this case, the optimization of both the curtain gas flow rate and the sampling plate voltage (Fig. 6.7d) enhanced the signal level obtained from using only strong declustering conditions to generate the strontium signal level shown in Fig. 6.7b. Background ion signals are also strongly attenuated in Fig. 6.7d This is perhaps indicative of increased energy requirements to decluster a doubly charged solution ion relative to a singly charged solution ion.

Strontium signal levels are plotted in Fig. 6.8 as a function of curtain gas flow rate. The importance of a flow of dry curtain gas on the intensity of electrosprayed ions is again emphasized by this plot. The sum of strontium ion signal intensities rises rapidly between curtain gas flow rates of 0.15 lpm and 0.39 lpm, thereafter the sum of strontium signals plateaus. In addition to plotting the sum of strontium ions, the signals for $^{88}Sr(MeOH)_2^{2+}$, $^{88}Sr(MeOH)_1^{2+}$, and $^{88}Sr(MeO)_1^+$ ions are also plotted to illustrate the point that although the sum of strontium signals remains constant, the nature of the strontium species detected does not under the condition of an increasing curtain gas flow rate. The three strontium ion species plotted in Fig. 6.8 comprise most of the total strontium ion signal in the mass spectra at flow rates > 0.5 lpm. At curtain gas flow rates ≤ 0.3 lpm, the sum of strontium signals is comprised of $^{88}Sr(MeOH)_n^{2+}$, $n \geq 3$. Increasing the flow rate of curtain gas shifts the distribution of strontium clusters to lower values of n and charge reduced strontium species begin to appear in the mass spectrum.

The intertwined role of the sampling plate voltage bias and the curtain gas flow rate is further demonstrated by biasing the sampling plate to 190 V while increasing the curtain gas flow rate and observing the +2 and +1 alkaline earth species (M^{2+} and M^{+}). Under these conditions ions entrained in the jet expansion are subject to very harsh collisions with neutral curtain gas molecules causing extensive declustering. A higher flow rate of curtain gas is required to cause the bare doubly charged and singly charged alkaline earth ion signal profiles (Fig 6.9a and 6.9b) to maximize in the order Ca < Sr < Ba. Furthermore. for each alkaline earth the bare doubly charged ion signal intensity profile (Fig. 6.9a) maximizes at a lower flow rate than for the singly charged ion intensity profile (Fig. 6.9b).

The ion signals plotted in Fig. 6.9 are the final products of collisional pathways in the jet expansion that are represented by Eqns. 6.2 to 6.6 for the alkaline earths. Eqn. 6.2 describes the removal, or evaporation of loosely bound solvation sphere molecules from the atmospheric pressure ions . Eqns. 6.3 to 6.6 describe further declustering collisions of the ion. Simple ligand loss is described by Eqn. 6.3 and is in competition with charge reduction of the metal ion cluster (Eqn. 6.4). The chemistry of the charge reduction step has been discussed previously [12,17]. Eqn. 6.5 describes the collisional activation and subsequent breakup of the charged reduced cluster produced by Eqn. 6.4. Eqn. 6.6 describes an alternate path for generating M^{+}.

$$M(MeOH)_n^{2+} \longrightarrow M(MeOH)_2^{2+} + n(MeOH) \qquad (6.2)$$

$$M(MeOH)_2^{2+} \longrightarrow M(MeOH)_1^{2+} + MeOH \qquad (6.3a)$$

$$M(MeOH)_1^{2+} \longrightarrow M^{2+} + MeOH \qquad (6.3b)$$

$$M(MeOH)_2^{2+} \longrightarrow M(MeO)_1^{+} + H(MeOH)^{+} \qquad (6.4)$$

$$M(MeO)_1^{+} \longrightarrow M(H)^{+} + CH_2O \qquad (6.5a)$$

$$M(H)^{+} \longrightarrow M^{+} H \qquad (6.5b)$$

$$M(MeOH)_1^{2+} \longrightarrow M^{+} + MeOH^{+} \qquad (6.6)$$

Insight into the declustering reaction pathways important for each of the alkaline earths can be gained through a comparison of the relative signal levels of M^{2+}, $M(MeO)_1^{+}$, and M^{+}. For Ca the relative signal intensities were ($I(Ca^{2+}) \sim I(Ca^{+}) \sim I(Ca(MeO)_1^{+})$, thus all collision induced dissociation product pathways (Eqns. 6.3 to 6.6) are important for calcium. The relative strontium ion signal levels were $I(Sr^{2+}) > I(Sr^{+}) > I(Sr(MeO)_1^{+})$, implying that Eqn. 6.3 is the favored collision induced dissociation pathway for strontium clusters. In decreasing importance in the collision induced dissociation of strontium clusters is Eqn. 6.4 followed by Eqn. 6.6. Finally, only Eqn. 6.3 is important in the

declustering of barium ions based on the relative signal intensities $I(Ba^{2+}) >> I(Ba^{+}) \sim I(Ba(MeO)_1^{+})$.

These relative signal trends between the alkaline earths can be qualitatively explained based on differences in the ionization potentials of Ca, Sr, and Ba. The first and second ionization potentials are 6.11 and 11.87 eV for Ca, 5.69 and 11.03 eV for Sr, and 5.21 and 10.00 eV for Ba. Charge reduction of the doubly ionized metal ion with oxidation of a solvent molecule (Eqn. 6.4) sets in when there are not enough solvent molecules in the cluster to stabilize the plus-two state. Thus, as the plus-two cluster is progressively declustered, charge reduction sets in first for Ca. Thus, even at a low curtain gas flow rate the Ca^{2+} signal peaks out and the Ca^{+} signal appears (see Fig. 6.9a and 6.9b). After further declustering, Sr^{+} appears and finally a weak signal for Ba^{+} is seen at high curtain gas flow rates. However, for barium, the Ba^{2+} remains the dominant species.

6.3.3 A Transition Metal: Cobalt II

The transition metal cobalt (II) is used to further distinguish the role of the sampling plate voltage bias from the role of the curtain gas flow rate in elemental ES-MS. To begin, a series of spectra obtained at increasing flow rates of curtain gas and constant sampling plate voltage bias (40 V) are shown in Fig. 6.10. The data for Fig. 6.10a were acquired with the flow rate of curtain gas set to 0 lpm. Under these source conditions a flat distribution of $^{59}Co(MeOH)_n^{2+}$ clusters is obtained and signal levels are low. The ion peak at m/z = 65 is $H(MeOH)_2^{+}$. Increasing the flow rate to 0.2 lpm (Fig. 6.10b) increases the total cobalt cluster signal level by approximately two orders of magnitude. It would also appear that the cobalt distribution has shifted to higher values of n. A further increase in curtain gas flow rate to 0.4 lpm (Fig. 6.10c) causes the $^{59}Co(MeOH)_n^{2+}$ to funnel into the $^{59}Co(MeOH)_4^{2+}$ cluster. The $^{59}Co(MeOH)_4^{2+}$ cluster is prominent in the respect that further loss of ligand is in competition with the charge reduction step. A very large increase to 1.93 lpm flow rate of curtain gas (Fig. 6.10d) is required before the $^{59}Co(MeOH)_4^{2+}$ cluster is effectively removed from the mass spectrum through charge reduction to form $^{59}Co(MeO)_1(MeOH)_2^{+}$ and $^{59}Co(MeO)_1(MeOH)_1^{+}$. Note that the first and second ionization potentials of Co are 7.86 and 17.05 eV, both larger than those for the alkaline earths. Thus the charge reduction reaction (Eqn. 6.8) sets in at a higher clustered state than was seen for the alkaline earths.

In contrast to the spectra shown in Fig. 6.10, the spectra in Fig. 6.11 were obtained by holding the curtain gas flow rate constant while increasing the sampling plate voltage bias. The $^{59}Co(MeOH)_n^{2+}$ distribution shown in Fig. 6.11a was obtained with the sampling plate voltage bias at 35 V. With the electrospray ion source conditions used to acquire the spectra in Fig. 6.11a, the flow rate of the curtain gas (0.4 lpm) was critical in observing cobalt ion clusters. Decreasing the curtain gas flow rate resulted in a near complete loss of cobalt ion signal. The peaks at m/z 33, 65, 97 are protonated methanol clusters ($H(MeOH)_n^+$). Increasing the sampling plate voltage bias to 44 V (Fig. 6.11b) caused the $^{59}Co(MeOH)_n^{2+}$ distribution to shift to lower values of n and the appearance of charge reduced cobalt clusters (($^{59}Co(MeO)(MeOH)_n^+$), n=1 and 2) could be observed. Formation of the charge reduction product ion $^{59}CoH(MeOH)_1^+$ was not favored until the sampling plate voltage bias was increased to 70 V (Fig. 6.11c) implying that the $^{59}CoH(MeOH)_1^+$ is formed through more energetic collisions in the jet expansion. Also first appearing in Fig. 6.11c is $^{59}CoH^+$. Increasing the sampling plate voltage bias to 120 V (Fig. 6.11d) causes more complete declustering to the extent that $^{59}Co^+$ is the most abundant ion in the spectrum.

The sampling plate voltage bias is used to control the collision induced dissociation energy that analyte ion clusters are subjected to in the region between the sampling plate and skimmer. The spectra of a solution of cobalt chloride in Fig. 6.11 are indicative of the wide range of cobalt ions that can be produced.

The differences between the effect of the curtain gas flow rate versus the effect of sampling plate voltage bias on the ES-MS of a solution of cobalt are summarized by the cobalt ion signal profile plots of Fig. 6.12a and Fig. 6.12b respectively. In Fig. 6.12a, a threshold curtain gas flow rate is observed (~ 0.25 lpm), below which gas phase cobalt ion clusters are detected with low efficiency and above which the sum of cobalt ion signal intensities remains high. The dominant individual cobalt ion clusters present in the mass spectra are also plotted in Fig. 6.12. Closer inspection of Fig. 6.12a reveals that at flow rates between 0.25 to 0.70 lpm, the sum of cobalt ion signal intensities is comprised predominately of doubly charged cobalt clusters. These clusters are converted to charged reduced clusters at flow rates greater than 0.70 lpm. The high curtain gas flow rates also cause the appearance of cobalt chloride and cobalt hydride clusters. These observations are summarized by Eqns. 6.7 to 6.10. High flow rates of curtain gas (> 0.70 lpm) cause Eqn. 6.7 to proceed, but Eqns. 6.8 through 6.10 are likely driven almost entirely by collisions in the jet expansion with the curtain gas.

$$Co(MeOH)_n^{2+} \longrightarrow Co(MeOH)_4^{2+} + n\text{-}4(MeOH) \quad (6.7)$$

$$Co(MeOH)_4^{2+} \longrightarrow Co(MeO)_1(MeOH)_2^{+} + H(MeOH)^{+} \quad (6.8)$$

$$Co(MeO)_1(MeOH)_2^{+} \longrightarrow Co(MeO)_1(MeOH)_1^{+} + MeOH) \quad (6.9)$$

$$Co(MeO)_1(MeOH)_1^{+} \longrightarrow Co(H)(MeOH)_1^{+} + CH_2O \quad (6.10)$$

In marked contrast, a very different cobalt ion signal intensity profile results when data were acquired by holding the curtain gas flow rate constant (and above the threshold at 0.4 lpm) while the sampling plate voltage bias was increased (Fig. 6.12b). The sum of cobalt ion signal intensities has three local maxima at 44 V, 70 V, and another at 100 V. The local maxima of the total cobalt ion signal profile at 44 V was comprised principally of doubly charged cobalt ion clusters. At a 70 V bias on the sampling plate, the local maximum was comprised in large by cobalt hydride species. The final local maximum occurs when the sampling plate voltage bias is 100 V and is attributed to the appearance of the bare singly charged cobalt ion. Increasing the sampling plate voltage bias clearly causes more extensive declustering in the jet expansion. In addition to the reactions described in Eqns. 6.8 to 6.10 at low sampling plate voltage biases (40 V), Eqns. 6.11 to 6.12 describe the collision induced dissociation processes occurring at higher sampling plate voltage bias.

$$Co(H)(MeOH)_1^{+} \longrightarrow CoH^{+} + MeOH \quad (6.11)$$

$$CoH^{+} \longrightarrow Co^{+} + H \quad (6.12)$$

Over the same voltage range, collision induced dissociation of analyte counter-ion clusters, derived from the salt being electrosprayed, also plays a role in determining the relative intensities of analyte molecular species [see Figs. 7 and 8 in reference 17]. The amount of molecular cobalt ion species ($^{59}CoH^{+}$, $^{59}CoOH^{+}$, $^{59}CoCl^{+}$) remaining in the spectrum shown in Fig. 6.11d represent potential spectral interferences on other analytes. These molecular species can be strongly attenuated through optimization of the sampling plate voltage bias and the curtain gas flow rate. This is illustrated by the data shown in Fig. 6.13. Within Fig. 6.13, which was obtained by electrospraying a solution of cobalt nitrate, in going down each column the curtain gas flow rate is increased from 0.085 to 0.39 to 0.70 lpm while the sampling plate voltage bias was held constant. Across each row, the sampling plate voltage was increased from 130 V to 230 V while the curtain gas flow rate was held constant. The same scales were used for each plot in Fig. 6.13 to facilitate visual comparison of the spectra. Clearly, neither increasing the sampling plate voltage bias (compare spectra in Figs. 6.13a to 6.13b) nor increasing the curtain gas flow rate (compare

spectra in Fig. 6.13a to Figs. 6.13c and 6.13e) effectively cause elimination of charge reduced cobalt molecular ions from the mass spectrum. Simultaneous increases in the curtain gas flow rate and increased sampling plate voltage bias do effectively discriminate against charge reduced cobalt molecular ions (compare Fig. 6.13a to Fig. 6.13f) and can result in a "clean" $^{59}Co^{+}$ spectrum (Fig. 6.13f).

The data contained in Fig. 6.13 are summarized by plotting the bare cobalt ion ($^{59}Co^{+}$) signal intensity and the sum of all charge reduced cobalt molecular ion species (Σ(cr-$^{59}Co^{+}$)) (Fig. 6.14b) signal intensities obtained at a flow rate of curtain gas of 0.70 lpm over the range of sampling plate voltage bias from 130 to 230 V. Although slightly different electrospray source conditions were used, Fig. 6.14 can be considered as an extension of Fig. 6.12b. Electrospray source conditions that allow for generating a maximum analyte signal intensity do not coincide with a minimum in the analyte molecular signal intensity. Operating the electrospray source to minimize the analyte molecular signal intensity (see Fig. 6.14 at sampling plate voltage bias > 190 V) is achieved at the expense of the bare analyte ion (M^{+}) signal intensity.

Several other transition metals were studied (Mn, Zn, Fe(II), Ni, Cd) and each was found to behave similarly to cobalt. The trivalent transition metals tested (Cr(III), Fe(III)) also behaved very similarly to cobalt even though these ions undergo two stages of charge reduction.

6.4 Conclusions

The nature of the mass spectrum observed in elemental electrospray mass spectrometry is critically dependent on source and interface parameters. In this study, the two most important variables were found to be the curtain gas flow rate and the sampling plate voltage. The primary role of the curtain gas is to dry the electrospray aerosol and to promote desolvation of ion solvent clusters while the sampling plate voltage sets the driving force for declustering collisions in the first stage of the vacuum interface. At low values of these parameters (*i.e.* mild conditions) the mass spectra are dominated by ion solvent clusters which have a mass to charge ratio indicative of the valence state of the cation in solution. At high values of these two parameters, simple mass spectra result consisting mainly of bare singly charged metal ions. Intermediate conditions produce a wide range of metal ion clusters involving solvent, oxidized solvent, and anions.

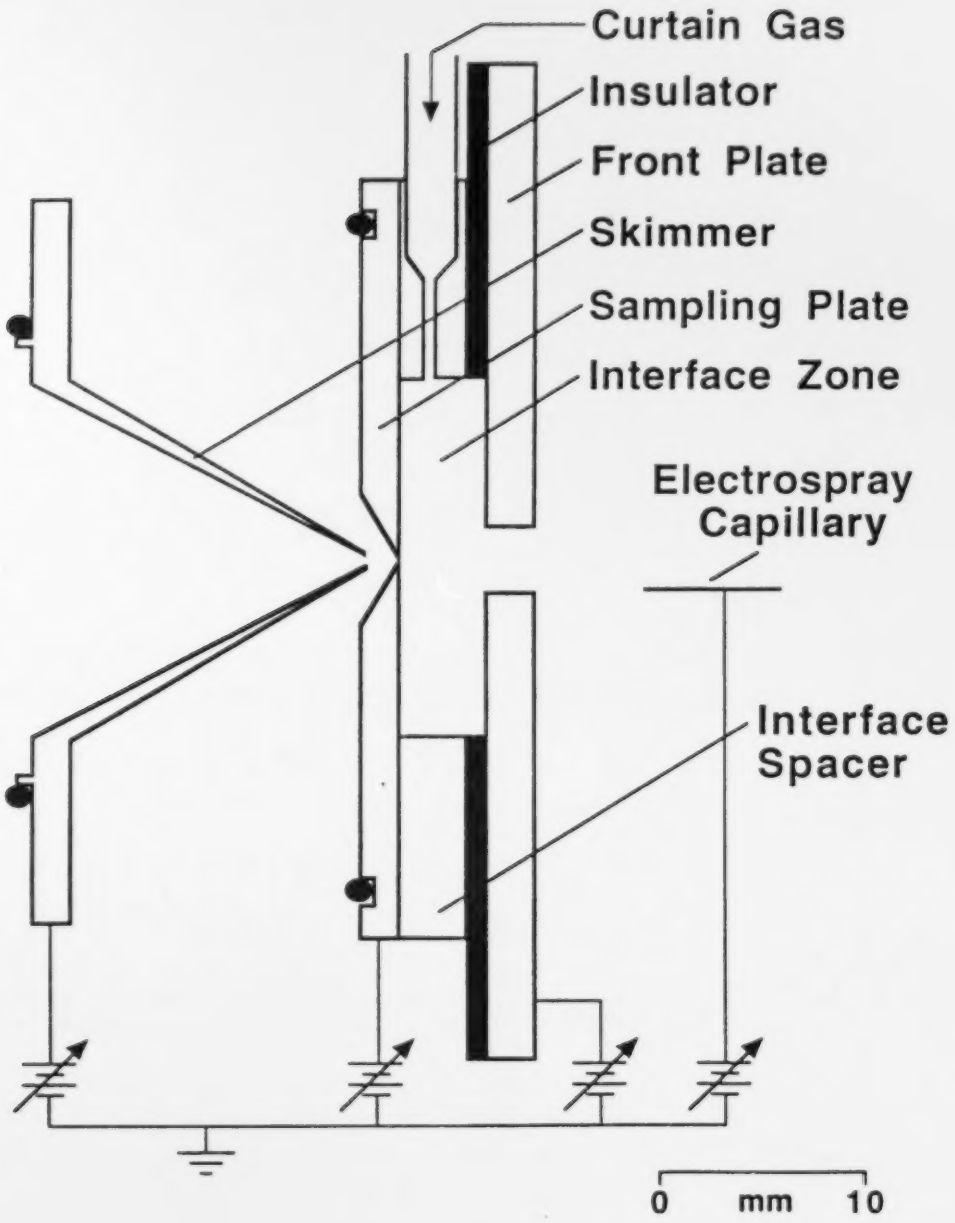

Figure 6.1 Schematic diagram of the electrospray ion source. The barrel ion extractor lens (not shown) was located 3 cm downstream of the skimmer.

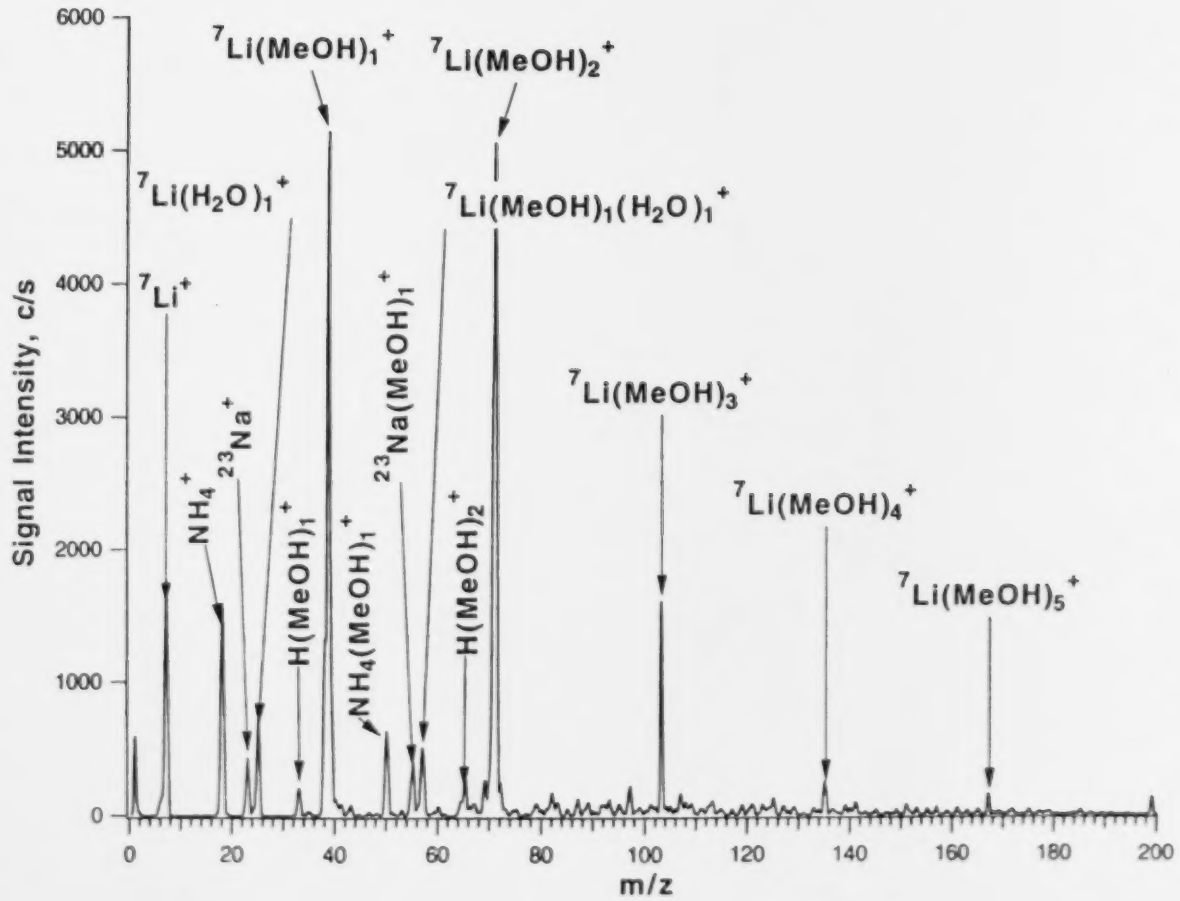

Figure 6.2 Mass spectrum of lithium chloride in 97:3 methanol:water. Electrospray capillary 4.0 kV, front plate 600 V, sampling plate 40 V, and curtain gas flow rate 0.2 lpm.

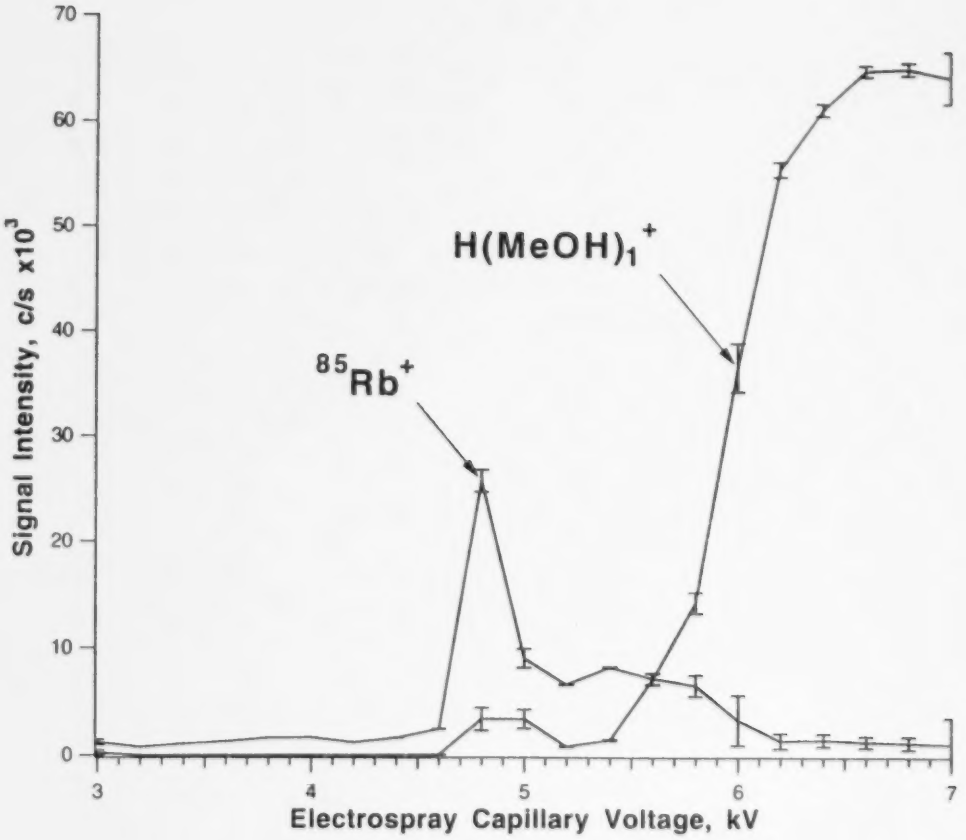

Figure 6.3 Effect of electrospray capillary voltage bias on $^{85}Rb^+$ and $H(MeOH)_1^+$ signal intensities. Electrospray source conditions were: front plate 950 V, sampling plate 160 V, and curtain gas flow rate .085 lpm. The solution contained Li, Na, K, Rb, and Cs chloride each at 1×10^{-4} molar.

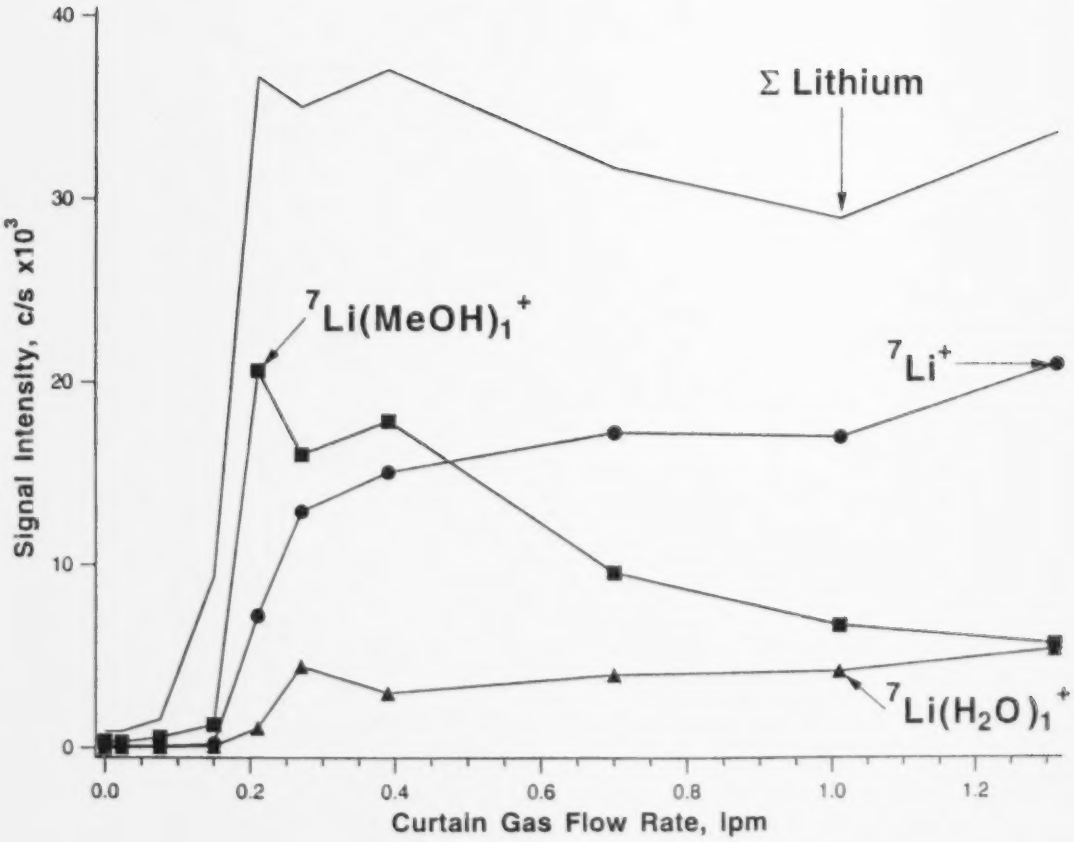

Figure 6.4 Effect of curtain gas flow rate on the total lithium signal. Response curves are also shown for the dominant lithium ion species. Electrospray capillary 4.0 kV, front plate 600 V, sampling plate 40 V, and skimmer 9.0 V.

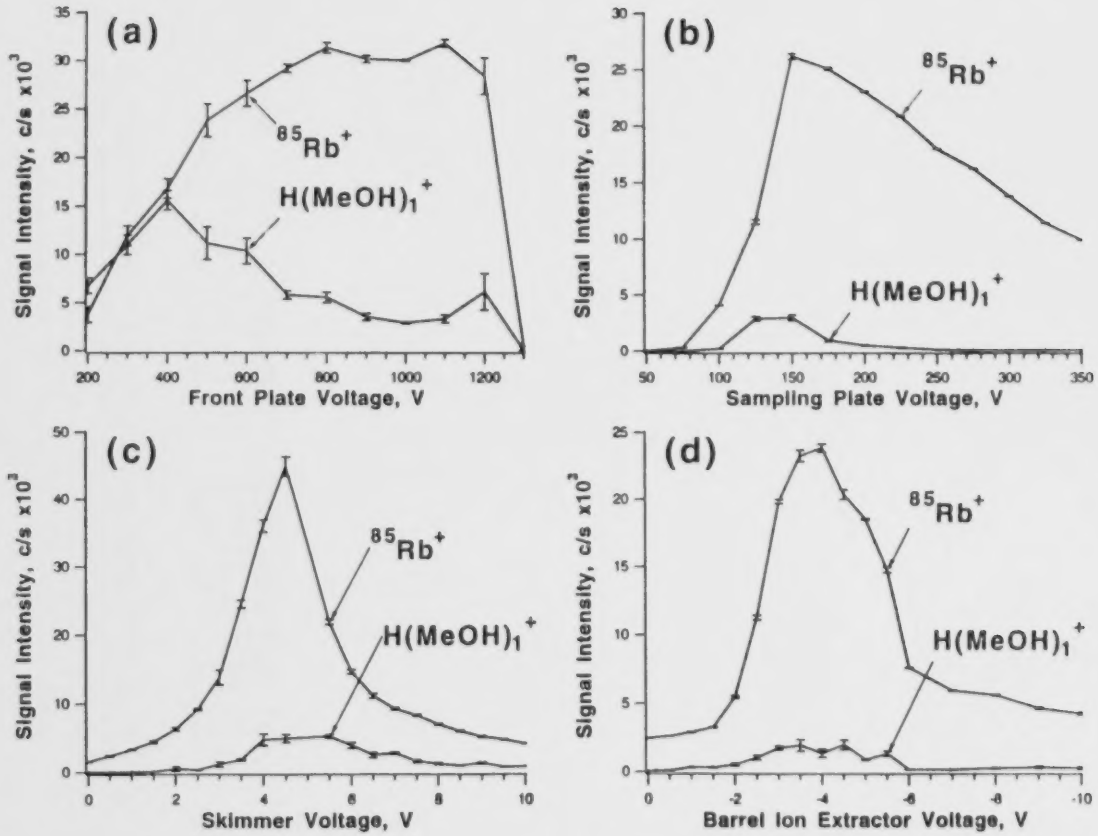

Figure 6.5 $^{85}Rb^+$ and $H(MeOH)_1^+$ signal intensities for (a) front plate voltage, (b) sampling plate voltage, (c) skimmer voltage, and (d) Barrel ion extractor voltage. Electrospray capillary 5.0 kV, front plate 950 V, sampling plate 160 V, skimmer 3.5 V, Barrel ion extractor -2.5 V, and curtain gas flow rate 0.085 lpm. The solution contained Li, Na, K, Rb, and Cs chloride each at 1×10^{-4} molar.

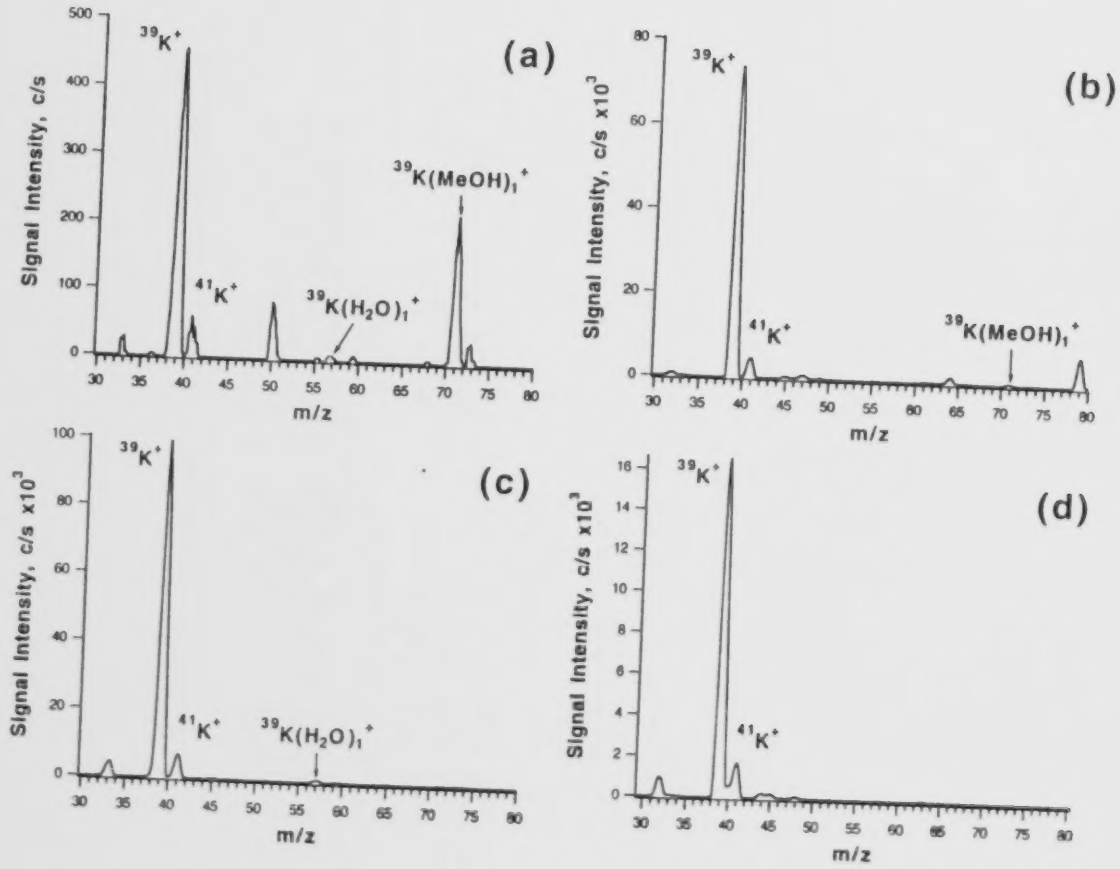

Figure 6.6 Mass spectra of potassium chloride. (a) sampling plate 40 V, curtain gas flow rate 0 lpm, (b) sampling plate 190 V, curtain gas flow rate 0 lpm, (c) sampling plate 40 V, curtain gas flow rate 0.58 lpm, and (d) sampling plate 190 V, curtain gas flow rate 0.58 lpm. Electrospray capillary 4.0 kV, front plate 600 V.

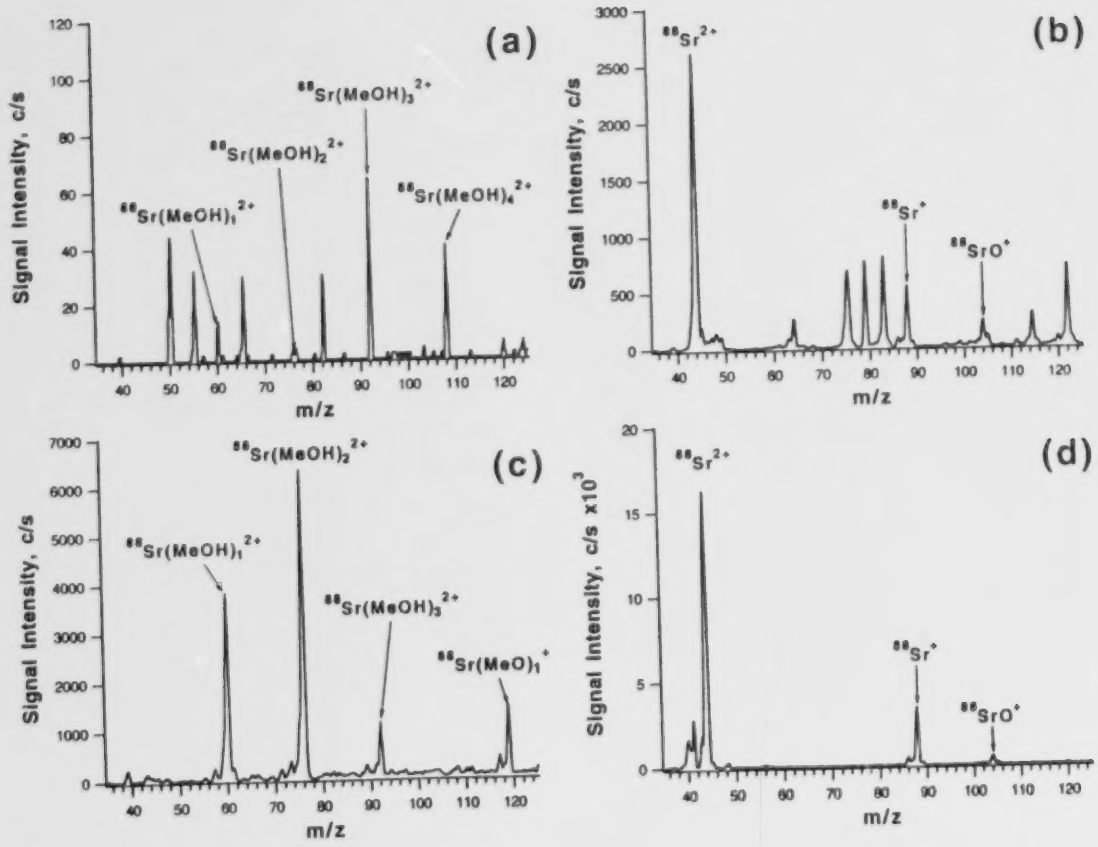

Figure 6.7 Mass spectra of strontium chloride. (a) sampling plate 40 V, curtain gas flow rate 0.085 lpm, (b) sampling plate 190 V, curtain gas flow rate 0.085 lpm, (c) sampling plate 40 V, curtain gas flow rate 0.70 lpm, and (d) sampling plate 190 V, curtain gas flow rate 0.70 lpm. Electrospray capillary 4.0 kV, front plate 600 V.

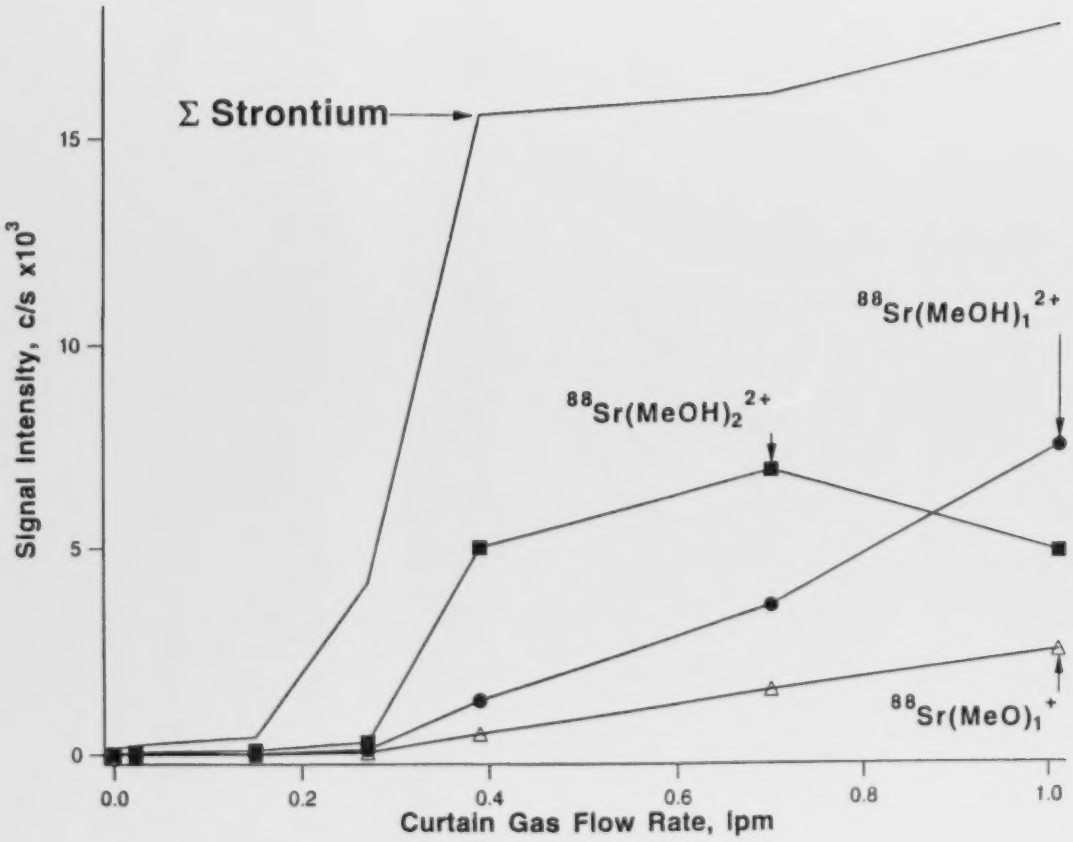

Figure 6.8 Effect of curtain gas flow rate on the total strontium signal. Response curves are also shown for the dominant strontium ion species. Electrospray capillary 4.0 kV, front plate 600 V, sampling plate 40 V, and skimmer 9.0 V.

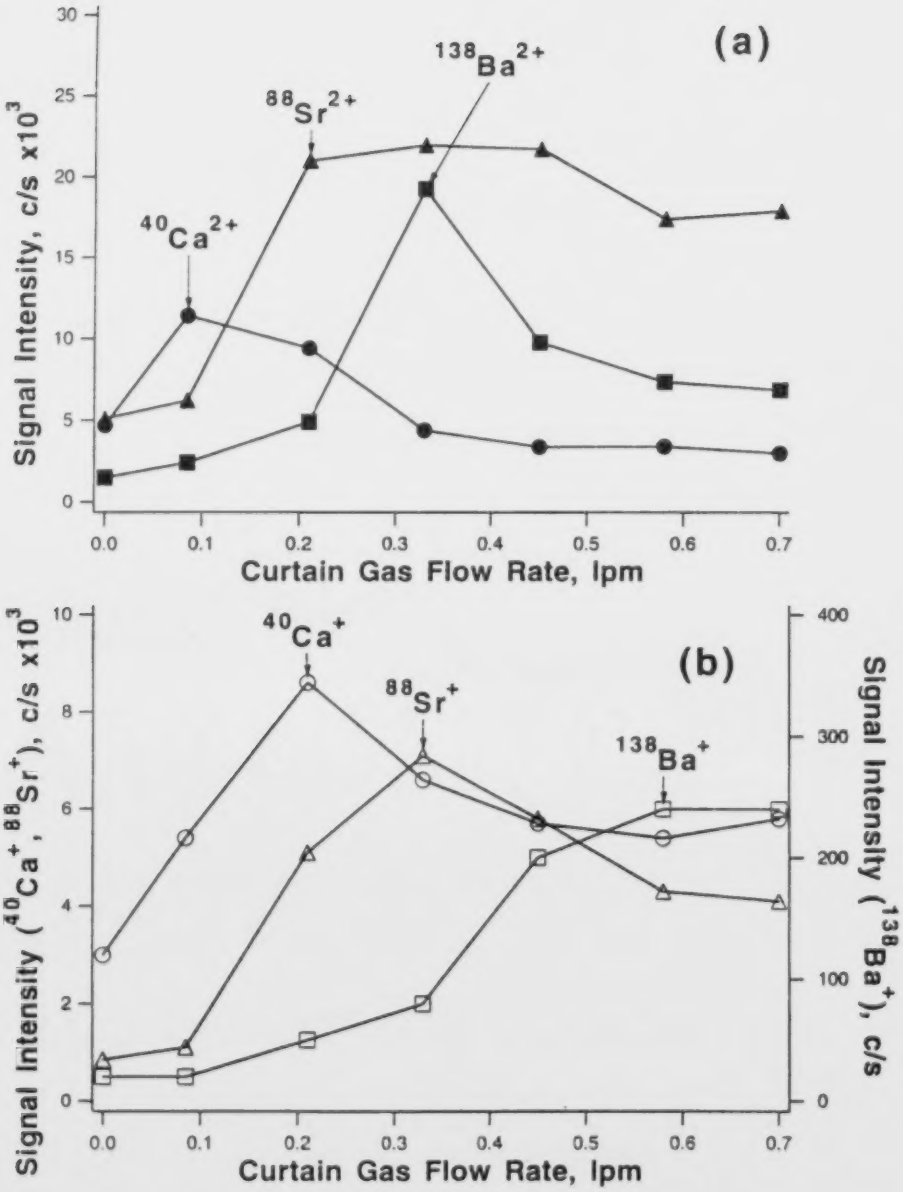

Figure 6.9 Effect of curtain gas flow rate on (a) doubly charged bare alkaline earths and (b) bare singly charged alkaline earths. Electrospray capillary 5.0 kV, front plate 950 V, sampling plate 190 V.

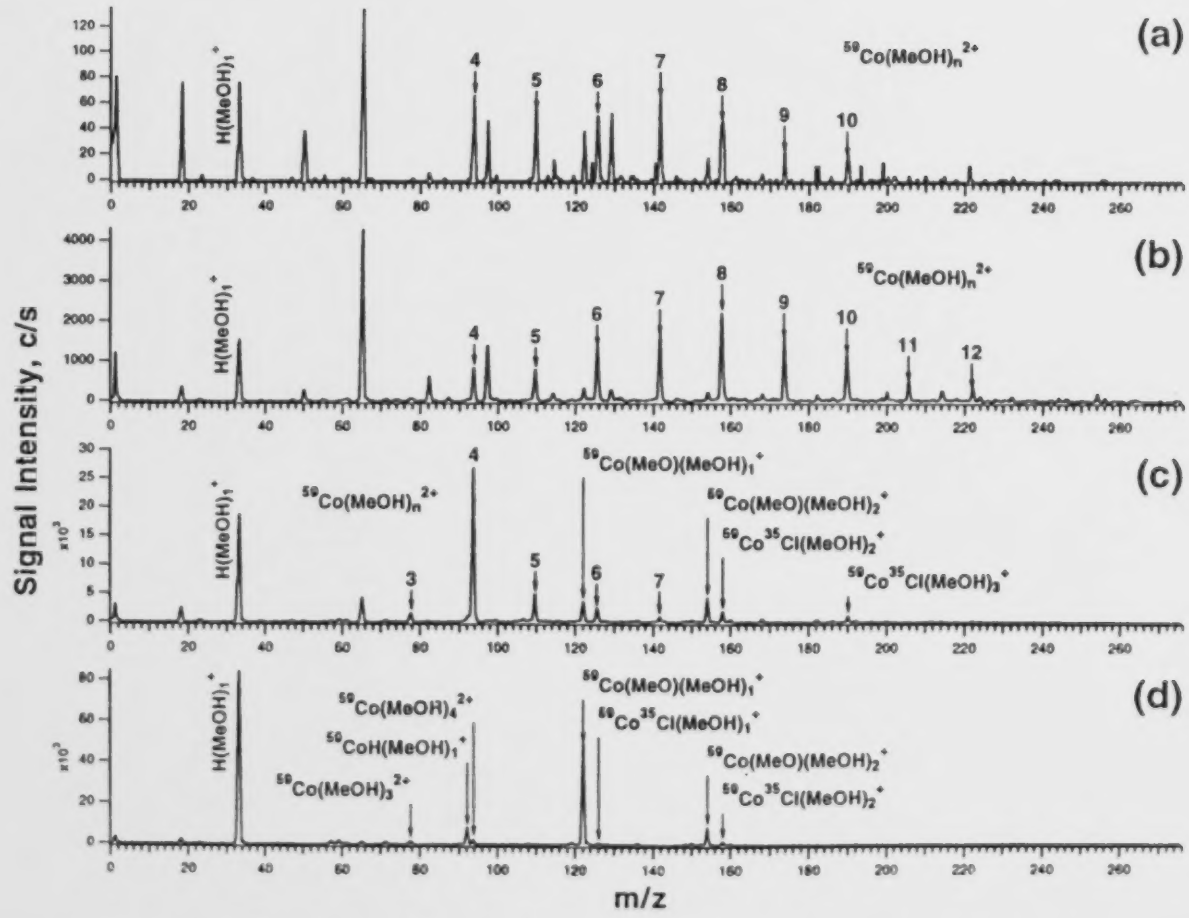

Figure 6.10 Mass spectra of cobalt chloride. Curtain gas flow rate was (a) 0 lpm, (b) 0.21 lpm, (c) 0.39 lpm, and (d) 1.93 lpm. Electrospray capillary 4.0 kV, front plate 600 V, sampling plate 40 V.

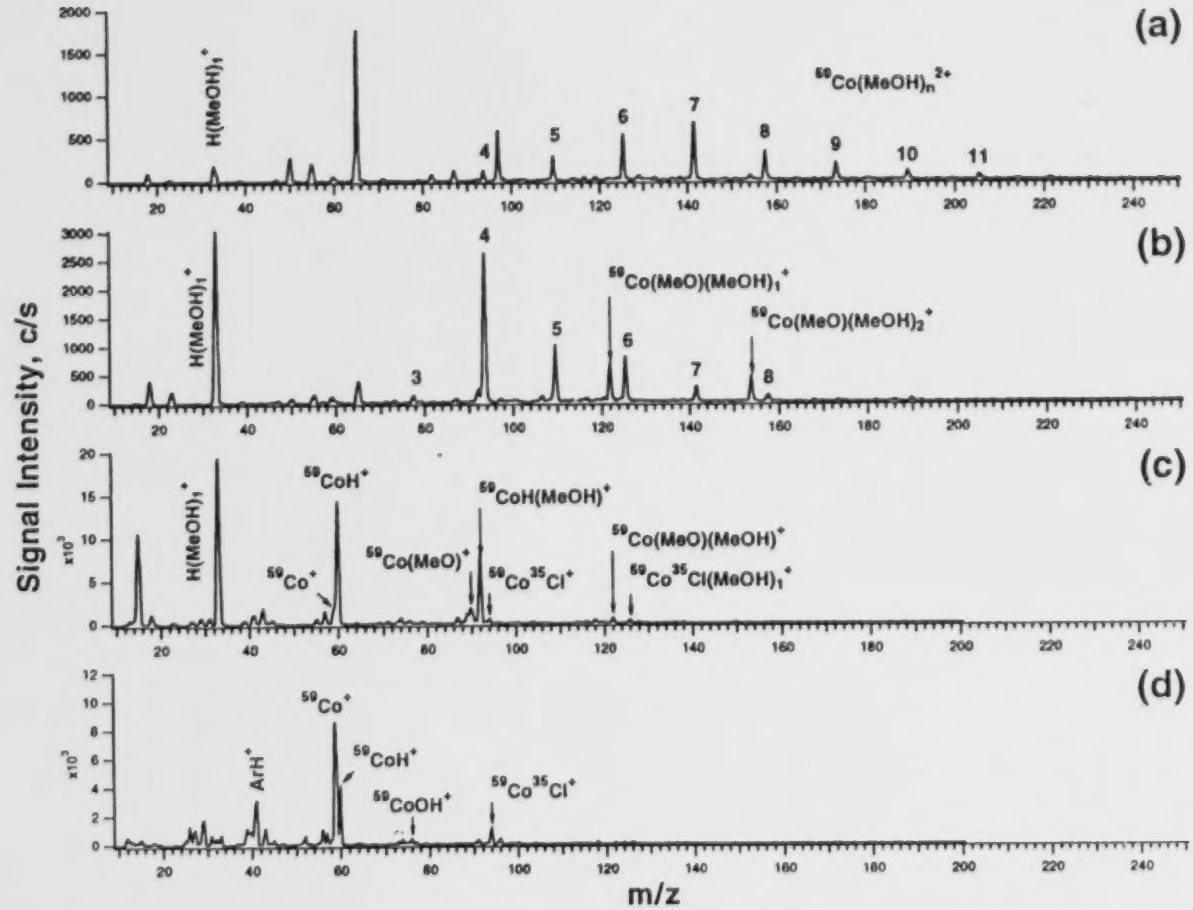

Figure 6.11 Mass spectra of cobalt chloride. Sampling plate voltage was (a) 35 V, (b) 44 V, (c) 70 V, and (d) 120 V. Electrospray capillary 4.0 kV, front plate 600 V, curtain gas flow rate 0.39 lpm.

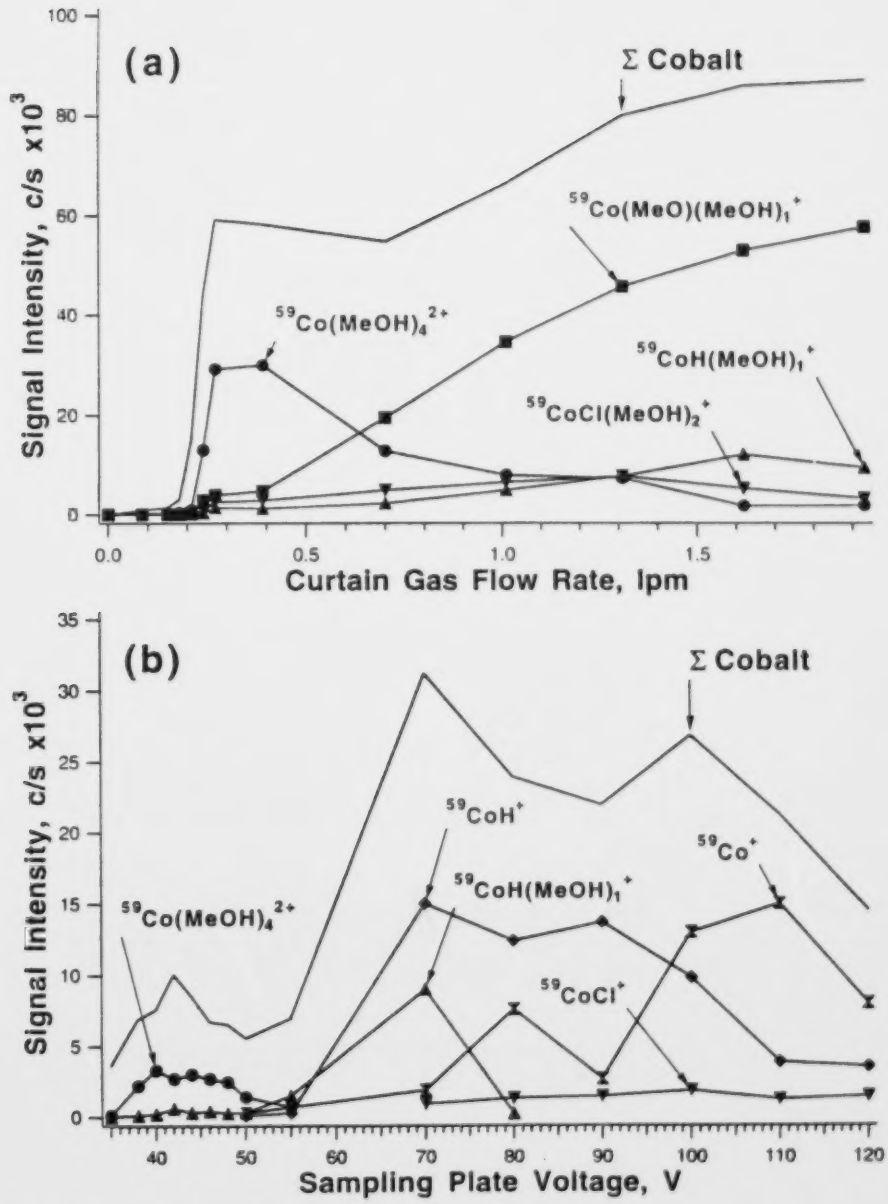

Figure 6.12 Major ion intensities from Fig. 6.10 as a function of (a) curtain gas flow rate and from Fig. 6.11 as a function of (b) sampling plate voltage.

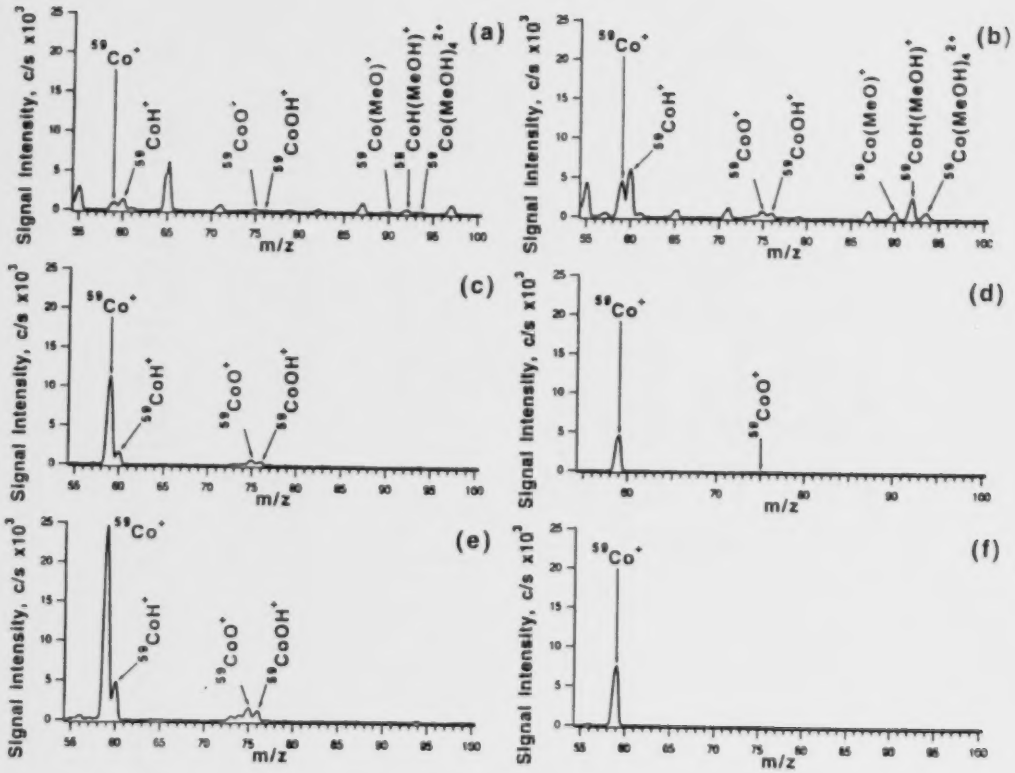

Figure 6.13 Mass spectra of cobalt nitrate acquired while varying the sampling plate voltage and the curtain gas flow rate: (a) sampling plate voltage 130 V, curtain gas flow rate 0.085 lpm, (b) sampling plate voltage 230 V, curtain gas flow rate 0.085 lpm, (c) sampling plate voltage 130 V, curtain gas flow rate 0.39 lpm, (d) sampling plate voltage 230 V, curtain gas flow rate 0.39 lpm, (e) sampling plate voltage 130 V, curtain gas flow rate 0.70 lpm, (f) sampling plate voltage 230 V, curtain gas flow rate 0.70 lpm.

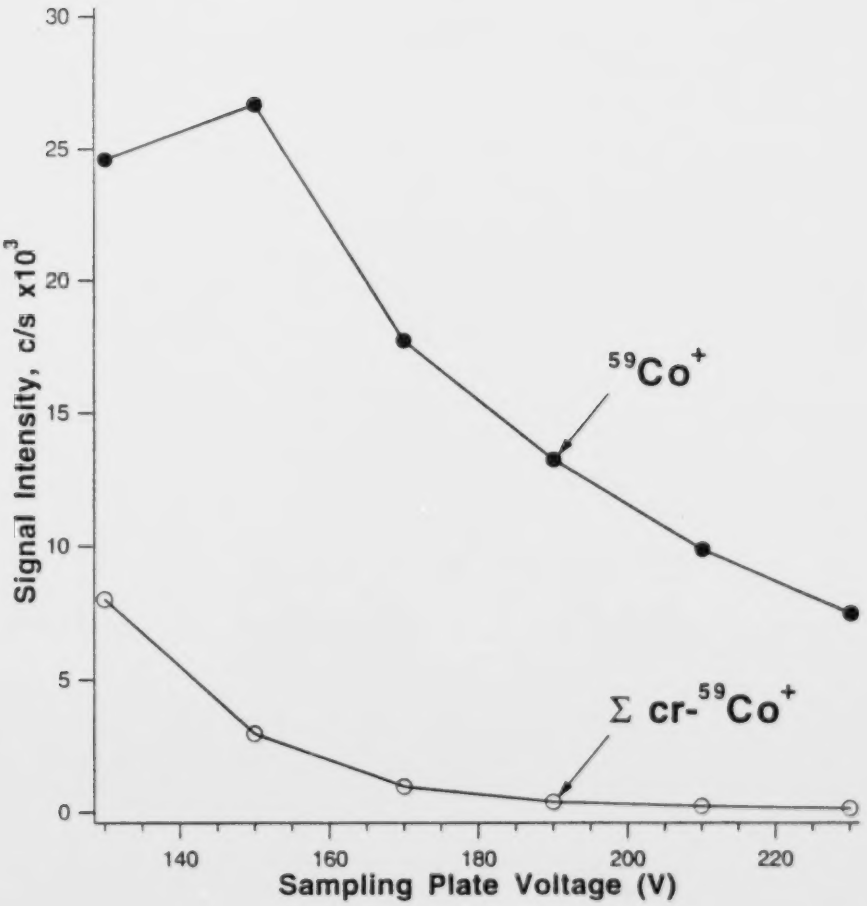

Figure 6.14 (a) $^{59}Co^{+}$ and (b) the sum of charge reduced cobalt molecular ion (Σ(cr-$^{59}Co^{+}$)) signal intensities as a function of sampling plate voltage bias at the curtain gas flow rate of 0.70 lpm. Electrospray capillary 5.0 kV and front plate 950 V.

6.5 References

1. P. Kebarle and L. Tang, Anal. Chem., 65, 972A (1993).

2. D. C. Taflin, T. L. Ward, and E. J. Davis, Langmuir, **5**, 376 (1989).

3. L. Tang and P. Kebarle , Anal. Chem., **65**, 3654 (1993).

4. J. B. Fenn, J. Am. Soc. Mass Spectrom., **4**, 524 (1993).

5. B. E. Winger, K. J. Light-Wahl, R. R. Ogorzalek Loo, H. R. Udseth, and R. D. Smith, J. AM. Soc. Mass Spectrom., **4**, 536 (1993).

6. M. Dole, L. L. Mack, R. L. Hines, R. C. Mobley, L. D. Ferguson, and M. D. Alice, J. Chem. Phys., **49**, 2240 (1968).

7. L. L. Mack, P. Kralik, A. Rheuda, and M. Dole, J. Chem. Phys., **52**, 4977 (1970).

8. G. Schmelzeisen-Redeker, L. Butfering, and F. W. Rollgen, Int. J. Mass Spectrom. Ion Processes, **90**, 139 (1989).

9. J. V. Iribarne and B. A. Thomson, J. Chem. Phys., **64**, 2287 (1976).

10. B. A. Thomson and J. V. Iribarne, J. Chem. Phys., **71**, 4451 (1979).

11. P. Jayaweera, A. T. Blades, M. G. Ikonomou, and P. Kebarle, J. Am. Chem. Soc., **112**, 2452 (1990).

12. A. T. Blades, P. Jayaweera, M. G. Ikonomou, and P. Kebarle, Int. J. Mass Spectrom. Ion Processes, **102**, 251 (1990).

13. A. T. Blades, P. Jayaweera, M. G. Ikonomou, and P. Kebarle, Int. J. Mass Spectrom. Ion Processes, **101**, 325 (1990).

14. A. T. Blades, P. Jayaweera, M. G. Ikonomou, and P. Kebarle, J. Chem. Phys., **92**(10), 5900 (1990).

15. M. Yamashita and J. B. Fenn, J. Phys. Chem., **88**, 4451 (1984).

16. G. Agnes and G. Horlick, Appl. Spectrosc., **46**(3), 401 (1992).

17. G. Agnes and G. Horlick, "Determination of Solution Ions by Electrospray Mass Spectrometry," Appl. Spectrosc. (accepted for publication).

18. M. Yamashita and J. B. Fenn, J. Phys. Chem., **88**, 4671 (1984).

19. M. G. Ikonomou, A. T. Blades, and P. Kebarle, Anal. Chem., **62**(9),957 (1990).

20. M. G. Ikonomou, A. T. Blades, and P. Kebarle, Anal. Chem., **63**(18), 1989 (1991).

21. M. G. Ikonomou, A. T. Blades, and P. Kebarle, Anal. Chem., **63**(19), 2109 (1991).

22. K. W. M. Siu, R. Guevremont, J. C. Y. LeBlanc, R. T. O'Brian, and S. S. Berman, Org. Mass Spectrom., **28**, 579 (1993).

Chapter 7

Elemental Speciation Measurements with Electrospray Mass Spectrometry: An Assessment

7.1 Introduction[5]

Elemental speciation is the determination of all chemical forms of an element in a sample. With respect to solution samples, chemists characterize the chemical forms of an element with parameters such as the oxidation state and associated ligands in the inner and outer coordination spheres of the analyte. Based on these parameters for the differentiation of chemical forms of an element, the study of such species requires methodology and technology that possesses specificity, selectivity, and sensitivity. Furthermore, measurement of the species distribution should not perturb the system in question.

With increasing frequency, chemistry is being asked to make these difficult measurements in order to understand the properties of individual chemical forms in biological, geological, food, agricultural, and environmental systems. However to date no one single measurement technique capable of measuring all chemical forms of an element in a solution sample has been developed. Measurements have thus been limited to the determination of a single chemical form of an element, unless kinetically inert forms of an element are being determined. Kinetically inert chemical forms are defined as being stable, or unaffected by any changes (physical or chemical) to the system being measured in the time required to determine the chemical form.

7.2 Speciation Strategies

With respect to the determination of kinetically inert chemical forms, the most successful speciation strategy couples the specificity of a separation technique with the selectivity and sensitivity of an atomic spectroscopy technique. A wide variety of separation methods (GC [1,2], SFC [3,4], preconcentration [5-7], and LC [8-11]) and atomic spectroscopic methods (ICP [12-19], MIP [20],and AA [21-23]) have been utilized in this marriage of analytical techniques. Of the atomic based techniques utilized, LC-ICP-MS has received by far the most recent attention from researchers in this field.

---

[5] A version of this chapter has been submitted for publication. George R. Agnes and Gary Horlick, Anal. Chem.

Kinetically labile species, chemical forms that are affected by any change to the system, are inherently a much more difficult measurement to make than kinetically inert chemical forms. The requirement that the system be unaffected during the measurement step is valid only when a non-invasive technique is used to measure the chemical forms. However in attaining adequate selectivity, developments in this area have been forced to utilize a selective interaction engineered into the measurement device with the chemical form being measured [24-32]. These measurement devices must therefore be brought into contact with the solution or system being measured. This approach is therefore invasive and any measurements performed with such devices assume that perturbation of the system is negligible. Alternatively, development of a method that removes species from solution would selectively isolate sought for species physically, rather than chemically. Yamashita and Fenn made this alternative a reality in 1984 when they introduced electrospray mass spectrometry (ES-MS) [33,34].

An electrospray source relies on phenomena associated with the spraying of a solution from a capillary held at a high potential to transfer ions in solution to the gas phase [35-39]. The chemical form of the solution ion is thought to be preserved since the ion remains solvated while being transferred from solution to the gas phase. Selective and sensitive mass spectrometric detection of the specific chemical forms introduced to the gas phase by the electrospray source is called electrospray mass spectrometry. Numerous reports utilizing ES-MS for a host of speciation related investigations have appeared in the literature: Toxic inorganic species [40-45], inorganic complexes [46-51], metalloporphyrins [52,53], metal ion coordination in bio-organic molecules [54-59], anti-cancer drugs [60], tagging of neutral organic molecules with metal ions [61], phosphopeptides [62], and environmental contaminants such as pesticides and parasiticides [63-65] have all been determined.

The present work is an assessment of the capabilities and limitations of elemental speciation measurements by ES-MS. While this study focuses on inorganic species, the results and conclusions implied herein are applicable to the broad spectrum of speciation applications summarized above.

7.3 Experimental

A schematic of the in-house constructed electrospray source is shown in Fig. 7.1. A 10 µl/min. flow of sample solution was pumped through the electrospray capillary. This

capillary (0.1 mm ID. x 0.2 mm OD.) was biased to a high voltage (3 - 4 kV) relative to the front plate voltage bias. The droplets produced at the electrospray capillary tip are charged due to an excess of charged ions that are the same polarity as the electrospray capillary. The charged droplets are electrostatically driven to the front plate by the electric field between the electrospray capillary tip and the front plate. Some of these charged droplets pass through the hole in the front plate into the interface zone where a countercurrent flow of drying gas (curtain gas) sweeps solvent vapor out of this region causing the rate of solvent loss from the charged droplets to accelerate. After losing a portion of its original mass due to solvent evaporation, the droplet becomes unstable due to the excess charge still contained in the droplet and a Rayleigh fission occurs. Rayleigh fission is a process that a charged droplet undergoes in which excess destabilizing charges in the droplet are expelled, allowing the charged droplet to re-attain stability [66,67]. Ultimately individual solvated ions are produced in this region from the evaporating charged droplets by, as yet an unproven mechanism(s). See references 35-37 for more detailed discussions of the overall electrospray process.

Gas phase ions located near the sampling plate orifice (0.1 mm dia.) are then sampled into the mass spectrometer (SCIEX/Perkin Elmer ELAN Model 250). Through careful selection of the atmospheric pressure interface parameters, namely the sampling plate voltage bias and the flow rate of curtain gas, Agnes and Horlick demonstrated the ability to make direct determinations of the chemical form of the element from the solution state (valence and oxidation state, ligands, counter-ions) [44]. The sampling plate voltage bias controls the collisional energy of the ion in the jet expansion, and hence the extent of solvent declustering from the ion. The flow rate of curtain gas in the interface zone is used to control the vapor pressure of the solvent, hence the evaporation rate of the charged droplets produced at the electrospray capillary [68]. The flow of curtain gas also sweeps solvent molecules away from the sampling plate orifice reducing solvent molecule cluster growth around ions in the jet expansion [69].

Studies were carried out utilizing both positive and negative electrospray modes. In positive mode electrospray the data obtained reflect the cationic composition of the solution and in the negative mode the data reflect the anionic composition of the solution.

Converting from positive to negative ES-MS required switching the polarity of the deflector and detector power supply boards on the mass spectrometer and on the electrospray source power supplies. Unless otherwise stated, the electrospray source operating parameters

employed in this study are listed in Table 7.1. Oxygen was used as the curtain gas in the negative ion mode to suppress electric discharges. In addition, alternating between positive and negative ES-MS warranted cleaning of the sampling plate orifice. Immersion of the sampling plate into boiling water for several minutes sufficed to remove charged droplet residues. If this step was not performed the total ion current reaching the detector rapidly decreased to zero over approximately fifteen minutes of operation, presumably due to the buildup of a salt bridge over the sampling plate orifice (i.e. negatively charged droplets depositing a layer of negative ions over an existing layer of positive ions).

Samples were prepared by dissolving the ACS grade salt in distilled deionized water followed by a 100-fold dilution with HPLC grade methanol. The mass scan rate was 0.1 sec./point with ten points per amu, unless otherwise stated. No background correction procedures were applied. Data were transferred to a Mac IIci computer for processing (5 point box smoothing algorithm in Igor (Wavemetrics, Lake Oswego, OR, USA)).

7.4 Results and Discussion

7.4.1 Differentiation of Kinetically Inert Species with Different Oxidation States and Different Inner Coordination Sphere Composition

Perhaps the simplest differentiation of chemical forms of an element in solution is when the sought for chemical forms are kinetically inert and there are differences in the molecular form of the element. For example, the equilibria between chloride, chlorate, and perchlorate ions is slow and these ions are best represented as $Cl^-(Sol)_a$, $ClO_3^-(Sol)_b$, and $ClO_4^-(Sol)_c$ where the subscripts a, b, and c the solvation sphere of these ions. Furthermore these representations of the chlorine species in solution remain valid, even after conversion to the gas phase at atmospheric pressure by the electrospray process. In this case, differentiating these forms of chlorine in the gas phase was accomplished by adjusting the ES-MS interface conditions to cause removal of the solvation sphere (i.e. the solvent molecules) while leaving the molecular form intact. The solvation sphere was removed by collisions with neutrals in the jet expansion between the front plate and the skimmer orifices. The resultant mass spectra of these chlorine species are shown in Figs. 7.2a to 7.2c. Incomplete removal of the solvation sphere ligands (methanol) would cause spectral overlap of $Cl^-(MeOH)_{n+1}$ on $ClO_3^-(MeOH)_n$, degrading the ClO_3^- detection limit.

Conditions of the electrospray interface were adjusted for minimal collisional decomposition while electrospraying sodium perchlorate, which readily decomposed at sampling plate voltage biases in excess of -50 V, while minimizing $ClO_4^-(Sol)_c$ ion signal intensities. The mass spectrum obtained by electrospraying an equimolar mixture of these three chlorine species is shown in Fig. 7.2d.

A potential application of the ES-MS is the simultaneous monitoring of ionic chlorination by-products. The chemistry of chlorine dioxide disinfection in water treatment utilities is well known as are the toxic properties of two of the by-products, chlorite and chlorate [70]. Current analytical methodology for the determination of chlorite and chlorate utilizes sequential spectrophotometry [71] or ion chromatography[70].

The background ion peaks (in Fig. 2) at -m/z = 16, 32, 48, 64, and 96 are attributed to oxygen and/or oxygen-methanol species, presumably generated by an electrical discharge at the electrospray capillary tip. The origin of the peaks at -m/z = 75 and 77 were tentatively assigned as $N_2O(MeO)_1^-$ and $NO_2(MeO)_1^-$ since the signal intensity of these peaks is related to the known discharge peak at -m/z = 48 which is O_3^- (and/or $O(MeOH)_1^-$). Assignment of the origin of background ion peaks at -m/z = 45, 46, and 60 was not made. A future design modification of the electrospray source used in this study will include a plenum chamber surrounding the entire electrospray source such that the environment between the electrospray capillary and the front plate be purged with the curtain gas (and also contain potentially toxic species eliminating the risk of exposure to the investigator) [72].

Electrospraying the analogous iodine species was not as successful. The mass spectrum obtained with negative ES-MS of a solution of potassium iodide is shown in Fig. 7.3a. The iodate ion (Fig. 7.3b) was observed with low sensitivity and the periodate (mass spectrum not shown) was not detected. Presumably the periodate and to a lesser degree the iodate species oxidized the methanol solvent. If simple collisional decomposition of the iodate and periodate were occurring, a large iodide signal would have been observed in Fig. 7.3b.

A variety of sulfur species were electrosprayed in this third and final example of using ES-MS to differentiate between kinetically inert forms of an element having different molecular forms. The mass spectra obtained while electrospraying the sodium salt of thiocyanate, sulfite, sulfate, thiosulfate, and peroxodisulfate are shown in Figs. 7.4a to 7.4e

respectively. Sulfite is introduced into the environment from a variety of sources (fossil fuel emissions, the sulfite lyes used in the paper industry, and from the food industry which uses sulfur (IV) as a preservative) and also, because of its role in acid rain, much effort has gone into developing techniques to selectively measure sulfite [30]. The mass spectrum of a solution of sodium sulfite in HPLC grade methanol is shown in Fig. 7.4b. Most of the sulfur ion signal (90%) was in the SO_2^- form and the remainder in the HSO_3^- species. For the solution conditions used, bisulfite (-m/z = 81) and bisulfate ion (-m/z = 97) were the major forms in each of the respective solutions. A small amount of the mono-sodium sulfite and sulfate were also detected. While sulfite and sulfate were mono-protonated under the solution conditions employed, the thiosulfate species was detected in two forms [$S_2O_3^-/HS_2O_3^-$ ~ 2], indicative of a lower basicity of $S_2O_3^-$ relative to SO_4^{2-}. The peroxodithiosulfate was likely detected as SO_4^- and not as $S_2O_8^{2-}$ because dichromate ion, another oxygen bridged dimer did not remain intact without a solvation sphere and was detected as CrO_3^- [44]. Only a very small ion signal was observed for $S_2O_8^-$ (< 50 counts/second). The mass spectrum obtained when an equimolar mixture ($3x10^{-5}$ molar) of the sodium salt of thiocyanate, sulfite, sulfate, thiosulfate, and peroxodithiosulfate was electrosprayed is shown in Fig. 7.5. Sensitivity differences of these sulfur species (thiocyanate and sulfite (~9000 counts/second), the products of peroxodisulfate decomposition (~7500 counts/second), sulfate (~6000 counts/second) and thiosulfate (~ 3500 counts/second)) are attributed to mass bias as the ion optics were tuned to -m/z = 58 (SCN^-). For this reason, implications regarding the mechanism by which gas phase ions are ultimately produced in the electrospray process should not be inferred from this data.

These examples have led the authors to speculate on some potential uses of ES-MS that hold particular promise. First, the determination of elements that suffer from atomic or molecular-argon ion spectral interferences in ICP-MS such as potassium, calcium, iron, selenium and arsenic is troublesome [73]. ES-MS will likely not be handicapped by this spectral interference. When the electrospray source is operated as described above in conjunction with Figs. 7.2 and 7.4, determination of the oxo-anions of selenium and arsenic by ES-MS should be quite feasible. Indeed, Corr and Douglas did just that when they directly differentiated selenite and selenate [43]. While it would be extremely naive to think that ES-MS will not be without its own characteristic spectral interferences, there will certainly be niche applications where ES-MS performance may exceed that of ICP-MS, particularly in light of the fact that ES-MS can **directly** differentiate various kinetically inert species. Second, elements in organic matrices are problematic for ICP-MS analyses [74]. Conversely, organic solvents are more desirable than aqueous based solvents in ES-

MS based analyses. As pointed out by Boorn and Browner, the value of solvent extraction is often overlooked in efforts to avoid the introduction of organic matrices into the ICP wherever possible [75]. They do however, point out that sample preconcentration and physical separation of analyte from a matrix can be achieved quite efficiently through solvent extractions. A third example of a use of ES-MS may be for the determination of organometallics, an application that is discussed in section 7.4.4 below.

7.4.2 Differentiation of Kinetically Inert Species with Different Oxidation States

The question of differentiating two kinetically inert oxidation states of an element in solution was investigated for the case of the ferrous/ferric species. These two species exist as $Fe^{2+}(MeOH)_6(Sol)_d$ and $Fe^{3+}(MeOH)_6(Sol)_e$ (d and e = 0, 1, 2, ...) in methanol solution where ligands of the inner coordination sphere are represented as MeOH and ligands in the outer coordination sphere (also methanol molecules) are represented as $(Sol)_{(d\ or\ e)}$. In this example there is no advantage gained by removal of the outer coordination sphere, as was the case for the chlorine, iodine, and sulfur species discussed above to expose the different molecular form of the species. Furthermore the ferric ion does not remain stable in the gas phase cluster and charge reduction of a ligand occurs producing $[Fe(MeO)(MeOH)_{n-1}]^{2+}$. This cluster differs by only 0.5 amu from the ferrous cluster $[Fe(MeOH)_n]^{2+}$. (The nomenclature used to distinguish inner and outer sphere coordination ligands in solution has been dropped for the gas phase clusters and the charge, while still localized on the iron atom, applies to the entire gas phase cluster.) The chemistry of the charge reduction step has been discussed in detail by Blades et. al. [48].

Unfortunately the ELAN Model 250 mass spectrometer is capable of only unit resolution under optimal conditions and clearly differentiating these ions would be tenuous at best. In order to solve this problem the ES-MS interface parameters were adjusted such that the iron clusters were charge reduced to the plus one clusters $[Fe(MeO)(MeOH)_s]^+$ and $[Fe(MeO)_2(MeOH)_t]^+$ which are resultant from ferrous and ferric iron species respectively. The mass spectrum obtained for a ferrous iron solution is shown in Fig. 7.6a. In addition to observing the $[Fe(MeO)(MeOH)_s]^+$ species, several other forms of the ferrous ion were detected and are labeled in Fig. 7.6a. Fig. 7.6b shows the mass spectrum obtained under similar conditions for a solution of ferric iron where the doubly charge reduced $[Fe(MeO)_2(MeOH)_t]^+$ cluster is observed. An equimolar mixture of ferrous and ferric iron

was electrosprayed to generate the mass spectrum shown in Fig. 7.6c and both solution oxidation forms of iron were detected. No explanation can be given for the low signal intensity of $[Fe(MeO)_2(MeOH)_4]^+$ at m/z = 150 in Fig. 7.6c. For quantitation purposes of the total iron present in solution, both ferrous and ferric iron can be declustered down to the bare metal Fe^+ (Fig. 7.6d). Declustering is accomplished by increasing the electric field gradient across the jet expansion between the sampling plate orifice and the skimmer orifice to ~950 V/cm [68].

7.4.3 Inorganic Complexes

The silver-cyanide and ferric-fluoride complexes were used to demonstrate the usefulness of ES-MS for speciation of inorganic complexes. The silver-cyanide complex formation constant in water is $pK_f = 20.48$ [76]. The mass spectrum obtained by electrospraying a $3x10^{-4}$ molar solution of sodium cyanide is shown in Fig. 7.7a and the CN^- and MeO^- peaks are labeled. The CN^- signal intensity (~ 2000 counts/second) is representative of the equilibrium of CN^- with HCN in the methanol solution. Background ion signals were not labeled in Fig. 7.7. Upon addition of silver nitrate, the appearance of the $Ag(CN)_2^-$ complex is observed at -m/z = 159 and 161 (Fig. 7.7b). Associated with the appearance of the $Ag(CN)_2^-$ complex was an increase in the CN^- signal level in Fig. 7.7b. Collisional decomposition of the $Ag(CN)_2^-$ complex in the jet expansion after removal of all solvation ligands from the cluster is the only explanation for the increase in the CN^- signal intensity. Decomposition of the solvated $Ag(CN)_2(MeOH)_n^-$ complex would produce HCN and MeO^-. Using positive mode ES-MS, the free silver ion concentration was below the detection limit (est. ~ 10^{-7} molar) [77].

With respect to the collisional decomposition of the silver-cyanide complex in the jet expansion, decreasing the sampling plate voltage bias (reduction of the electric field gradient across the jet expansion) decreased the degree of collisional declustering of $Ag(CN)_2^-$ as monitored by an increase in the signal intensity ratio $Ag(CN)_2^-/CN^-$. Unfortunately, a reduction of the total ion current reaching the detector was associated with a reduced sampling plate voltage bias. Therefore the sampling plate voltage bias of -40 V used for this study was an arbitrary optimum between collisional decomposition of the complex while minimizing the number of $Ag(CN)_2(MeOH)_n^-$ detected. For these reasons, and especially because the instrument used has not been calibrated with respect to mass bias, an estimate of the degree of collisional decomposition of $Ag(CN)_2^-$ was not possible.

This silver-cyanide example shows in principle that it is possible to monitor the ionic chemical forms of metal-ligand(s) complex equilibria. Certainly techniques that can measure the free (uncomplexed) metal are useful because the free metal is usually the most toxic chemical form of the element. Extending on that same argument, it would be more informative to the investigator if the entire system could be measured. ES-MS should be able to provide identification of all complexing ligands in the system and how the analyte element is distributed in that system, particularly in the case when the most toxic form(s) of the analyte element is not the free metal.

The second example of complex equilibria to be discussed is the iron fluoride complex. The mass spectrum of ferric nitrate at $1x10^{-4}$ molar in methanol is shown in Fig. 7.8a. The same ES-MS operating conditions used to acquire the mass spectra in Figs. 7.6a to 7.6c were used for the acquisition of the mass spectra that are shown in Fig. 7.8.

Addition of sodium fluoride to the ferric nitrate solution such that the total ferric iron and fluoride were both $1x10^{-4}$ molar, yielded the mass spectrum shown in Fig. 7.8b. Using the aqueous FeF^{2+} formation constant of $pK_f = 6$ [76] yields that 90 % of the iron should be complexed with fluoride. In support of solution species concentrations based on the FeF^{2+} formation constant in water of $pK_f = 6$, the sum of the free iron signal intensities did decrease by approximately 90%, in qualitative agreement with the aqueous formation constant. It is immediately apparent however in Fig. 7.8b that an FeF^{2+} complex was not detected.

In the inset in Fig. 7.8b, there are ion signals that can only have been derived from the ferric iron-nitrate complex. To explain, the $Fe(NO_3)^{2+}$ complex in water is $pK_f \sim 1$ [76] and a concentration for the $Fe(NO_3)^{2+}$ ion in solution was calculated as $\sim 3x10^{-7}$ molar. An Fe^{3+} concentration of $\sim 9.97x10^{-5}$ molar was calculated assuming the aqueous value of the iron-nitrate formation constant in the solvent methanol. The solution ion $[Fe(NO_3)(MeOH)_n]^{2+}$ is transferred intact to the gas phase, but readily decomposes to $[FeO(MeO)]^+$ and $[FeO(H)(MeOH)_l]^+$ according to Eqns. 7.1 to 7.5. Eqn. 7.1 refers to the loss of solvent molecules due to solvent evaporation from $Fe(NO_3)(MeOH)_m^{2+}$. The charge reduction step is expressed by Eqn. 7.2. Decomposition of the nitrate ligand (Eqn. 7.3) occurs with further solvent loss from the charge reduced ion cluster. Loss of the last solvent molecules from the ion cluster is expressed by Eqn. 7.4, after which the ion cluster further decomposes via Eqn. 7.5a with loss of a methanol molecule or by Eqn. 7.5b which

involves decomposition of the methoxy-group with loss of formaldehyde. The $FeO(MeO)^+$ and $FeO(H)(MeOH)_l^+$ products in Eqn. 7.5 are labeled in the inset of Fig. 8b.

$$Fe(NO_3)(MeOH)_m^{2+} \longrightarrow Fe(NO_3)(MeOH)_n^{2+} + m\text{-}n(MeOH) \quad (7.1)$$

$$Fe(NO_3)(MeOH)_n^{2+} \longrightarrow Fe(NO_3)(MeO)(MeOH)_{n-2}^{+} + H(MeOH)^+ \quad (7.2)$$

$$Fe(NO_3)(MeO)(MeOH)_{n-2}^{+} \longrightarrow FeO(MeO)(MeOH)_p^{+} + n\text{-}2\text{-}p(MeOH) + NO_2 \quad (7.3)$$

$$FeO(MeO)(MeOH)_p^{+} \longrightarrow FeO(MeO)(MeOH)_l^{+} + p\text{-}1(MeOH) \quad (7.4)$$

$$FeO(MeO)(MeOH)_l^{+} \longrightarrow FeO(MeO)^+ + MeOH \quad (7.5a)$$

$$FeO(MeO)(MeOH)_l^{+} \longrightarrow FeO(H)(MeOH)_l^{+} + CH_2O \quad (7.5b)$$

The ferric iron-fluoride complex in solution should have produced $FeF(MeO)^+$ and/or $FeF(H)(MeOH)_l^+$, according to Eqns. 7.1 to 7.5 (after modification of these equations to read fluoride in-place of nitrate anion). The $FeF(MeO)^+$ and $FeF(H)(MeOH)_l^+$ clusters were expected at m/z = 106 and 108 respectively (see inset in Fig. 7.8b). The FeF^{2+} complex in solution was very likely not transferred to the gas phase by the electrospray process, else the gas phase FeF^{2+} complex, or the collisional decomposition products of such a complex would have been detected. Additionally, the semi-quantitative signal intensity observed for the sodium ion is remarkably similar to the observed sodium signal intensity from a solution containing only sodium fluoride. Hence it is entirely probable that Na^+ competes only with the free Fe^{3+} and $Fe(NO_3)^{2+}$ but not with FeF^{2+} for the charge sites in the charged droplets. Competition for the charge sites in a charged droplet are to a first approximation statistical [35] and the high sensitivity for sodium ions from this solution was very surprising. K. Chaudhuri and N. S. Islam have reported that the octahedral FeF_6^{3-} ion has sharing fluoride ions in crystalline salts [78]. An explanation of the failure to observe the FeF^{2+} complex is that fluoride ions are shared in solution even when the stoichiometry for Fe^{3+} and F^- is 1:1. Along these lines a polymerization of the ferric iron-fluoride monomers to form $[-(FeF^{2+})_n-]$ provides a better picture of this complex in methanol solvent. Such a polymer would be very different from the inorganic polymers [i.e. $(-CH_2O-)_nNa^+$ and $(-CH_2O-)_nSO_4^{2-}$] used by Cody et. al. for mass calibration

purposes [79] and by J. B. Fenn and co-workers in their investigative studies of the electrospray process [80,81].

Electrospraying a solution containing $1x10^{-4}$ molar iron (III) nitrate and $3x10^{-4}$ molar sodium fluoride produced the mass spectrum shown in Fig. 7.8c. Nearly all of the iron is complexed by fluoride as the free iron concentration is calculated to be ~ $5x10^{-7}$ molar in this solution (~ 0.5 % of the total iron added to the solution). The FeF^{2+} complex was however, detected from this solution (see inset in Fig. 7.8c). The collisional decomposition product of $FeF(MeOH)_m^{2+}$ was $[FeF(H)(MeOH)_1]^+$ indicating a slightly different charge reduction scheme (see Eqns. 7.6 to 7.9) than was observed for $Fe(NO_3)(MeOH)_m^{2+}$. $FeF(MeO)^+$ was not a stable gas phase ion whereas $FeO(MeO)^+$ was. Compare Eqns. 7.5a and 7.5b with Eqn. 7.9 and the insets in Fig. 7.8b and 7.8c. Decomposition products from the ferric iron-nitrate complex are no longer detected in Fig. 7.8c.

$$FeF(MeOH)_m^{2+} \longrightarrow FeF(MeOH)_r^{2+} + m\text{-}r(MeOH) \qquad (7.6)$$

$$FeF(MeOH)_r^{2+} \longrightarrow FeF(MeO)(MeOH)_{r-2}^{+} + H(MeOH)^+ \qquad (7.7)$$

$$FeF(MeO)(MeOH)_{r-2}^{+} \longrightarrow FeF(MeO)(MeOH)_1^{+} + r\text{-}3(MeOH) \qquad (7.8)$$

$$FeF(MeO)(MeOH)_1^{+} \longrightarrow FeF(H)(MeOH)_1^{+} + CH_2O \qquad (7.9)$$

The mass spectrum obtained when the concentration of the sodium fluoride in the solution being electrosprayed is increased to $9x10^{-4}$ molar while keeping the total iron (III) present in the system at $1x10^{-4}$ molar is shown in Fig. 7.8d. The free iron remaining in solution (est. $1x10^{-7}$ molar) was not detected due to competition for the excess charge within the droplets with Na^+ ($9x10^{-4}$ molar) even though this concentration of iron (III) is just at the detection limit when a solution containing only an iron(III) salt in solution is being electrosprayed. One must realize that the free iron competes on a statistical basis for the excess charge in the charged droplets with the sodium ions that are $9x10^{-4}$ molar.

7.4.4 Organometallics

Ions with increasing hydrophobic character produce increasingly larger electrosprayed ion signal intensities [35,36]. Therefore, ES-MS should prove ideal for detection of organometallics. This potential was recognized early by K. W. M. Siu and co-workers when they determined tributyltin in reference standard PACS-1 with ES-MS [40]. A mass spectrum of trimethyl generated in this laboratory is shown in Fig. 7.9. (The significance of this mass spectrum is that an identical concentration of inorganic tin (IV) produced an ion signal intensity ~ 200 counts/second with the same ES-MS conditions.)

The analysis of neutral species by ES-MS was not thought to be an analytically viable method. On the contrary, neutral species complexation with metal ions have shown otherwise [46,52,53,61]. In fact, recent reports of elemental speciation within bio-molecules using ES-MS indicate that this technique will be an invaluable diagnostic tool in deciphering the role of metals in bio-molecules [54-59]. Coupled with the fact that ES-MS has "opened the door to high molecular weight bio-molecule analysis," [36-39,82-92] it is speculated that ES-MS will prove instrumental in the measurement of all the elements of the periodic table within bio-molecules that serve important physiological roles.

7.5 Summary

In light of the examples presented here, using ES-MS for speciation measurements of inorganic ions in solution (chlorine, sulfur, iron, the silver-cyanide system, and the iron-fluoride system), and in addition to those presented by others and cited in the introduction, it should be clear to the reader that speciation investigations with ES-MS are quite feasible. However, several problems associated with the technique were alluded to in the results section and these problems are brought to the forefront in this summary with a comparison of ES-MS to the characteristics of an ideal speciation measurement technique.

First, a previous report by Agnes and Horlick showed quantitative analyses by ES-MS requires the use of an electrospray stabilizer and also an internal standard [77]. In the context of that report, an electrospray stabilizer was simply an inert electrolyte (i.e. KCl) added to the solution being electrosprayed. While a number of methods of injecting the electrospray stabilizer and internal standard are available, the reality is that an external electrolyte is being added to the system, potentially affecting species distribution in

solution. This point is certainly a matter of concern with respect to kinetically labile species distributions, but not when kinetically inert species are the target of the investigation.

Secondly, all mass spectra in this report are of ions derived from methanol solution. The electrospraying of aqueous solution is not as efficient with respect to the transfer of ions to the gas phase for mass spectrometric purposes [93]. Attempts to facilitate the electrospraying of aqueous solutions were, modification of the conductivity of the solution through addition of an organic acid such as acetic acid and the use of a sharpened electrospray capillary tip to increase the electric field strength [93], or sheathing the electrospray capillary with SF_6 to suppress electric discharge [94] in a variation of pneumatically assisted electrospray [72,95]. Indications are that the recently introduced "ultraspray ion source" which adds ultrasonic vibration to the charged electrospray capillary to assist droplet formation is capable of generating ions with high efficiency from aqueous solutions [96].

Before discussing the third point, it is noteworthy to re-iterate that ES-MS is capable of selectively monitoring all ionic species of an element in solution, a feature that is unique among kinetically labile speciation techniques. Kebarle and Tang suggested that diffusion driven equilibria within the charged droplet permits equilibration of the bulk electrolyte with the excess charge sites within the droplet [35,97,98]. It followed that ions from the bulk electrolyte statistically compete for the excess charge sites. In the iron (III) fluoride complexation example discussed in conjunction with Fig. 7.8b, Na^+, Fe^{3+}, $Fe(NO_3)^{2+}$, and FeF^{2+} account for all positively charged species in a solution of $Fe(NO_3)_3$ and NaF where each electrolyte was $1x10^{-4}$ molar. In light of the fact that FeF^{2+} was not detected in the mass spectrum shown in Fig. 7.8b, it can be assumed that only Na^+, Fe^{3+}, and $Fe(NO_3)^{2+}$ competed for the surface charge sites. While it is this characteristic of the electrospray process that allows the detection of all ionic species present in solution, it can not be overlooked that the Na^+ ion competition for surface charge sites with the analyte iron species is undeniably the source of a matrix effect in the gas phase generation of iron species from these droplets. In consideration of the number of possible concomitant ions present in a real sample and how these ions affect the sensitivity of analyte ion species, the method of standard additions will most certainly be required for reliable quantitation measurements.

It is the manner with which gas phase ions are generated by the electrospray process that permits monitoring of ionic species populations in solution that is itself the most serious

flaw with respect to kinetically labile speciation measurements. To explain, ions are not released into the gas phase until after the charged droplet has lost solvent molecules due to evaporation and the droplet has undergone several Rayleigh fissions, thus affecting the solution state species distribution. Furthermore, the calculations of Kebarle and Tang [35,97,98] that are based on the independent work by Taflin et. al. (15 % of the charge and only 2% of the mass is released on average during a Rayleigh fissional process [67]) show that the Rayleigh fissional product droplets have a higher ratio of excess surface charges to the population of the bulk ions than the charge releasing droplet. The degree to which kinetically labile species distributions are altered in the product droplets of Rayleigh fission was not ascertained in this study due to the lack of reliable formation constants in methanol solutions. Estimates of the bulk electrolyte concentration increase due to the solvent evaporation process is by a factor $\leq$ ~200 [35]. A bulk electrolyte concentration increase by a factor of 200 would negligibly alter the silver-cyanide equilibria. However when the formation constant is not as favorably large, measurable perturbation of the solution species equilibria can be predicted. Qualitatively though the iron fluoride complex behavior was modeled using the value of the aqueous formation constant, perhaps indicating that the increase in bulk electrolyte concentration through solvent evaporation may be offset by the increase in the ratio of excess charges to bulk electrolyte in the Rayleigh fission product droplets. The validity of this hypothesis is questionable at best and determination of the degree to which kinetically labile species distributions may be altered by the electrospray process was the subject of a separate investigation [99].

7.6 Conclusions

In the discussion of the results obtained it was made clear that ES-MS is not an "ideal speciation technique," however, it must be realized that there are no "ideal speciation techniques." In spite of this, several examples were provided indicating a very real potential for kinetically inert speciation determinations. The ability to directly measure all ionic species present in solution by the transfer of these species unchanged in the gas phase was noted as the most important advantage of ES-MS. This feature of ES-MS should prove useful in the monitoring of kinetically labile equilibria in dynamic systems. The inorganic applications of this technique are expected to be, but not necessarily limited to, samples that are difficult to analyze by ICP-MS. It is perhaps more constructive to view ES-MS and ICP-MS as two complementary techniques. Finally, because ES-MS is not limited to inorganic species determinations, this technique will continue to be utilized in the

investigation of novel research areas, thereby adding to the already impressive list of applications to which ES-MS has been successfully applied.

Table 7.1 Electrospray source and interface parameter set points.

Parameter	Positive Ion Mode	Negative Ion Mode
Electrospray Capillary (kV)	4.0	-3.0
Front Plate (V)	600	-600
Sampling Plate (V)	40	-30
Skimmer (V)	9	-9
Barrel Ion Extractor (V)	-1	1
Curtain Gas Flow Rate (lpm)	0.4 (N_2)	0.4 (O_2)

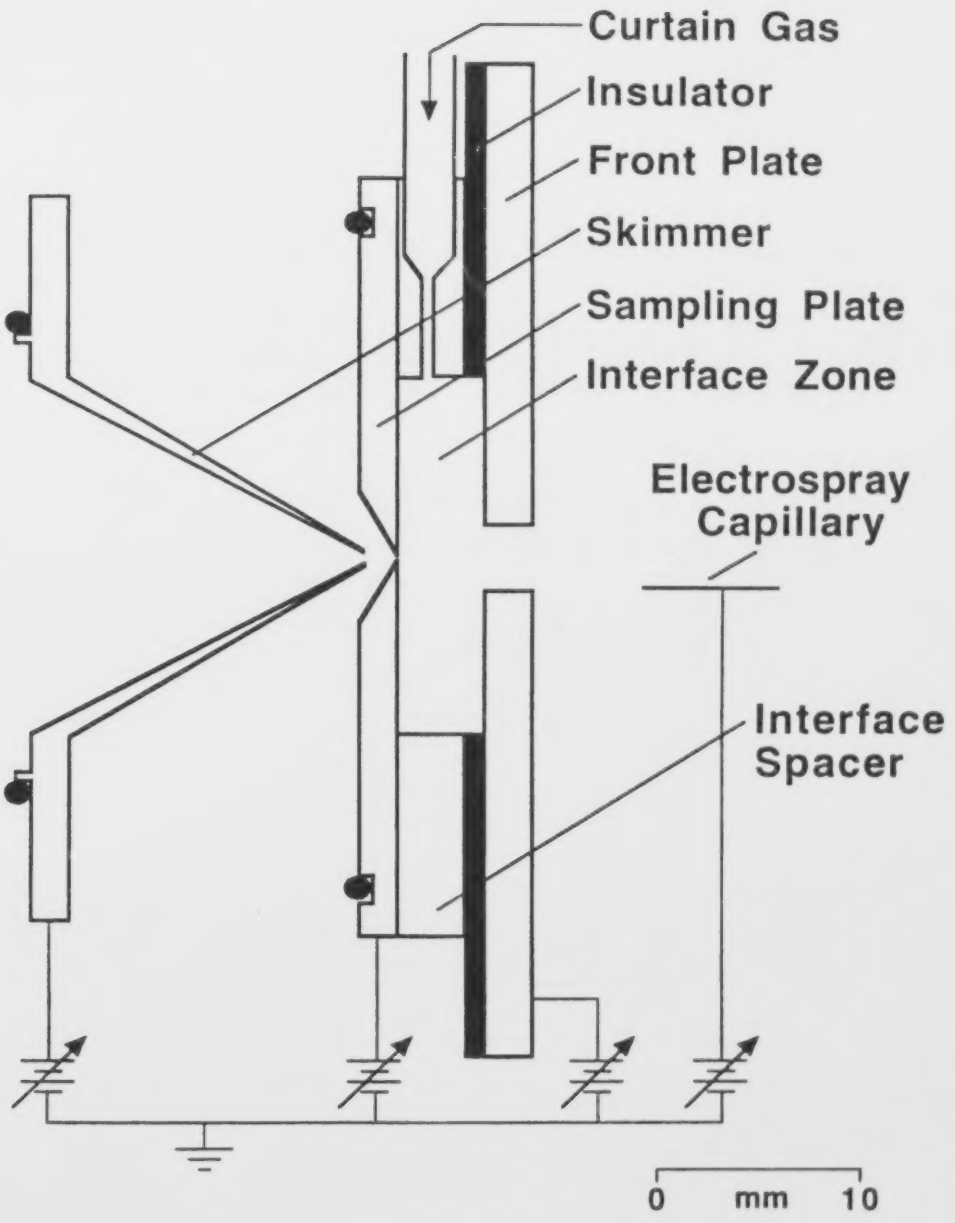

Figure 7.1 A schematic diagram of the Electrospray source and interface.

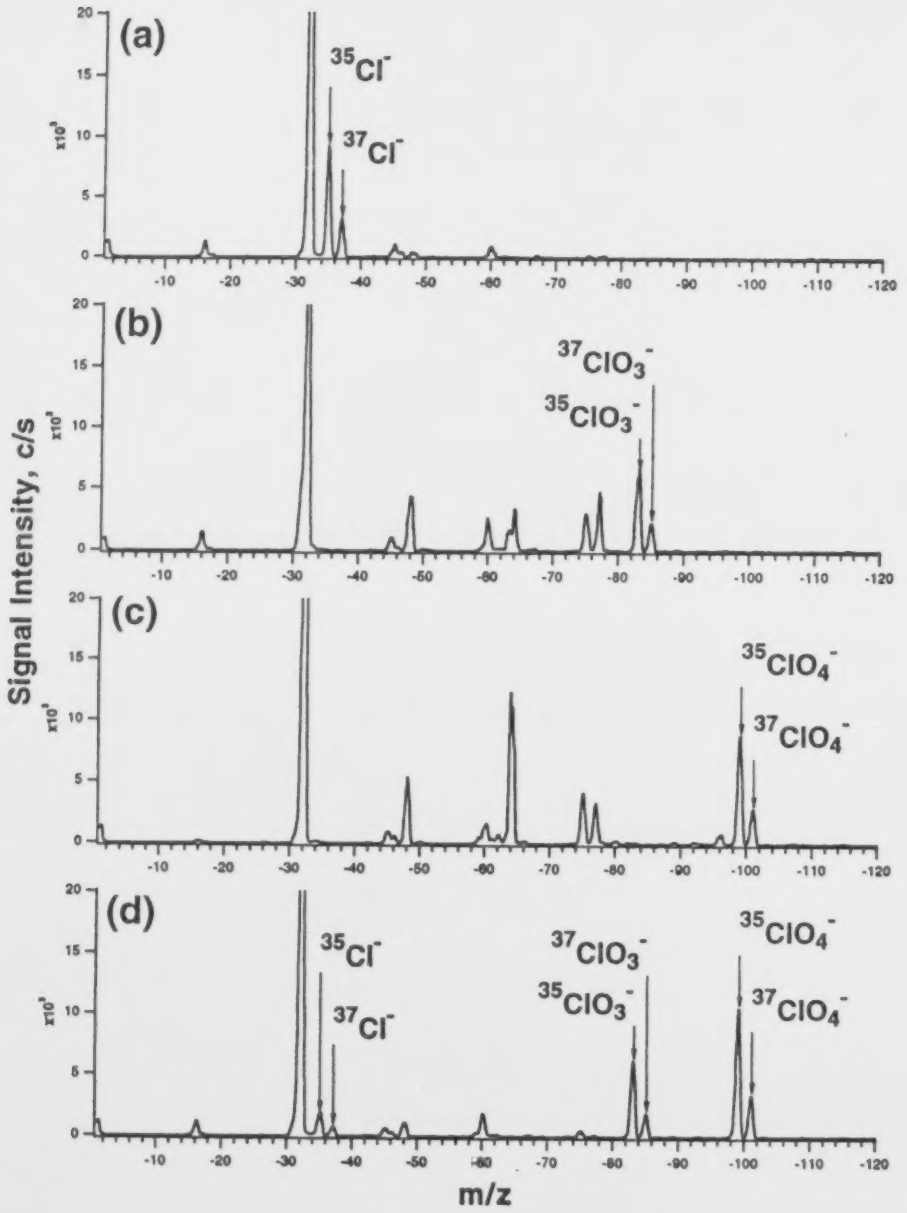

Figure 7.2 Mass spectra of (a) chloride, (b) chlorate, (c) perchlorate, and (d) an equimolar mixture of chloride, chlorate, and perchlorate acquired with negative mode ES-MS. All chlorine species concentrations were $1x10^{-4}$ molar.

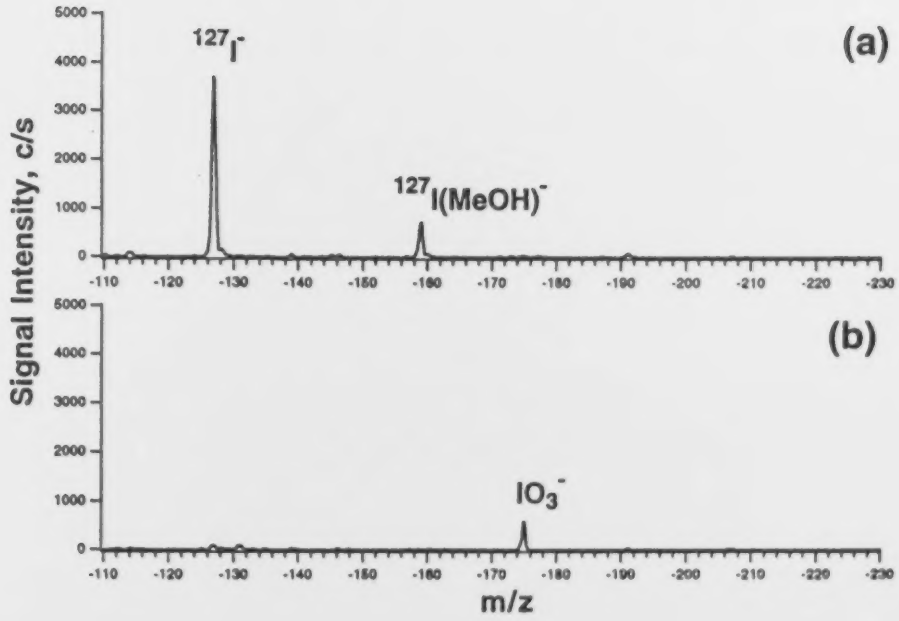

Figure 7.3 Mass spectra of (a) iodide and (b) iodate acquired with negative mode ES-MS. All iodine species concentrations were $1x10^{-4}$ molar.

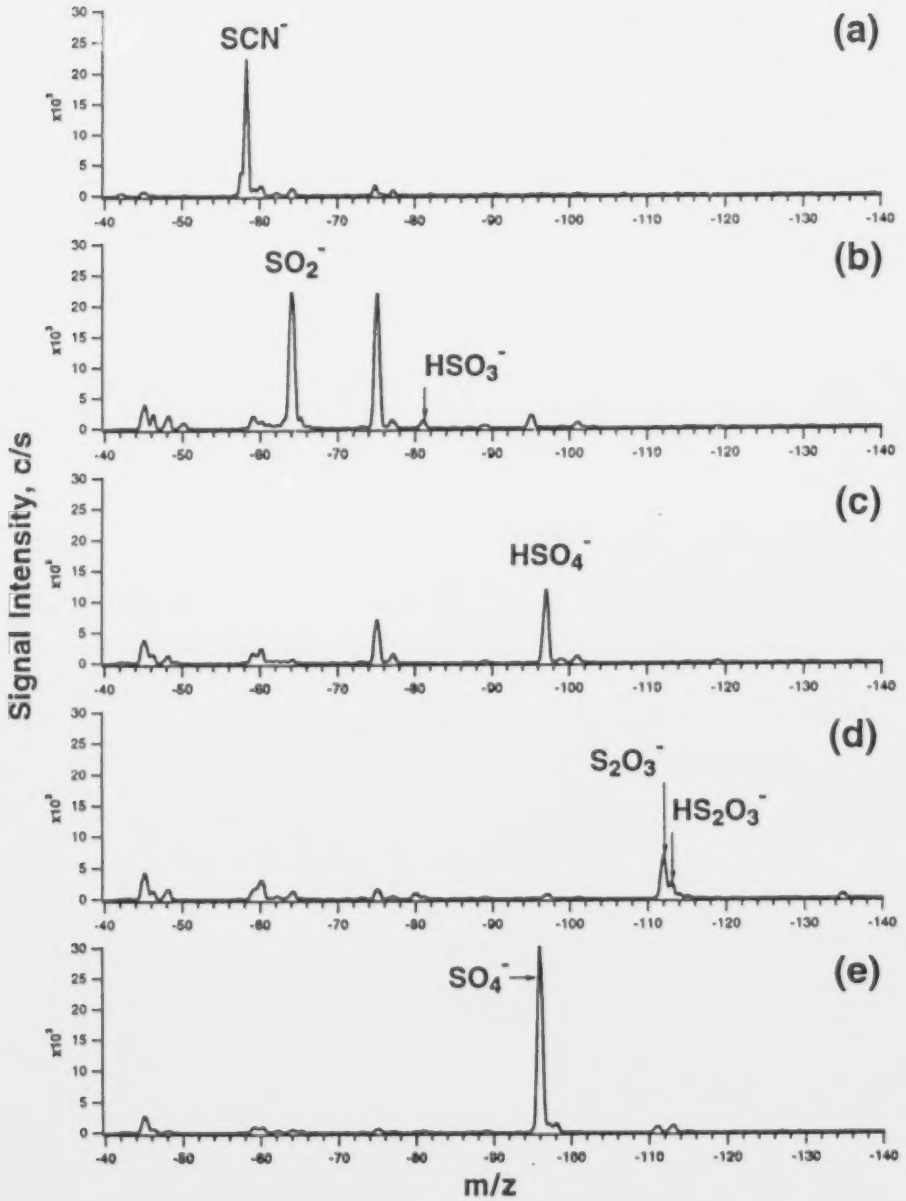

Figure 7.4 Negative mode ES-MS spectra of (a) thiocyanate, (b) sulfite, (c) sulfate, (d) thiosulfate, and (e) peroxodisulfate. All sulfur species concentrations were $1x10^{-4}$ molar.

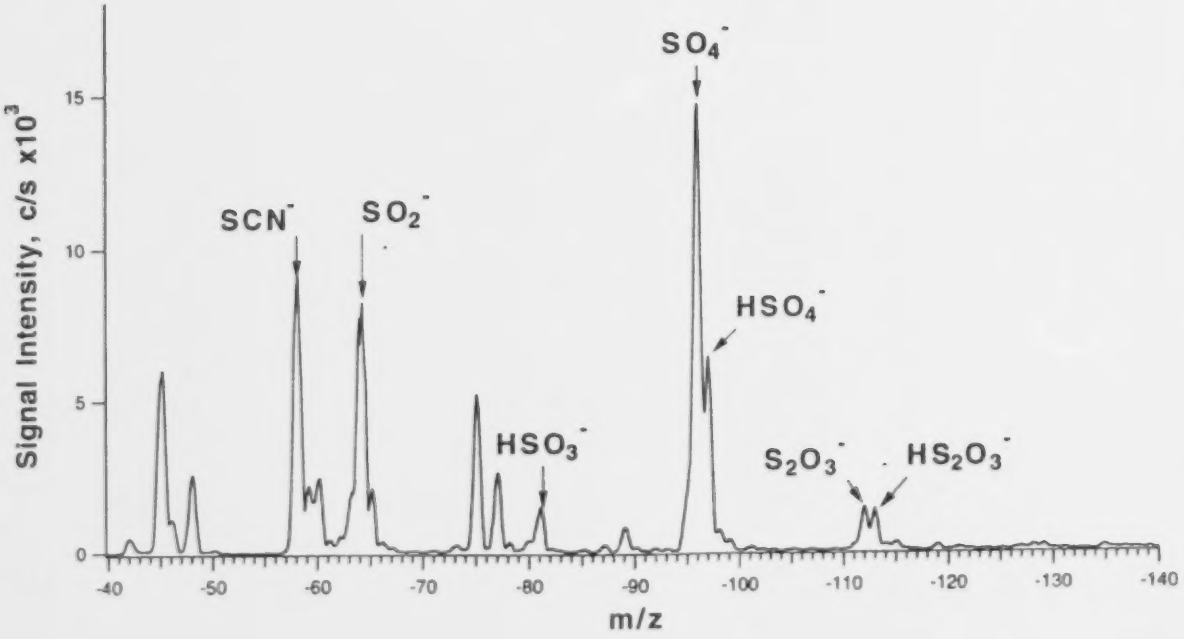

Figure 7.5 Negative mode mass spectrum of an eqimolar mixture ($3x10^{-5}$ molar) of thiocyanate, sulfite, sulfate, thiosulfate, and peroxodisulfate. The SO_4^- at -m/z = 96 is from the decomposition of peroxodisulfate.

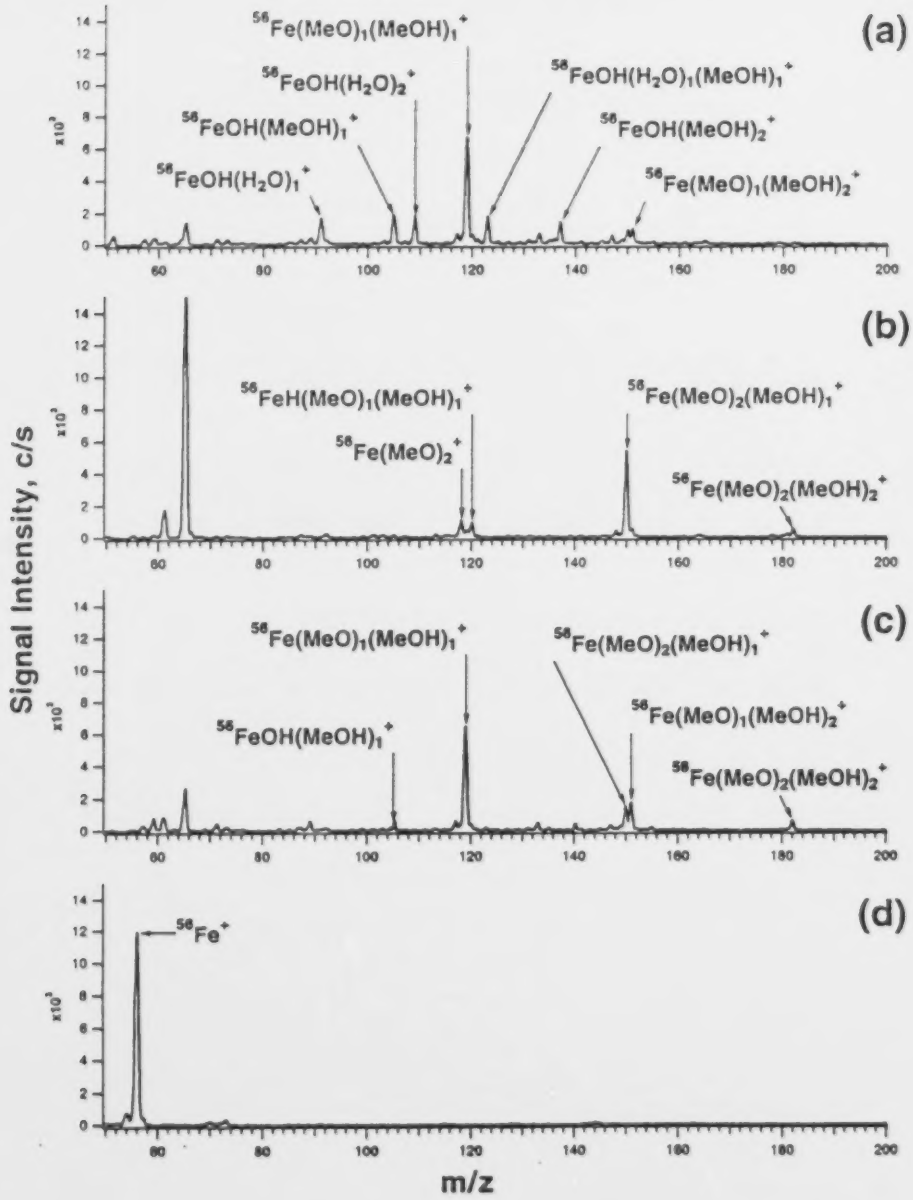

Figure 7.6 Positive mode mass spectra of (a) Fe(II), (b) Fe(III), and an equimolar mixture of Fe(II) and Fe(III) for both (c) and (d). Each of the iron species concentration was $1x10^{-4}$ molar. The mass spectrum in Fig. 7.6d was obtained under very harsh declustering conditions which were; Electrospray capillary 4.0 kV, front plate 950 V, sampling plate 190 V, and the flow rate of curtain gas was 0.7 lpm. See text for discussion.

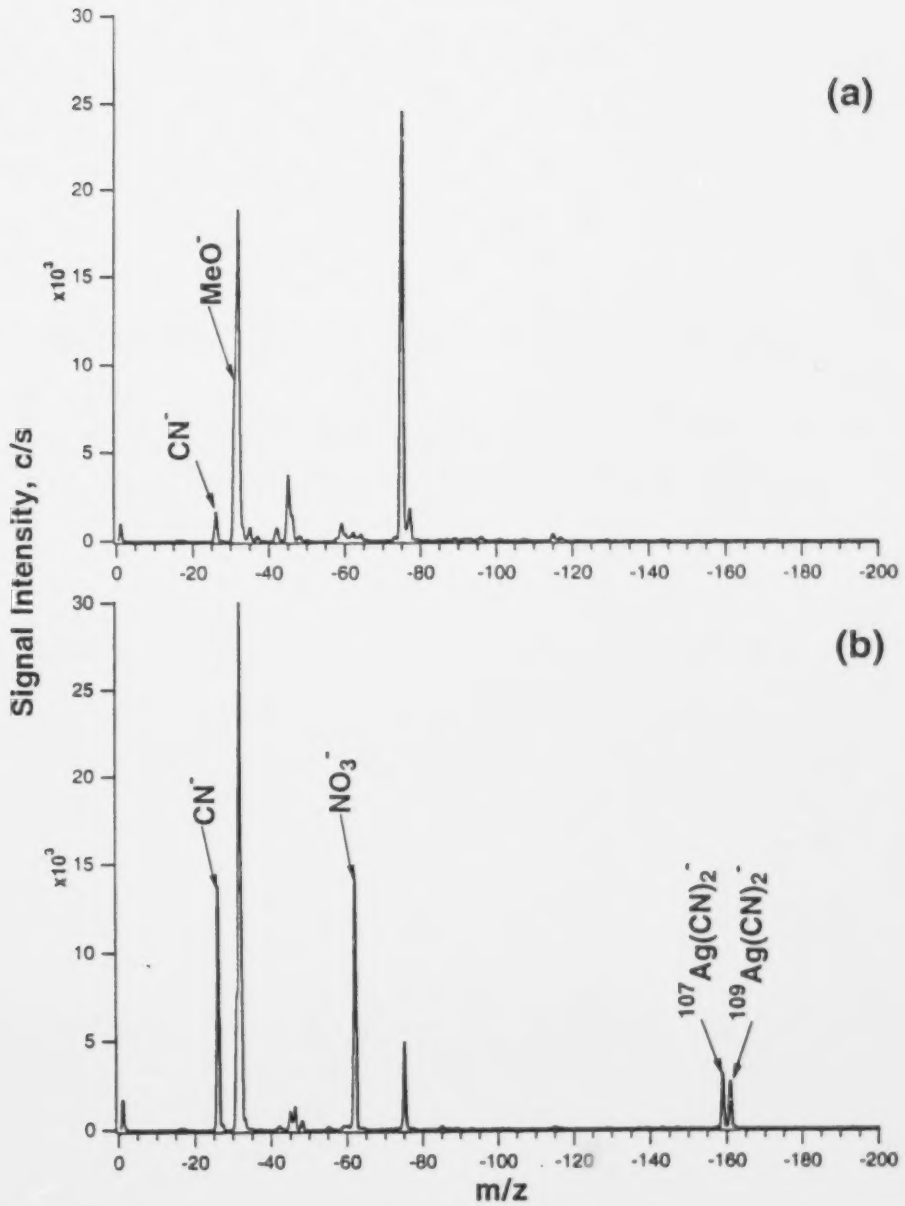

Figure 7.7 Negative mode mass spectra obtained while electrospraying (a) no Ag^+ added and (b) $1x10^{-4}$ molar Ag^+ in the presence of a fixed level of CN^- ($3x10^{-4}$ molar).

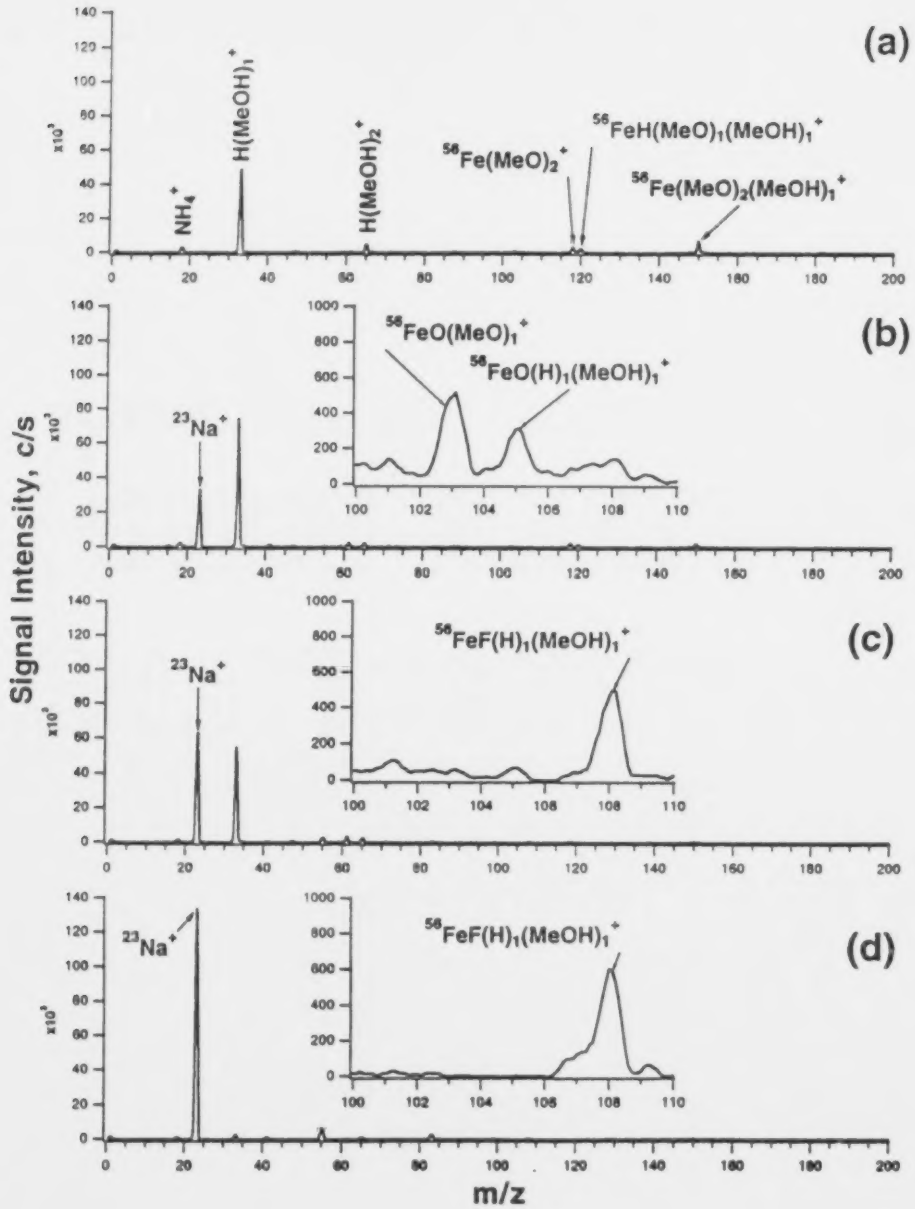

Figure 7.8 Positive mode mass spectra obtained while electrospraying a solution of (a) no added F^-, (b) $1x10^{-4}$ molar F^-, (c) $3x10^{-4}$ molar F^-, and (d) $9x10^{-4}$ molar F^-. A fixed level of Fe(III) ($1x10^{-4}$ molar) was present in each of the solutions electrosprayed.

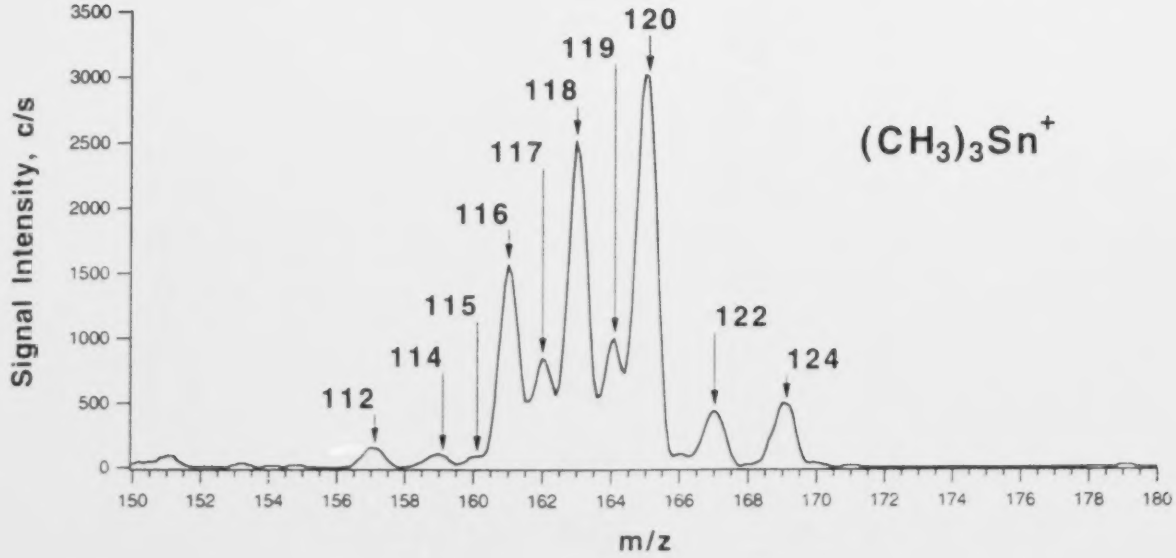

Figure 7.9 Electrospray mass spectrum of trimethyltin chloride ($1x10^{-4}$ molar).

7.7 References

1. R. Lobinski, W. M. R. Dirk, M. Ceulemans, and F. C. Adams, Anal. Chem., **64**, 159 (1992).

2. R. Lobinski, C. F. Boutron, J.-P. Candelon, S. Hong, J. Szpunar-Lobinska, and F. C. Adams, Anal. Chem., **65**, 2510 (1993).

3. K. A. Forbes, J. F. Vecchiarelli, P. C. Uden , and R. M. Barnes, Anal. Chem., **62**, 2033 (1990).

4. W.-L. Shen, N. P. Vela, B. S. Sheppard, and J. A. Caruso, Anal. Chem., **63**, 1491 (199).

5. S. D. Hartenstein, J. Ruzica, and G. D. Christian, Anal. Chem., **57**, 21 (1985).

6. C. W. Mcleod, I. G. Cook, P. J. Worsfold, J. E. Davies, and J. Queay, Spectrochim. Acta., **40B**, 67 (1985).

7. B. Patel, S. J. Haswell, and R. Grzeskowiak, J. Anal. At. Spectrom. **4**, 195 (1989).

8. R. S. Houk and S. J. Jiang, in *Trace Element Analysis and Speciation*, I. S. Krull, Ed., Elsevier: Amsterdam, 1991; Chapter 5.

9. R. M. Harrison and S. Rapsomanikis, *Environmental Analysis Using Chromatography Interfaced with Atomic Spectroscopy*; John Wiley and Sons: New York, 1989.

10. S. C. K. Shum and R. S. Houk, Anal. Chem., **65**, 2972 (1993).

11. L. C. Alves, L. A. Allen, and R. S. Houk, Anal. Chem, **65**, 2468 (1993).

12. N. P. Vela and J. A. Caruso, J. Anal. At. Spectrom., **8**, 787 (1993).

13. S. J. Hill, J. Bloxham, and P. J. Worsfold, J. Anal. At. Spectrom., **8**, 499 (1993).

14. C. Vanecasteele, H. Vanhoe, and R. Dams, J. Anal. At. Spectrom., **8**, 781, (1993).

15. E. Larsen, G. Pritzi, and S. H. Hansen, J. Anal. At. Spectrom., **8**, 557 (1993).

16. J. Goossens, L. Moens, and R. Dams, J. Anal. At. Spectrom., **8** 921 (1993).

17. L. C. Alves, L. A. Allen, and R. S. Houk, Anal. Chem. **65**, 2468 (1993).

18. V. V. Salov, J. Yoshinaga, Y. Shibata, and M. Morita, Anal. Chem., **64**, 2425 (1992).

19. J. R. Pretty, E. A. Blubaugh, and J. A. Caruso, Anal. Chem., **65**, 3396 (1993).

20. N. P. Vela, L. K. Olson, and J. A. Caruso, Anal. Chem., **65**, 585A (193).

21. J. Posta, H. Berndt, S. K. Luo, and G. Schaldach, Anal. Chem., **65**, 2590 (1993).

22. C. P. Hanna, J. F. Tyson, and S. McIntosh, Anal. Chem., **65**, 653 (1993)

23. J. Posta, H. Berndt, S.-K. Luo, and G. Schaldach, Anal. Chem., **65**, 2590 (1993).

24. Z. Gao, G. Wang, P. Li, and Z. Zhao, Anal. Chem., **63**, 953 (1991).

25. J. A. Sweileh, D. Lucyk, B. Kratochvil, and F. F. Cantwell, Anal. Chem., **59**, 586 (1987).

26. F. F. Cantwell, J. Nielsen, and S. R. Hrudey, Anal. Chem., **54**, 1498 (1982).

27. S. L. Beli and A. Zirino, Anal. Chem., **65**, 2583 (1993)--J. Huang and M. S. Wrighton, Anal. Chem., 65, 2740 (1993).

28. J.-M. Zen and M. L. Lee, Anal. Chem., **65**, 3238 (1993).

29. B. A. Moyer, G. N. Case, S. D. Alexandratos, and A. A. Kriger, Anal. Chem., **65**, 3389 (1993).

30. M. Kuratli, M. Badertscher, B. Rusterholz, and W. Simon, Anal. Chem., **65**, 3473 (1993).

31. K. Suzuki, H. Yamada, K. Sato, K. Watanabe, H. Hisamoto, Y. Tobe, and K. Kobiro, Anal. Chem., **65**, 3404 (1993).

32. J. Janata, Anal. Chem., **64**, 921A, (1992).

33. M. Yamashita and J. B. Fenn, J. Phys. Chem., **88**, 4451 (1984).

34. M. Yamashita and J. B. Fenn, J. Phys. Chem., **88**, 4671 (1984).

35. P. Kebarle and L. Tang, Anal. Chem., **65**, 972A (1993).

36. J. B. Fenn, J. Am. Soc. Mass Spectrom., **4**, 524 (1993).

37. B. E. Winger, K. J. Light-Wahl, R. R. Ogorzalek Loo, H. R. Udseth, and R. D. Smith, J. Am. Soc. Mass Spectrom., **4**, 536 (1993).

38. J. B. Fenn, M. Mann, C. K. Meng, S. F. Wong, and C. M. Whitehouse, Mass Spectrom. Rev., **9**, 37 (1990).

39. R. D. Smith, J. A. Loo, R. R. Ogorzalek Loo, M. Busman, and H. R. Udseth, Mass Spectrom. Rev., **10**, 359 (1991).

40. K. W. M. Siu, G. J. Gardner, S. S. Berman, Anal. Chem., **61**, 2320 (1989).

41. K. W. M. Siu, R. Guevremont, J. C. Y. Le Blanc, G. J. Gardner, and S. S. Berman, J. of Chromatogr., **554**, 27 (1991).

42. J. M. Curtis and R. K. Boyd, Rapid Commun. Mass Spectrom., **7**, 409 (1993).

43. J. J. Corr and D. J. Douglas, "Elemental Ionspray-Mass Spectrometry: Analysis of Solutions of Metal Salts", in *Proceedings of the 41st ASMS conference on Mass Spectrometry and Allied Topics*, San Francisco, CA, May 30-June 4, 1993, page 732a.

44. G. Agnes and G. Horlick, "Determination of Solution Ions by Electrospray Mass Spectroscopy," Appl. Spectrosc. (accepted for publication).

45. G. R. Agnes And G. Horlick, Appl. Spectrosc., **46**, 401 (1992).

46. V. Katta, S. K. Chowdhury, and B. T. Chait, J. Am. Chem. Soc., **112**, 5348 (1990).

47. A. T. Blades, P. Jayaweera, M. G. Ikonomou, and P. Kebarle, J. Phys. Chem., **10**, 5900 (1990).

48. A. T. Blades, P. Jayaweera, M. G. Ikonomou, and P. Kebarle, Int. J. Mass Spectrom. Ion Processes, **102**, 251 (1990).

49. A. T. Blades, P. Jayaweera, M. G. Ikonomou, and P. Kebarle, Int. J. Mass Spectrom. Ion Processes, **101**, 325 (1990).

50. J. M Curtis, P. Blay, N. Burford, T. M. Parks, and S. Mason, "A Study of Air Sensitive Compounds Containing Low Coordinate Cationic Phosphenium and Arsenium Centers by Electrospray Mass Spectrometry", in *Proceedings of the 41st ASMS conference on Mass Spectrometry and Allied Topics*, San Francisco, CA, May 30-June 4, 1993, page 1033a.

51. Z. L. Cheng, K. W. M. Siu, R. Guevremont, and S. S. Berman, J. Am. Soc. Mass Spectrom., **3**, 281 (1992).

52. G. J. Van Berkel, S. A. McLuckey, and G. L. Glish, Anal. Chem., **64**, 1586 (1992).

53. G. J. Van Berkel, S. A. McLuckey, and G. L. Glish, Anal. Chem., **63**, 1098 (1991).

54. A. Fura and J. A. Leary, Anal. Chem., **65**, 2805 (1993).

55. R. P. Schneider, M. J. Lynch, J. F. Ericson, and H. G. Fouda, Anal. Chem., **63**, 1789 (1991).

56. Y.-T. Li, Y.-L. Hsieh, J. D. Henion, and B. Ganem, J. Am. Soc. Mass Spectrom., **4**, 631 (1993).

57. X. Yu, M. Wojciechowski, and C. Fenselau, Anal. Chem., **65**, 1355 (1993).

58. M. Jaquinod, E. Leize, N. Potier, A.-M. Albrecht, A. Shanzer, and A. Van Dorsselaer, Tetrahedron Lett., **34**, 2771 (1993).

59. E. Leize, R. Kramer, J. M. Lehn, and A. Van Dorsselaer, "Formation Study of Metal Complexes Self-Assembly by ESMS", in *Proceedings of the 41st ASMS conference on Mass Spectrometry and Allied Topics*, San Francisco, CA, May 30-June 4, 1993, page 878a.

60. G. K. Poon, G. M. F. Bisset, and P. Mistry, J. Am. Soc. Mass Spectrom., **4**, 588 (1993).

61. S. R. Wilson and Y. Wu, J. Am. Soc. Mass Spectrom., **4**, 596 (1993).

62. M. J. Huddleston, R. S. Annan, M. F. Bean, and S. A. Carr., J. Am. Soc. Mass Spectrom., **4**, 710 (1993).

63. B. M. Hughes, D. E. McKenzie, and K. L. Duffin, J. Am. Soc. Mass Spectrom., **4**, 604 (1993).

64. H.-Y. Lin and R. D. Voyksner, Anal. Chem., 65, 451 (1993).

65. J. V. Headley, M. S. Wong, P. W. Brooks, K. M. Peru, and A. Phillips, "Evaluation of Electrospray and FAB for Mass Spectrometry of Organometallic

Parasiticides", in *Proceedings of the 41st ASMS conference on Mass Spectrometry and Allied Topics*, San Francisco, CA, May 30-June 4, 1993, page 636a.

66. Lord Rayleigh, Philos. Mag., **14**, 184 (1882).

67. D. C. Taflin, T. L. Ward, and E. J. Davis, Langmuir, **5**, 376 (1989).

68. G. R. Agnes and G. Horlick, Appl. Spectrosc., submitted.

69. A. P. Bruins, Mass Spectrom. Rev., **10**, 53 (1991).

70. A. M. Dietrich, T. D. Ledder, D. L. Gallagher, M. N. Grabeel, and R. C. Hoehn, Anal. Chem., **64**, 496 (1992).

71. B. Chiswell and B. Keller-Lehmann, Analyst, **118**, 1457 (1993).

72. In *The API III Book*: SCIEX, Thornhill, Ontario, Canada.

73. E. H. Evans and J. J. Giglio, J. Anal. At. Spectrom., **8**, 1 (1993).

74. G. A. Meyer and P. N. Keiliher, "An Overview of Analysis by Inductively Coupled Plasma-Atomic Emission Spectrometry", in *Inductively Coupled Plasmas in Analytical Atomic Spectrometry*, A. Montaser and D. W. Golightly, Ed., VCH Publishers, New York, 2nd ed.

75. A. W. Boorn and R. F. Browner, "Application: Organics", in *Inductively Coupled Plasma Emission Spectroscopy, Part II: Applications and Fundamentals*, P. W. J. M. Boumans, Ed., John Wiley and Sons, 1987.

76. In *Critical Stability Constants*, Vol 4; by A. E. Martell and R. M. Smith, Plenum Press, 1977 New York.

77. G. Agnes and G. Horlick, "Electrospray Mass Spectrometry as a Technique for Elemental Analysis: Quantitative Aspects," Appl. Spectrosc. (accepted for publication).

78. K. Chaudhuri and N. S. Islam, Inorg. Chem., **25**, 3749 (1986).

79. R. B. Cody, J. Tamura, and B. D. Musselman, Anal. Chem., **64**, 1561 (1992).

80. T. Nohmi and J. B. Fenn, J. Am. Chem. Soc., **114**, 3241 (1992).

81. S. F. Wong, C. K. Meng, and J. B. Fenn, J. Phys. Chem., **92**, 546 (1988).

82. J. B. Fenn, M. Mann, C. K. Meng, S. F. Wong, and C. M. Whitehouse, Science, **246**, 64 (1989).

83. R. D. Smith, J. A. Loo, C. G. Edmonds, C. J. Barinaga, and H. R. Udseth, Anal. Chem., **62**, 882 (1990).

84. J. A. Loo, R. R. Ogorzalek Loo, K. J. Light, C. G. Edmonds, and R. D. Smith, Anal. Chem., **64**, 81 (1992).

85. T. Matsuo, T. Sakurai, H. Ito, and Y. Wada, Int. J. Mass Spectrom. Ion Processes, **118/119**, 635 (1992).

86. M. Mann, Org. Mass Spectrom., **25**, 576 (1990)

87. R. D. Smith, J. H. Wahl, D. R. Goodlett, and S. A. Hofstadler, Anal. Chem., **65**, 574A (1993).

88. S. C. Beu, M. W. Senko, J. P. Quinn, F. M. Wampler, and F. W. McLafferty, J. Am. Soc. Mass Spectrom., **4**, 557 (1993).

89. B. E. Winger, S. A. Hofstadler, J. E. Bruce, H. R. Udseth, and R. D. Smith, J. Am. Soc. Mass Spectrom., **4**, 566 (1993).

90. E. C. Huang, B. N. Pramanik, A. Tsarbopoulos, P. Reichert, A. K. Ganguly, P. P. Trotta, T. L. Nagabhushan, and T. R. Covey, J. Am. Soc. Mass Spectrom., **4**, 624 (1993).

91. R. Feng and Y. Konishi, J. Am. Soc. Mass Spectrom., **4**, 638 (1993).

92. C. L. Stevenson, R. J. Anderegg, and R. T. Borchardt, J. Am. Soc. Mass Spectrom., **4**, 646 (1993).

93. S. K. Chowdhury and B. T. Chait, Anal. Chem., **63**, 1660 (1991).

94. M. G. Ikonomou, A. T. Blades, and P. Kebarle, J. Am. Soc. Mass Spectrom., **2**, 497 (1991).

95. M. G. Ikonomou, A. T. Blades, and P. Kebarle, Anal. Chem., **63**, 1989 (1991).

96. J. W. Finch, B. D. Musselman, J. F. Banks, and C. M. Whitehouse, "Electrospray Ionization at LC Compatible Flow Rates on a Magnetic Sector," in *Proceedings of the 41st ASMS conference on Mass Spectrometry and Allied Topics*, San Francisco, CA, May 30-June 4, 1993, page 287a.

97. L. Tang and P. Kebarle, Anal. Chem., **63**, 3654 (1993).

98. Tang, Ph. D. dissertation, Univeristy of Alberta, Edmonton, Alberta, Canada, 1992.

99. G. R. Agnes and G. Horlick, Appl. Spectrosc., submitted for publication.

Chapter 8

Mechanistic Investigations of Electrospray Mass Spectrometry: Part I, On the Transfer of Ions from within a Charged Droplet to the Gas Phase

8.1 Introduction[6]

The use of electrospray mass spectrometry (ES-MS) has seen prolific growth over the past decade. The now famous use of ES-MS for molecular weight determinations of large biomolecules [1], an area of mass spectrometric research that was not amenable with traditional ionization sources, attracted the attention of the entire mass spectroscopy community and beyond. Early reports promoting this technique cited (1) soft ionization, (2) multiple charging, (3) no thermal requirements of the ion source and as well, (4) the electrospray source is simply a small capillary held at a high DC potential through which a solution is pumped. Almost any laboratory that has access to a mass spectrometer can easily construct an electrospray source and quickly evaluate this new ion source first hand. Consequently ES-MS has been used for a vast array of applications [2-4].

As with any novel technique, early mechanistic investigations into the unknown often lead to conflicting reports regarding the underlying processes involved. With time, more detailed and focused studies begin to unravel the mechanistic aspects of the technique. To date there has been considerable effort spent directly investigating the nature of the electrospray source or indirectly through observations from applied studies. While the use and success of a technique is not directly related to an understanding of the technique, clearly future instrumental developments and the success of forays into novel research areas depend on a detailed understanding of the technique.

Assessment of the current understanding of the electrospray source is reviewed to provide background for this study of the mechanism by which ions in the charged droplets are transferred to the gas phase.

8.2 A Review of the Literature

The first step in the electrical dispersion of a liquid is the application of a high DC voltage ($\geq$ 2 kV) to a capillary through which a solution is pumped. The second step involves the

---

[6] A version of this chapter has been submitted for publication. George R. Agnes and Gary Horlick, Appl. Spectrosc.

formation of a Taylor cone at the end of the electrospray capillary from which a jet of liquid emerges. The jet that emerges from the cone ultimately breaks apart due to electrical shearing forces exceeding the surface tension of the liquid and charged droplets are created [5-8]. The charge in the droplets is due to an excess of positive ions over negative ions (for positive electrospray). A. T. Blades et. al. have proposed an electrophoretic mechanism wherein oxidation of either solvent or anions within the electrospray capillary leaves a surplus of positively charged ions [9].

Once the charged droplets have formed they drift towards a counter electrode due to the electric field. The lifetime of the charged droplets is limited by the drift time between the electrospray capillary tip and the counter electrode which has been estimated to be on the order of a few milliseconds [10]. Before the droplets impact on the surface of a counter electrode, some of the excess charges within the droplet are released into the gas phase at atmospheric pressure. The charged species (solvated ions) can then be sampled into a mass spectrometer for mass to charge analysis.

The process by which the charges are expelled from the droplets is initiated by solvent evaporation from the droplet and this causes the surface field strength of the droplets to increase as the surface area of the droplet decreases. At a certain field strength described by the Rayleigh instability relation (Eqn. 8.1) [11] the surface electrostatic repulsion of the charges within the charged droplets exceed the binding energy of the droplet (surface tension) and a Rayleigh fission occurs. (Rayleigh fission has also been called an electrohydrodynamic breakdown.) In Eqn. 8.1, q is the charge in the droplet, R is the radius of the droplet, E_o is the permitivity or dielectric strength of the ambient medium, and s is the surface tension. D. Taflin et. al. used a levitation device to measure the physical changes of a charged droplet due to a Rayleigh fission and found that 15 % of the charge and 2 % of the mass of the droplet is released in a single Rayleigh fission event [12]. They also found that the charged droplets underwent fission prematurely at a radius of ~ 80 % from that defined by Eqn. 8.1 ($q_D/q_R \sim 0.8$ where q_D is the charge measured in the droplets and q_R is the charge contained in a Rayleigh or ideal droplet).

$$q^2 = (64\pi^2 E_o s)R^3 \qquad (8.1)$$

The solvent evaporation followed by Rayleigh fission cycle proceeds until very small droplets are produced. Kebarle and Tang have provided calculations of the physical parameters of the charged droplets as a function of charge and radius as it proceeds through

several solvent evaporation Rayleigh fission cycles based on the measurements of Taflin et. al. [13,14]. From the calculations by Kebarle and Tang, the charge and mass released by the Rayleigh fission was divided into 20 product droplets whose radius was ~1/10 the radius of the charged droplet that underwent Rayleigh fission. The calculations by Kebarle and Tang indicated that after three cycles, charged droplets were produced containing more excess charge (~ 280) than ion pairs (~ 80) in a droplet having a radius of ~ 29 nm. They concluded that the most efficient transfer of ions from solution to the gas phase was from such droplets.

It is however the precise mechanism by which the ions are transferred to the gas phase that remains controversial. The first person to explore mass spectrometric measurements of electrosprayed solutions was M. Dole and co-workers [15,16]. They explained their results on the basis of a charged residue model (CRM) where ultimately very small droplets were produced containing a single ion. Kebarle and co-workers have renamed this mechanism the single ion droplet theory (SIDT) in light of their calculations on the uneven Rayleigh fissional process [13,14]. The Rayleigh fissional process was termed uneven because a Rayleigh fission does not cause the droplet to split into two equal fragments. Significantly, the calculations by Kebarle and Tang on the physical characteristics of an evaporating charged droplet was that for the first time, the SIDT was shown to be theoretically plausible.

The only other alternative mechanistic explanation for the transfer of ions from within the charged droplets to the gas phase is known as the Ion Evaporation Theory (IET) which was proposed by Iribarne and Thomson [17,18]. The IET is based on the direct electrostatic desorption of a solvated ion from the surface of a charged droplet containing approximately 80 charges and having a radius of about 8 nm. Iribarne and Thomson were unable to observe gas phase ions produced from doubly charged solution ions in their experiments. They rationalized that the solvation energy of a doubly charged solution ion was too great for such ions to be electrostatically desorbed from the charged droplet at an appreciable rate. Hence their model included ion dependent variables such as the solvation energy and radius of the solvated ions where it was assumed that multiply charged solution ions would not surmount the activation energy barrier for ion evaporation. The IET predicts preferential desorption of ions from the charged droplets based on the properties of the individual ions in the charged droplet.

A number of investigations have been directed at deducing the mechanism by which solution ions in the charged droplet are transferred to the gas phase. J. B. Fenn observed increasing signal intensities as the organic content (read hydrophobic character) increased when a homologous series of quaternary ammonium ions was electrosprayed [19]. This observation was rationalized by correlating the ion signal intensities with an estimate of the free energies of solvation of the ions tested, in support of the IET. M. Sakairi et. al. utilized a series of amino acids where the observed signal intensities were correlated to differences in the solvation energy of the organic side chain of the amino acid in an effort to determine the validity of the IET [20]. They did find a correlation between the solvation energy and ion signal intensity, but also noted that the observed ion signal dependence on solvation energy was much lower than would be predicted from the ion evaporation theory alone. Tang and Kebarle also noted a very low dependence on the solvation energy on the observed ion signal intensity for a variety of test ions [14]. For this reason, they suggested that their results could also be explained by the SIDT theory with the assumption that the hydrophobic character of an ion be used as a measure of the relative surface activity of that ion which is in turn reflected by the relative signal intensity of that ion.

Smith and co-workers have long questioned the validity of the IET, particularly with respect to their observations of non-covalently bound complexes by ES-MS [21]. Furthermore, Rollëgen has supported the SIDT by arguing that Rayleigh fission occurs which prevents the droplet surface electric field strength required by the IET from being reached [22].

Estimates of the required surface field strength for positive ion emission is on the order of ~ 10^{10} V/m and for electron emission ~ 10^{9} V/m [23]. P. Reist however calculated a lower surface field strength of ~ 10^{8} V/m for electron emission [24]. The field strength of dried solute residues from charged droplets has been measured by V. Katta et. al. to be on the order of ~ 10^{9} V/m [25]. According to the IET a field strength of ~ 10^{9} V/m is required before ion evaporation is kinetically feasible. Therefore, if the field strength of the charged droplets increases to ~ 10^{9} V/m through solvent evaporation, then in negative mode ES-MS and assuming validity of the IET, there would be no ions observed as only electrons would be spontaneously emitted from the droplets. While the IET does hold physical validity, the IET requires that charges are only released into the gas phase from charged droplets having a narrow range of radii ($0.6 < r < 1$ nm) and also a narrow range of the number of excess charges within the droplet ($60 < q < 100$). What is known though is that whatever mechanism(s) is responsible for the release of the charges within a droplet, that mechanism

is not very efficient as the salt residues, remaining after all solvent has evaporated, have surface field strengths on the order of 10^9 V/m.

Essentially the two mechanisms considered here (IET and SIDT) to govern the electrospray process of transferring an ion in the charged droplet to the gas phase at atmospheric pressure requires that the ion be solvated. It is, however, the degree of ion solvation that distinguishes these two mechanisms. The IET implies that the ion be solvated by a solvation sphere during the transfer step whereas the SIDT can be thought of as a nano-droplet containing a single ion during the transfer step. This investigation had the objective to ascertain the degree to which either the IET or the SIDT controls the conversion of ions in the charged droplets to the gas phase. In particular, the electrospraying of well defined simple electrolyte salts in solution [4, 26-30] as opposed to loosely defined analyte ions such as bio-polymers proved to be very informative as a diagnostic tool regarding the subtle nuances of the electrospray source.

8.3 Experimental

A schematic diagram of the in-house constructed electrospray ion source and the interface to the atmospheric pressure sampling mass spectrometer is shown Fig. 8.1. The electrospray capillary used was 0.1 mm I.D. by 0.065 mm wall. The flow rate of solution used throughout the study was 10 µl/minute. The sampling plate orifice was 0.1 mm dia. and the skimmer orifice was 1 mm dia. The flow rate of curtain gas (drying gas) was controlled with a micrometer valve. Further details of this ion source are provided elsewhere [30].

Manipulation ion clusters sampled from atmospheric pressure by variation of the interface parameter set-points, namely the sampling plate voltage and the curtain gas flow rate, was recently described [28]. It was shown that depending on the set-point of the interface parameters, the solvation sphere of the inorganic ion could be preserved using gentle ion sampling interface conditions or removed from the ion with harsh interface ion sampling conditions, depending on the nature of the information sought. Gentle ion sampling was characterized by a low sampling plate voltage ($\leq$ 40 V). Harsh ion sampling interface conditions were characterized by a relatively high sampling plate voltage bias (> 80 V) and with such conditions there was not a threshold curtain gas flow rate required before an analyte ion signal could be observed. A variety of interface conditions used to acquire the

data reported and as such, the interface parameters used to acquire each set of data are included with the individual figure or table caption.

The mass spectrometer used was a SCIEX/Perkin-Elmer ELAN Model 250 and the ion optical arrangement used in this mass spectrometer is shown in Fig. 8.2. A high speed oscilloscope (HP 54542A) and a high resolution counter (Philips PM 5193 programmable synthesizer/function generator and Philips PM 6654 programmable high timer/counter) used in section 4.5 were used to provide monitoring of the ion signal independent of the ELAN Model 250 ion signal processing electronics.

All solutions were prepared from ACS grade salts which were dissolved in distilled deionized water. Unless otherwise stated, these stock solutions were then diluted by a factor of $\geq$ 100 with HPLC grade methanol before being electrosprayed and the concentration of the test analyte ion in each solution electrosprayed was $1x10^{-4}$ molar.

8.4 Results and Discussion

8.4.1 Suppression of Ion Signal Intensity Levels from Solutions with High Total Electrolyte Concentrations

The efficiency of the electrospray process is known to suffer as the total electrolyte concentration exceeds ~ $3x10^{-4}$ molar [10,31]. See for example the cesium calibration curve plotted in Fig. 8.3. The cesium ion signal intensity does not have unity slope at any point in the log log calibration plot. In fact at cesium concentrations ranging from $3x10^{-5}$ molar to $3x10^{-3}$ molar the slope of the log log calibration plot approaches zero. This characteristic of the electrospray process is confusing in light of the fact that the electrospray capillary current increases as the solution electrolyte concentration increases (see Table 8.1). A first intuition would be to expect the number of excess charges per droplet to increase due to the increased current, in turn producing a proportionately greater analyte ion signal intensity. This does not occur and in fact analyte signal levels decrease at high currents ($> 0.8x10^{-6}$ Amperes which corresponds to a cesium chloride concentration $\geq$ $3x10^{-3}$ molar in Fig. 8.3). See also reference 10 for further discussion of this electrospray phenomena.

This characteristic of the electrospray process is further demonstrated by the Cl^- and CH_3COO^- signal intensities shown in Fig. 8.4 for a solution containing a fixed concentration of chloride and acetate (each $1x10^{-4}$ molar) while the concentration of sodium hydroxide in the solution was increased. Below an added base concentration of $1x10^{-4}$ molar, the Cl^- and the CH_3COO^- signal intensities are relatively unresponsive to the added base. Increasing the total electrolyte concentration with the addition of base to $1x10^{-3}$ molar sodium hydroxide causes the ion signal intensities of both Cl^- and CH_3COO^- to fall to ~ 1,000 counts/second.

It has been suggested previously that the current carried by an electrosprayed droplet is limited [31,32]. If this is true, then conceptually, there will be a relative insufficiency of charge sites on the droplet surface at high electrolyte concentrations resulting in a less than unity slope for the log-log calibration plot. When the current imparted to the droplet is limited, as is the case for solutions having a total electrolyte concentration above $1x10^{-4}$ molar, ES-MS is inherently less sensitive towards multiply charged solution ions than singly charged solution ions. The simplified explanation that follows assumed a total of 100 charge sites available in the droplet (in reality there are likely several thousand). For the case of analyte M_a^{1+} being the only ion present in solution, 100 M_a^{1+} ions carry the charge within the droplet. When a solution of M_b^{2+} is electrosprayed there will be a total of 50 M_b^{2+} ions carrying the charge within the droplet. Similarly, there will be 33 M_c^{3+} when a triply charged analyte ion in solution is electrosprayed.

An early explanation regarding ion signal intensity reduction at high electrolyte concentrations was proposed by Iribarne and Thomson as the solid residue limit [17]. The solid residue limit was described simply as the radius of the charged droplet when all solvent has evaporated and it was assumed that at high initial electrolyte concentrations (> $1x10^{-3}$ molar) that the droplet dried to a salt residue before all charges in the droplet that would otherwise experience ion evaporation, evaporated. The IET requires a minimum surface electric field strength on the surface of the charged droplet before ion evaporation can proceed. Iribarne and Thomson therefore assumed that the required surface field strength was not reached before the droplet dried to a solid residue. This model seemed plausible until recently when Kebarle and Tang showed through calculations of the uneven Rayleigh fission process that a large portion of the charge carried by the droplet, can be released well before the solid residue limit is reached [13,14].

Tang and Kebarle explicitly showed the importance of the solution conductivity in ES-MS applications [31]. In that report, they presented Eqn. 8.2 that describes how the presence of a concomitant electrolyte (E) in the solution will suppress the analyte ion signal intensity (Eqn. 9 in reference 31). $I(A^+,g)$ is the gas phase ion current at atmospheric pressure, I is the total electrospray current, k_A and k_E are constants that express the rate of transfer of the ion from the droplets to the gas phase, $[A^+]$ and $[E^+]$ are the electrolyte concentrations of the ions, and f was defined as a proportionality factor to represent the fraction of droplet charge that gets converted into gas phase ions.

$$I(A^+,g) = If\ [\ k_A[A^+] / (k_A[A^+] + k_E[E^+])\ ] \qquad (8.2)$$

Kebarle and Tang used Eqn. 8.2 to determine the relative ion evaporation rate constant k of individual ions by measuring relative ion signal intensities when two ions were present in the solution being electrosprayed. Unfortunately Kebarle and Tang were not able to conclusively state the role of SIDT versus IET during the transfer step [14].

On the assumption that the solvophobic character of the test analyte ions employed by Kebarle and Tang was solely responsible for the differences in the observed relative signal intensities, then the use of inorganic ions that have no hydrophobic character simplifies Eqn. 8.2 in that the ion evaporation rate constant k is the same for all inorganic ions. Eqn. 8.3 was written on the assumption that the ion evaporation rate constants are unity for all inorganic ions.

$$I(A^+,g) = If\ [[A^+] / ([A^+] + [E^+])\ ] \qquad (8.3)$$

In this report a comparison of the predicted analyte ion signal intensity suppression with the measured relative suppression was used as the basis of investigation in an effort to determine the mechanism by which ions are transferred from the charged droplets to the gas phase at atmospheric pressure. Specifically, the signal intensity of an ion was measured both with and without the presence of a concomitant electrolyte in an effort to obtain relative signal intensity suppressions. Furthermore, measurement of the relative ion signal intensity suppression of an individual analyte ion removes any mass bias errors that would otherwise be a source of error.

To summarize, if an SIDT mechanism dominates in the ion transfer step from solution to the gas phase, then the analyte ion signal intensity suppression can be statistically predicted

by Eqn. 8.2. If, however, the IET mechanism dominates, then the relative ion signal intensity suppressions would not be statistically predicted in which case a correlation between the ion signal intensity suppression and the solvation energy would permit a qualitative assessment of the role of the IET in the transfer step.

8.4.2 Is there a Preferential Desorption Mechanism?

Under conditions that do not favor the evaporation of the charged droplets (i.e. very low curtain gas flow rates) it might be expected that a depletion process as described by Tang and Kebarle would be exposed because if the charge releasing droplets are not efficiently dried then one ion only would be preferentially detected [14]. The depletion mechanism described by Tang and Kebarle assumed the IET was valid and taken literally, the ions in solution that have a very much higher ion evaporation rate constant will be desorbed from the charged droplet first, before any other ions of lower ion evaporation rates desorb. Equilibration of the surface excess charges with the bulk electrolyte population in the droplet is assumed to continually replenish the surface charge site population of the ion with the higher evaporation rate. The preferential detection of one ion when a two component mixture was electrosprayed would invalidate Eqn. 8.3 where the assumption made was that the relative rates of ion evaporation for inorganic ions was equal for all inorganic ions.

The signal intensity of rubidium ion clusters as a function of curtain gas flow rate is plotted in Fig. 8.5. Fig. 8.5 was acquired with gentle ion sampling interface conditions. If the data contained in Fig. 8.5 were taken literally, then at low flow rates of drying gas (< 0.2 lpm) the charged droplets would not experience sufficient solvent evaporation to cause release of the charges from within the droplet to the gas phase. Conversely, at flow rates above 0.4 lpm, the charged droplets release all possible excess charge within the droplet to the gas phase. Intermediate flow rates between 0.2 and 0.4 lpm would thus create conditions where the charged droplets are only partially dried. Observation of preferential desorption of one ion over another would be most easily observed at intermediate curtain gas flow rates (between 0.2 and 0.4 lpm).

Since the absolute signal intensities were not corrected for mass bias, each ion signal intensity profile in Figs. 8.6 and 8.7 was normalized. Also, only equimolar solutions were employed except for Fig. 8.7b. A simultaneous increase of both ion signal intensity

profiles between curtain gas flow rates of 0.2 to 0.4 lpm was taken to indicate that no preferential desorption was occurring. In Fig. 8.6a the signal intensity profile for rubidium and cesium are plotted. The rubidium signal intensity profile experiences an onset of the rapid signal intensity increase at a lower relative flow rate than does the cesium ion signal intensity profile. This observation was originally taken to imply that there was a preferential desorption mechanism acting, in which case the charged droplet was only being partially dried and in turn only a fraction of the total charge in the droplet was being released at the intermediate curtain gas flow rates. This behavior was reproducible and the same trend was observed for rubidium versus strontium and also for rubidium versus yttrium. However, this trend was only observed when one of the ions in the pair was rubidium. A mass bias associated with the sampling plate voltage bias was suspected and by reducing the sampling plate voltage bias from 40 V to 20 V, both the cesium and rubidium ion signal profiles exhibited a similar response profile as a function of curtain gas flow rate (Fig. 8.6b).

The mass bias associated with the sampling plate voltage bias has its origins in the nature of the collisional declustering that occurs in the jet expansion between the sampling plate orifice and the skimmer orifice. Eqn. 8.4 is a representation of the declustering that occurs in the jet expansion. Consideration that a sampling plate voltage bias of 40 V was optimal for the preferential transfer of rubidium clusters through the jet expansion, relative to other ions clusters, a relative difference in the onset of the rise in the rubidium ion signal profile versus cesium in Fig. 8.6a was the result.

$$Rb(MeOH)_n^+ \longrightarrow Rb(MeOH)_1^+ + n\text{-}1(MeOH) \qquad (8.4)$$

Additionally, ion signal intensities as a function of curtain gas flow rate are shown in Fig. 8.7 for dissimilarly charged test ions. The test ions were chosen to include a singly charged solution ion and a doubly charged solution ion because the doubly charged solution ion was expected to have a much lower ion evaporation rate than a singly charged solution ion. The potassium and strontium ion signal intensity profile both experience a simultaneous rise in response to the increasing flow rate of curtain gas. No preferential desorption could be inferred from the data contained in Fig. 8.7a. The signal intensity as a function of curtain gas flow rate in Fig. 8.7b was obtained while electrospraying a solution of sodium and cobalt where the molar concentration of sodium was twice the molar concentration of cobalt. The separation of the sodium and cobalt ion signal profiles in Fig. 8.7b above curtain gas flow rates of 0.2 lpm was attributed to the charge reduction of

cobalt clusters to $Co(MeO)(MeOH)_m^+$ which may benefit from a higher relative transfer efficiency than its precursor ion cluster $Co(MeOH)_n^{2+}$. See reference 28 for further details regarding the nature of the inorganic ions detected under these conditions.

8.4.3 Suppression Effects Due to Similarly Charged Ions

In the previous section, a preferential desorption mechanism could not account for all observations. It was therefore surmised that the SIDT may be responsible for the transfer of ions in solution to the gas phase and not the IET. An investigation of analyte ion signal intensity suppression due to competition for the surface charge sites was used to substantiate the hypothesis that the SIDT was the primary mechanism by which ions are transferred from solution to the gas phase. Validity of this hypotehsis was ascertained with a comparison between the predicted ion signal intensity suppressions according to Eqn. 8.3 and the experimentally measured ion signal intensity suppressions.

To simplify the presentation of this statistical argument of analyte ion signal intensity suppression due to charge allocation within a charged droplet, it was assumed that there is a total of 100 charges available in the droplet. The test solution contains either the analyte electrolyte only in solution or the analyte electrolyte plus an equimolar amount of another inorganic electrolyte. Also it was assumed that the number of excess charges in the droplet is limited meaning that there will be competition between the equimolar ions in solution for the charge sites (for the purpose of the discussion, 100 charge sites were assumed) . The last condition is valid for total electrolyte concentrations $\geq \sim 1 \times 10^{-4}$ molar.

Recall that an electrosprayed solution containing only M_A^{1+} (or M_E^{1+}) would have 100 charge sites occupied by M_A^{1+} (or M_E^{1+}). When two singly charged ions M_A^{1+} and M_E^{1+} are present in solution there will be 50 M_A^{1+} and 50 M_E^{1+} ions carrying the charge within the droplet (the subscript A and E refer to the analyte and the added electrolyte respectively). Therefore a signal suppression of 50 % would be expected for both M_A^{1+} and M_E^{1+} when the ion signal intensities from the equimolar mixture of these two ions are compared to the ion signal intensities from the solution containing only M_A^{1+} or M_E^{1+}, if there is no preferential desorption mechanism. Importantly, the bulk electrolyte population within the charged droplet ($[M_a^{1+}]_{bulk} = [M_d^{1+}]_{bulk}$) will be equal to the ion charge carrying (or surface charge site) equilibrium of $[M_A^{1+}]_{scs} = [M_E^{1+}]_{scs}$ where the subscript scs indicates a surface charge site. This argument is unchanged for equimolar mixtures of two

similarly charged ions (i.e. C_i^{x+} and C_{ii}^{x+} for positive electrospray or A_i^{x-} and A_{ii}^{x-} for negative electrospray). Measurement of the relative signal intensity suppressions of both ions in solution will thus expose any mechanism acting that favors the desorption of one ion over the other ion in the charged droplet.

The measured ion signal intensity suppression effects due to a similarly charged concomitant ion, equimolar with the analyte ion are presented in Table 8.2. The signal intensity sum tabulated in column 3 was obtained by electrospraying two separate solutions in which a single electrolyte was dissolved in each. The ion signal intensities were then measured by electrospraying a solution containing both analytes (column 4). The standard deviation of the measured signal intensities was approximately 6 %, hence the uncertainty of the measured ion signal intensity suppression tabulated in column 5 was +/- 9 %. Thus a mechanism favoring the preferential desorption of one ion over another would have to be quite pronounced in order for such a mechanism to be uncovered by this method. To enhance any potential preferential desorption, test analyte ion pairs were selected such that the solvation energy of the two ions would be large (i.e. for the alkali metals, lithium has the largest solvation energy, cesium the lowest).

The suppression of an analyte ion signal is dependent on the conductivity of the solution. A higher relative level of suppression was expected for solutions of multiply charged ions versus solutions of two singly charged ions, even though the analyte ion concentration in all solutions was $1x10^{-4}$ molar. For the case of the singly charged solution ions, the relative signal intensity suppression was less than the predicted 50%, likely because the assumption that the current was limited was not valid. Importantly though, the relative suppression of lithium and cesium was equal for both ions at the two different flow rates. However, the absolute ion signal intensity suppression was greater at a lower flow rate of curtain gas (trial 1) versus at a higher flow rate (trial 2) in Table 8.2. An explanation for the relative signal intensity suppression dependence on the curtain gas flow rate can not be made at this time, although it would seem reasonable that these measurements are dependent on temporal and spatial nuances of the electrospray interface (the sampling of the charged droplets by the sampling plate hole, temporally and spatially where charges are released from the charged droplet, and also the sampling of gas phase ion clusters by the mass spectrometer sampling plate orifice are all affected by the flow rate of curtain gas).

In Table 8.2, the measured relative signal intensity suppressions for the doubly charged solution ions of ~ 50% were predicted by the statistical argument of charge allocation in the

droplet (see trials 3 and 4). As was observed with the singly charged solution ions tested, the relative signal intensity suppression was also equal, within experimental error for the doubly charged solution ion pairs tested. If a mechanism for preferential desorption of one ion over another is present, then that mechanism is not predominant in the process by which ions are transferred from the charged droplets to the gas phase.

8.4.4 Suppression Effects Due to Dissimilarly Charged Ions

When two electrolytes are present in the solution being electrosprayed, the question to be asked is "how does the available charge distribute between the two analyte ions?" Consider the case when an equimolar solution of M_a^{1+} and M_b^{2+} is electrosprayed. Are the charges, or charge sites evenly divided amongst the two analyte ions based on the populations of these two ions or does the charge get unequally divided so that the population equilibrium of the charge carriers remains equal to the bulk analyte population?

If the 100 droplet charges are divided amongst the two analyte ions based on an equimolar ratio, 50 charge sites will be occupied by M_a^{1+} and 50/2 charge sites will be occupied by M_b^{2+}. A signal suppression of 50 % would be predicted for both M_a^{1+} and M_b^{2+} when the ion signal intensities from the equimolar mixture of these two ions are compared to the ion signal intensities from the solution that contained only M_a^{1+} or M_b^{2+}. If this distribution of charge sites is valid, the population of droplet surface charge sites $[M_a^{1+}]_{scs} = 2[M_b^{2+}]_{scs}$ is not equal to the bulk electrolyte population equilibrium $[M_a^{1+}]_{bulk} = [M_b^{2+}]_{bulk}$.

If however the charge within the droplet is divided unequally then the equilibrium distribution of surface charge sites $[M_a^{1+}]_{scs} = [M_b^{2+}]_{scs}$ would be equal to the bulk electrolyte population $[M_a^{1+}]_{bulk} = [M_b^{2+}]_{bulk}$. In this case, there would be 33 M_a^{1+} and 33 M_b^{2+} ions carrying the 100 charges within the droplet. A signal suppression of 67% and 33% would be predicted for M_a^{1+} and M_b^{2+} respectively. A similar argument can be made for the case when an equimolar solution of M_a^{1+} and M_c^{3+} is electrosprayed where the predicted ion signal intensity suppression would be 75% and 25% respectively, if the available charge was divided unequally.

Initial measurements of the signal intensity suppression caused by a dissimilarly charged ion in solution were not reproducible. In searching for a cause, a time dependency on the relative suppression was observed. An example of the time dependency on the signal

intensity suppression is provided in Table 8.3. An increase of the relative suppression of the cesium ion signal intensity with elapsed time after applying high voltage to the electrospray tip was noted while a simultaneous decrease of the relative suppression of the magnesium ion signal intensity occurred.

What these results indicate is that upon application of the DC potential to the electrospray capillary, the charge in the first droplets to be produced is statistically divided amongst the ions present in solution. This observation could be expected if an electrophoretic mechanism was responsible for the charge in the droplets produced. Oxidation of solution species (either anions or solvent) in a positively biased electrospray capillary would not be selective as to what cations would be left unpaired. The equilibrium inequality of the charge sites, or ions carrying the charge, with the bulk electrolyte present in the droplet immediately after applying the high voltage to the electrospray capillary is not corrected during the lifetime of the droplet. Therefore the rate at which the charge carrying sites equilibrate with the bulk electrolyte in a charged droplet is slow compared to the lifetime of the charged droplet. To account for these observations, it is pointed out that the excess charges within the droplet are rigidly held on the surface of the droplet by mutual electrostatic repulsion from the other charges within the droplet. The charge carrying sites within the droplet would therefore be expected to have a low tendency to undergo a charge site occupancy exchange with an ion from the bulk electrolyte. Ion pairing in the relatively low dielectric strength solvent methanol may also contribute to the inability of the charge carrying sites to equilibrate with the bulk electrolyte during the lifetime of the droplet.

Significantly, the population equilibrium of the charge carriers present in the droplet at the instant the droplet formed can therefore be considered special, and ES-MS may permit accurate measurement of kinetically labile species distributions present in the solution (i.e. solvent evaporation from the charged droplets may not significantly affect the charge carrying site distribution). This argument pertains to inorganic ions only. Results from L. Tang imply that if two ions present in solution having significantly different hydrophobic moieties, then the charge carrying site distribution may be altered during the course of the lifetime of the droplet [13,14].

With the passage of time (minutes) after application of the high voltage to the electrospray tip, the charge carrying population inequality with the bulk electrolyte population is significantly reduced or even negated as observed by the increased ion signal intensity suppression for the cesium and the reduced ion signal intensity suppression for magnesium

(see Table 8.3). This observation implies that the electrospray capillary current is not generated solely at the capillary tip where the Taylor cone forms, but that the equilibrium between charge carriers and the bulk electrolyte that was observed occurs in the electrospray capillary, not in the charged droplets. Oxidation of a species within the electrospray capillary leaves a surplus of charges in the capillary where the electric field is imposed by the capillary walls. Even though the excess charges will be found on the capillary wall double layer, the surplus ions are not locked in space by mutual electrostatic repulsion since the imposed electric field is imposed by the capillary wall. Within the confines of the capillary walls, it would be possible for these excess charges to equilibrate with the bulk electrolyte population. Immediately after exiting the electrospray capillary (i.e. in the Taylor cone and in the charged droplets) the excess charges themselves impose the electric field, meaning that the charge carriers move to the surface of the liquid and become locked in space preventing or very strongly reducing the ability to exchange with the bulk electrolyte once free of the capillary walls. The low flow rate (10 µl/min) within the large electrospray capillary, which connects the syringe to the electrospray capillary tip, may account for the long time behaviour equilibration.

A consequence of the time dependent behavior on the charge allocation in a multicomponent system may pose difficulties for the quantitative use of flow injection techniques for ES-MS, which may not allow sufficient time for the equilibration of charge carrying sites described here. Furthermore, quantitation of chromatographically separated components may also experience similar time dependent signal intensity suppression effects.

Table 8.4 contains the experimental signal intensity suppressions observed 10 minutes after application of the DC voltage to the electrospray capillary. The statistical argument presented above regarding unequal distribution of the charge sites in the droplets where the population distribution of charge carrying sites has equilibrated with the bulk electrolyte population predicts the measured suppressions to within experimental error. In light of these results it is not surprising that a preferential desorption mechanism was not found as a function of the curtain gas flow rate in section 8.4.2.

Ion solvation energy and the distance that the ion cluster lies below the surface of the charged droplet (i.e. the effective radius of the ion solvation sphere) are two analyte dependent variables of the IET. Because the measurements of signal intensity suppression were observed experimentally, due to a similarly and dissimilarly charged concomitant ion in solution were predicted from a statistical viewpoint for a wide range of analyte ions

(different solvation energies and different solvation sphere radii), a mechanism favoring the desorption of one ion over another is likely not predominant in the transfer of an ion from within the charged droplet to the gas phase.

8.4.5 Indirect Evidence of a Single Ion Droplet Mechanism

In a previous report on the effect of the interface parameters between the electrospray source and the mass spectrometer, it was noted that when the curtain gas flow rate was shut off an appreciable analyte ion signal could be obtained by increasing the sampling plate voltage bias from 40 V to 190 V, creating an electric field gradient in the jet expansion on the order of 950 V/m. Refer to reference 28 for further details. The assumption was that the increased electric field gradient caused the charged droplets to be broken apart by collisions with neutral curtain gas molecules, in the jet expansion between the sampling plate and the skimmer. During the course of this study, the ability to collisionally break apart a charged droplet was revisited in an attempt to decipher the composition of the charged droplets that are the source of the analyte ion signal under such conditions.

Proceeding on the basis that the ions observed at the conditions indicated in the caption for Fig. 8.8 originated as nano-droplets containing one excess charge at atmospheric pressure, a minimum size of the nano-droplet was estimated in the following manner. The difference in the energy required to collisionally decompose a charged droplet from $M(MeOH)_n^+$ to $M(MeOH)_{n-1}^+$ was used to correlate the sampling plate voltage with the flow rate of curtain gas used to the number of methanol molecules in the charged droplet at atmospheric pressure, before being sampled into the mass spectrometer. In Fig. 8.8a the sampling plate voltage was 50 V. Increasing the sampling plate voltage bias to 55 V (Fig. 8.8b), the distribution of lithium clusters detected was shifted lower on the mass to charge axis by the loss of two additional methanol ligands from $Li(MeOH)_5^+$ to $Li(MeOH)_3^+$. From this information, the nano-droplets being sampled from atmospheric pressure into the mass spectrometer contained approximately 22 methanol molecules. Such a qualitative estimate of the size of the charged droplets at atmospheric pressure holds more validity as long as inner coordination sphere ligands are not involved. Unfortunately, the inner coordination sphere of lithium has been measured by NMR as having an inner coordination sphere of 4 ligands in methanol/water solvents. Hence the estimate of 22 methanol molecules (i.e. $M(MeOH)_{22}^+$) is likely higher than what is actually present at atmospheric pressure. Further increases in the sampling plate voltage (Fig. 8.8c) did shift the lithium cluster

distribution to lower coordination numbers, but the total signal intensity of the lithium clusters increased. It is our interpretation that the lithium ions being detected under these conditions were present at atmospheric pressure as nano-droplets as $Li(MeOH)_z^+$ where $z > 25$ and the range of z is very large. If the range of z was not large, then observation of the nano-droplets with detectable signal to background ratios would be observed with mass spectrometers that have an extended mass to charge ratio capability. No reports of such observations of nano-droplets have been reported, although Smith and co-workers have recently reported the observation of charged droplet residues of a high mass to charge ratio ($m/z > 10{,}000$) [21]. Furthermore, by increasing the sampling plate voltage, more and more of the larger nano-droplets (high z) were being collisionally decomposed and funneled into a few species ($Li(MeOH)_y^+$ where $y < 5$).

Similar results were obtained by repeating this procedure for several combinations of sampling plate voltage biases and curtain gas flow rates, showed that the minimum number of methanol molecules associated with the nano-droplet being sampled into vacuum decreased as the flow rate of curtain gas was increased. At very high curtain gas flow rates, lithium clusters detected were $Li(MeOH)_m(H_2O)_n^+$ where $(m + n) < 6$ with very little or no collisional decomposition during the sampling step required.

Alternatively, it is possible that the IET was responsible for the production of the lithium clusters that were detected. If an "ion evaporation droplet" did release charge to the gas phase at atmospheric pressure, then methylated lithium clusters would be ejected from the charged droplets into the ambient atmospheric pressure environment in the interface zone as $Li(MeOH)_{7(+/-1)}^+$. (Tang and Kebarle calculated a minimum in the solvation energy of lithium as seven water ligands (no thermodynamic data exists for methanol) [13,14].) If conditions at atmospheric pressure were such that a large charged droplet evaporated enough to release charge (i.e. from an "ion evaporation type droplet" (radius of droplet is ~ 6 to 10 nm and q ~ 60 to 100)) then growth at atmospheric pressure of the $Li(MeOH)_{7(+/-1)}^+$ clusters to $Li(MeOH)_z^+$ would not be expected. More likely to occur would be the displacement of the methanol ligands by water vapor present in the curtain gas would occur, hence forming $Li(H_2O)_{7(+/-1)}^+$. Hydrated lithium clusters were not observed with gentle ion sampling conditions (zero electric field gradient in the jet expansion) combined with a low flow rate of curtain gas.

If however, the Ion Evaporation charged droplets did not release charge at atmospheric pressure, but released charge after being sampled into the mass spectrometer then ions

arriving at the detector should be temporally packed and the number and temporal delay from the time of detecting the first ion to the last ion in a packet would be indicative of the physical parameters of an "ion evaporation type droplet". The assumption made was that if the analyte ion signal was observed with nanosecond time resolution for any given count rate per second, then a histogram of the number of counts per 0.1 or 1 msecond integration period would be indicative of the nature of the charged droplets being sampled. A histogram with a normal distribution centered about the nominal count rate obtained with a one second integration period divided by a factor equal to the integration period reduction would be indicative of an SIDT type droplet (ie. a nano droplet containing a single ion) being sampled into the mass spectrometer. On the other hand, if the histogram was not normal, a case for charged droplets containing numerous charges could be made in that the ions arriving at the detector would arrive in ion packets that are indicative of the charged droplet composition at atmospheric pressure. It was assumed that the "ion evaporation type droplets" would be very highly charged and that collisions in the jet expansion would release a small fraction of charges from these droplets leading to temporal packing of the ions detected.

Experimental conditions were adjusted so as to channel the analyte ion distribution into a single ion species in order to more easily observe any ion signal temporal packing. This was most easily achieved for cesium ions. The histograms shown in Fig. 8.9 were obtained at the observed count rate for two different interface parameter conditions. In Fig. 8.9a, the ion monitored was $Cs(H_2O)^+$ by setting the interface conditions for gentle ion sampling (electric field gradient across the jet expansion < 1 V/cm and a high flow rate of curtain gas). Displacement of methanol ligands by water vapor present as an impurity in the curtain gas is indicative that the ions detected were present as free individual (solvated) ions at atmospheric pressure. This ligand exchange would not be expected if the ions being detected were collisionally released from an "ion evaporation type droplet" in the jet. In Figure 8.9b, the observed analyte signal histogram was obtained with harsh ion sampling interface conditions, characterized by a high sampling plate voltage electric field gradient across the jet expansion was 950 V/cm with no flow of curtain gas. The ion signal count rate histogram shown in Figure 8.9b is normal implying that there was no packing of the ion signal observed.

It should be pointed out that large droplets containing numerous charges and on the same order of size as an "ion evaporation type droplet" (radius ~ 6 to 10 nm and the number of excess charges between ~ 60 and 100) normally requires conventional atomic spectroscopic

methods to measure the composition of such droplets (i.e. a flame or plasma to desolvate, vaporize, then excite the atoms that were in the droplet). In consideration of the time and energy requirements to collisionally dislodge an ion from an "ion evaporation type droplet", then collisional strip the solvent from the ion that was released so that it can be detected with a mass spectrometer with an upper m/z of 300 Daltons, all within the jet expansion is not feasible.

8.5 Conclusions

The mechanism by which ions in the charged droplet are released to the gas phase for the inorganic ions used in the investigations presented were most easily rationalized with the SIDT. The suppression measurements of inorganic ion signal intensities were well predicted by a statistical argument based on Eqn. 8.3. A consequence of this is that no preferential desorption of solution ions from the charged droplets, as would be predicted by the IET, was observed. From these investigations it is likely that the source of ions detected with a mass spectrometer from an electrospray source are derived from nano-droplets ($M(MeOH)_z^{x+}$ where $z > \sim 22$ and the range of z is large) that contain a single ion at atmospheric pressure. Even when conditions are not optimal for production of the nano-droplets (i.e. little or no flow rate of curtain or drying gas), they are still present at atmospheric pressure at a high population. This was ascertained by employing collisional break-up of the nano-droplets by energetic collisions in the jet expansion to generate small ion clusters that were then detected with a mass spectrometer.

Equilibrium between excess charges and the bulk electrolyte occurs within the confines of the electrospray tip, not in the charged droplets. Charge carrying sites within the droplets are not significantly affected by an increase in the bulk concentration by evaporation of solvent from the charged droplets. This result implies that ES-MS may potentially be used for kinetically labile speciation measurements. Conversely, the time dependence of the equilibration of charge carrying sites with the bulk solution must be considered in the quantitation of analyte ions by ES-MS when coupled with transient signal generating techniques such as FIA or chromatography.

Table 8.1 Measured electrospray capillary current as a function of the total electrolyte concentration in HPLC grade methanol.

Total Electrolyte Concentration (molar)	Current (μAmpere)
$1x10^{-5}$	0.2
$3x10^{-5}$	0.3
$1x10^{-4}$	0.4
$3x10^{-4}$	0.5
$1x10^{-3}$	0.6
$3x10^{-3}$	0.8

Table 8.2 Experimentally observed suppressions in the analyte ion signal intensity as predicted by Eqn. 8.3 from a similarly charged ion in solution, equimolar with the analyte ion. Curtain gas flow rate was 1 lpm except for trial 2 where a curtain gas flow rate of 1.62 lpm was used, ([a]) mean of 45 measurements (RSD of signal intensities ~ 6 %), ([b]) relative error is +/- 9 %.

Trial	Monitored Ions	Signal Intensity (single ion)[a]	Signal Intensity (mixture)[a]	Suppression (%)[b]
1	ΣLi^+	34,667	21,345	38
	ΣCs^+	58,984	32,296	45
2*	ΣLi^+	24,015	17,764	26
	ΣCs^+	82,265	60,306	27
3	ΣCo^{2+}	52,483	23,694	55
	ΣBa^{2+}	53,086	26,031	51
4	ΣMg^{2+}	54,126	29,146	46
	ΣBa^{2+}	50,703	24,747	51

Table 8.3 Experimentally observed suppressions in the analyte ion signal intensity as predicted by Eqn. 8.3 from a dissimilarly charged ion in solution, equimolar with the analyte ion. Curtain gas flow rate was 1 lpm, ([a]) elapsed time after application of the 4.0 kV to the electrospray tip to when data acquisition began, ([b]) mean of five measurements (RSD of signal intensities ~ 6 %), ([c]) the relative error is +/- 9%.

Trial	Elapsed Time (minutes)[a]	Monitored Ions	Signal Intensity (single ion)[b]	Signal Intensity (mixture)[b]	Suppression (%)[c]
1	1	ΣCs^+	55,874	31,698	43
		ΣMg^{2+}	49,389	30,297	39
	4	ΣCs^+	56,694	19,706	65
		ΣMg^{2+}	41,417	31,674	24
	7	ΣCs^+	56,396	16,856	70
		ΣMg^{2+}	44,998	29,954	33
2	1	ΣCs^+	75,012	24,907	67
		ΣMg^{2+}	46,451	21,311	54
	4	ΣCs^+	62,778	16,328	74
		ΣMg^{2+}	46,112	28,376	38
	7	ΣCs^+	56,810	12,982	77
		ΣMg^{2+}	42,440	35,377	17

Table 8.4 Experimentally observed suppressions in the analyte ion signal intensity as predicted by Eqn. 8.3 from a dissimilarly charged ion in solution, equimolar with the analyte ion. Curtain gas flow rate was 1 lpm. ([a]) an elapsed time of ten minutes after application of 4.0 kV to the electrospray tip to when data acquisition began, ([b]) mean of five measurements (RSD of signal intensities ~ 6 %), ([c]) the relative error is +/- 9%.

Trial	Monitored Ions	Signal Intensity (single ion)[a,b]	Signal Intensity (mixture)[a,b]	Suppression (%)[c]
1	ΣCs^+	84,584	22,475	73
	ΣBa^{2+}	48,373	35,718	26
2	ΣK^+	77,492	30,729	60
	ΣLa^{3+}	26,306	19,164	27

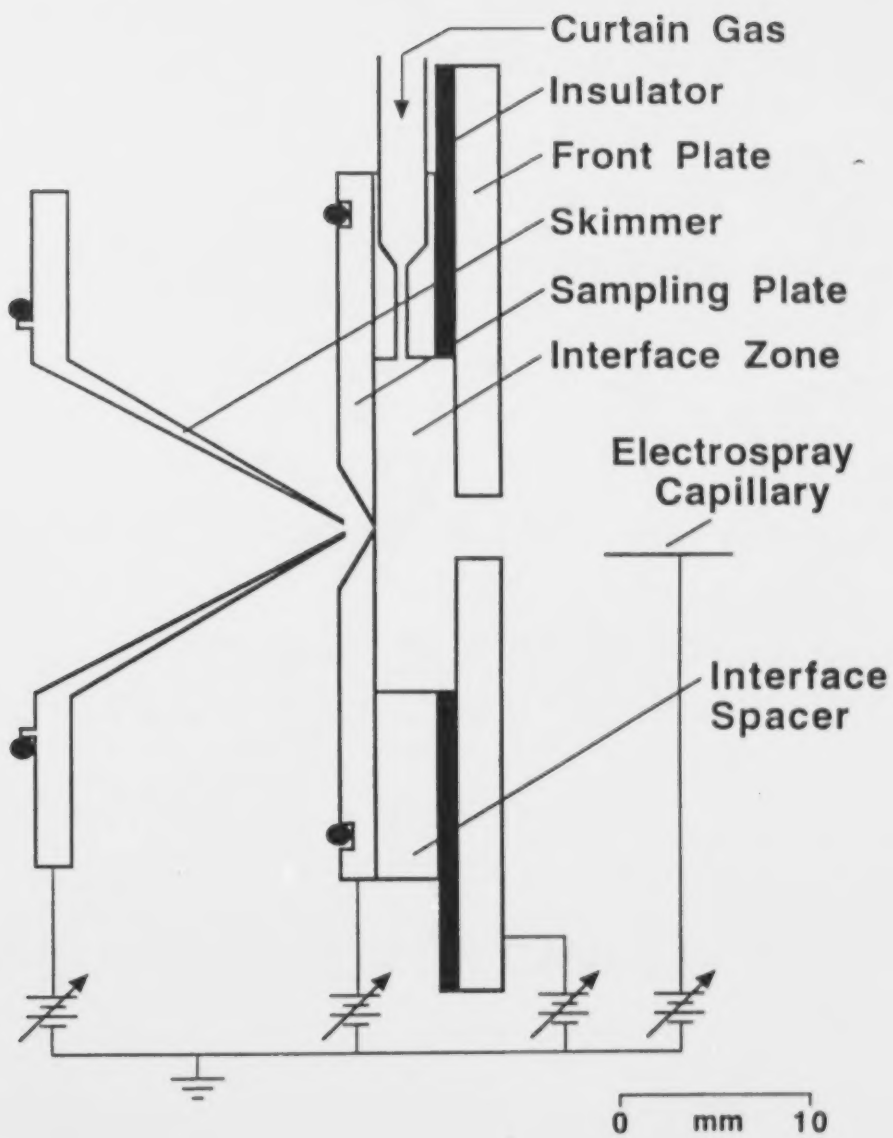

Figure 8.1 A schematic diagram of the electrospray source and interface to the mass spectrometer.

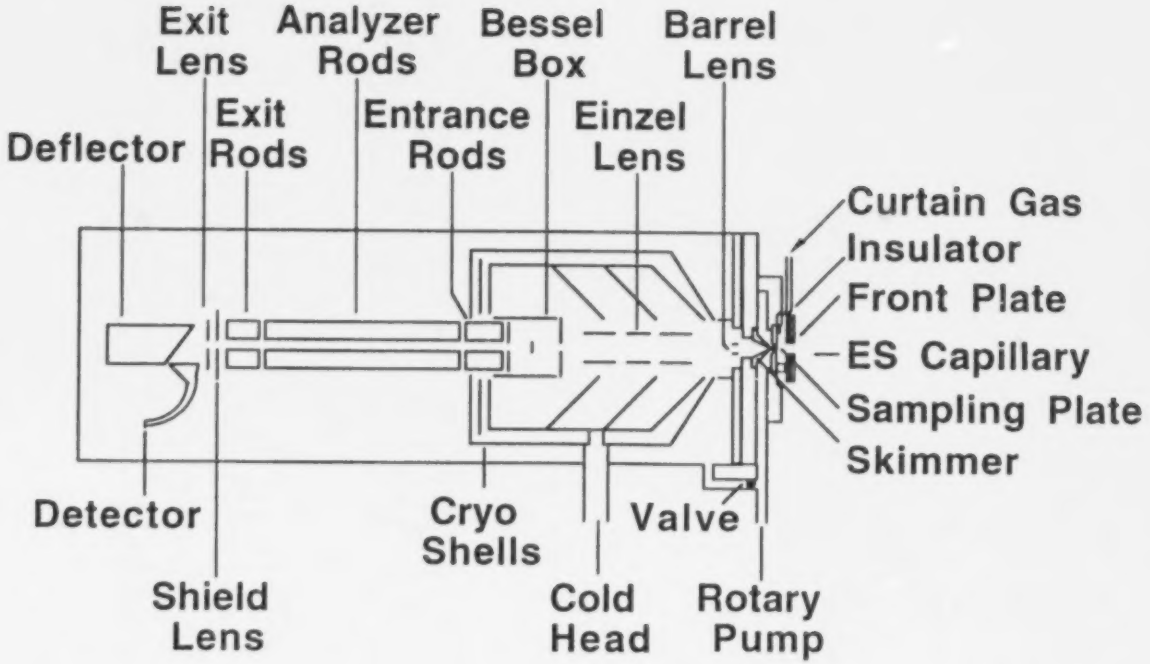

Figure 8.2 A schematic diagram of the SCIEX/Perkin-Elmer ELAN Model 250 mass spectrometer interfaced with the electrospray source.

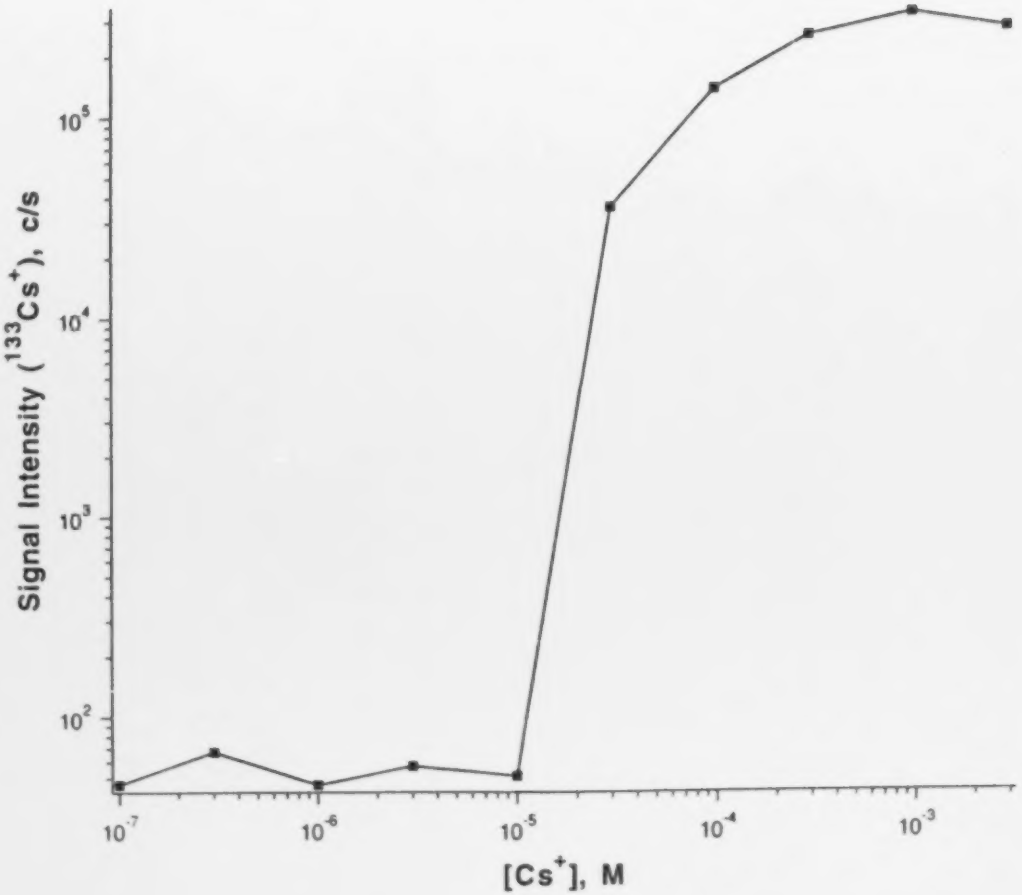

Figure 8.3 Attempted calibration curve for cesium nitrate in HPLC grade methanol. Source conditions were electrospray capillary 5.0 kV, front plate 950 V, sampling plate 190 V, skimmer 5 V, and curtain gas flow rate 0.1 lpm.

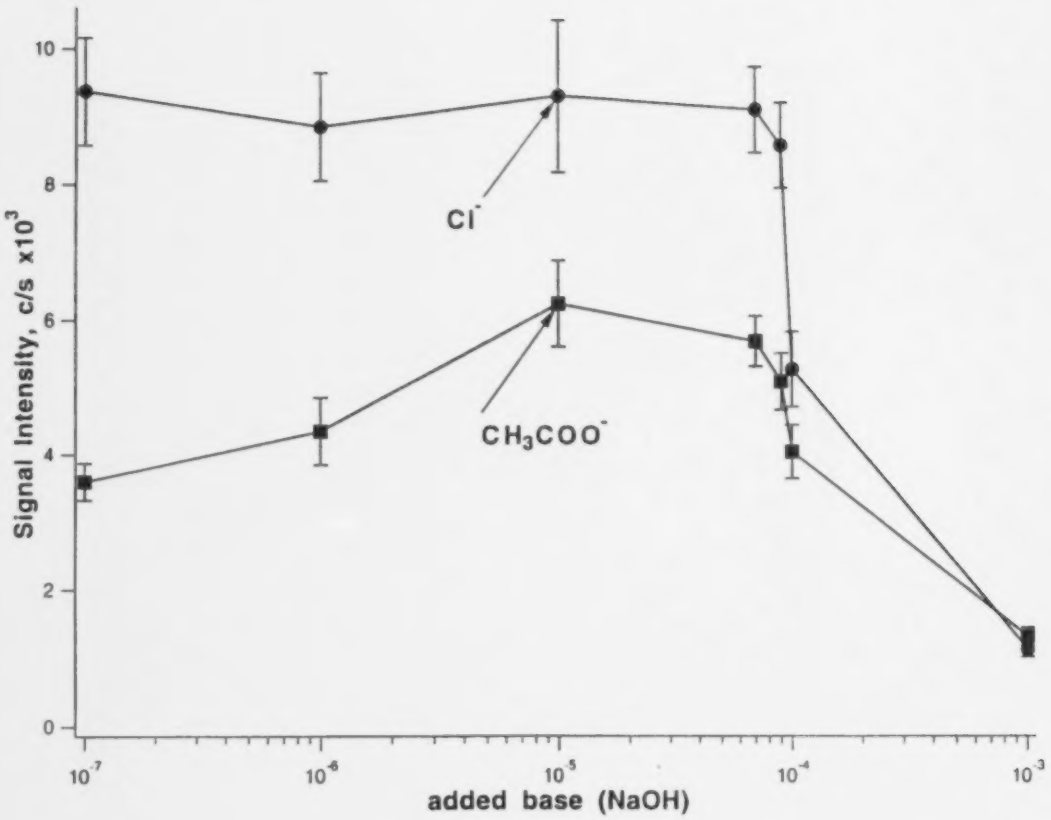

Figure 8.4 Dependency of ES-MS analyte signal intensities (Cl^- and CH_3COO^- at $1x10^{-4}$ molar) as a function of sodium hydroxide concentration. Source conditions were electrospray capillary -3.0 kV, front plate -950 V, sampling plate -40 V, skimmer -8 V, and curtain gas flow rate 0.7 lpm oxygen.

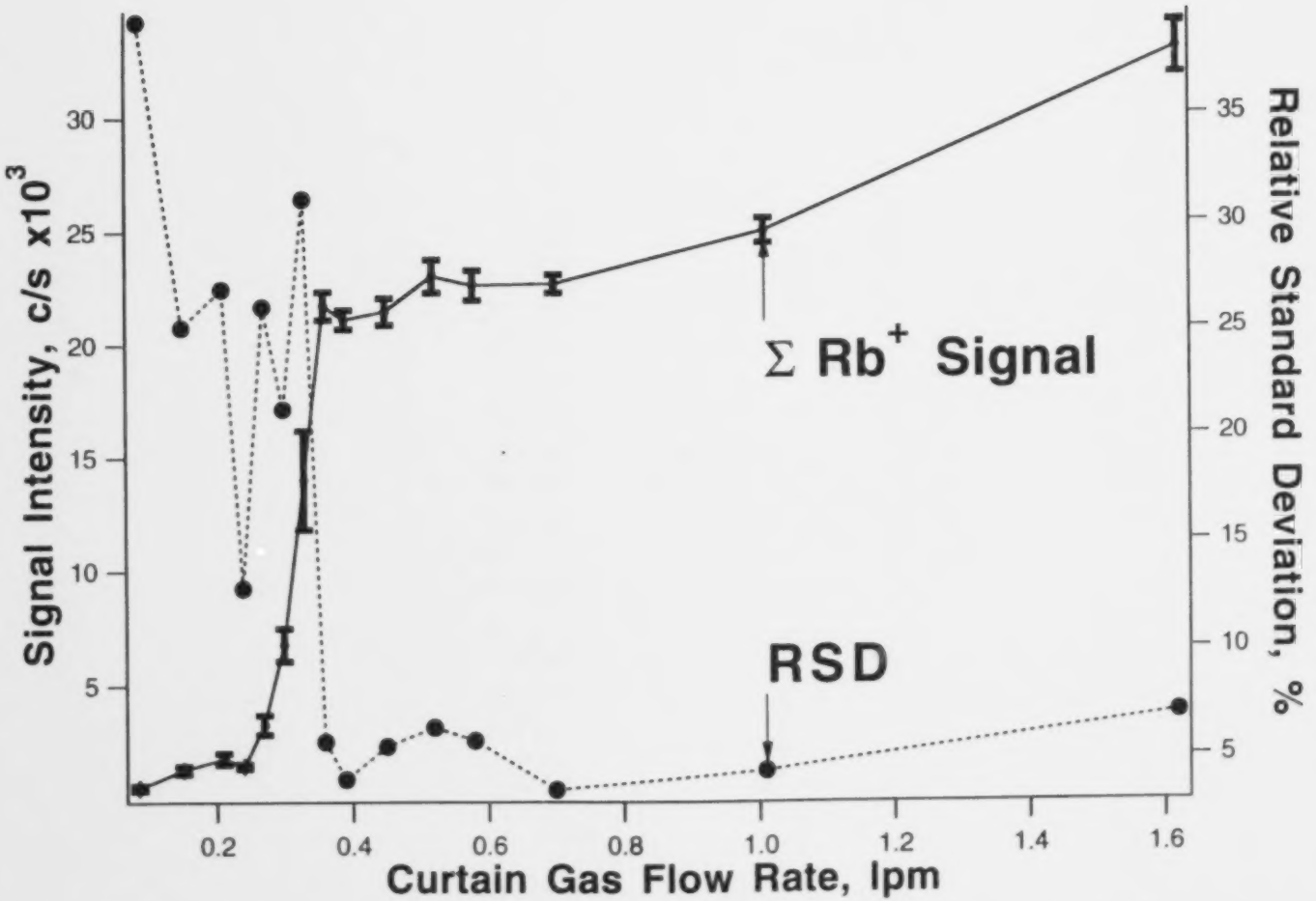

Figure 8.5 Total rubidium ion signal as a function of the curtain gas flow rate. RbCl was 1×10^{-4} molar. Source conditions were electrospray capillary 4.0 kV, front plate 600 V, sampling plate 40 V, and skimmer 9 V.

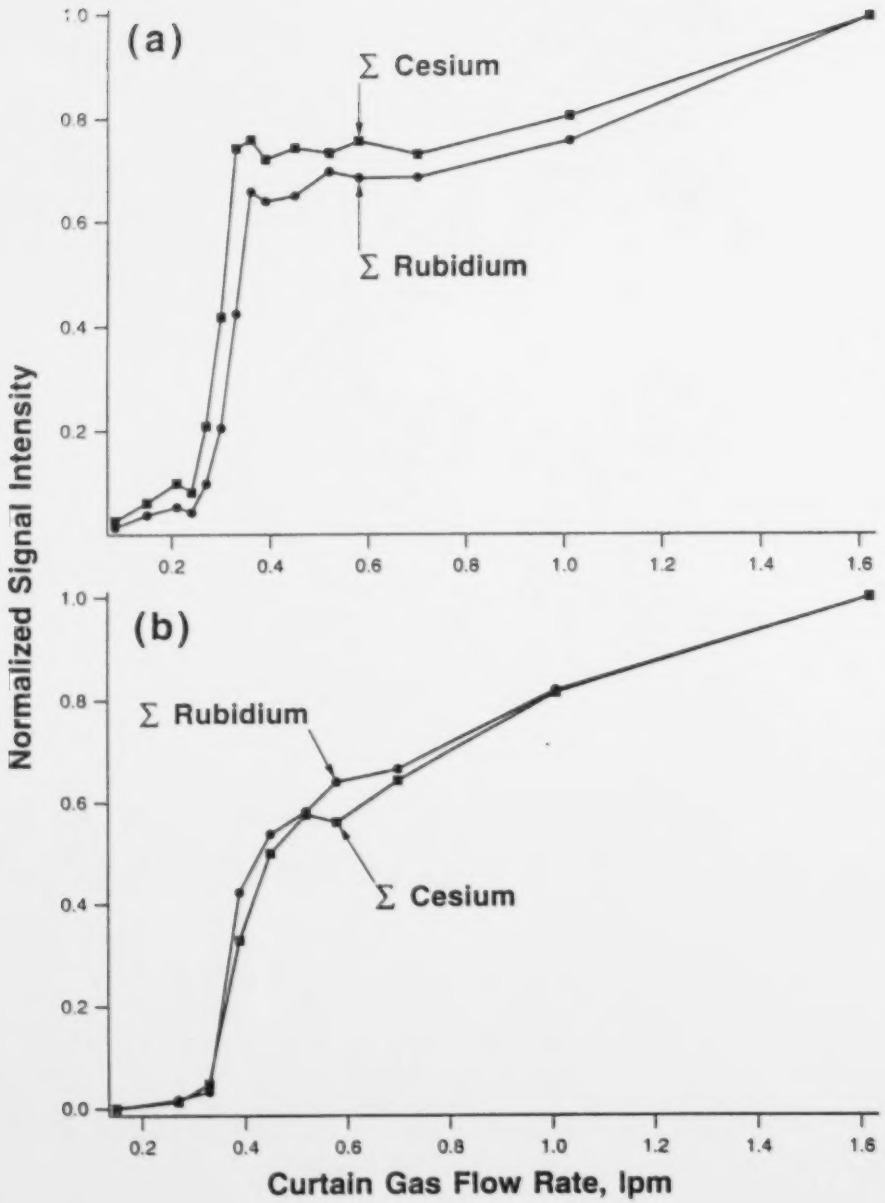

Figure 8.6 Normalized total ion signal intensities for an equimolar ($1x10^{-4}$ molar) two component mixture of rubidium and cesium as a function of curtain gas flow rate. Sampling plate voltage bias was (a) 40 V and (b) 20 V. Source conditions were electrospray capillary 4.0 kV, front plate 600 V, and skimmer 9 V.

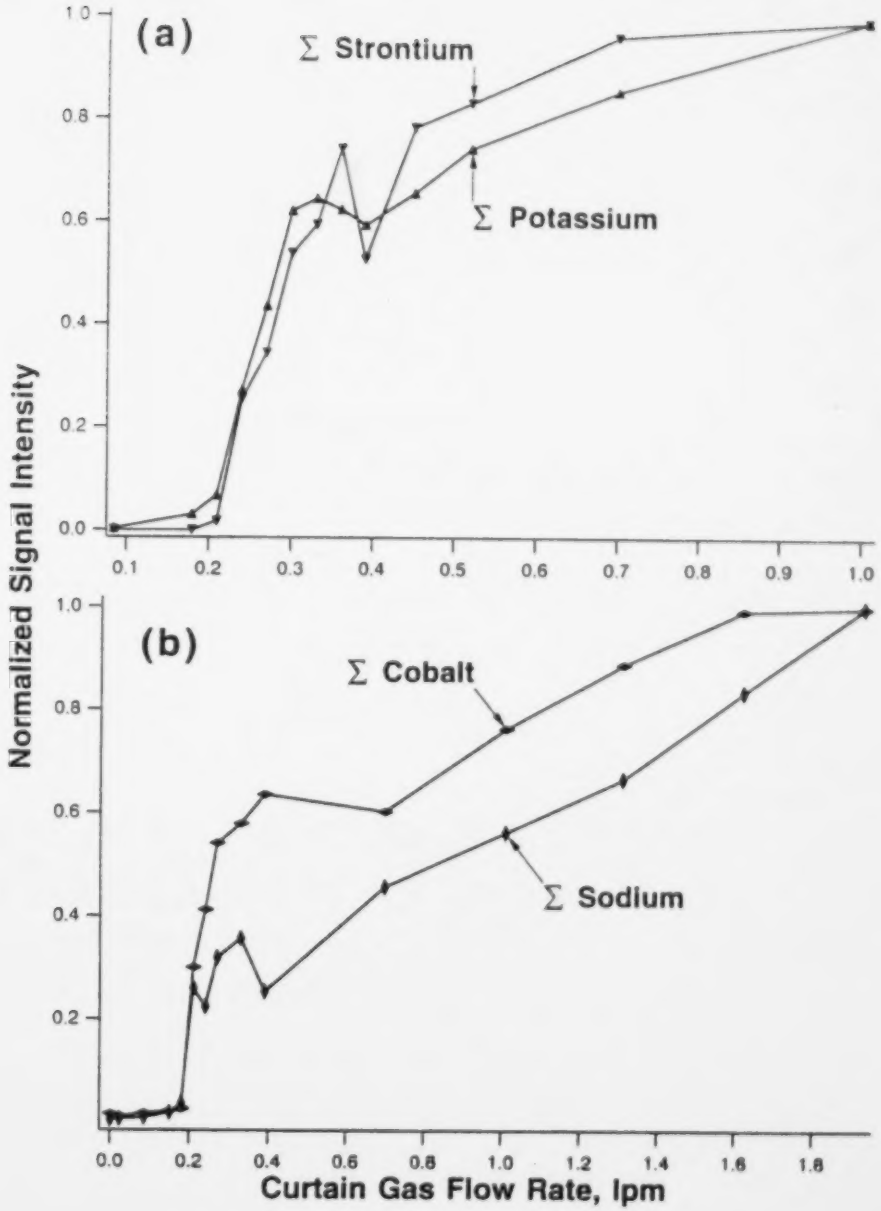

Figure 8.7 Normalized total ion signal intensities for a two component mixture of (a) potassium and strontium where both analyte ions were $1x10^{-4}$ molar and (b) sodium ($2x10^{-4}$ molar) and cobalt ($1x10^{-4}$ molar) as a function of curtain gas flow rate. Source conditions were electrospray capillary 4.0 kV, front plate 600 V, sampling plate 40 V, and skimmer 9 V.

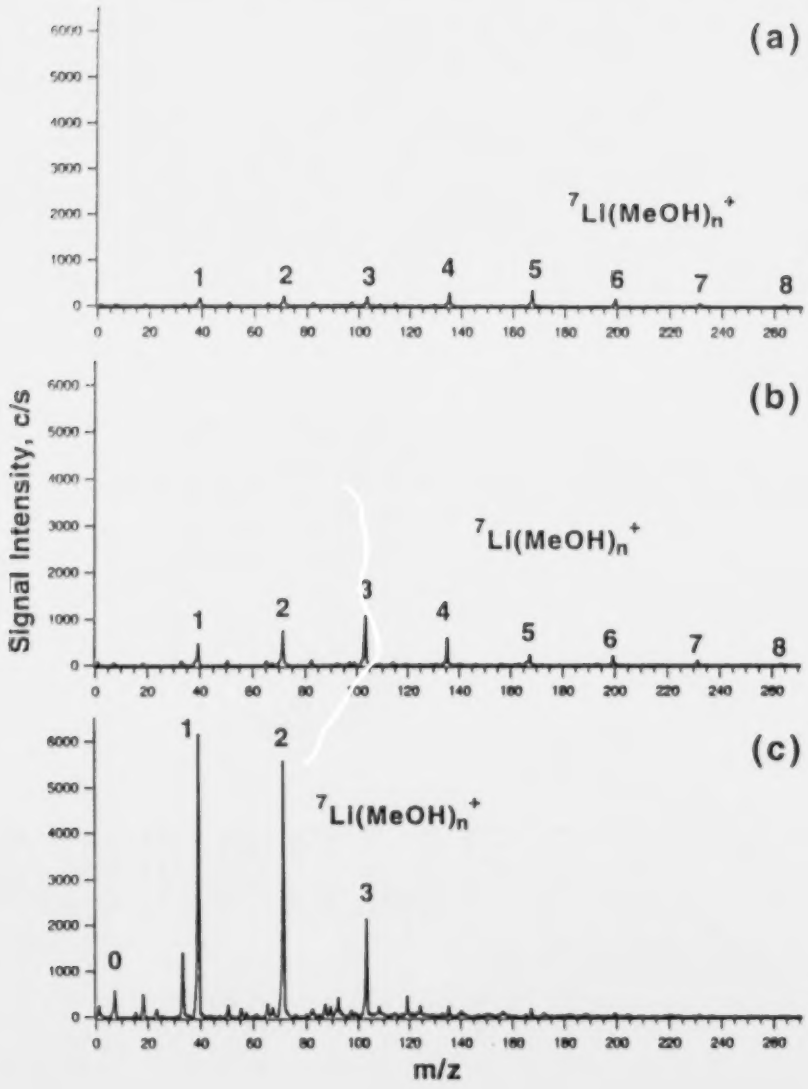

Figure 8.8 Lithium ion cluster distributions being shifted to lower ligand coordination numbers. An increased electric field gradient across the jet expansion brought about by increasing the sampling plate voltage bias subjects ion clusters in the jet to experience increased energetic collisions with neutrals and loss of coordination ligands. Sampling plate voltage bias was (a) 50 V, (b) 55 V, and (c) 90 V. Other source conditions were electrospray capillary 4.0 kV, front plate 600 V, skimmer 10 V, and curtain gas flow rate 0.15 lpm. Lithium concentration was 1×10^{-4} molar.

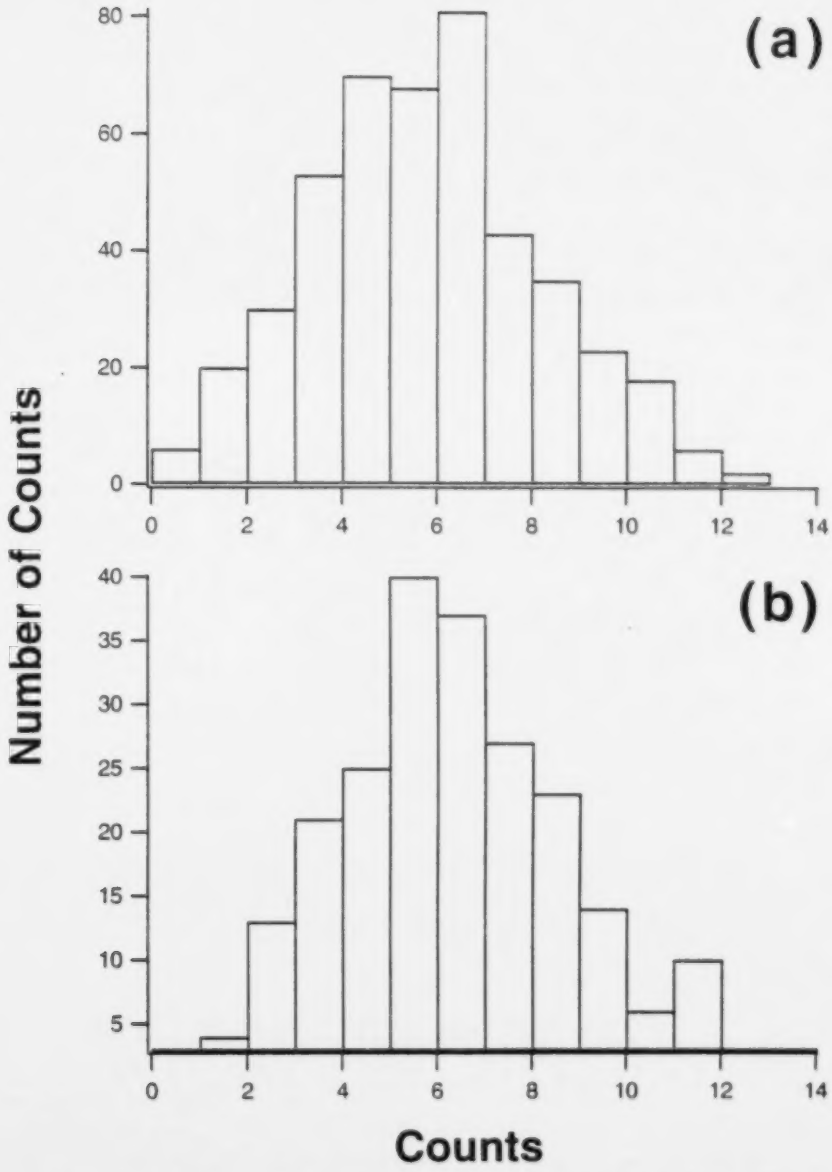

Figure 8.9 Histogram of the number of ion counts per integration period for two different electrospray interface operating conditions. (a) ion monitored was $Cs(H_2O)_1^+$ per 0.1 msecond, sampling plate voltage 10 V and curtain gas flow rate was 1.62 lpm and (b) ion monitored was Cs^+ per 1 msecond, sampling plate voltage bias 190 V and curtain gas flow rate 0 lpm. Nominal count rate per second was a) 5,279 +/- 976 and b) 58,341 +/- 6,910. cesium chloride was $1x10^{-4}$ molar. Other source conditions were electrospray capillary 4.0 kV, front plate 600 V, and skimmer 10 V.

8.6 References

1. J. B. Fenn, M. Mann, C. K. Meng, S. K. Wong, and C. M. Whitehouse, Science, **246**, 64 (1989).

2. Volumes 4 and 5: Special Issues devoted solely to Electrospray Mass Spectrometry, J. Am. Soc. Mass Spectrom., 1993.

3. R. D. Smith, J. H. Wahl, D. R. Goodlett, and S. A Hofstadler, Anal. Chem., **65**, 574A (1993).

4. G. R. Agnes and G. Horlick, Anal. Chem., submitted.

5. I. Hayati, A. I. Bailey, and TH. F. Tadros, Nature, **319**, 41 (1986).

6. I. Hayati, A. I. Bailey, and TH. F. Tadros, J. Colloid Interface Sci., **117**, 205 (1987).

7. I. Hayati, A. I. Bailey, and TH. F. Tadros, J. Colloid Interface Sci., **117**, 222 (1987).

8. M. Cloupeau and B. Prunet-Fóch, J. Electrostatics, **25**, 165 (1990).

9. A. T. Blades, M. G. Ikonomou, and P. Kebarle, Anal. Chem., **63**, 2109 (1991).

10. M. G. Ikonomou, A. T. Blades, and P. Kebarle, Anal. Chem., **62**, 957 (1990).

11. Lord Rayleigh, Philos. Mag., **14**, 184 (1882).

12. D. C. Taflin, T. L. Ward, and E. J. Davis, Langmuir, **5**, 376 (1989).

13. P. Kebarle and L. Tang, Anal. Chem., **65**, 972A (1993).

14. L. Tang and P. Kebarle, Anal. Chem., **65**, 3654 (1993).

15. M. Dole, L. L. Mach, R. L. Hines, R. C. Mobley, L. P. Ferguson, and M. B. Alice, J. Chem. Phys., **49**, 2240 (1968).

16. L. L. Mach, P. Kralik, A. Rheude, and M. Dole, J. Chem. Phys., **52**, 4977 (1970).

17. J. V. Iribarne and B. A. Thomson, J. Chem. Phys., **64**, 2287 (1976).

18. B. A. Thomson and J. V. Iribarne, J. Chem. Phys., **71**, 4451 (1979).

19. J. B. Fenn, J. Am. Soc. Mass Spectrom., **4**, 524 (1993).

20. M. Sakairi, A. L. Yergey, K. W. M. Siu, J. C. Y. Le Blanc, G. Guevremont, and S. S. Berman, Anal. Chem., **63**, 1488 (1991).

21. B. E. Winger, K. J. Light-Wahl, R. R. Ogorzalek Loo, H. R. Udseth, and R. D. Smith, J. Am. Soc. Mass Spectrom., **4**, 536 (1993).

22. G. Schmelzeisen-Redeker, L. Bütfering, and F. W. Röllgen, Int. J. Mass Spectrom. Ion Processes, **90**, 139 (1989).

23. A. J. Kelly, J. Appl. Phys., **47**, 5264 (1976).

24. R. C. Reist, Introduction to Aerosol Science; MacMillan: New York, 1984.

25. V. Katta, A. L. Rockwood, and M. L. Vestal, Int. J. Mass Spectrom. Ion Process, **103**, 129 (1991).

26. G. R. Agnes and G. Horlick, "Determination of Solution Ions by Electrospray Mass Spectrometry," Appl. Spectrosc. (accepted for publication).

27. G. R. Agnes and G. Horlick, "Electrospray Mass Spectrometry as a Technique for Elemental Analysis: Quantitative Aspects," Appl. Spectrosc. (accepted for publication).

28. G. R. Agnes and G. Horlick, Appl. Spectrosc., submitted for publication.

29. I. Stewart and G. Horlick, J. Anal. At. Spectrosc., submitted for publication.

30. G. R. Agnes and G. Horlick, Appl. Spectrosc., **46**, 401 (1992).

31. L. Tang and P. Kebarle, Anal. Chem., **63**, 2709 (1991).

32. M. Mann, Org. Mass Spectrosc., **25**, 575 (1990).

Chapter 9

Mechanistic Investigations of Electrospray Mass Spectrometry: Part II, Prediction of the Physical Parameters of the Charged Droplets

9.1 Introduction[7]

Electrostatic dispersion of liquids has been used for a variety of diverse applications ranging from propulsion jets to agricultural crop spraying [1]. Fundamental investigations of the process of electrical atomization of liquids by the application of a high electric field have typically been performed with optical spectroscopic techniques [2-7]. Optical investigations of electrostatic dispersion of liquids have shown that numerous parameters are involved in the stable electrical dispersement of liquids [1]. The steps leading up to the creation of charged droplets in an electrospray source are (1) pumping of a solution through a small capillary (< 20 μl/min.), (2) bias the electrospray capillary to a high potential relative to a counter electrode (> ~ 2 kV) which causes a flow of current (< 1 μAmpere), (3) formation of a cone of liquid at the tip of the electrospray capillary from which a jet of liquid emerges [8], (4) break-up of the jet into small droplets [7], and (5) release of solvated ions into the gas phase from the small charged droplets. Steps 1 to 5 take place at atmospheric pressure [9]. A detailed understanding of some of these steps is lacking due to the complexity of the step and in particular, steps 3 to 4 are very difficult to study experimentally and a satisfactory model describing the electrostatic atomization processes is consequently lacking.

What is known however, is that for the particular solution that is being electrosprayed, maintaining stable electrostatic atomization (smallest droplet size and the narrowest droplet size distribution) requires re-optimization of the physical parameters of the electrospray source variables (flow rate and geometry (electrospray capillary tip to counter electrode separation distance and the applied voltage)) [5]. The properties of the solution that effect the charged droplet generation process are conductivity, viscosity, and surface tension [1, 5-7]. These parameters are depicted in the cartoon shown in Fig. 9.1.

The cartoon in Fig. 9.2 depicts what is observed at the tip of an electrospray capillary. An inverted cone of liquid (commonly called the Taylor cone) forms at the end of the electrospray capillary. This cone forms as a result of the balance between the charges in

---

[7] A version of this chapter has been submitted for publication. George R. Agnes and Gary Horlick, Appl. Spectrosc.

the solution residing on the surface of the cone and the binding forces (surface tension) of the liquid. The unpaired, or excess ions in the Taylor cone are accelerated in a direction normal to the tip of the electrospray capillary. Close to the base of the Taylor cone, the binding forces within the droplet are greater than the tangential electrostatic repulsion. With increasing distance from the tip of the electrospray capillary, the excess charges continue to be accelerated causing the radius of the cone to decrease with increasing distance from the electrospray capillary tip. The filament jet likely forms at the point where the electrostatic repulsion forces have exceeded the surface tension of the liquid. The excess charges are further accelerated in the filament jet and ultimately, the jet breaks apart into droplets.

The use of mass spectrometry to probe the nature of the droplets produced by an electrospray source was pioneered by M. Dole and co-workers [10,11]. Since then fundamental investigations of the electrospray process have been overshadowed by the overwhelming number of novel research areas that have been made possible with electrospray mass spectrometry (ES-MS) [12-24]. That is not to say that diagnostic investigations of the electrospray source using a mass spectrometer as the spectroscopic probe of the source have not been performed. The properties of the solution being electrosprayed [9,25,26] and the physical processes that occur in a capillary biased to a high potential have also been investigated by mass spectroscopic techniques [27,28]. An electrophoretic mechanism is believed to occur in the electrospray capillary where the most easily oxidized species are oxidized (when the electrospray capillary is positively biased). Such a process is thought to leave a surplus of positive charges in the solution being electrosprayed. The excess charges are transported away from the electrospray capillary tip by the atomized droplets. It is the high charge density within the droplets that causes ions to be released to the gas phase at atmospheric pressure. The mechanism by which ions are transferred from within the droplets to the gas phase at atmospheric pressure has itself generated considerable discussion [29-33].

While an understanding of the mechanism of solvated ion transfer from solution phase to gas phase is of fundamental interest, such investigations did not directly query the physical processes involved in the formation of the charged droplets themselves. Furthermore, it is believed that a large fraction of the total mass spectrally detected ion signal current from an electrospray ion source originates from the charged droplets [9,34], and not directly from the electrospray capillary tip as has been suggested by Siu et. al. [35,36]. Therefore a physical description of an electrospray source necessarily requires an examination of the charged droplet formation processes that occur at the electrospray capillary tip.

In a quantitative investigation of the electrospray process as monitored by a mass spectrometer, Agnes and Horlick uncovered an inherently non-linear response for concentration calibration curves of simple solutions consisting of simple inorganic electrolytes dissolved in a pure methanol solvent [37]. See Fig. 9.3. The assumption that is made here is that the behavior depicted in the calibration curve plotted in Fig. 9.3 is a direct monitor of the processes governing charged droplet formation. Below a certain concentration of electrolyte ($< 3x10^{-5}$ molar) dissolved in a pure methanol solvent (HPLC grade), an electric discharge could not be avoided when such solutions were electrosprayed at the conditions employed. At intermediate electrolyte concentrations, the slope of the log-log concentration calibration plot for a simple inorganic salt approached zero and ion signal intensities decrease when solutions of very high electrolyte concentration ($> 3x10^{-3}$ molar) are electrosprayed. In a certain respect, this behavior can be described as being digital in nature in that for a certain range of electrolyte concentrations dissolved in a pure methanol solvent, the ion signal intensity response was high. Outside the empirically defined range of solution electrolyte concentration the analyte ion signal intensity was low. These observations, which were very real and reproducible, had not previously been reported and a model describing this fundamental characteristic of the electrospray source was lacking.

When electrospray is employed for mass spectrometric purposes, it is the physical parameters of the electrospray source that are fixed and the solution properties that are varied (or unknown in the case of real samples). Of fundamental importance is an understanding of how the droplet formation process is altered by variation of the properties of the solutions being electrosprayed. The present report reviews the knowns and unknowns concerning the stable electrical atomization of liquids in an attempt to explain the observations summarized above regarding the quantitative nature of an electrospray source. In doing so, a detailed look at how electrical atomization is brought about was necessarily required. A model was proposed to predict the physical parameters of the charged droplets. Calculations based on this model can be used to qualitatively explain the quantitative behavior of an electrospray source.

9.2 Experimental

A schematic diagram of the electrospray source and interface is shown in Fig. 9.4. The dimensions of the stainless steel electrospray capillary are 0.1 mm ID x 0.065 mm wall. The sample solution was pumped at a flow rate of 10 µl/min. Nitrogen was used as the curtain gas and the voltage bias applied to each conductor in the electrospray source and interface is included with each figure caption. Stock solutions (10 mM) were prepared daily by dissolving an ACS grade salt in distilled deionized water. The stock solutions were then diluted by a factor of 100 with HPLC grade methanol before electrospraying.

Results

Gentle ion sampling interface conditions were characterized by an electric field gradient across the jet expansion < 150 V/cm. With gentle interface conditions, the ion clusters detected by the mass spectrometer are thought to be representative of the ion clusters or nano-droplets that are present at atmospheric pressure. The mass spectra thus obtained consist of numerous analyte ion peaks ($M(MeOH)_n^{x+}$) [34]. The data plotted in Fig. 9.5 were obtained under such conditions and hence each data point plotted in Fig. 9.5 represents the sum of all lithium ion signal intensity peaks in the mass spectrum as a function of the flow rate of the drying gas for several methanol/water solvent mixtures. The percentage of water in each solution is indicated beside the respective data curve and a decreasing total lithium ion cluster signal intensity was observed as the percentage of water in the electrosprayed solution was increased. For each solution electrosprayed, as the flow rate of drying gas was increased, the total lithium ion signal intensity consistently experienced a sharp onset, or threshold, at a flow rate of 0.2 lpm. A slight reduction of the total lithium ion cluster signal intensity was observed by increasing the flow rate of curtain gas to 0.27 lpm, after which the total lithium ion cluster signal intensity was not affected by further increases in the flow rate of the curtain gas.

Two possible explanations for this data set are considered. The first will be to assume that the efficiency of the mechanism by which ions within the charged droplet are transferred to the gas phase degraded as the percentage of water in the solution increases. The mechanism known as ion evaporation, from the Ion Evaporation Theory (IET), which describes the transfer for ions from within the charged droplet to the gas phase will be assumed for this argument [38,39]. The IET predicts an ion signal intensity dependence on

the solvation energy of a particular ion solvent cluster. Further discussion of the IET can be found in references [29,32,33]. As the percentage of water in the solution increases so do the number of water ligands present in the solvation sphere of the lithium ions in solution. This argument would then require that the minimum free energy of hydration of lithium is greater than the minimum free energy of methylation, thus reducing the ion evaporation rate. The individual total lithium ion signal intensity curves each show a maximum at the curtain gas flow rate of 0.2 lpm. This observation could be explained by stating that evaporation conditions optimal for ion cluster release into the gas phase from the charged droplets caused ions to be released immediately in front of the sampling plate orifice, thus optimizing the sampling efficiency of the analyte ions into the mass spectrometer.

However, this argument based on the IET requires that the electrostatic atomization process be independent of the methanol/water solvent ratio in the solution electrosprayed. This assumption could be interpreted because the mass flow rate of the solution and also the current was unchanged as a function of percent water in the solution. But if the physical description of the charged droplets (radius and number of excess charges) are unaffected by an increased percentage of water in the solution electrosprayed, then an electrostatic desorption mechanism for ion transfer from the surface of the charged droplet to the gas phase, such as the IET, does not predict the observed decrease in ion signal intensity.

An alternative explanation of the lithium ion signal intensity response trends in Fig. 9.5 would be to assume that an increase in water content in the solution being electrosprayed adversely affects the charged droplet production process to a much larger degree than the extent to which the ion transfer efficiency from within the charged droplets to the gas phase is adversely affected. To explain, recall that the evaporation of small droplets (< 1 μm dia.) is governed by kinetics and not by thermodynamic considerations [9,40-42]. Thus the rate of solvent evaporation from small droplets is independent of the methanol/water composition. In turn, the size of the evaporating charged droplets in an electrospray source will be a constant function of the droplet spatial position (i.e. distance from the electrospray capillary tip). Each lithium ion cluster signal intensity curve plotted in Fig. 9.5 displays a sharp rise at the curtain gas flow rate of 0.2 lpm. This observation suggests that the release of the solvated ions from the charged droplets is indeed governed by electrostatic repulsive forces. However, notice that the magnitude of the sharp rise in the lithium ion cluster signal intensity plots decreases with an increasing percentage water of content in the solution electrosprayed. This observation implies that a change in the size of the

electrosprayed droplets produced has occurred as a function of the percentage of water in the solution electrosprayed because the charged droplets are no longer releasing the excess charge spatially close to the sampling orifice of the mass spectrometer.

Furthermore, with respect to a reduction of the total lithium signal intensity with increased percent water in the solution being electrosprayed, D. P. Smith stated that solvents having a surface tension greater than 0.05 Nm can not be easily and reliably electrosprayed [7]. This fact has been emphasized in the publications of the 'new' practitioners of electrospray who use mass spectroscopy to measure the ions produced with this source [43,44]. For the data presented in Fig. 9.5, the electrospray source was initially optimized for maximum lithium ion signal intensity from solutions of lithium chloride dissolved in pure HPLC grade methanol, with the added condition that electrospraying a 50:50 methanol:water solvent mixture would not cause an electric (corona) discharge to be sustained. Optimal electrospray source conditions are characterized by a small charged droplet size and also a small droplet size distribution. Increasing the percentage of water in the methanol/water solvent being electrosprayed may destabilize the Taylor cone and the filament jet. Hence, the electrostatic atomization of the methanol/water solutions to form a particular size of charged droplets and the droplet size distribution would necessarily be affected. A smaller fraction of the charged droplets produced per unit time from which ions are efficiently transferred from within a charged droplet to the gas phase was proposed as the reason for the reduction of the lithium ion cluster signal intensity as the percentage of water in the solution being electrosprayed increased.

9.4 Discussion: Charged Droplet Composition Prediction with a Constant Surface Electric Field Model

A brief background of the literature is provided as a review of the knowns and unknowns with respect to electrostatic atomization of liquids. An electrostatic atomization model is proposed that describes quantitatively the results obtained in Fig. 9.3, but only qualitatively describes the observations made from the data plotted in Fig. 9.5. The model is based on the assumption that the surface electric field strength of the charged droplets is a constant. Equations used to predict the physical parameters of the charged droplets based on this assumption are provided and a discussion of the significance of the proposed model follows.

A photograph of a capillary jet being drawn from a Taylor cone (See Fig. 1 in Reference 6) has astounding similarities to the photograph of a charged droplet undergoing Rayleigh fission where a long capillary is drawn from the droplet before breaking into droplets (See inset in Fig. 3 in Reference 9). Rayleigh fission is a process by which a charged droplet that is unstable due to a high electric surface field strength ejects 15% of the total droplet charge and 2% of the total droplet mass [45]. It was hypothesized that charged droplet production from the Taylor cone/filament jet is a Rayleigh fissional process of the first kind that can be envisioned as a "steady state droplet jet". If this hypothesis is correct, then the physical dimensions that the Taylor cone and filament jet can be used to predict the physical characteristics of the charged droplets themselves using the interpretation of the charged droplet Rayleigh fissional process described by Kebarle and Tang [9,32]. The calculations from Kebarle and Tang were based on the assumption that the charge and mass ejected by a Rayleigh fission are divided into ~ 20 product droplets and the radius of each product droplet was ~ 1/10 the radius of the unstable droplet undergoing Rayleigh fission. The assumptic made here was that the radius of the droplet can be replaced with the dimensions of a Taylor cone.

The dimensions of the stainless steel capillary used in this work was 0.1 mm I.D. x 0.06 mm wall. Using the terminology of Cloupeau and Prunet-Foch who have studied the different modes of electrostatic spraying of liquids, the multi-jet variant of the cone-jet mode was the mode with which the electrospray investigations reported from this laboratory were acquired (see Fig. 11.b in reference 1). In this mode of operating the electrospray source, the blunt end or wall of the electrospray capillary is wetted by the solution, and this serves as the source of the charged droplets. A "steady state-droplet jet" model of droplet formation would predict a maximum charged droplet radius on the order of ~ 1/10 the wall thickness radius of the electrospray capillary.

Pfeifer and Hendricks developed Eqn. 1 relating the electric field strength of the electrospray capillary to be calculated knowing the applied voltage and geometry of the capillary [46]. Their equation is extended here to reflect the geometry of the "steady state-droplet jet" based on the argument of Cloupeau and Prunet-Foch that the surface of the Taylor cone is nearly equi-potential with the potential applied to the electrospray capillary tip [1]. Using an equivalent radius of $r = 3x10^{-6}$ m (1/10 the radius of the wall of the electrospray capillary on the assumption that the radius of the end of the capillary serves as the source of the "steady state-droplet jet"), the distance to the counter electrode d = 0.01 m, and an applied voltage to the electrospray tip of V = 3,400, an effective field strength of

2.4×10^8 V/m is obtained for a multijet variant of the cone-jet. The field strength of 2.4×10^8 V/m can be thought of as being the radius of the Taylor cone at the position where the filament jet begins to form (see Fig. 9.2). A filament jet of $r = 3 \times 10^{-6}$ m is expected to produce charged droplets having a radius of ~ 3 μm. The estimate of droplets having a radius ~ 3 μm is assumed to be the upper radius limit for which stable electrical atomization will be observed.

$$E = 2V / r \ln(4d/r) \tag{9.1}$$

A lower limit to the size of the charged droplets produced is not limited by the dimensions of the electrospray tip, but by the field strength at which the ambient dielectric medium will break down. A field strength of ~ 10^9 V/m is very high and electrical discharge can be expected at field strengths in excess of 10^9 V/m. An effective field strength of 1.9×10^9 V/m is obtained if an equivalent filament jet radius of $r = 0.3 \times 10^{-6}$ m is used from which charged droplets with radii on the order of ~ 0.3 μm are expected. In this manner the "steady state-droplet jet" model predicts stable charged droplet production for droplets having radii in the range defined as ~0.3 μm < r < 3 μm.

From the data provided in Figure 3 in Reference 9, where a charged droplet was depicted as having a radius of 1.5 μm and 51,250 charges, a 3.3×10^7 V/m surface field strength of such a droplet was calculated. A reduction of the surface field strength from that at the Taylor cone ~ 2.4×10^8 V/m (up to 1.9×10^9 V/m) to ~3×10^7 V/m on a charged droplet can be expected as a result of electrostatic atomization. Unfortunately, surface field strengths on charged droplets immediately after formation have not been measured for a wide variety of experimental conditions. For reasons to be explained below, the assumption of constant droplet surface field strength for all droplets produced (4.8×10^7 V/m) was made.

D. P. Smith measured changes of the radius and length of the filament jet drawn from the apex of the Taylor cone due to changes in the composition of the solution being electrosprayed [7]. Solutions of higher electrolyte concentration produced shorter filament lengths with smaller filament radii than solutions having a lower electrolyte concentration (see Table 1 and Table 2 in Reference 7). The length of a filament jet is determined by the tangential electrostatic repulsion of the charge carrier velocity in the filament jet exceeding the surface tension of the solution at which point, the filament breaks apart into droplets. Higher tangential electrostatic repulsion is created by smaller filament jet radii, this in turn causes higher charge carrier velocities, greater tangential shear stress, and shorter filament

jets result. The observations by D. P. Smith provided much of the insight behind the hypothesis that electrostatically atomized droplets have a constant surface electric field.

As the velocity of the charge carriers increases within the filament jet, current conservation requires that the current flux be constant. Therefore a decreasing charge density per unit cross sectional volume along the filament jet with increasing distance from the electrospray capillary tip can be expected. Therefore the surface electric field strength of the droplets produced must be less than the field strength at the origin of the "steady state-droplet jet". It is on this point that this model disagrees with the model proposed by Willoughby et. al. where they have argued that the droplets produced are close to the Rayleigh limit [47]. The model by Willoughby et. al. was derived from consideration of the flux of matter (charges, ion pairs, solvent) going in to the Taylor cone requires an outlet for an equivalent flux of matter out of the cone. However, because the signal intensity of the inorganic ions derived from an electrospray source are dependent on the flow rate of a curtain gas, the droplets produced are below the Rayleigh instability limit (see Fig. 9.5) [34]. A certain minimum or threshold flow rate of drying gas is required to induce solvent evaporation from the charged droplets before mass spectrally detected ion currents are dramatically increased via Rayleigh fissional processes [33].

The assumption made in this report that the filament jet radius dictates the radius of the resulting charged droplets contradicts an earlier model proposed by I. Hayati et. al.. They suggested that the filament jet was considered to break apart into droplets when the electric field strength tangential to the direction of flow was equal to the electric field strength normal to the directional flow of the filament jet [6,48]. It is this analogy that causes the single filament jet to split into multiple jets. Siu et. al. have explained their glycerol solvent data in a similar manner where they have argued that solvent evaporation is not a necessary requirement for mass spectral detection of ions produced by an electrospray source [35,36]. In the limit, this model would predict that droplets containing a single ion would be produced from successive splitting of the filament jet. But because the relative ion yield from the charged droplets produced from non-volatile solvents is very low relative to when a volatile solvent is electrosprayed, this mechanistic interpretation can only be a minor source of gas phase ion production in the electrospray process. When solvent evaporation does not occur to an appreciable extent, electrosprayed ion currents are very low (see Fig. 9.5 at curtain gas flow rates below 0.1 lpm), but under optimal curtain gas flow rate conditions, a much larger electrosprayed ion current can be observed (see Fig. 9.5 at curtain gas flow rates above 0.3 lpm).

The point at which the filament jet breaks into droplets is determined by the tangential electrical shear stress and the binding forces of the particular solution being electrosprayed. The assumption made here was that the surface field strength of charged droplets produced solely by electrical atomization is independent of the filament jet radius from which it was produced. This assumption of a constant droplet surface field strength while electrospraying solutions of inorganic electrolytes at different concentrations will be valid provided the surface tension of the solutions are to a first approximation independent of the electrolyte concentration. This condition is met for simple electrolytes (i.e. inorganic electrolytes) dissolved in ethanol [49].

Recall that the surface electric field strength reduction from the Taylor cone generating the charged droplets is greater for droplets derived from a Taylor cone having a smaller radius. On the assumption that all charged droplets produced have a surface field strength of 4.8×10^7 V/m, arbitrary selection of a mean droplet radius was then made to initiate calculations to predict the physical parameters of the charged droplets. For example, consider a solution of a simple electrolyte in methanol at 3×10^{-5} molar. Selection of a droplet radius of 0.71 μm allows the calculation of the droplet volume in cm^3 by Eqn. 9.2.

$$V_d = (4/3)\pi R^3 \tag{9.2}$$

The number of droplets produced per second was obtained with Eqn. 9.3 knowing that the solution flow rate was 10 μl/min. From Eqn. 9.2, the volume of a droplet with a 0.71 μm radius is 1.50×10^{-12} ml and the number of droplets produced per second is 1.11×10^8.

$$\text{drops/sec} = (10\ \mu\text{l/min}) \times (60\ \text{sec/min})^{-1} \times (10^{-3}\ \text{ml/}\mu\text{l}) \times (V_d\ \text{ml})^{-1} \tag{9.3}$$

From Table 9.1, a current of 0.3 μAmperes or 1.8×10^{12} charges/sec was produced by the electrospray tip when a solution containing an electrolyte solution concentration of 3×10^{-5} molar was electrosprayed. The number of charges per droplet was determined with Eqn. 9.4 to be 16,800 charges/drop.

$$\text{charges/drop} = (\text{charges/sec}) / (\text{drops/sec}) \tag{9.4}$$

The surface electric field strength (SEFS) of the droplet could then be calculated using Eqn. 9.5. If the surface electric field strength was not $4.8(+/-0.1) \times 10^7$ V/m, a new charged

droplet radius was selected and the calculations of Eqns. 9.2 to 9.5 were repeated iteratively until the proper droplet radius was determined. An error of the estimated field strength of the charged droplets of $4.8(+/-2)x10^7$ V/m produces an error in the radius of charged droplets of 0.71(+0.30/-0.29) μm produced by electrospraying a solution with an electrolyte concentration of $3x10^{-5}$ molar.

$$SEFS = q / 4\pi E_o R^2 \tag{9.5}$$

The values obtained for the sample calculation for a simple electrolyte concentration of $3x10^{-5}$ molar has been included in Table 9.2 along with calculations for several other solution electrolyte concentrations. The designation CD1′ in Table 9.2 refers to the physical description of a charged droplet immediately after formation. The number of ion pairs per droplet was determined simply from the number of ion pairs per droplet volume in the solution being electrosprayed, had no current been generated. (A correction to subtract the number of charges produced from the total number of ion pairs present was not made.)

CD1′′ refers to the charged droplet at the instant immediately prior to Rayleigh fission where the only physical change to the droplet in going from CD1′ to CD1′′ was solvent evaporation. The radius at which CD1′′ will experience Rayleigh fission was determined based on the experimental evidence provided by Taflin et. al. [45] according to Eqn. 9.6. q is the number of charges in the droplet, E_o the permitivity, or dielectric strength, of the ambient atmosphere, s is the surface tension of the solution, and R_R is the radius of the droplet when fission occurs. Eqn. 9.6 reflects the experimental observations of Taflin et. al. where charged droplets were found to undergo fission with only 80% of the charge that can be predicted by the Rayleigh equation.

$$q^2/0.8 = 64\pi^2 E_o s R_R^3 \tag{9.6}$$

Solving Eqn. 9.6 for the radius at which the droplet undergoes fission allowed the calculation of the droplet radius and number of charges before (CD1′′) and after ($CD1^{(''),'}$) the fission as well as the physical parameters of the very small product droplets (radius, number of charges, and number of ion pairs) ejected from the droplet that underwent Rayleigh fission. The droplet undergoing the Rayleigh fission expels 15% of its charge along with 2% of its mass. Similar calculations have been carried out previously by Kebarle and co-workers [9,32] and they assumed that the matter expelled by the Rayleigh fission was divided into 20 equivalent droplets. These product droplets have been termed

CD2′ where the 2 refers to a second generation droplet and ′ refers to the physical parameters of these droplets at the moment of formation.

These equations were used to calculate the physical description of charged droplets for three cycles, or generations, of solvent evaporation-Rayleigh fission. Third generation droplets produced from electrosprayed solutions of high electrolyte concentration ($\geq 1x10^{-4}$ molar) were undefined from the standpoint that less than one charge per droplet was calculated using the procedure outlined above (see Table 9.2). A ? was used to denote that the composition of such droplets could not be predicted from the simple procedure used here.

Having explained the calculations and assumptions used to describe the physical parameters of the charged droplets at atmospheric pressure in an electrospray source, it is now useful to assess the significance of the charged droplet parameters that were calculated and tabulated in Table 9.2. The radii of the first generation droplets (CD1′) that are summarized in Table 9.2 extend over two orders of magnitude of electrolyte concentration and the calculated values provide some explanation as to the reason why solutions of low total electrolyte concentration ($< 3x10^{-5}$ molar) and high total electrolyte concentration ($> 1x10^{-3}$ molar) are difficult to electrospray. Refer to Fig. 9.3 where the calibration curve for a simple electrolyte salt dissolved in pure methanol is plotted. The electrospray current increases as the electrolyte concentration was increased (Table 9.1). For a fixed solution flow rate, the only way for the charged droplets to carry more current is to increase the surface area to volume ratio through a reduction of the charged droplet radii. This is reflected in Table 9.2 for the CD1′ droplets where the radius of the charged droplets produced decreases from 1.1 μm to 0.27 μm when the concentration of the electrolyte in solution is increased from $1x10^{-5}$ molar to $3x10^{-3}$ molar. The respective surface area to volume ratio increase is from $2.7x10^{4}$ to $1.4x10^{5}$.

Under the CD1′ heading in Table 9.2, the number of charges per droplet and the number of ion pairs per droplet are tabulated. As mentioned previously, the number of excess ions calculated per droplet were not subtracted from the number of ion pairs per droplet. Assuming that the source of the current generated in the electrospray capillary was only from oxidation of anions, then the number of excess ions per droplet should be subtracted from the number of ion pairs remaining. Performing this subtraction for electrospraying an electrolyte solution at $3x10^{-5}$ molar, the number of ion pairs actually remaining in the droplet containing $1.7x10^{4}$ charges is $1.0x10^{4}$. At very high electrolyte concentrations (>

$1x10^{-3}$ molar), the number of excess charges per droplet is small relative to the number of ion pairs per droplet, and this correction becomes less important. However, for solution electrolyte concentrations $\leq 1x10^{-5}$ molar, subtracting the number of excess ions from the number of ion pairs in the droplet results in a corrected number of ion pairs per droplet less than zero. This is in fact not a fault of the constant surface electric field strength droplet assumption because electrospraying solutions of low electrolyte concentrations ($\leq 1x10^{-5}$ molar) does not produce a stable analytical ion signal (see Fig. 9.3).

Correction of the number of ion pairs remaining in the droplet, by subtracting the calculated number of ion pairs assuming no electrospray current was generated (as was the case for the data contained in Table 9.2) from the calculated number of excess ions was performed for the values in Table 9.3. The number of excess charges and the number of ion pairs per average CD3´ is 1 and 0.01 respectively, for an initial solution concentration of 3x10-5 molar. However, for an initial solution concentration of 3x10-3 molar, the calculated average number of excess charges and ion pairs is 0.1 and 3 respectively. With consideration of these calculations, the fundamental nature of an electrospray calibration curve, as depicted by the fundamental electrospray response function of the ES-MS calibration curve plotted Fig. 9.3, may be easily rationalized.

The assumption of a constant droplet surface electric field strength can also be used to explain why the addition of an electrospray stabilizer was able to linearize the calibration curve plotted in Fig. 9.3. Solutions that have trace electrolyte concentrations ($\leq 1x10^{-5}$ molar) in pure methanol solvent can not be electrosprayed without adjustment of the operating conditions of the source. (The threshold for stable electrospray was dependent on the electrospray capillary applied voltage and a reduction from 5.0 kV to 4.0 kV allowed solutions of $1x10^{-5}$ molar KCl to be electrosprayed in the absence of an electric discharge. But a reduction of the electric field strength at the electrospray capillary tip would alter the surface electric field strength of the droplets produced.) Addition of an electrospray stabilizer, an inert electrolyte at a fixed level to all solutions, changes the solution properties of the test solution such that stable droplets can be produced by electrical atomization. Establishment of stable charged droplet formation through the addition of an electrospray stabilizer then permits quantitation of trace solution components. (See reference 37 for further details.)

Non-mass spectrometric investigators of electrostatic spraying phenomena explain the inability of low electrolyte solutions to form a Taylor cone because the electric field of the

electrospray capillary does not penetrate the liquid to form a Taylor cone [4-7]. A qualitative explanation for the inability to generate stable charged droplet production at low electrolyte concentrations (< $3x10^{-5}$ molar) is afforded by the "steady state droplet jet" interpretation where production of charged droplets from the Taylor cone is Rayleigh fission of the first kind. Charged droplets generated when the solution electrolyte concentration was $1x10^{-5}$ molar were calculated to be 1.07 μm on the assumption of a droplet surface field strength of $4.8x10^{7}$ V/m. Such a droplet radius is approaching the maximum droplet radius permitted by the "steady state droplet jet" interpretation (~ 3 μm dia. droplets).

For the case of high electrolyte solutions (> $1x10^{-4}$ molar) being electrostatically atomized, smaller charged droplets are produced with fewer number charges per droplet. The calculated number of charges per droplet decreases by a factor of approximately three in going from a solution electrolyte concentration of $3x10^{-5}$ molar to $3x10^{-3}$ molar, but because of the constant surface electric field assumption the number of charges per unit surface area remains constant. Consideration of the ratio of the number of excess charges to the number of ion pairs per droplet at high electrolyte concentrations provides an explanation for the observed low analyte sensitivities. A consequence of the lower number of charges per droplet are that third generation droplets (CD3′) are ill-defined with respect to the number of charges per CD3′. For example, for solution electrolyte concentrations > $3x10^{-5}$ molar, less than one charge per CD3′ was calculated. This result is of significance because it is reasonable to expect that ion transfer from solution to the gas phase is most efficient from CD3′ that have the highest ratio of the number of excess charges per number of ion pairs. A CD3′ droplet derived from electrospraying a solution with an electrolyte concentration of $3x10^{-5}$ molar contains on average one excess charge per droplet but only a single ion pair per 33 CD3′ produced.

Hayati et. al. observed that the charge to mass ratio (q/m) of the filament jet produced increases with increasing conductivity. (See Figure 9 in Reference 5.) On the assumption that a q/m increase in the filament jet will be directly reflected by a similar increase of the q/m ratio in the droplets, then from Table 9.2 the q/m ratio of the CD1′ droplets at electrolyte concentrations of $3x10^{-5}$ molar and $3x10^{-3}$ molar is $2.3x10^{-3}$ and $6.1x10^{-3}$ respectively. From this it follows that the first generation droplets initially produced from solutions with an electrolyte concentration of $3x10^{-5}$ molar and $3x10^{-3}$ molar were at 45% and 61% of the Rayleigh limit respectively. The smaller charged droplets are closer to the Rayleigh limit, as determined with Eqn. 9.6 than larger droplets that are produced solely by

electrostatic atomization. The calculations made here based on the assumption of a constant surface electric field strength droplet model can be used to explain the fundamental quantitative behavior of an electrospray source and to also explain the observation made by Hayati et. al that the charge to mass ratio of the filament jet increases with increasing solution conductivity.

No attempt has been made to quantitatively explain the observations made concerning the lithium ion signal intensity trends plotted in Fig. 9.5, but speculation on the observations discussed in the results section will now be offered. From the first generation droplet parameters that were calculated and tabulated in Table 9.2, an increase of the charge to mass ratio of the droplets resulted in smaller droplets being produced from solutions of higher electrolyte concentrations. From Eqn. 9.6, for an increase in the surface tension of the solution being electrosprayed, as would be the case for an increasing water to methanol solvent ratio, the charge to mass ratio (actually the q^2/R_R^3 ratio) of the droplets should increase proportionally by the factor $1/R_R^3$ (at constant current), causing smaller charged droplets to be produced (at constant electrospray current). Smaller charged droplets would have a lower number of excess charges per droplet and hence a lower ion signal intensity would be observed. Qualitatively, if smaller charged droplets are produced, then the surface electric field strength of the droplets produced would decrease with an increasing level of water content in the solution being electrosprayed because the electrospray current was not dependent on the water to methanol solvent composition. This observation may also imply that the source of current in the electrospray capillary is due to oxidation of anions, not oxidation of solvent.

9.5 Conclusions

A qualitative method of predicting charged droplet composition based on a "steady state-droplet jet" interpretation of the Taylor cone together with an assumption that a constant surface electric field strength on different sized charged droplets is constant has been developed. The steady state droplet jet interpretation allowed estimation of the field strength at the apex of a Taylor cone where the filament jet originates and also estimation of the decrease in field strength along the filament jet. The surface field strength of the electrostatically atomized droplets is lower than the field strength at the Taylor cone by an estimated factor of ~ 4 to 50, depending on the solution being electrosprayed. The surface field strength of the droplet was assumed here to be 4.8×10^7 V/m. Furthermore, the

assumption of a constant surface electric field strength on droplets produced by electrostatic atomization from solutions having variable electrolyte concentrations has allowed the calculation of the physical parameters of charged droplets that were used to explain numerous experimental observations.

Experiments are being prepared to establish validity of the assumptions made and also to incorporate a mathematical description of the effect of physical properties of the solution (conductivity and surface tension) being electrosprayed.

Table 9.1 Measured electrospray capillary current as a function of electrolyte concentration in HPLC grade methanol.

Total Electrolyte Concentration (molar)	Current (μAmpere)
$1x10^{-5}$	0.2
$3x10^{-5}$	0.3
$1x10^{-4}$	0.4
$3x10^{-4}$	0.5
$1x10^{-3}$	0.6
$3x10^{-3}$	0.8

Table 9.2 Predicted charged droplet composition for electrospraying simple inorganic electrolytes dissolved in methanol. A constant droplet surface electric field strength of 4.8×10^7 V/m was assumed. A ? indicates the physical parameters of the droplet are undefined with respect to defining a Rayleigh fission product droplet based on the available charge in the droplet undergoing the fission. See text for details of calculations.

Droplet	Parameter	Initial Electrolyte Concentration (molar)				
		1×10^{-5}	3×10^{-5}	1×10^{-4}	3×10^{-4}	3×10^{-3}
CD1′	radius (μm)	1.1	0.71	0.54	0.43	0.27
	V_d (10^{-12} ml)	5.1	1.5	0.66	0.33	0.08
	droplet/second (10^9)	0.03	0.1	0.3	0.5	2
	charges/drop (10^4)	3.8	1.7	1.0	0.6	0.24
	ion pairs/droplet (10^4)	3.1	2.7	3.9	5.9	14
	surface area to volume ratio (10^2)	2.8	4.2	5.5	7.0	11
CD1″	radius (μm)	0.78	0.45	0.31	0.23	0.12
	surface field strength (10^8 V/m)	0.9	1.2	1.4	1.7	2.3
CD1$^{(\prime\prime)\prime}$	radius (μm)	0.77	0.45	0.31	0.23	0.12
	surface field strength (10^8 V/m)	0.8	1.1	1.2	1.4	2.0
CD2′	radius (μm)	0.08	0.05	0.03	0.02	0.01
	charges/drop	288	126	72	46	18
	ion pairs/droplet	31	27	39	59	144
	surface field strength (10^8 V/m)	0.7	0.9	1.1	1.3	1.7
CD2″	radius (μm)	0.03	0.02	0.01	0.009	0.005
	surface field strength (10^8 V/m)	4.7	6.1	7.4	8.6	12
CD3′	radius (μm)	0.003	0.002	?	?	?
	charges/drop	2	1			
	ion pairs/droplet	0.03	0.03			

Table 9.3 Corrected third generation charged droplet composition for electrospraying simple inorganic electrolytes dissolved in methanol. Subtraction of the number of excess charges from the number of ion pairs per droplet (assuming no electrospray current) was performed to provide a more accurate estimate of the third generation charged droplet composition. These calculated values in this table were derived from the values contained in Table 9.2 With this correction method, the calculated number of ion pairs in the droplet is a negative value for initial solution concentrations of 1x10-5 molar, hence such droplets are undefined. See text for details of calculations.

Droplet	Parameter	Initial Electrolyte Concentration (molar)				
		$1x10^{-5}$	$3x10^{-5}$	$1x10^{-4}$	$3x10^{-4}$	$3x10^{-3}$
CD3´	radius (μm)	?	0.002	0.03	0.002	0.001
	charges/drop		1	0.5	0.3	0.1
	ion pairs/droplet		0.01	0.6	1	3

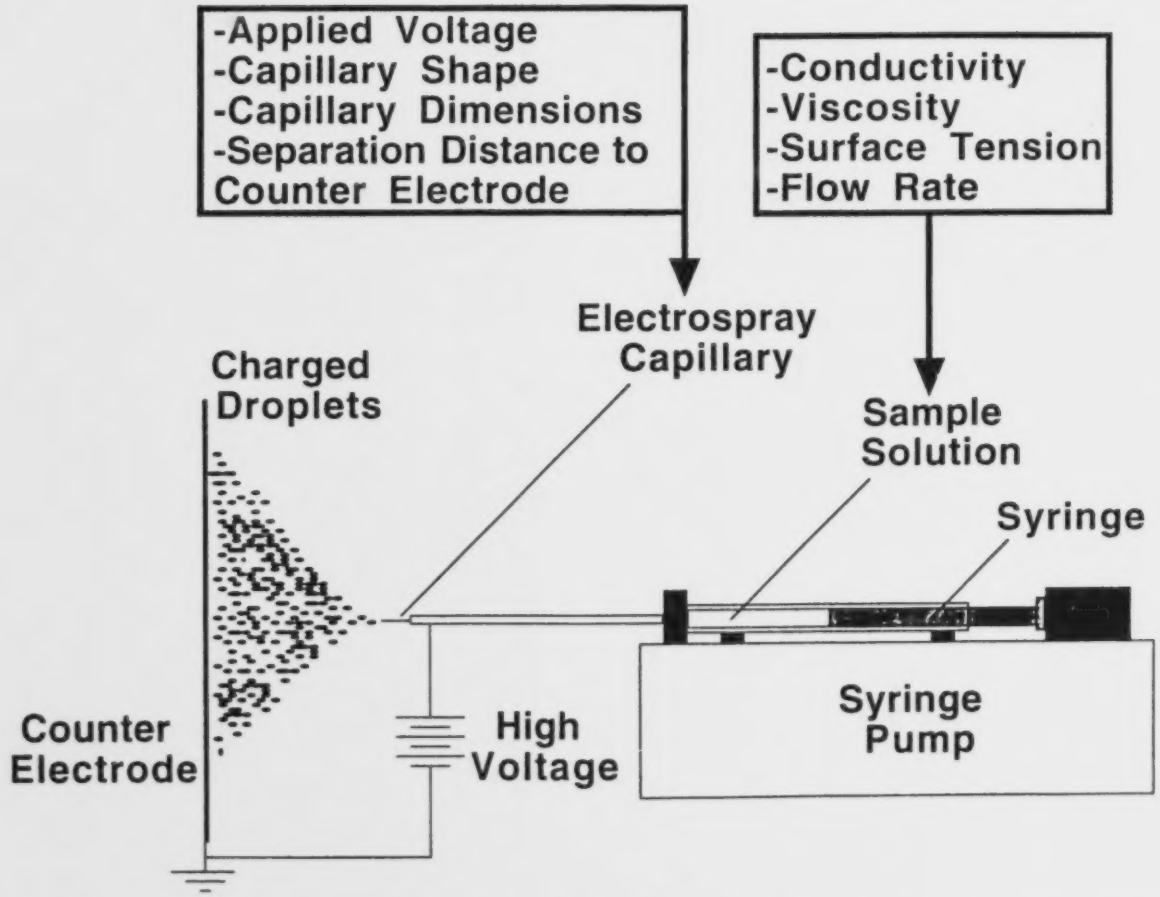

Figure 9.1 Cartoon depicting electrostatic atomization of a liquid. The solution exiting the charged capillary is dispersed by electrical forces into droplets.

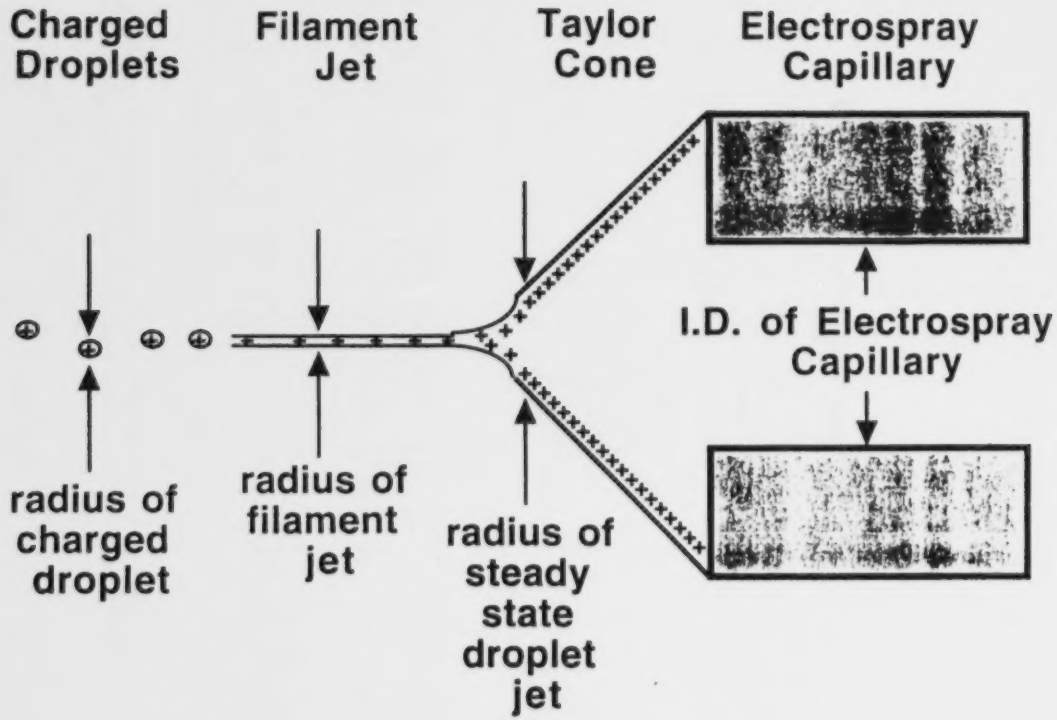

Figure 9.2 Cartoon that depicts the electrostatic atomization steps occurring at the electrospray capillary tip. An oxidation process occurs within a positively biased electrospray capillary to create an excess of positive charges. The positive charges flow along the surface of the Taylor cone. When the electrostatic forces begin to exceed the binding forces of the solution, a filament jet emerges from the apex of the Taylor cone which ultimately breaks apart to form charged droplets.

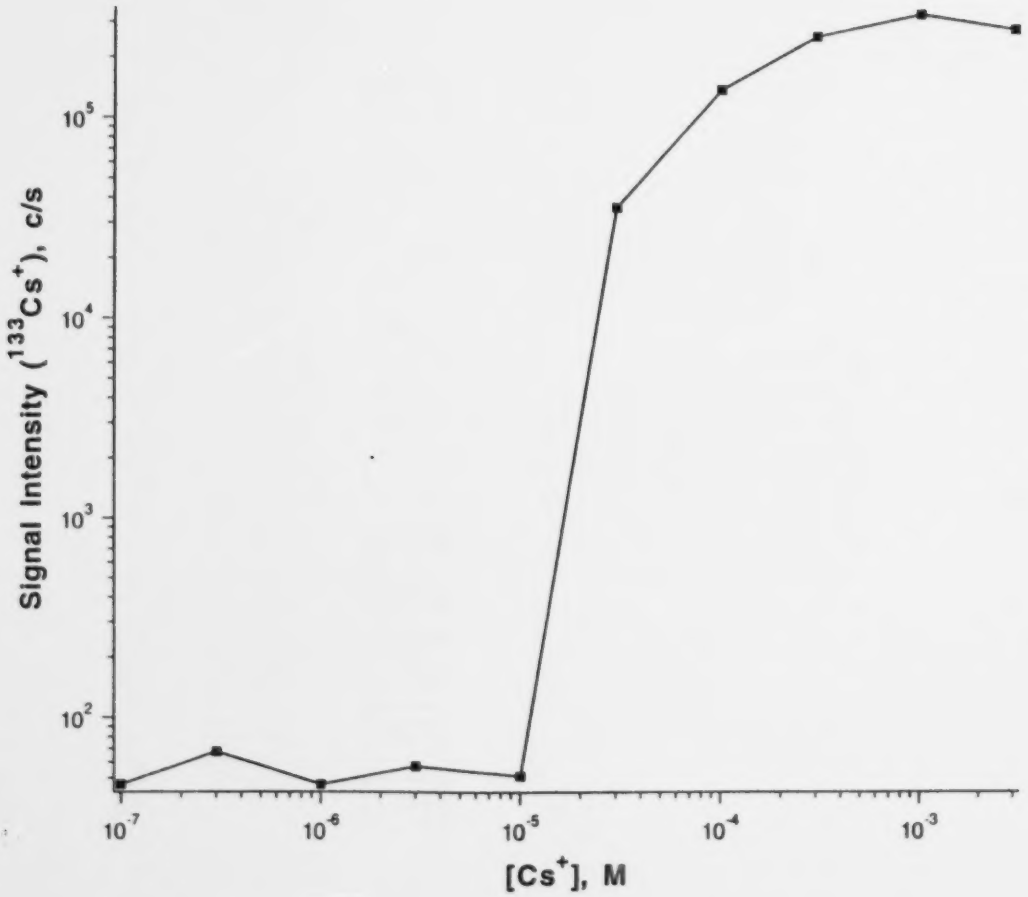

Figure 9.3 Attempted calibration curve for cesium nitrate in HPLC grade methanol. Source conditions were electrospray capillary 5.0 kV, front plate 950 V, sampling plate 190 V, skimmer 5 V, and curtain gas flow rate 0.1 lpm.

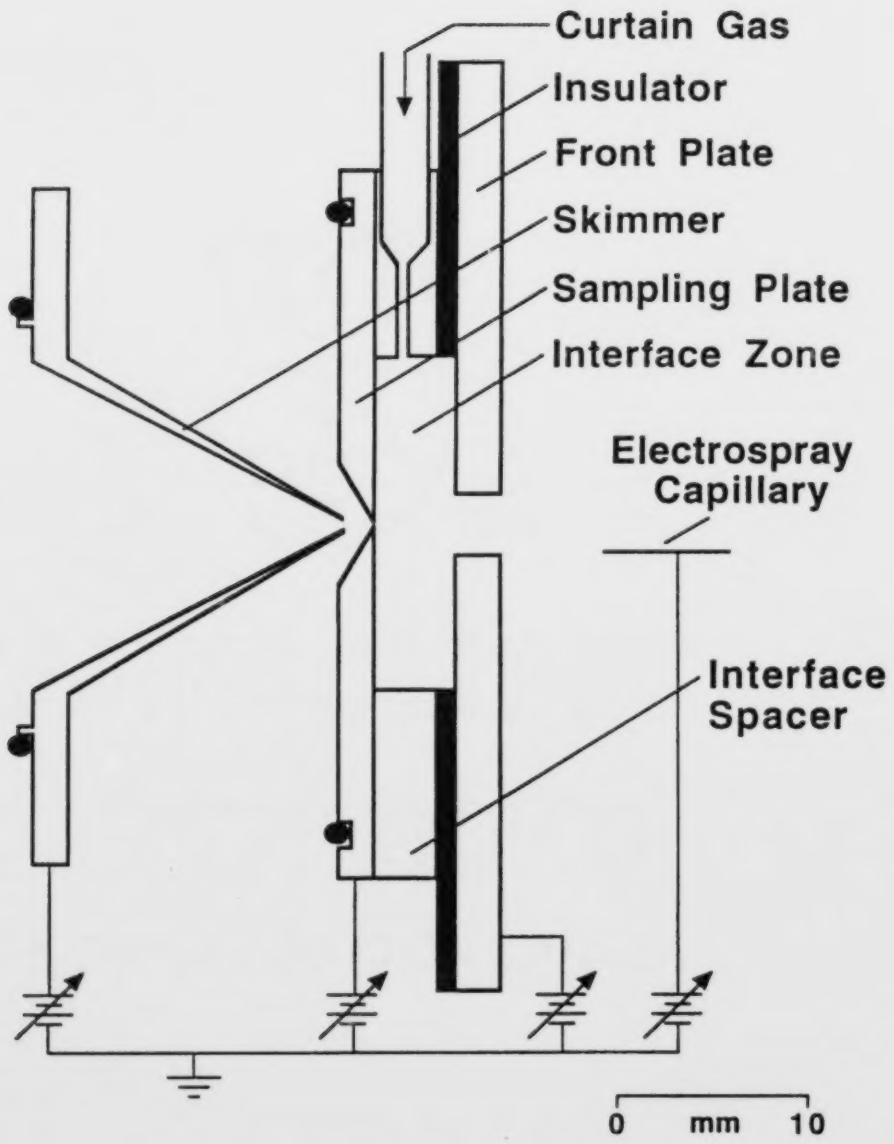

Figure 9.4 A schematic diagram of the electrospray source and interface.

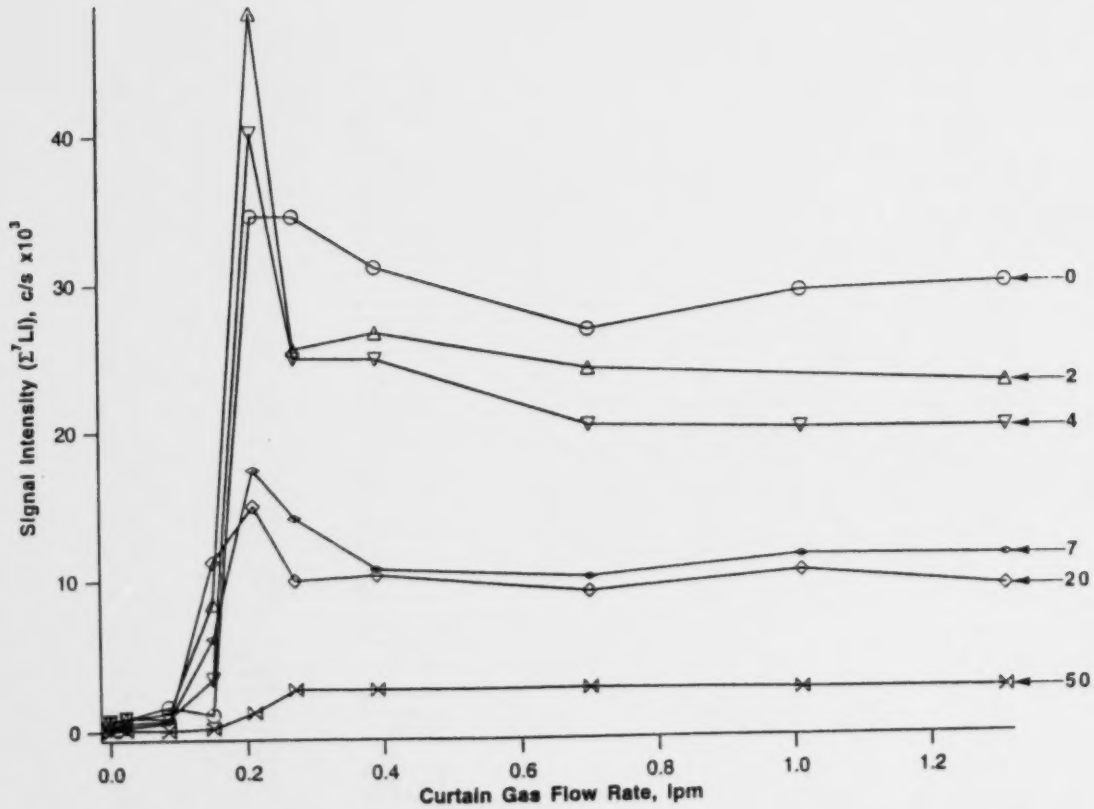

Figure 9.5 Total lithium ion signal as a function of the curtain gas flow rate as the composition of the water/methanol solvent was changed. The percentage water in each mixture is indicated in the figure. Lithium chloride was 1×10^{-4} molar in all solutions. Source conditions were electrospray capillary 4.0 kV, front plate 600 V, sampling plate 40 V, and skimmer 9 V.

9.6 References

1. M. Cloupeau and B. Prunet-Foch, J. Electrostatics, **25**, 165 (1990).

2. V. G. Drozin, J. Colloid Sci., **10**, 158 (1955).

3. A. Doyle, D. R. Moffett, and B. Vonnegut, J. Colloid Sci., **19**, 136 (1964).

4. D. W. Horning and C. D. Hendricks, J. Appl. Phys., **50**, 2614 (1979).

5. I. Hayati, A. I. Bailey, and Th. F. Tadros, J. Colloid Interface Sci., **117**, 205 (1987).

6. I. Hayati, A. I. Bailey, and Th. F. Tadros, J. Colloid Interface Sci., **117**, 222 (1987).

7. D. P. H. Smith, IEEE Trans. Ind. Appl., **1A-22**, 527 (1986).

8. G. I. Taylor, Proc. R. Soc. London, **A280**, 383 (1964).

9. P. Kebarle and L. Tang, Anal. Chem., **65**, 972A (1993).

10. M. Dole, L. L. Mach, R. L. Hines, R. C. Mobley, L. P. Ferguson, and M. B. Alice, J. Chem. Phys., **49**, 2240, (1968).

11. L. L. Mach, P. Kralik, A. Rheude, and M. Dole, J. Chem. Phys., **52**, 4977 (1970).

12. J. B. Fenn, M. Mann, C. K. Meng, S. K. Wong, and C. M. Whitehouse, Science, **246**, 64 (1989).

13 R. D. Smith, J. H. Wahl, D. R. Goodlett, and S. A. Hofstadler, Anal. Chem., **65**, 574A, (1993).

14. S. C. Beu, M. W. Senko, J. P. Quinn, F. M. Wampler, and F. W. McLafferty, J. Am. Soc. Mass Spectrom., **4**, 557 (1993).

15. B. E. Winger, S. A. Hofstadler, J. E. Bruce, H. R. Udseth, and R. D. Smith, J. Am. Soc. Mass Spectrom., **4**, 566 (1993).

16. G. J. Van Berkel, G. L. Glish, and S. A. McLuckey, Anal. Chem., **62**, 1284 (1990).

17. S. R. Wilson, and Y. Wu, J. Am. Soc. Mass Spectrom., **4**, 596 (1993).

18. B. M. Hughes, D. E. McKenzie, and K. L. Duffin, J. Am. Soc. Mass Spectrom., **4**, 604 (1993).

19. E. C. Huang, B. N. Pramanik, A. Tsarbopoulos, P. Reichert, A. K. Ganguly, P. P. Trotta, T. L. Nagabhushan, and T. R. Covey, J. Am. Soc. Mass Spectrom.., **4**, 624 (1993).

20. R. Feng and Y. Konishi, J. Am. Soc. Mass Spectrom., **4**, 638 (1993).

21. V. Katta, S. K. Chowdhury, and B. T. Chait, J. Am. Chem. Soc., **112**, 5348 (1990).

22. P. Jayaweera, A. T. Blades, M. G. Ikonomou, and P. Kebarle, J. Am. Chem. Soc., 112, 2452 (1990).

23. K. W. M. Siu, G. J. Gardner, and S. S. Berman, Anal. Chem., 61, 2320 (1989).

24. G. R. Agnes and G. Horlick, Anal. Chem., submitted.

25. L. Tang and P. Kebarle, Anal. Chem., **63**, 2709 (1991).

26. K. L. Duffin, J. D. Henion, and J. J. Shieh, Anal. Chem., **63**, 1781 (1991).

27. G. J. Van Berkel, S. A. McLuckey, and G. L. Glish, Anal. Chem., **64**, 1586 (1992).

28. A. T. Blades, M. G. Ikonomou, and P. Kebarle, Anal. Chem., **63**, 2109 (1991).

29. J. B. Fenn, J. Am. Soc. Mass Spectrom., **4**, 524 (1993).

30. B. E. Winger, K. J. Light-Wahl, R. R. Ogorzalek Loo, H. R. Udseth, and R. D. Smith, J. Am. Soc. Mass Spectrom., **4**, 536 (1993).

31. G. Schmelzeisen-Redeker, L. Butfering, and F. W. Rollegen, Int. J. Mass Spectrom. Ion Processes, **90**, 139 (1989).

32. L. Tang and P. Kebarle, Anal. Chem., **65**, 3654 (1993).

33. G. R. Agnes and G. Horlick, Appl. Spectrosc., submitted for publication.

34. G. Agnes and G. Horlick, Appl. Spectrosc., submitted for publication.

35. K. W. M. Siu, R. Guevremont, J. C. Y. LeBlanc, R. T. O'Brien, and S. S. Berman, Org. Mass Spectrom., **28**, 579 (1993).

36. R. Guevremont, J. C. Y. LeBlanc, R. and K. W. M. Siu, Org. Mass Spectrom., **28**, 1345 (1993).

37. G. R. Agnes and G. Horlick, "Electrospray Mass Spectrometry as a Technique for Elemental Analysis: Quantitative Aspects", Appl. Spectrosc. (accepted for publication).

38. J. V. Iribarne and B. A. Thomson, J. Chem. Phys., **64**, 2287 (1976).

39. B. A. Thomson and J. V. Iribarne, J. Chem. Phys., **71**, 4451 (1979).

40. A. G. Childers and G. M. Hieftje, Anal. Chem., **65**, 2753 (1993).

41. A. G. Childers and G. M. Hieftje, Anal. Chem., **65**, 2761 (1993).

42. C. N. Davies, In *Fundamentals of Aerosl Science*, D. T. Shaw, Ed., John Wiley and Sons, New York, 1978, p. 154.

43. M. G. Ikonomou, A. T. Blades, and P. Kebarle, J. Am. Soc. Mass Spectrom., **2**, 497 (1991).

44. S. K. Chowdhury and B. T. Chait, Anal. Chem., **63**, 1660 (1991).

45. D. C. Taflin, T. L. Ward, and E. J. Davis, Langmuir, **5**, 376 (1989).

46. R. J. Pfeifer and C. D. Hendricks, J. AIAA, **6**, 496 (1968).

47. R. Willoughby, E. Sheehan, A Jarrell, R. Peddar, T. Marecic, and S. Penn, "Studies of the Physical Processes of Electrospray," in *Proceeding of the 41st ASMS Conference on Mass Spectrometry and Allied Topics*, San Francisco, CA, May 30-June 4, 1993, p. 765a.

48. I. Hayati, A. I. Bailey, and Th. F. Tadros, Nature, **319**, 41 (1986).

49. In Table "Surface Tension of Inorganic Solutes in Organic Solvents," in *CRC Handbook of Chemistry and Physics*, 59th edition, R. C. Weast, Ed., CRC Press, 1978.

Chapter 10

Conclusions

10.1 Summary

Several reasons were outlined in the introduction as to why this project was undertaken. The single most important reason fueling the development of ES-MS as a tool for elemental analysis was the potential for this technique to make species determinations.

Chapter 7 dealt specifically with the potential for ES-MS to make species determinations of kinetically inert and kinetically labile species in solution. ES-MS is indeed a wonderfully simple technique with which most ionic chemical forms of an element in solution may be studied. It is the unique nature of the electrospray source whereby solution ions are stabilized by solvent molecules during the transfer to the gas phase at atmospheric pressure.

The ease with which chemical forms of an element were able to be differentiated was made possible by understanding how the nano-droplets present at atmospheric pressure may be manipulated during the sampling step by the ES-MS interface parameter set-points. Control over the extent to which an ion cluster is declustered en-route to the mass analyzer permitted the acquisition of information specific to the solution state of the ion. Ion sampling with gentle interface conditions allowed for a survey of the oxidation state and also any ligands associated with the analyte ion. Interface conditions set for harsh ion sampling were used to differentiate chemical forms through collisional removal of the solvation sphere. A survey of these capabilities were presented in Chapter 5 with a detailed investigation of the interface parameters following in Chapter 6. The acquisition of the speciation data presented in Chapter 7 was made possible having gained knowledge regarding how manipulation of the interface parameters affected the ion sampling process.

Quantitation of inorganic ions in solution was demonstrated with harsh ion sampling interface conditions such that the analyte ion flux arriving at the detector consisted primarily of a single analyte ion form, typically the bare ion M^+. Mass spectra acquired with harsh ion sampling interface conditions were similar in appearance to that which is obtained using an ICP ion source.

At the time that the quantitation experiments were performed (see Chapter 3), an explanation of the calibration curves obtained by electrospraying a solution consisting of a simple inorganic electrolyte (A^+B^-) dissolved in a pure solvent was not available. Since that time several developments in the understanding of the electrospray process appeared in

the literature. The electrospray mechanistic thoughts of other workers that were reported greatly assisted the formulation of the model that was used to predict the physical parameters of electroatomized droplets that was presented in Chapter 9. The model was based on a "steady state-droplet jet" interpretation of the droplet formation step and also on the assumption of a constant surface electric field strength on the charged droplets. The success with which experimental results were rationalized with this model certainly warrants further investigation to ascertain the validity of the constant surface electric field strength assumption inherent to the model.

Another development of significance was the clarification of the mechanism by which ions within charged droplets are transferred to the gas phase (Chapter 8). The suppression of the analyte ion signal intensity caused by the introduction of another ion into the solution being electrosprayed was used to investigate the ion transfer mechanism. The results of such experiments were well modeled with a statistical, or ion population based argument of surface charge site competition between solution ions. This lead to the conclusion that the single ion droplet theory (SIDT) for ion transfer mechanism provides a satisfactory explanation of the mechanism by which solution ions with in the charged droplets are transferred to the gas phase. Furthermore, the experiments that were performed and discussed in Chapter 8 discount the ion evaporation theory (IET) of ion transfer because no preferential desorption of one ion over another, as would be predicted by the IET, was observed.

10.2 Future Directions

10.2 Potential Applications for Elemental ES-MS

The greatest potential use of ES-MS in the scheme of elemental determinations would be to exploit this technique for what it is ideally suited; solution speciation determinations. From this perspective, realistic expectations of ES-MS applications for elemental determinations of real samples will very likely evolve around niche assays that are difficult to perform by other methods.

In reality, ES-MS will likely not compete with ICP-MS as a general purpose elemental analysis technique. Severe analyte signal intensity suppressions caused by the presence of

any concomitant electrolyte ions in solution are observed. These suppressions are a fundamental flaw of this technique and its utility to determine the elemental composition of unknown samples. Therefore the direct analysis of elemental composition of solution samples containing high electrolyte concentrations can be precluded apriori from useful ES-MS applications.

With these considerations in mind, the following applications may be particularly well suited for elemental ES-MS;

i) Inorganics in organic solvents.

ii) Species that are difficult to determine by other methods, such as the organotins.

iii) Assessing the entire species distribution of an element in a solution sample when several different complexing ligands are present.

iv) Elemental composition of naturally occurring (peptides, proteins, sugars) and synthesized organometallics (thermally unstable compounds, dyes, pesticides).

10.2.1 Recommended Instrumentation Modification

A future hardware modification to the mass spectrometer could, and should include an ion optic arrangement suited to an electrospray source. RF-only quadrupoles would be an ideal replacement for the required ICP-related ion optical arrangement of Einzel lenses and a Bessel box. For safety reasons, addition of a plenum chamber to surround the electrospray capillary prior to electrospraying toxic materials is required. A plenum chamber will alter the characteristics of the electrospray interface from that which was described in Chapter 6.

A question frequently asked following presentation of elemental ES-MS results at scientific meetings is, "can aqueous solutions be electrosprayed?" Admittedly, electrical atomization of aqueous solutions may be the Achilles' heel of electrospray. Several reports have appeared in the literature describing the electrical atomization of aqueous samples.

Application of the reported technology has however been slow, implying that alternative approaches to solve this problem remain to be developed.

Several non-reproducible observations regarding the behavior of ES-MS were briefly discussed in Chapter 4. The observations were short term drift, day to day sensitivity changes, and the structured background spectral characteristics. As was clearly delineated in Chapter 4, a clear explanation of any one of these observations could not easily be made from the limited data set that was compiled. Further investigation into any one of these areas of poor understanding could evolve into a thesis of its own. Such mechanistic investigations can lead to technological breakthroughs. However, as was the case for the interesting results presented in this thesis, the advancement of knowledge was more often than not achieved through the serendipitous combination of doing several things incorrectly to learn something entirely different than what was originally sought.